Characterisation of Submarine Landslides on the Eastern Slopes of the Eivissa Channel, Western Mediterranean Sea

DISSERTATION

zur Erlangung des

Doktors der Naturwissenschaften (Dr. rer. nat.)

der Mathematisch-Naturwissenschaftlichen Fakultät der

Christian-Albrechts-Universität zu Kiel

vorgelegt von

Thore Falk Sager

Kiel, 2023

Erste Gutachterin: Prof. Dr. Morelia Urlaub (GEOMAR)

Zweiter Gutachter: Prof. Dr. Christian Berndt (GEOMAR)

Tag der mündlichen Prüfung: 12. September 2023

Dekan

Eidesstattliche Erklärung

Die Abhandlung ist, abgesehen von der Beratung durch meine Betreuer und die Zuhilfenahme der angegebenen Mittel, nach Inhalt und Form eine eigenständige und nur mit den angegebenen Hilfsmitteln verfasste Arbeit. Diese hat weder zum Teil bereits an anderer Stelle im Rahmen eines Prüfungsverfahrens vorgelegen, noch wurde sie veröffentlicht oder wurde zur Veröffentlichung eingereicht. Die Arbeit ist unter Einhaltung der Regeln guter wissenschaftlicher Praxis der Deutschen Forschungsgemeinschaft entstanden. Ich versichere, dass mir noch kein akademischer Grad entzogen wurde.

Thore Falk Sager Ort, Datum

Summary

Submarine landslides pose a risk to offshore infrastructure and can generate devastating tsunamis. There exist a range of hypotheses about pre-conditioning factors and trigger mechanisms, yet the understanding of landslide development and emplacement processes has been limited to a few case studies. On the one hand, this is partly because the study of sub-seafloor structures is limited to sediment echosounder profiles and 2D and rarely 3D reflection seismic data. However, because these data are expensive to acquire, data coverage is sparse and often of low resolution. On the other hand, historical records of landslide-generated tsunamis are rare, and can often not be differentiated from tsunamis generated exclusively by earthquakes. In addition, the study of active slope failures is mainly based on the 2D and 3D reflection seismic analysis of their remnants – the mass transport deposits (MTDs) – meaning that slope failure development and emplacement processes can only be interpreted from these remains. Interpretation of reflection seismic data is a highly ambiguous task and depends on the data which includes resolution and penetration depth and the experience of the interpreter. Monitoring of active failure processes has only been successful to a limited extent, for instance by measurements of landslide velocities deduced from telecommunication cable breaks. Because of the large size of submarine landslides, it is becoming more and more evident that they can deform seafloor sediments to significant depth. Furthermore, stations and platforms installed directly on the seafloor can be damaged or buried by landslide material or even be incorporated into the slope failure.

Understanding the underlying controls that govern submarine slope failure is critical to assess geohazards and predicting future events. Knowledge and understanding gained from small-scale examples can be extrapolated to large-scale events. To this end, one main contribution of this thesis is the evaluation of development and emplacement processes, the volume assessment of actually mobilised landslide material, and a re-evaluation of destabilising factors that control slope failures in the study area. The main results of the analysis are that one of these landslides, Ana Slide located in the Eivissa Channel between the Iberian Peninsula and the islands of Eivissa (Ibiza) and Formentera, developed during two stages of failure referred to as the primary and secondary failure separated by a significant time lag of around 240 ka (thousand years). Both stages in turn show multi-stage retrogressive development for instance from a stepped headscarp and several lobes inside the sink area. The detailed understanding of Ana Slide is used to estimate the volume of material actually mobilised by the initial failure through the reconstruction of the pre-failure seafloors. Furthermore, results are used to analyse potential destabilising factors at play for other landslides in the Eivissa

Channel. It was found that these factors are a combination of the presence of weak layers, changes in pore pressure through sub-seafloor fluid and gas migration, and local recurrent fault activity.

This thesis investigates submarine landslide occurrences in the Eivissa Channel from the integrated analyses of marine geophysical data. The main methodology uses 2D and 3D reflection seismic data and sediment echosounder profile interpretation to map the internal structure of landslides.

To broaden the understanding of submarine landslide development, emplacement processes, pre-conditioning factors, and potential trigger mechanisms, geophysical data from the Eivissa Channel is analysed. This thesis documents that small submarine landslides have the potential to deform large amounts of seafloor sediment to significant depth. Knowledge gained of the development and emplacement processes of Ana Slide is used to assess the volume of landslide material involved through reconstructions of pre-failure seafloors. In addition, the volume of apparently deformed seafloor sediment from chaotic, transparent, or disrupted seismic facies significantly overestimates the initially failed volume. From the integrated analysis of a wide range of geophysical data, this thesis presents findings that contribute to a revised assessment of destabilising factors that make the eastern slopes of the Eivissa Channel prone to slope instability.

Zusammenfassung

Submarine Hangrutsche stellen eine Gefahr für Offshore-Infrastrukturen dar und können verheerende Tsunamis auslösen. Es gibt viele Hypothesen darüber, wie Hangrutsche entstehen und wie sie Tsunamis auslösen, jedoch gibt es noch viel zu lernen über die Entstehungs- und Ablagerungsprozesse und die inhärenten Vorbedingungen und Auslösemechanismen, die zu Hangrutschen entlang von Kontinentalrändern führen. Während die Untersuchung der Auslösemechanismen viel wissenschaftliche Aufmerksamkeit erhalten hat, ist das Verständnis der Entwicklungs- und Ablagerungsprozesse von Hangrutschen noch auf wenige Fallstudien beschränkt. Dies liegt zum einen daran, dass sich die Untersuchungen der Strukturen unter dem Meeresboden auf Sedimentecholotprofile und primär 2D- und vereinzelte 3D-reflexionsseismische Daten beschränken. Diese Daten sind teuer in der Beschaffung, so dass die Datenabdeckung spärlich ist und oft von geringer Auflösung. Andererseits sind historische Aufzeichnungen von durch Hangrutsche ausgelöste Tsunamis begrenzt und können oft nicht von Tsunamis unterschieden werden, die durch Erdbeben verursacht wurden. Darüber hinaus basiert die Untersuchung von aktiven Hangrutschen hauptsächlich auf der Analyse von 2D- und 3D-reflexionsseismischer Daten und der Interpretation ihrer Überreste, der Massentransportablagerungen (MTDs), was bedeutet, dass die Entwicklung und die Ablagerungsprozesse von Hangrutschen nur von diesen Überresten aus interpretiert werden können. Die Interpretation von reflexionsseismischen Daten ist eine höchst mehrdeutige Aufgabe und hängt von den Daten selbst ab, d. h. von der Auflösung und Eindringtiefe und vor allem von der Interpretationserfahrung. Die Beobachtung von aktiven Hangrutschen ist nur in begrenztem Umfang möglich, z. B. durch Messungen von Hangrutschgeschwindigkeiten, die von Telekommunikationskabelbrüchen abgeleitet wird. Wegen des großen Ausmaßes von submarinen Hangrutschen wird nun immer deutlicher, dass Meeresbodensediment zu einer beträchtlichen Tiefe unterhalb des Meeresboden deformiert werden kann, so dass direkt am Meeresboden installierte Infrastruktur beschädigt, von Hangrutschmaterial begraben oder sogar in Hangrutschen inkorporiert werden kann.

Das Verständnis der zugrundeliegenden Faktoren, die das Versagen submariner Hänge beeinflussen, ist von entscheidender Bedeutung für die Bewertung möglicher Geohazards und das Vorhersagen zukünftiger Ereignisse. Die Erkenntnissen von Fallstudien kleiner Hangrutsche können auf größere Ereignisse extrapoliert werden. Bei den submarinen Hangrutschen im Eivissa-Kanal, der zwischen der Iberischen Halbinsel und den Inseln Eivissa (Ibiza) und Formentera im westlichen Mittelmeer liegt, wurde durch die Bewertung der Entwicklungs- und Ablagerungsprozesse des Ana Slides eine Abschätzung des tatsächlich mobilisierten

Rutschungsmaterials durchgeführt und es wurden potentielle Destabilisationsfaktoren, die Hangrutsche im Untersuchungsgebiet kontrolliert haben, untersucht.

Einer der wichtigsten Ergebnisse dieser Arbeit ist, dass der Ana Slide sich in zwei Hauptphasen des Versagens entwickelt hat. Diese werden als die 'Primär'- und 'Sekundär'-Stadien bezeichnet, welche durch eine erhebliche zeitliche Verzögerung von etwa 240.000 Jahren voneinander getrennt sind. Beide Stadien zeigen eine mehrstufige retrogressive Entwicklung auf. Das detaillierte Verständnis des Ana Slides wurde genutzt, um die Volumina unterschiedlicher Hangrutschmaterialien abzuschätzen, sowie für die Rekonstruktion des Meeresbodens vor der Hangrutschung im Quellenbereich, von wo aus Hangrutschmaterial evakuierte wurde. Darüber hinaus wird das detaillierte Verständnis vom Ana Slide genutzt, um mögliche Destabilisationsfaktoren zu analysieren, die bei anderen Hangrutschen im Eivissa-Kanal eine Rolle gespielt haben. Die Analyse zeigt, dass eine Kombination von Faktoren eine Rolle gespielt hat und diese bestehen aus dem Vorhandensein schwacher Schichten und Veränderungen des Porendrucks durch die Migration von Flüssigkeiten und Gasen unter dem Meeresboden entlang von Verwerfungsstrukturen, die mit wiederkehrender Verwerfungstätigkeit zeitlich zusammenfallen.

Ziel dieser Arbeit ist es, das Vorkommen submariner Hangrutsche im Eivissa-Kanal anhand der integrierten Analyse geophysikalischer Daten zu untersuchen. Die Hauptmethode verwendet die Interpretation von 2D- und 3D-reflexionsseismischen Daten, um die internen Strukturen von Hangrutschen zu kartieren und Einblicke in die Entwicklungs- und Ablagerungsprozesse zu gewinnen.

Um das Verständnis der Prozesse der Entwicklung und Ablagerung submariner Hangrutsche sowie der Destabilisationsfaktoren und potenziellen Auslösemechanismen zu erweitern, bietet eine umfassende Analyse des Ana Slides einen entscheidenden Einblick in die Kontrollprozesse für Hangrutsche im Eivissa-Kanal. Diese Erkenntnisse wurden genutzt, um Destabilisationsfaktoren zu untersuchen, die das Auftreten der Ana, Joan, Nuna und Jersi slides sowie des verschütteten pre-Ana Slides, der sich unterhalb des Ana Slides befindet, kontrollierten. Auf der Grundlage der integrierten Analyse einer Vielzahl geophysikalischer Daten werden in dieser Arbeit Erkenntnisse vorgestellt, die zu einer Neubewertung der Hypothesen über die Destabilisationsfaktoren beitragen, die die östlichen Hänge des Eivissa-Kanals anfällig für Hanginstabilitäten machen. Darüber hinaus dokumentiert diese Arbeit, dass kleine submarine Hangrutsche das Potenzial haben, große Mengen an Meeresbodensediment in beträchtliche Tiefen zu deformieren, und dass das Volumen von scheinbar deformiertem Meeresbodensediment aus chaotischen, transparenten oder gestörten seismischen Fazies überschätzt wird.

Contents

Eidesstattliche Erklärung i

Summary iii

Zusammenfassung v

1 Motivation and Outline 1

1.1 Motivation . . . 1

1.2 Thesis Outline . . . 2

References . . . 6

2 Introduction 7

2.1 Submarine Landslides . . . 8

2.2 Landslide Terminology . . . 9

2.3 Studying Mass Transport Deposits (MTDs) . . . 9

2.4 Eivissa Channel Landslides . . . 10

2.5 Data, Methodology, and Processing . . . 11

2.5.1 Database . . . 11

2.5.1.1 Multi-beam Bathymetry Maps . . . 13

2.5.1.2 Sub-bottom Profiler (TOPAS) . . . 13

2.5.1.3 Reflection Seismic Data . . . 14

2.5.2 Methodology . . . 14

2.5.2.1 Seismic Interpretation and Stratigraphy . . . 15

2.5.2.2 Pre-failure Seafloor Reconstruction . . . 15

2.5.3 Additional Seismic Processing . . . 16

2.5.3.1 Re-processing Workflow . . . 19

2.6 TRISCO Project (UR 226/3-1 & GR 1024/35-1) . . . 21

2.7 Study Objectives . . . 22

References . . . 28

3 Development and Emplacement of Ana Slide, Eivissa Channel, Western Mediterranean Sea 29

Abstract . . . 30

Plain Language Summary . . . 30

3.1 Introduction . . . 31
3.2 Terminology . . . 32
3.3 Geological Background and Previous Studies . . . 33
3.4 Data and Methodology . . . 35
3.4.1 Additional Seismic Processing . . . 35
3.5 Results . . . 38
3.5.1 Morphology of Ana Slide . . . 38
3.5.2 3D seismic Interpretation . . . 39
3.5.3 Seismic units . . . 40
3.5.4 Faults and Crown-Cracks . . . 41
3.5.5 MTD Kinematic Domains . . . 43
3.6 Discussion . . . 46
3.6.1 Chronology of Ana Slide . . . 46
3.6.2 Headscarp Retrogression During the Primary and Secondary Failures . 47
3.6.3 Evolution and Emplacement of the Primary Failure . . . 48
3.6.4 Evolution and Emplacement of the Secondary Failure . . . 49
3.6.5 Structural and Morphological Controls on Landslide Emplacement . . 51
3.6.6 Causal Factors Between Fault Activity and Landsliding . . . 53
3.6.7 Identification of the Basal Shear Surfaces . . . 54
3.6.8 *In-Situ* Deformation Beneath Landslide Deposit . . . 54
3.6.9 Implications for the Development and Emplacement of Submarine Landslides . . . 56
3.6.9.1 Intact Blocks . . . 56
3.6.9.2 Deformation of Underlying Sediment . . . 56
3.6.9.3 Complex Failure . . . 56
3.6.9.4 Landslide Volumes . . . 57
3.7 Conclusions . . . 57
Acknowledgements . . . 57
Author Contributions . . . 58
Data Availability Statement . . . 58
References . . . 58
Supporting Information . . . 63

4 Assessment of Submarine Landslide Volume **81**
Abstract . . . 82
Keywords . . . 82
4.1 Introduction . . . 82
4.2 Emplacement of Ana Slide . . . 83
4.2.1 Tectonic setting of the Ana Slide area . . . 85
4.2.2 Depositional environment in the Eivissa Channel . . . 86
4.3 Data . . . 86

4.4 Methods for volume estimation of submarine landslides through pre-failure seafloor reconstructions . . . 86
4.4.1 Uncertainties of volume estimations . . . 89
4.5 Results from volume assessments of Ana Slide . . . 90
4.6 Discussion . . . 93
4.6.1 Ana Slide volume assessment . . . 93
4.6.2 Volume assessment of unconfined and confined submarine landslides . 94
4.6.3 How to determine the initially failed volume of submarine landslides? 95
4.6.4 Limitations and assumption of submarine landslide volume assessments 97
4.7 Conclusions . . . 97
Acknowledgements . . . 98
Availability of Data and Material . . . 99
Author Contribution . . . 99
References . . . 99
Supporting Information . . . 103

5 Destabilizing Factors for Submarine Landslides in the Eivissa Channel, Western Mediterranean Sea 105
Abstract . . . 106
Plain Language Summary . . . 106
Key Points . . . 106
5.1 Introduction . . . 107
5.2 Geological setting of the Eivissa Channel . . . 108
5.2.1 Gas in the Eivissa Channel . . . 110
5.2.2 Messinian evaporites . . . 110
5.2.3 Terminology, local tectonic setting, and stratigraphy . . . 111
5.2.4 Characteristics and morphology of submarine landslides in the Eivissa Channel . . . 115
5.2.5 Development and emplacement of Ana Slide . . . 115
5.2.6 Hypotheses for pre-conditioning factors and trigger mechanisms of Ana Slide . . . 116
5.3 Data and methodology . . . 118
5.3.1 Data . . . 118
5.3.2 Methodology . . . 118
5.3.2.1 Local tectonic activity . . . 119
5.3.2.2 Observations of in-situ deformation . . . 119
5.3.2.3 Age determination of landslides . . . 121
5.4 Results . . . 121
5.4.1 Geomorphometry of landslides . . . 121
5.4.2 Internal structure of landslides . . . 122
5.4.3 Reconstructing fault activity . . . 122

5.4.3.1 Ana Slide Complex . . . 122
5.4.3.2 Joan Slide . . . 123
5.4.3.3 Nuna Slide . . . 124
5.4.3.4 Jersi Slide . . . 124
5.4.4 Repeated slope failure in the Eivissa Channel . . . 128
5.4.5 Sedimentary features . . . 128
5.5 Discussion . . . 128
5.5.1 Sedimentation history . . . 129
5.5.2 Inherent changes in the sediment's physical properties . . . 131
5.5.3 Local external factors . . . 132
5.5.4 Far-field external factors . . . 133
5.6 Conclusions . . . 134
Acknowledgements . . . 134
Author Contribution . . . 135
Data Availability Statement . . . 135
References . . . 135
Supporting Information . . . 141

6 Conclusions and Outlook **143**
6.1 Conclusions . . . 143
6.2 Implications . . . 145
6.3 Outlook . . . 146
References . . . 148

List of Figures **149**

List of Tables **151**

Acknowledgements **153**

Curriculum Vitae **155**

List of Publications **157**

Appendix **159**
References . . . 168

1 Motivation and Outline

1.1 Motivation

Submarine landslides can damage and destroy offshore infrastructure and generate devastating tsunamis (e.g., Varnes, 1978; Farrell, 1984; Prior et al., 1984; Bondevik et al., 2005; Haugen et al., 2005; Løvholt et al., 2017). The historical record of such events is incomplete, but mass transport deposits (MTDs) have been identified to reach volumes of up to several thousands of cubic kilometres have been observed from the Mediterranean Sea (e.g., Frey-Martinez et al., 2005; Frey-Martinez et al., 2006; Moscardelli and Wood, 2015), offshore Norway (e.g., Kvalstad et al., 2005a; Kvalstad et al., 2005b; Haflidason et al., 2005), and presumably offshore East Africa (e.g., Dingle, 1977). These submarine landslides could have generated devastating tsunamis. It remains unclear how different processes and failure mechanisms affect the tsunamigenic potential of submarine landslides, yet the most important factors are the landslide mechanism and the volume of mobilised material (e.g., Harbitz et al., 2014).

Several pre-conditioning factors can decrease slope stability. Irrespective of geological setting and depositional environment major pre-conditioning factors have been identified to be linked to the presence of weak layers (Locat et al., 2014; Gatter et al., 2021; Wu et al., 2023). These layers consist of material with distinct geo-mechanical properties or weaker or stronger materials such as contourites (e.g., Kvalstad et al., 2005b), diatom oozes (Urlaub et al., 2018), foraminifera-enriched intervals (Sawyer and Hodelka, 2016), or of altered volcanic deposits (Miramontes et al., 2018). These can act as detachment surfaces or develop into basal shear surfaces resulting from the slope failure itself, be deposited, or be influenced by successive burial and consolidation. Furthermore, the presence of shallow gas within the sub-surface (e.g., Sultan et al., 2004b; Lafuerza et al., 2012) or gas hydrate dissociation potentially affected by climatic variability were proposed to be pre-conditioning factors for submarine slope failures (e.g., Elger et al., 2018).

A trigger mechanism acts as an external primer for slope instability and will ultimately cause slope failures (Sultan et al., 2004a). According to Lee et al. (2002), the most common trigger mechanisms for submarine landslides are seismic loading, rapid sediment accumulation and under-consolidation, gas hydrate dissociation, and glacial loading. Some of these can simultaneously act as pre-conditioning factors for instance over-steepening and climatic variability

that may control overpressure generation within the seafloor. To better understand the interaction between these pre-conditioning factors and trigger mechanisms it is thus critical to first constrain local geological conditions to make predictions about slope stability and future events.

The assessment of pre-conditioning factors and trigger mechanisms and their distinction can provide critical information about potential future slope failures. For a given study area, previously identified pre-conditioning factors may act as trigger mechanisms and vice versa, as the physiographic setting, geological conditions, sedimentary environments, and the lithology of slope sediments varies temporally and spatially. It is thus vital to first develop slope failure models for processes and mechanisms for a given landslide to assess potential pre-conditioning factors over a larger area. For a given landslide, local conditions that lead to inherently unstable slopes are more important to the understanding and prediction of future events than the ultimate trigger mechanism(s). For instance, the lithology of slope sediment, local seafloor morphology, and the presence of weak layers have a significant impact on the potential for a slope failure to develop into a large slope failure or to frontally emerge and generate a turbidity current and erode seafloor sediment.

Ana Slide, located in the western Mediterranean Sea between the Iberian Peninsula and the Eivissa Islands of Ibiza and Formentera, provides a natural laboratory for the analysis of local pre-conditioning and trigger mechanisms. From an extensive dataset comprised of multibeam echosounder maps, sediment echosounder profiles, side-scan sonar imagery, 2D and 3D reflection seismic data, in situ gravity core samples and geotechnical cone-penetration tests with pore pressure measurements (CPTu), development and emplacement processes of Ana, Joan, Nuna, and Jersi slides located on the eastern slopes of the Eivissa Channel, western Mediterranean Sea were investigated. The findings are relevant for the study of future events and to re-evaluate the interaction between several pre-conditioning factors and trigger mechanisms. Further, knowledge about development and emplacement processes from small submarine landslides could be extrapolated to far bigger ones that are potentially governed by similar pre-conditioning factors and trigger mechanisms.

1.2 Thesis Outline

This thesis is comprised of six chapters. Chapter 1 describes the motivation behind this thesis. Chapter 2 introduces submarine landslides and provides an overview of geophysical data used to address the objectives of this thesis. Chapters 3, 4, and 5 respectively contain published, re-submitted, and submitted manuscripts that represent the scientific output. Chapter 6 provides conclusions and future perspectives.

Chapter 3 presents a detailed analysis of Ana Slide, Eivissa Channel, western Mediterranean Sea. It documents the development and emplacement processes from the comprehensive coverage of multibeam echosounder maps and 3D reflection seismic data and re-processed

2D reflection seismic profiles. Ana Slide developed during two events: the primary and secondary stages which are separated by a significant time lag of around 240 ka. While the source area was evacuated in a frontally emergent manner the accumulated landslide material inside the sink area was able to deform shallow strata in situ to a significant depth beneath the pre-failure seafloor. Beneath the sink area, a local fault system affected the seafloor morphology before the failures of Ana Slide. For the analysis of Ana Slide the existing 3D reflection seismic data were re-processed because receiver-ghost artefacts were identified throughout the 3D cube. Chapter 3 is written in American English and the notation is not changed for this thesis.

Chapter 3 is published as:

Sager, T. F., Urlaub, M., Kaminski, P., Lastras, G., Canals, M., Papenberg, C., Berndt, C. (2022). *Development and Emplacement of Ana Slide, Eivissa Channel, Western Mediterranean Sea. Geochemistry, Geophysics, Geosystems (G^3)*, `https://doi.org/10.1029/2022GC010469`

Author contributions: *TFS, MU, and CB designed the study. TFS discussed all results and interpretations with all co-authors. TFS, MU, and CB wrote the original draft and TFS, MU, PK, GL, MC, and CB reviewed and edited the paper. MU and CB acquired funding. TFS produced Figures 1 – 10 and performed all formal analyses and investigations. All authors reviewed the manuscript.*

Chapter 4 presents a volume assessment of Ana Slide, Eivissa Channel, western Mediterranean Sea. This study estimates the amount of evacuated and accumulated landslide material from the source and inside the sink area from several approaches for pre-failure seafloor reconstruction. This article proposes a new nomenclature for volumes of landslide material and slope sediment either affected by or involved in slope failure and highlights pitfalls for submarine landslide volume assessments. Furthermore, it presents a workflow for frontally confined and unconfined landslides based on available geophysical data. Chapter 4 is written in American English and the notation is not changed for this thesis.

This manuscript was previously submitted to Geo-Marine Letters (GML) and rejected for publication with major comments by an anonymous reviewer and Dave Tappin of BGS (British Geological Survey). Consequently, the manuscript is completely rewritten following the comments.

Chapter 4 is re-submitted as:

Sager, T. F., Urlaub, M., Berndt, C.: *Assessment of Submarine Landslide Volume* to GML.

Author contributions: *Conceptualisation: TFS, MU, CB; Methodology: TFS; Formal analysis and investigation: TFS; Writing original draft preparation: TFS; Writing - review and editing: TFS, MU, CB; Funding acquisition: MU, CB; Resources: CB; Supervision: MU, CB. TFS produced Figures 1 – 4. All authors reviewed the manuscript.*

Chapter 5 investigates pre-conditioning factors and trigger mechanisms that destabilised slopes in the Eivissa Channel. Probable destabilising factors at play for the Ana, (pre-Ana), Joan, Nuna, and Jersi slides are discussed using high-resolution multibeam echosounder maps, sediment echosounder profiles, and 2D and 3D reflection seismic data. The analysis shows that all submarine landslides in the Eivissa Channel are strikingly similar and were controlled by identical pre-conditioning factors related to shallow vertical and lateral fluid and gas migration and the presence of a weak layer. These pre-conditioning factors were ultimately unable to trigger landslides in the Eivissa Channel and an external trigger mechanism such as an earthquake was necessary to cause slope failure. Chapter 5 is written in American English and the notation is not changed for this thesis.

Chapter 5 is submitted to G^3 as:

Sager, T. F., Urlaub, M., Kaminski, P., Lastras, G., Canals, M., Papenberg, C., Berndt, C. (2023). *Destabilizing Factors for Submarine Landslides in the Eivissa Channel, Western Mediterranean Sea.*

Author contributions: *Conceptualisation: TFS, MU, CB; Methodology: TFS, MU, CB; Formal analysis and investigation: TFS; Writing original draft: TFS, MU, CB; Writing - review and editing: TFS, MU, PK, GL, MC, CB; Visualisation: TFS has produced Figures 1 -– 12; Funding acquisition: MU, CB; Data curation: GL, MC, CB; Project administration: MU, CB. All authors reviewed the manuscript.*

References

Bondevik, S., F. Løvholt, C. Harbitz, J. Mangerud, A. Dawson, and J. Inge Svendsen (2005). The Storegga Slide Tsunami – Comparing Field Observations with Numerical Simulations. In: *Marine and Petroleum Geology* 1-2, pp. 195–208. DOI: 10.1016/j.marpetgeo.2004.10.003.

Dingle, R. V. (1977). The Anatomy of a Large Submarine Slump on a Sheared Continental Margin (SE Africa). In: *Journal of the Geological Society* 134.3, pp. 293–310. DOI: 10.1144/gsjgs.134.3.0293.

Elger, J., C. Berndt, L. Rüpke, S. Krastel, F. Gross, and W. H. Geissler (2018). Submarine Slope Failures Due to Pipe Structure Formation. In: *Nature Communications* 9.1, p. 715. DOI: 10.1038/s41467-018-03176-1.

Farrell, S. (1984). A Dislocation Model Applied to Slump Structures, Ainsa Basin, South Central Pyrenees. In: *Journal of Structural Geology* 6, pp. 727–736. DOI: 10.1016/0191-8141(84)90012-9.

Frey-Martinez, J., J. Cartwright, and B. Hall (2005). 3D Seismic Interpretation of Slump Complexes: Examples from the Continental Margin of Israel. In: *Basin Research* 1, pp. 83–108. DOI: 10.1111/j.1365-2117.2005.00255.x.

Frey-Martinez, J., J. Cartwright, and D. James (2006). Frontally Confined versus Frontally Emergent Submarine Landslides: A 3D Seismic Characterisation. In: *Marine and Petroleum Geology* 5, pp. 585–604. DOI: 10.1016/j.marpetgeo.2006.04.002.

Gatter, R., M. Clare, J. Kuhlmann, and K. Huhn (2021). Characterisation of Weak Layers, Physical Controls on their Global Distribution and their Role in Submarine Landslide Formation. In: *Earth-Science Reviews* 223, p. 103845. DOI: 10.1016/j.earscirev.2021.103845.

Haflidason, H., R. Lien, H. P. Sejrup, C. F. Forsberg, and P. Bryn (2005). The Dating and Morphometry of the Storegga Slide. In: *Marine and Petroleum Geology* 1-2, pp. 123–136. DOI: doi.org/10.1016/j.marpetgeo.2004.10.008.

Harbitz, C. B., F. Løvholt, and H. Bungum (2014). Submarine Landslide Tsunamis: How Extreme and How Likely? In: *Natural Hazards* 3, pp. 1341–1374. DOI: 10.1007/s11069-013-0681-3.

Haugen, K. B., F. Løvholt, and C. B. Harbitz (2005). Fundamental Mechanisms for Tsunami Generation by Submarine Mass Flows in Idealised Geometries. In: *Marine and Petroleum Geology* 1-2, pp. 209–217. DOI: 10.1016/j.marpetgeo.2004.10.016.

Kvalstad, T. J., L. Andresen, C. F. Forsberg, K. Berg, P. Bryn, and M. Wangen (2005a). The Storegga Slide: Evaluation of Triggering Sources and Slide Mechanics. In: *Marine and Petroleum Geology* 22.1-2, pp. 245–256. DOI: 10.1016/B978-0-08-044694-3.50025-1.

Kvalstad, T. J., F. Nadim, A. M. Kaynia, K. H. Mokkelbost, and P. Bryn (2005b). Soil Conditions and Slope Stability in the Ormen Lange Area. In: *Marine and Petroleum Geology* 1-2, pp. 299–310. DOI: 10.1016/j.marpetgeo.2004.10.021.

Lafuerza, S., N. Sultan, M. Canals, G. Lastras, A. Cattaneo, J. Frigola, S. Costa, and C. Berndt (2012). Failure Mechanisms of Ana Slide from Geotechnical Evidence, Eivissa Channel, Western Mediterranean Sea. In: *Marine Geology*, pp. 1–21. DOI: 10.1016/j.margeo.2012.02.010.

Lee, S. E., P. J. Talling, G. G. Ernst, and A. J. Hogg (2002). Occurrence and Origin of Submarine Plunge Pools at the Base of the US Continental Slope. In: *Marine Geology* 185.3-4, pp. 363–377. DOI: 10.1016/S0025-3227(01)00298-5.

Locat, J., S. Leroueil, A. Locat, and H. Lee (2014). "Weak layers: Their Definition and Classification from a Geotechnical Perspective". In: *Submarine mass movements and their consequences: 6th international symposium*. Springer, pp. 3–12. DOI: 10.1007/978-3-319-00972-8_1.

Løvholt, F., S. Bondevik, J. S. Laberg, J. Kim, and N. Boylan (2017). Some Giant Submarine Landslides Do Not Produce Large Tsunamis: Giant Landslide Tsunamis. In: *Geophysical Research Letters* 16, pp. 8463–8472. DOI: 10.1002/2017GL074062.

Miramontes, E., N. Sultan, S. Garziglia, G. Jouet, E. Pelleter, and A. Cattaneo (2018). Altered Volcanic Deposits as Basal Failure Surfaces of Submarine Landslides. In: *Geology* 46.7, pp. 663–666. DOI: 10.1130/G40268.1.

Moscardelli, L. and L. Wood (2015). Morphometry of Mass-Transport Deposits as a Predictive Tool. In: *Geological Society of America Bulletin*, B31221.1. DOI: 10.1130/B31221.1.

Prior, D. B., B. D. Bornhold, and M. W. Johns (1984). Depositional Characteristics of a Submarine Debris Flow. In: *The Journal of Geology* 6, pp. 707–727. DOI: 10.1086/628907.

Sawyer, D. E. and B. Hodelka (2016). "Tiny Fossils, Big Impact: The Role of Foraminifera-Enriched Condensed Section in Arresting the Movement of a Large Retrogressive Submarine Landslide in the Gulf of Mexico". In: *Submarine Mass Movements and their Consequences: 7th International Symposium*. Springer, pp. 479–486. DOI: 10.1007/978-3-319-20979-1_48.

Sultan, N., P. Cochonat, M. Canals, A. Cattaneo, B. Dennielou, H. Haflidason, J. Laberg, D. Long, J. Mienert, F. Trincardi, R. Urgeles, T. Vorren, and C. Wilson (2004a). Triggering Mechanisms of Slope Instability Processes and Sediment Failures on Continental Margins: A Geotechnical Approach. In: *Marine Geology* 213.1-4, pp. 291–321. DOI: 10.1016/j.margeo.2004.10.011.

Sultan, N., P. Cochonat, J.-P. Foucher, and J. Mienert (2004b). Effect of Gas Hydrates Melting on Seafloor Slope Instability. In: *Marine Geology* 213.1-4, pp. 379–401. DOI: 10.1016/j.margeo.2004.10.015.

Urlaub, M., J. Geersen, S. Krastel, and T. Schwenk (2018). Diatom Ooze: Crucial for the Generation of Submarine Mega-Slides? In: *Geology* 4, pp. 331–334. DOI: 10.1130/G39892.1.

Varnes, D. J. (1978). Slope Movement Types and Processes. In: *Special Report*, pp. 11–33.

Wu, N., C. A.-L. Jackson, M. A. Clare, D. M. Hodgson, H. D. Nugraha, M. J. Steventon, and G. Zhong (2023). Diagenetic Priming of Submarine Landslides in Ooze-Rich Substrates. In: *Geology* 51.1, pp. 85–90. DOI: 10.1130/G50458.1.

2 Introduction

Submarine landslides occur on continental margins and around ocean islands. They can generate devastating tsunamis with the potential to inundate coastal areas and destroy offshore infrastructure. With the expanding usage of the seafloor for offshore hydrocarbon platforms and exploration, seafloor telecommunication cables, as well as offshore wind farm constructions that go into increasingly deeper waters, it is critical to understand processes that control submarine slope failures and reshape seafloor morphology.

Large buried submarine mass-transport deposits (MTDs) have been described from many areas such as offshore Bahamas (Principaud et al., 2015), offshore Shetland (e.g., Wilson et al., 2004), offshore north-western Australia (e.g., Nugraha et al., 2022), Ulleung Basin, South Korea (e.g., Riedel et al., 2012; Sun et al., 2018), Gulf of Mexico (e.g., Dugan, 2012), and Antarctica (Imbo et al., 2003; Canals et al., 2016). These diverse settings demonstrate that submarine landslides can occur on inclined slopes with a wide range of depositional environments. Submarine landslides can reach sizes of up to several hundreds of kilometres in length such as the Storegga Slide, in western Norway (e.g., Haflidason et al., 2004; Moscardelli and Wood, 2015), MTDs along the South American margin (e.g., Alves and Cartwright, 2009; Jackson, 2011; Steventon et al., 2019), and the Sahara and Cape Blanc slides, western Africa (e.g., Krastel et al., 2019; Tang et al., 2022). Remarkably, the largest submarine landslides imaged occurred on slopes less than 2° that are characterised by relatively low accumulation rates ($\sim$ 0.15 m/ka) (Urlaub et al., 2012; Urlaub et al., 2015).

Studies agree that earthquake-induced peak ground accelerations (PGAs) have triggered many submarine slope failures (e.g., Lastras et al., 2004; Bryn et al., 2005b; Lackey et al., 2018). This mechanism acts as the ultimate trigger but slopes were previously preconditioned by a plethora of destabilising factors. One of the most common destabilising factors is the presence of weak layers facilitating failure along a stratigraphic plane (e.g., Lastras et al., 2004; Locat et al., 2014; Miramontes et al., 2018; Gatter et al., 2021). The deposition of these weak layers is controlled by the prevailing depositional environment with sedimentation of materials with distinct geo-mechanical properties such as coarser material interbedded by finer materials. This has been observed for the Storegga Slide where intervals of glacially and inter-glacially derived sediments appear to generate regional weak layers (e.g., Haflidason et al., 2004; Lindberg et al., 2004). Other destabilising factors include slope over-steepening from tectonic faulting, differential compaction, toe and canyon erosion, and contourite deposition (e.g., Shan et al., 2022). Furthermore, in situ changes of the weak layer from the generation of overpressure, disassociation of gas hydrates, and the presence

of sub-seafloor gas or injected gas can subsequently affect slope stability (e.g., Sultan et al., 2004; Elger et al., 2018; Kaminski et al., 2021). On a larger scale, sea level rise and fall related to climatic variability can affect the pressure regimes in the sub-seafloor (e.g., Talling et al., 2014). The response of the sub-seafloor pressure regime is delayed compared to relatively fast increases and decreases of the hydrostatic pressure during glacial cycles on the time scale of some hundred thousand years from sea level rise to fall. Further, destabilising factors themselves are more important for the development and emplacement processes of submarine slope failures than the trigger mechanism, although the interplay of these is poorly constrained. It remains unclear how the pre-conditioning and triggering of slope failures relate to the tsunamigenic potential of submarine landslides and how this relates to the amount of initially failed landslide material and the landslide mechanism (e.g., Harbitz et al., 2014).

2.1 Submarine Landslides

Submarine landslides mobilise slope material from steep and shallow to deeper continental areas and on ocean basin floors. Landslides or more accurately their remnants called MTDs are sub-divided into two broad categories; those derived from open slope failures, for instance, Storegga Slide (e.g., Haflidason et al., 2004; Bryn et al., 2005b; Bryn et al., 2005a; Kvalstad et al., 2005) or the Israel Slump Complex (e.g., Frey-Martinez et al., 2005; Frey-Martinez et al., 2006) and those derived from volcanic flank collapses, for instance, Fogo Island in the Cape Verdes, offshore West Africa (Barrett et al., 2020) or offshore Sakar, Papua New Guinea (Kühn et al., 2021). Compared to terrestrial landslides, submarine landslides are orders of magnitude larger and can reach runout lengths of several hundred kilometres as mobilised slope material may readily mix with seawater creating suspension and turbidity currents. Studies have shown that these can erode the seafloor and destroy seafloor infrastructure (e.g., Clarke et al., 1990). The 1929 Grand Banks is a prime example, with a movement velocity of ca. $15 - 30$ m/s derived from submarine telecommunication cable breaks (Heezen et al., 1954; Hasegawa and Kanamori, 1987; Løvholt et al., 2019). Because modern communication is critically reliant on submarine telecommunication cables there is a need to better understand how these turbidity currents develop, how they are generated, and how these interact and erode seafloor sediments. Furthermore, knowledge gained from the development and emplacement processes of submarine landslides could be used to assess and predict future landslides and turbidity current events.

Submarine slope failures mobilise material from their original position of deposition such as river mouths and deltas to deep marine settings. Landslide material that reaches these deep marine settings is distinct from background sediments and usually more coarse-grained. MTD intervals are thus characterised by higher permeability and porosity materials that could act as reservoirs for freshened groundwater or hydrocarbons.

2.2 Landslide Terminology

The terminology of submarine landslides generally differentiates between the types of slope failure that are characterised by the internal architecture, type of movement, the type of material involved in slope failure and others. The literature describes different types of slopes failures such as creeps, debris and rock falls, avalanches, slides, slumps, debris flows, and turbidity currents controlled for instance by sediment properties of landslide material and landslide mechanisms (e.g., Hampton et al., 1996; Masson et al., 2002; Moscardelli and Wood, 2008), yet no unified terminology exist mainly because submarine landslides are complex geological structures. Furthermore, landslides are oftentimes poorly imaged and their potentially large-scale and complex development and emplacement history is rarely fully understood.

In this thesis, the term 'failure' is used to characterise the active process of 'landslide material' mobilisation and translation between the upslope evacuational 'source' and downslope accumulational 'sink' areas. Material that was mobilised between the source and sink areas is referred to as the mass-transport deposit. Notably, this material does not refer to the 'affected slope sediment' deformed in situ beneath the seafloor. This terminology applies to Ana Slide located in the Eivissa Channel, western Mediterranean Sea. The boundary of a landslide is called the landslide 'scar', while the upper extent is called the 'headscarp' which marks the location of the latest stage of retrogression. Throughout this thesis, the term 'source' area is used to describe the evacuation area also called the headwall domain (e.g., Bull et al., 2009) because it provides kinematic information, while the 'sink' area describes the accumulation area also called toe domain (e.g., Bull et al., 2009). In addition, with the detailed analysis of Ana Slide, landslide material that was mobilised, material that was deformed in situ, and slope sediment that was unaffected by the landslide are differentiated.

2.3 Studying Mass Transport Deposits (MTDs)

Submarine landslides can be imaged with geophysical data and investigated from in situ samples (e.g., Imbo et al., 2003; Haflidason et al., 2004; Lastras et al., 2004; Wilson et al., 2004; Cartwright and Huuse, 2005; Frey-Martinez et al., 2005; Frey-Martinez et al., 2006; Gee et al., 2006; Bull et al., 2009; Lackey et al., 2018). A slope failure is an instantaneous geological event and its remains will be buried by subsequent sedimentation. The surface morphology of submarine landslides will thus be successively buried making bathymetric surveys to study them viable only for relatively recent failures. In addition, the penetration depth of sediment echosounder profiles is generally limited to around 30 to 50 m (e.g., Lykousis et al., 2002; Lastras et al., 2004). Properties of the seafloor and sub-seafloor sediments are related to the penetration depth because the high-frequency signals used by this method quickly attenuate with depth beneath the seafloor. As an alternative, reflection seismic data have a larger penetration depth though at the cost of sub-seafloor resolution.

Thus, there is a trade-off between the imaging of deeply buried, potentially older and larger, submarine landslides and those that occurred in relatively recent times. Furthermore, gravity cores of up to 30 m can be obtained, but these have rarely penetrated complete landslide sequences (e.g., Lafuerza et al., 2012; Sammartini et al., 2021). Also, it remains unclear how the degree of deformation observed from the disrupted, chaotic, or transparent seismic facies relates to microscopic faults and fractures observed from gravity cores as the seismic signals get dissipated within MTD intervals (e.g., Ford et al., 2021). It is thus vital to integrate various data types such as multi-beam bathymetry maps, side-scan sonar imagery, sediment echosounder profiles, 2D and preferably 3D reflection seismic data, in situ samples such as those obtained by gravity cores, and geotechnical cone-penetration tests with pore pressure measurements (CPTu) to better understand pre-conditioning factors and trigger mechanisms that control slope failures.

Geophysical reflection seismic surveying is the most widely used method to image the offshore sub-seafloor (e.g., Cartwright and Huuse, 2005; Bull et al., 2009). This is mainly because seismic methods are widely applicable, processing software and techniques are readily available and constantly improving, legacy data can be included, and data can be compiled to cover whole basins for example the Mediterranean Sea (e.g., Driussi et al., 2015; Raad, 2022; Ochoa et al., 2015). Furthermore, this method is non-destructive and can be deployed from relatively small vessels and is relatively cheap. Reflection seismic data show impedance contrasts between stratigraphic layers and thus this method provides an indirect image of the sub-seafloor. These images are used in seismic interpretation which in itself is a highly interpretative and ambiguous task and biased towards the worker's experience (Sheriff and Geldart, 1995).

Unfortunately, in recent decades local governments have introduced many restrictions to seismic surveying to decrease the anthropogenic stress on marine mammals through the reduction of marine noise (e.g., Duarte et al., 2021). The collection of new seismic data thus becomes increasingly difficult. In some cases, the acquisition of new data is not possible and might instead necessitate the re-processing of legacy seismic data with new processing techniques (e.g., Raad, 2022). On the contrary, limitations of seismic surveying in shallow coastal areas pushed forward the development of new methods for seismic acquisition and processing such as using shallow sparker-based 3D reflection seismic surveying or creating 3D cubes from closely spaced sediment echosounder profiles (e.g., Müller et al., 2002; Müller et al., 2013; Gutowski et al., 2015; Shin et al., 2022).

2.4 Eivissa Channel Landslides

Four recent and shallowly buried submarine landslides are identified in water depths of 610 to 905 m on the eastern slopes of the Eivissa Channel located in the western Mediterranean Sea between the Iberian Peninsula and the islands of Eivissa (Ibiza) and Formentera (Lastras

et al., 2004; Lastras et al., 2006; Berndt et al., 2012) (Table 2.1 and Figure 2.1). From South to North, these are called Ana, Joan, Nuna, and Jersi slides with a distance of 20 km from each other (Figure 2.2). A buried landslide, the pre-Ana Slide, is located approximately 5 to 30 m beneath Ana Slide (Berndt et al., 2012) and is presented in Chapter 3. A brief list of geomorphometric parameters of these MTDs is provided in Table 2.1 which shows the many similarities between Ana, Joan, Nuna and Jersi slides including pre-Ana Slide using parameters proposed by Clare et al. (2019). A table with a complete list of geomorphometric parameters is presented in the appendix of this thesis (Table 6.2).

Slide Name	Latitude	Longitude	Water depth (m)	Height drop (m)	Slope angle (°)	Scarp height (m)	Maximum deposit thickness (m)	Area (km^2)	Volume (km^3)
pre-Ana	38°38'30"	0°48'20"	buried	buried	buried	20 m	48.75 m	8.2 km^2	$\ll$ 0.040 km^3
Ana	38°38'25"	0°48'50"	635 - 790	155 m	< 1 - 2.2°	30 m	39 m	4.8 km^2	0.040 km^3
Joan	38°41'00"	0°47'25"	610 - 870	260 m	< 1 - 1.1°	20 m	52.5 m	23.6 km^2	$\ll$ 0.40 km^3
Nuna	38°43'20"	0°47'35"	705 - 855	150 m	< 1 - 1.5°	50 m	45 m	10.2 km^2	$\ll$ 0.31 km^3
Jersi	38°47'20"	0°47'10"	750 - 905	155 m	< 1 - 2°	45 m	41.25 m	8.1 km^2	$\ll$ 0.19 km^3

Table 2.1: Geomorphometric table of pre-Ana, Ana, Joan, Nuna, and Jersi slides in the Eivissa Channel. Maximum deposit thickness is calculated from depth-converted sediment echosounder profiles using a seismic velocity of 1500 m/s. Parameters were compiled from Lastras et al. (2004), Lastras et al. (2006), and Lastras et al. (2007).

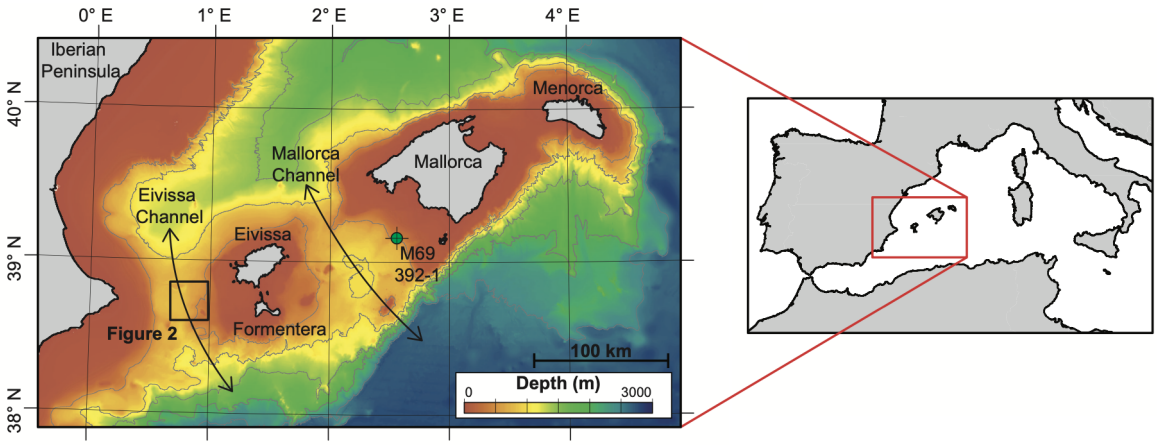

Figure 2.1: Location of the study area of the Eivissa Channel located in the western Mediterranean Sea between the Iberian Peninsula and the islands of Eivissa (Ibiza) and Formentera. This figure is taken from Chapter 4.

2.5 Data, Methodology, and Processing

2.5.1 Database

The database of this thesis comprises multi-beam bathymetry maps, sub-bottom profiler (TOPAS), and various 2D and 3D reflection seismic data (Figure 2.2). Additional data are available such as side-scan sonar imagery, geotechnical cone-penetration tests with pore pressure measurements (CPTu), sediment sampling (gravity core and multi-core), and video

transects, but these were not deemed relevant to the objectives of this thesis (e.g., G. Lastras, *personal communication*, December 16, 2022) (Table 6.1).

Because reflection seismic data presented in this thesis were acquired using different source and receiver set-ups, the term 'airgun' reflection seismic profile describes 2D seismic profiles acquired during the HERMESIONE cruise (HERMESIONE, 2009) (Table 6.1). The reflection seismic data acquired during the CD178 cruise are referred to as the '3D' and 're-processed 2D' reflection seismic data and profiles, respectively. Additional information on the re-processing of the 3D data and their raw files is provided in Chapter 2.5.3.

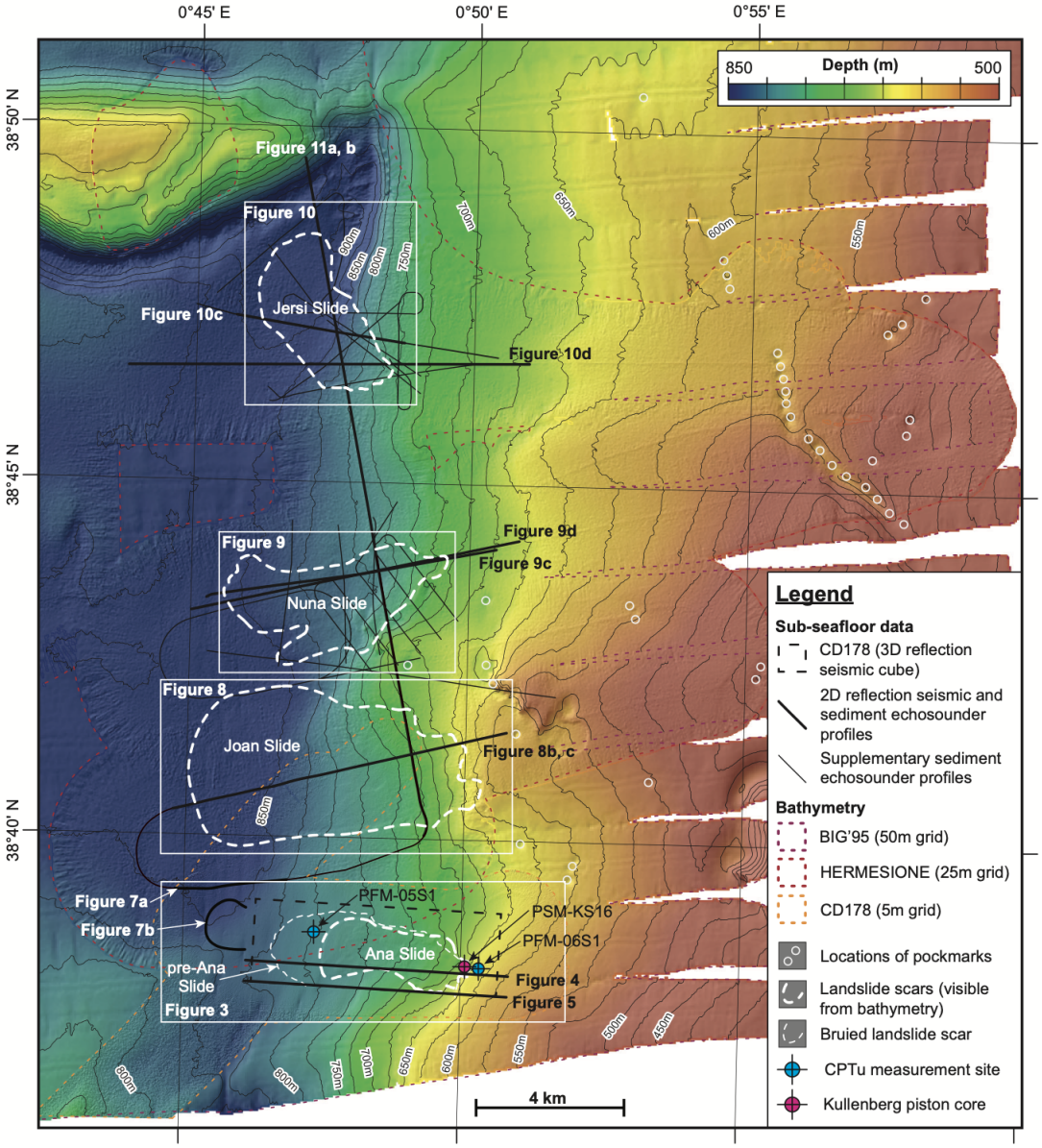

Figure 2.2: Bathymetric map of the study area located on the eastern slopes of the Eivissa Channel in the western Mediterranean Sea between the Iberian Peninsula and the islands of Eivissa (Ibiza) and Formentera (location indicated in Figure 2.1). This figure shows a regional map (BIG'95 bathymetric grid) of available bathymetric maps, sub-bottom profiler, and 2D and 3D reflection seismic data (Berndt et al., 2012) and Chapter 3. This figure is taken from Chapter 5.

2.5.1.1 Multi-beam Bathymetry Maps

In 1995, the Eivissa Channel was mapped for the first time in the framework of the BIG'95 cruise using the BIO (Buque de Investigación Oceanográfica) Hespérides. In 2002, the Jersi, Nuna, Joan, and Ana slides were revisited with the same vessel during the MARINADA cruise during which multi-beam bathymetric maps were collected. These maps were merged into a higher-resolution bathymetric grid that is used as a regional background grid for other bathymetric surveys of the Ana, Joan, Nuna, and Jersi slides (Table 6.1 and Figure 2.2).

During the CD178 cruise in 2006 with the RRS (Royal Research Ship) Charles Darwin, a very-high-resolution bathymetric grid (5 x 5 m) was acquired of Ana Slide. These data were acquired in parallel with complementing seismic surveying covering Ana Slide and the surrounding seafloor up to one kilometre towards the North and South (Figure 2.2). This resulted in a seafloor map of excellent quality that is used throughout this thesis and previously used by Berndt et al. (2012), Lafuerza et al. (2012), and Panieri et al. (2012) and presented in Chapter 3.

In 2007, during the EUROLEON cruise (BIO Hespérides), a high-resolution (20 x 20 m) bathymetric grid was acquired during sub-bottom profiler acquisition, partially covering all landslides (Figure 2.2). Additionally, a seamount located around 8 km upslope of Ana Slide has been covered by the AUV-mounted EM3000 multi-beam system (2 x 2 m) but this data is not considered further in this thesis.

In 2009, BIO Hespérides revisited the eastern slopes of the Eivissa Channel for the last time in the framework of the HERMESIONE cruise (HERMESIONE, 2009). During this cruise multi-corer samples, bathymetric maps, and airgun 2D reflection seismic profiles were collected. The bathymetric map has a lower resolution (25 x 25 m) with a larger swath width compared to the EUROLEON cruise which resulted in a lower processed resolution. Jersi, Nuna, and Joan Slide were completely covered (Figure 2.2).

2.5.1.2 Sub-bottom Profiler (TOPAS)

Submarine landslides in the Eivissa Channel have been imaged by numerous sub-bottom profiles (TOPAS) acquired during the MARINADA, EUROLEON, and HERMESIONE cruises (Table 6.1). TOPAS profiles acquired during the MARINADA cruise were initially presented by Lastras et al. (2004) but have also been used by Lafuerza et al. (2012). In this thesis, all available TOPAS profiles with fair quality were used that allowed the mapping of the basal shear surface (called *slip plane* by Lastras et al. (2004)) represented as the Reference reflector (Ref) in Chapters 3, 4, and 5 throughout the Eivissa Channel. Besides the reflection seismic data acquired during the CD178 and HERMESIONE cruises, these TOPAS profiles represent the only sub-surface data of submarine landslides located within the Eivissa Channel.

2.5.1.3 Reflection Seismic Data

In 2006, during cruise CD178 Ana Slide was covered by 3D reflection seismic data in its entirety (Berndt et al., 2012). At that time it was known that a previous landslide, pre-Ana Slide, is located beneath Ana Slide, yet its lateral extent was unknown and it was found to extend outside of the 3D reflection seismic data towards the South. In 2009 the Eivissa Channel was visited in the framework of the HERMESIONE cruise and additional 2D reflection seismic profiles (airgun) were acquired that image the sub-seafloor beneath the Joan, Nuna, and Jersi slides. These 2D reflection seismic data are still unpublished, but they are presented in the HERMESIONE cruise report HERMESIONE (2009) and are consequently included in Chapter 5 to show the sub-seafloor of Joan, Nuna, and Jersi slides in Figures 5.8, 5.9, and 5.10, respectively.

In 2006, a 3D reflection seismic cube was acquired of Ana Slide for academic purposes using the P-Cable system (Berndt et al., 2012). This system consists of two paravane doors that span a perpendicular cable called the P-cable in between onto which single channel streamers were attached (CD178, 2006). During this cruise, eleven 12.5 m-long single-channel Teledyne streamers were deployed with one malfunctioning (number 7) (Berndt et al., 2012). The seismic source consisted of four 40 in^3 Bolt 600B air guns spaced 0.75 m apart that were towed at an optimal depth of 1.5 m about 20 m behind the vessel. 3D reflection seismic processing included frequency filtering (35 – 350 Hz) before a 3D Stolt time migration with a migration velocity of 1500 m/s was applied. This data was used by Berndt et al. (2012) to discuss the repeated slope failure linked to the potential migration of gas and is used throughout this thesis to discuss development and emplacement processes (Chapter 3). Furthermore, this data is used for assessing submarine landslide volumes (Chapter 4) and to study destabilising factors for submarine landslides in the Eivissa Channel (Chapter 5).

During seismic acquisition, the P-Cable system passed over the study area 85 times with inlines orientated East-West (Figure 2.3). For 3D reflection seismic processing, data acquired in the turns between inlines orientated from East to West were removed, yet this data was recorded and provides sub-seafloor information outside the extent of the 3D cube.

2.5.2 Methodology

For the study area, all available sub-bottom profiler data (TOPAS), and airgun and reflection seismic data (3D and re-processed 2D profiles) were integrated, analysed, and interpreted in the seismic software IHS Kingdom® Suite 2018/2020. Although the reflection seismic data were acquired using different methods and source-receiver configurations, data were tied for all of the submarine landslides on the eastern slopes of the Eivissa Channel.

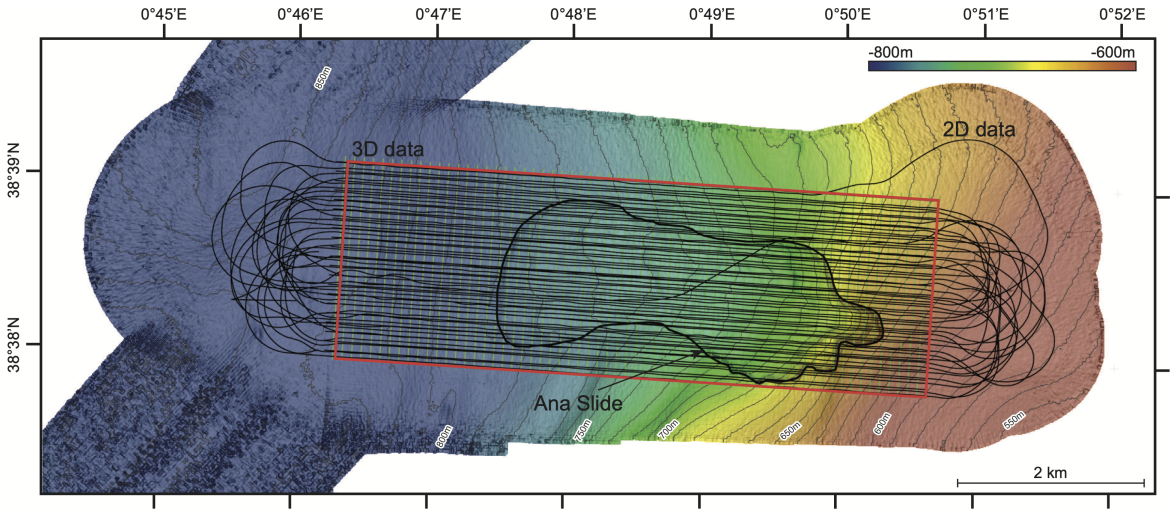

Figure 2.3: Location of reflection seismic data covering Ana Slide, Eivissa Channel, western Mediterranean Sea. Vessel tracks and turns extend outside the processed 3D data (red box). The black lines represent re-processed 2D reflection seismic profiles that extend East and West of the 3D data.

2.5.2.1 Seismic Interpretation and Stratigraphy

In seismic stratigraphy, seismic reflections are subdivided into genetically related sedimentary sequences (Kearey et al., 2002). Seismic data present impedance contrasts related to the seismic velocity and density of materials (Helbig, 1983). Reflectors in seismic profiles are picked laterally and tracked and comprise horizons that represent seismic surfaces in 3D. Their termination, lateral extent, seismic facies, and geometry provide information for instance about the depositional environment, physiography, and structural influences (e.g., Mitchum et al., 1977).

In this thesis, seismic interpretation of TOPAS profiles, 3D, airgun, and re-processed 2D reflection seismic profiles is used to map laterally extensive reflectors throughout the Eivissa Channel. Several reflectors are identified such as the seafloor (SFR), sub-reflectors R1, R2, and R3, the reference (Ref), and the top pre-Ana (tpAS) and base pre-Ana Slide (bpAS) reflectors from immediately beneath the seafloor to around 100 ms beneath the seafloor (e.g., Figure 3.3). Further information about these reflectors is provided in Chapters 3, 4, and 5.

2.5.2.2 Pre-failure Seafloor Reconstruction

The complete coverage of 3D reflection seismic data allowed the detailed reconstruction of the pre-failure seafloor before the failures of Ana Slide. This reconstruction is useful to estimate the amount of landslide material initially located inside the source area between the pre-failure and present-day seafloors. A similar approach was used by Omira et al. (2022), Webster et al. (2016), and Sun et al. (2018). In Chapter 4 the approach is adapted for Ana Slide and a volume assessment of the slide using previous hypotheses and methods is presented.

In Chapter 4 the pre-failure seafloor of Ana Slide is reconstructed assuming that the amount of mobilised landslide material evacuated from inside the source area is represented by the void space between the present-day and pre-failure seafloors (sensu Völker, 2010). In this thesis, the pre-failure seafloor before Ana Slide inside its source area is reconstructed by the 'contour-line' approach. For this approach the contour-lines before the failure are represented by contour-lines that follow the local trend throughout the source area. In Chapter 3 it is demonstrated that a local seafloor antithetic en echelon fault system modified the morphology of the seafloor inside the sink area before the failure of Ana Slide. Therefore, the contour-line approach does not realistically reconstruct the pre-failure seafloor inside the sink area. Nonetheless, the 3D reflection seismic data allows us to constrain the pre-failure seafloor morphology before the failure of Ana Slide by using the 'horizon-flattening' approach that assumes a predictable thickness of stratigraphic units. This thickness is then interpolated inside the sink area. Additional information about assumptions, limitations, results, and application of for instance the horizon-flattening approach are presented in Chapter 4.

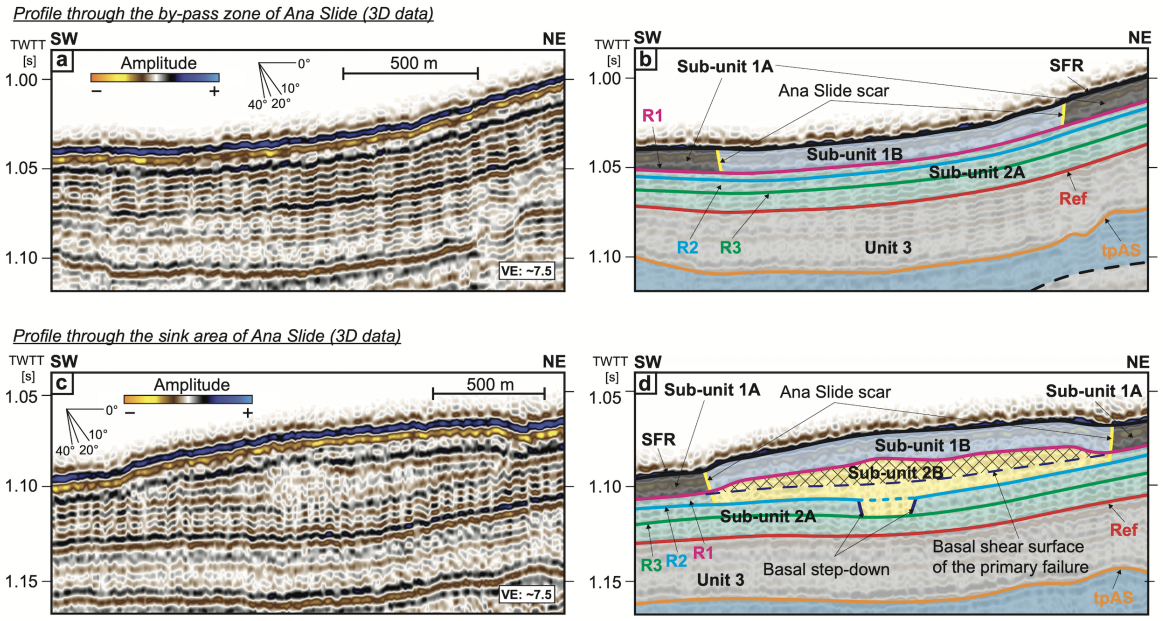

Figure 2.4: Seismic crosslines through Ana Slide extracted from the 3D data. **a)** Uninterpreted crossline profiles through the 'by-pass' zone and **c)** through the sink area of Ana Slide. **b)** and **d)** show the interpreted profiles respectively where the artefact is removed from the interpretation. This figure is taken from chapter 3 (Figure 3.7).

2.5.3 Additional Seismic Processing

During the initial analysis and interpretation of the 3D reflection seismic data, partial downward bending of reflections creating spatial incoherency were primarily observed on crosslines orientated North-South in the 3D cube (Figure 2.4). Similarly, seismic inlines orientated East-West were also affected, but the effects are less pronounced here (Figure 3.3). An example of these artefacts is presented in Figures 3.11, 3.12, and 3.13 from a crossline where

the seafloor reflector (SFR) is not continuous but has a pronounced 'garland' appearance. Deeper reflectors such as Ref are less affected by this artefact yet the effect is evident. Furthermore, isochore thickness maps between surfaces show E-W elongated artefacts (Figures 3.4, 3.8, and 5.6).

These issues were examined more closely after the initial data analysis by locating the original navigation and raw files. Initially, it was thought that the 'garland' artefacts on crosslines were the result of navigation issues introduced in the 3D reflection seismic data through processing. This hypothesis was tested by plotting the seafloor reflector and the wavelets of all streamers from individual shots (Figures 2.5 and 3.11). These wavelets in channels 3 to 4 are fully separated, those in channels $2, 5, 8$ and 12 are partially separated, and only those in channels 1 and 6 are concomitant. Contrary to the earlier belief that this separation was a result of the navigation and potentially the 3D seismic processing, the artefact was generated during seismic acquisition in 2006 using an early version of the P-Cable system.

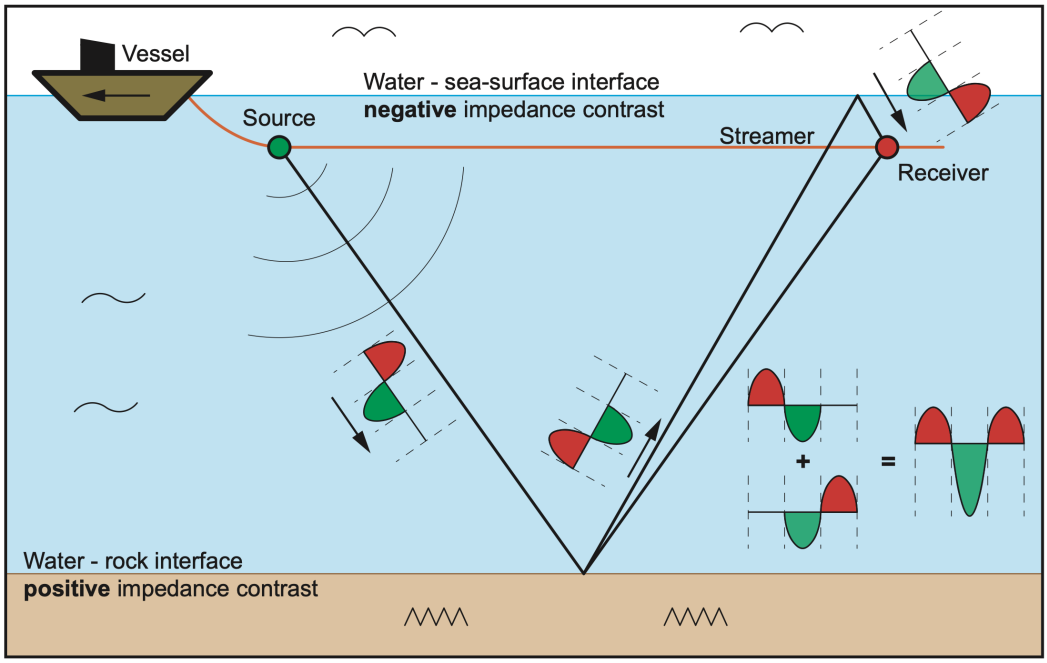

Figure 2.5: Principle sketch of receiver ghost artefact generation.

The principle of marine seismic surveying is shown in Figure 2.5. A vessel pulls a source or air gun and receivers embedded into streamers behind at shallow water depth. The air gun is triggered and creates a signal as a pressure wave that propagates as a wavelet in all directions. The 'direct wave' reaches the receiver first but it does not provide seafloor and sub-seafloor information and is consequently filtered out for this data. The 'primary' downward propagating wavelet (peak – trough) is reflected by the seafloor that has a *positive* impedance contrast and thus the reflected signal propagates upwards to the streamer as a peak – trough wavelet. This is recorded as the first arrival from the seafloor reflection on individual receivers in the streamer. The 'primary' wavelet that is reflected by the seafloor or water-rock interface propagates further upward and is reflected by the water – seasurface

interface with a *negative* impedance contrast. This reflected wavelet propagates downward to the streamer as a trough – peak wavelet. The resulting wavelet of the reflected primary wavelet and the wavelet reflector from the water – seasurface interface forms a peak – double trough – peak wavelet. This situation describes the optimal setup of marine seismic surveying, where both wavelets arrive at the receiver at the correct time delayed by a couple of milliseconds. In case the receiver is located too shallow or deep beneath the seasurface the wavelets may interfere constructively or destructively.

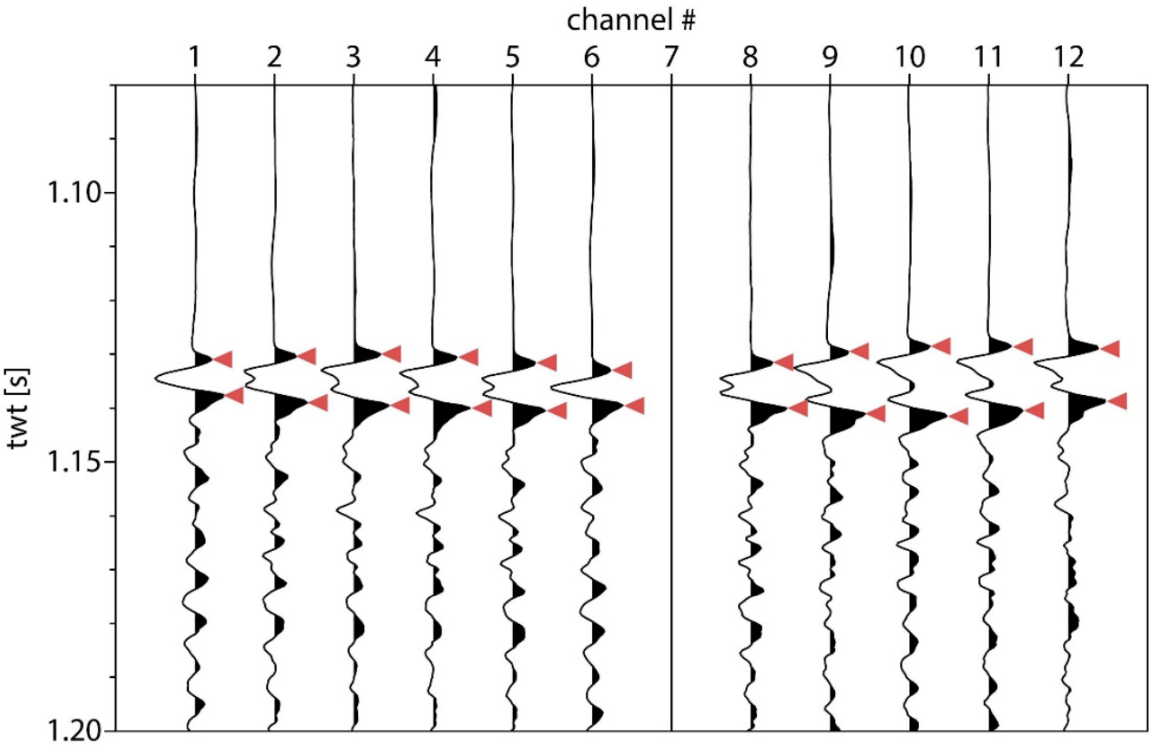

Figure 2.6: Seafloor reflection of a single shot; channels 3-4 and 9-11: heavy receiver ghost as both wavelets are fully separated, channels 2,5,8 and 12: moderate receiver ghost as both wavelets are partially separated, channels 1 and 6: 'tuned' receiver ghost as both wavelets are concomitant. Red arrows mark the automated pick pairs at the peak of both lobes to approximate the streamer depths. This figure is taken from the supplementary material of Chapter 3 (Figure 3.12).

Following Figure 2.6 (presented in the supplementary material of Chapter 3 and Figure 3.12 in this thesis) it is evident that the perpendicular cable sagged between streamers 2 and 5 and sagged even more significantly between streamers 7 and 12. Furthermore, streamers 10 and 11 show almost complete separation between the primary direct wave and the seafloor multiple. Receiver ghosts are not observed on streamers 1 and 6 likely because the depth was optimally defined as half the wavelets length. Streamer 1 was attached to the perpendicular cable next to one of the paravane doors, while streamer 6 was attached to a central buoy. Nonetheless, streamer 12 which was attached close to the other paravane door is heavily affected by the receiver ghost artefact. There could be several reasons for this such as fishnets caught in the streamer or strong currents. For instance, the receiver ghost is observed throughout the dataset and thus currents can be discarded.

3D reflection seismic data can be used to study lateral amplitude variations and to calculate seismic attributes (Chopra and Marfurt, 2005). They can highlight zones of interest and show geological features of faults, fractures, and discontinuities. The main aim of re-processing the raw data of Ana Slide was to remove and filter the receiver ghost artefact. Standard de-ghosting methods are applied in the f-k (wavenumber-frequency) domain or other spatial domains and thus need multi-trace (shot) gathers. Here, the P-Cable system used short 12.5 m single-channel streamers and none of the tested de-ghosting techniques were able to remove or filter the ghost artefacts. Instead, single-channel data from individual streamers were re-processed. These individual 2D profiles have higher resolution tuned for the shallow sub-surface compared to those from the 3D cube. A visual comparison between both data is provided in Figure 2.7. The re-processing workflow is described below following the approach presented in the supplementary material of Chapter 3.

2.5.3.1 Re-processing Workflow

This re-processing workflow is published and presented in Chapter 3 and detailed in detail in the supplementary material.

Raw data were frequency-filtered using an Ormsby-Bandpass at 18/42/250/500 Hz. Afterwards, data were de-spiked for burst-noise attenuation with a sliding Alpha Trim 11-trace mean filter in common receiver gather (trim factor 66) after which individual channels were binned onto a crooked line with a bin size of 12.5 m. Before stacking, a normal move-out (NMO) is applied with 1520 m/s below the seafloor and 1512 m/s above. This stack is migrated using the Stolt method with a constant velocity of 1520 m/s approximating the average seismic velocity in the uppermost sediments. It is worth noting that no automatic gain control is applied meaning that amplitudes of deeper reflections are not increased. Throughout this thesis, profiles presented from reflection seismic data acquired during cruise CD178 almost exclusively show re-processed 2D profiles while planview and isochore maps use the 3D cube where the ghost artefact is visible (e.g., Figures 3.4, 3.8, and 4.2).

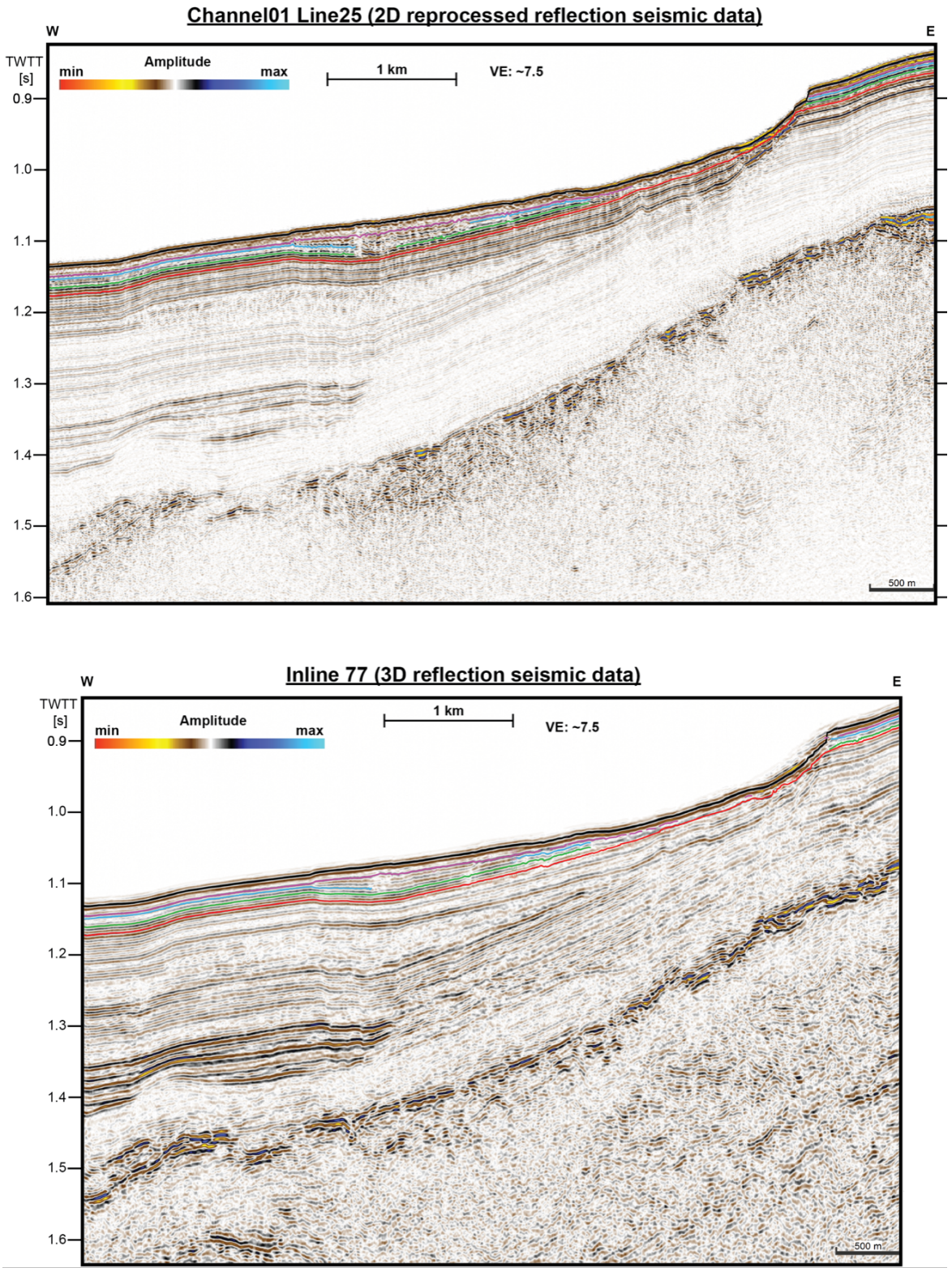

Figure 2.7: Visual comparison between reflection seismic profiles from the re-processed profiles (upper panel) and 3D data (lower panel). The re-processed data shows a clearer image of the subsurface with higher-resolution reflections compared to the bottom panel. The coloured horizons in both panels relate to the interpretation of reflectors presented but can be ignored for this part of this thesis. The figure is presented in the supplementary material of Chapter 3 (Figure 3.12).

2.6 TRISCO Project (UR 226/3-1 & GR 1024/35-1)

This thesis is the product of the Deutsche Forschungsgemeinschaft (DFG) funded TRISCO project – *Investigation of gas migration as a TRIggering mechanism for Submarine landslides on COntinental slopes*. GEOMAR Helmholtz Centre for Ocean Research Kiel, Kiel, Germany hosted the PhD student Thore F. Sager in collaboration with the Institute of Geotechnical Engineering & Construction Management, Hamburg University of Technology (TUHH) which hosted the PhD student Pauline Kaminski. Funding was acquired by Prof. Dr. Morelia Urlaub and Prof. Dr. Christian Berndt (GEOMAR) and Prof. Dr. Jürgen Grabe (TUHH). At GEOMAR the project started on the 1st of August 2019 with a cost-neutral extension for three months. Funding for the project ended on the 31st of October 2022.

The objective of this research project is to investigate the potential of shallow marine gas to cause submarine landslides. Additionally, the team aimed to investigate the interaction between different pre-conditioning factors and/or trigger mechanisms. A double-tracked approach was chosen involving geophysical data interpretation performed at GEOMAR while geotechnical measurements and new methods for geotechnical testing were performed and developed at TUHH. Further, a collaboration with the National Oceanographic Centre (NOC) in Southampton, UK was planned but this was not successful partly because of the COVID-19 pandemic, related logistical challenges and Brexit.

The work at GEOMAR involved seismic analysis of geophysical data in collaboration with project partners Dr. Galderic Lastras and Prof. Dr. Miquel Canals of the Department of Earth and Ocean Dynamics, CRG Marine Geoscience, University of Barcelona. Geophysical data of the study area located on the eastern slopes of the Eivissa Channel was provided by the project partner in Barcelona. These data comprise bathymetric maps, sub-bottom profiler data, side-scan sonar imagery, airgun, re-processed reflection seismic profiles and 3D data. The 3D reflection seismic data, that were the main focus of this thesis are property of Prof. Dr. Christian Berndt (GEOMAR). Further, the re-processing of reflection seismic data was performed at GEOMAR in collaboration with Dr. Cord Papenberg. In this thesis, the scientific output from three manuscripts is presented in Chapters 3, 4, and 5 while posters, presentations, and conference contributions are listed in Chapter 6.

The pandemic had a significant impact on work primarily affecting joint interdisciplinary collaboration. In-person meetings with the project partners in Barcelona were not possible and the cancellation of several scientific conferences negatively affected scientific exchange.

The main result of the TRISCO project is that slope stability can be affected by shallow marine gas. Nonetheless, the occurrence of marine gas alone acts exclusively as a pre-conditioning factor but never as a trigger mechanism. The analysis has shown that large earthquakes and significant PGAs ultimately trigger slope failures along the eastern slopes of the Eivissa Channel, western Mediterranean Sea. It is thus vital for submarine slope

stability analysis to integrate all conceivable destabilising factors that could lead to unstable slopes.

2.7 Study Objectives

- Integrate geophysical data from the Eivissa Channel to propose a revised model for the development of Ana Slide including emplacement, evacuation, and accumulation processes.
- Use the development model of Ana Slide to assess submarine landslide volumes from pre-failure seafloor reconstructions.
- Link knowledge from Ana Slide to landslides in the Eivissa Channel to correlate their occurrence with a re-assessment of pre-conditioning and trigger mechanisms that govern submarine slope failure.

This thesis aims to study the development of submarine slope failures and in particular how these are emplaced and what pre-conditions and ultimately triggers them. Here, geophysical data is presented such as multi-beam bathymetry maps, sub-bottom profiler data, and airgun, re-processed and 3D reflection seismic data covering Ana (pre-Ana) Slide and Joan, Nuna, and Jersi slides within the Eivissa Channel, western Mediterranean Sea.

In this thesis, I integrate geophysical data to answer the following questions:

- How did Ana Slide develop?
- Why is Ana Slide specifically located at this location?
- What processes controlled the repeated slope failure of pre-Ana and Ana slides? Are similar processes responsible for the retrogressive development of slope failures of the Joan, Nuna, and Jersi slides?
- What are the local and regional morphological and structural tectonic controls on the development and emplacement of slope failures in the Eivissa Channel?
- What is the geohazard potential of Ana Slide to generate a tsunami?
- What is the chronology of events that acted as pre-conditioning factors or trigger mechanisms for the repeated failure of the pre-Ana and Ana slides? Can this be extended to the Joan, Nuna, and Jersi slides?

References

Alves, T. M. and J. A. Cartwright (2009). Volume Balance of a Submarine Landslide in the Espírito Santo Basin, Offshore Brazil: Quantifying Seafloor Erosion, Sediment Accumulation and Depletion. In: *Earth and Planetary Science Letters* 3-4, pp. 572–580. DOI: 10.1016/j.epsl.2009.10.020.

Barrett, R., E. Lebas, R. Ramalho, I. Klaucke, S. Kutterolf, A. Klügel, K. Lindhorst, F. Gross, and S. Krastel (2020). Revisiting the Tsunamigenic Volcanic Flank Collapse of Fogo Island in the Cape Verdes, Offshore West Africa. In: *Geological Society, London, Special Publications* 1, pp. 13–26. DOI: 10.1144/SP500-2019-187.

Berndt, C., S. Costa, M. Canals, A. Camerlenghi, B. de Mol, and M. Saunders (2012). Repeated Slope Failure Linked to Fluid Migration: The Ana Submarine Landslide Complex, Eivissa Channel, Western Mediterranean Sea. In: *Earth and Planetary Science Letters*, pp. 65–74. DOI: 10.1016/j.epsl.2011.11.045.

Bryn, P., K. Berg, M. Stoker, H. Haflidason, and A. Solheim (2005a). Contourites and Their Relevance for Mass Wasting along the Mid-Norwegian Margin. In: *Marine and Petroleum Geology* 1-2, pp. 85–96. DOI: 10.1016/j.marpetgeo.2004.10.012.

Bryn, P., K. Berg, C. F. Forsberg, A. Solheim, and T. J. Kvalstad (2005b). Explaining the Storegga Slide. In: *Marine and Petroleum Geology* 22.1-2, pp. 11–19. DOI: 10.1016/j.marpetgeo.2004.12.003.

Bull, S., J. Cartwright, and M. Huuse (2009). A Review of Kinematic Indicators from Mass-Transport Complexes Using 3D Seismic Data. In: *Marine and Petroleum Geology* 7, pp. 1132–1151. DOI: 10.1016/j.marpetgeo.2008.09.011.

Canals, M., D. Amblas, J. Casamor, and G. Lastras (2016). Gebra Slide: Glacial and Tectonic Controls on Recurrent Submarine Landsliding off the Northern Tip of the Antarctic Peninsula. In: *Geological Society, London, Memoirs* 46.1, pp. 417–418. DOI: 10.1144/M46.152.

Cartwright, J. and M. Huuse (2005). 3D Seismic Technology: The Geological 'Hubble'. In: *Basin Research* 17.1, pp. 1–20. DOI: 10.1111/j.1365-2117.2005.00252.x.

CD178 (2006). *Cruise Report No. 03 R.R.S. Charles Darwin cruise CD178*. Douglas G. Masson and Christian Berndt: National Oceanography Centre (NOC), Southampton; 14th March -11th April: 2006 3D Seismic Acquisition over Mud Volcanoes in the Gulf of Cadiz and Submarine Landslides in the Eivissa Channel, Western Mediterranean Sea. URL: https://www.bodc.ac.uk/resources/inventories/cruise_inventory/report/7117/.

Chopra, S. and K. J. Marfurt (2005). Seismic attributes—A historical perspective. In: *Geophysics* 70.5, 3SO–28SO. DOI: 10.1190/1.2098670.

Clare, M., J. Chaytor, O. Dabson, D. Gamboa, A. Georgiopoulou, H. Eady, J. Hunt, C. Jackson, O. Katz, S. Krastel, R. Le0n, A. Micallef, J. Moernaut, R. Moriconi, L. Moscardelli, C. Müller, A. Normandeau, M. Patacci, M. Steventon, M. Urlaub, D. Völker, L. Wood, and Z. Jobe (2019). A Consistent Global Approach for the Morphometric Characterization of Subaqueous Landslides. In: *Geological Society, London, Special Publications* 1, pp. 455–477. DOI: 10.1144/SP477.15.

Clarke, J. E. H., A. N. Shor, D. J. Piper, and L. A. Mayer (1990). Large-scale Current-Induced Erosion and Deposition in the Path of the 1929 Grand Banks Turbidity Current. In: *Sedimentology* 37.4, pp. 613–629. DOI: 10.1111/j.1365-3091.1990.tb00625.x.

Driussi, O., A. Maillard, D. Ochoa, J. Lofi, F. Chanier, V. Gaullier, A. Briais, F. Sage, F. Sierro, and M. Garcia (2015). Messinian Salinity Crisis Deposits Widespread over the Balearic Promontory: Insights from New High-Resolution Seismic Data. In: *Marine and Petroleum Geology* 66, pp. 41–54. DOI: 10.1016/j.marpetgeo.2014.09.008.

Duarte, C. M., L. Chapuis, S. P. Collin, D. P. Costa, R. P. Devassy, V. M. Eguiluz, C. Erbe, T. A. Gordon, B. S. Halpern, H. R. Harding, et al. (2021). The Soundscape of the Anthropocene Ocean. In: *Science* 371.6529, eaba4658. DOI: 10.1126/science.aba4658.

Dugan, B. (2012). Petrophysical and Consolidation Behavior of Mass Transport Deposits from the Northern Gulf of Mexico, IODP Expedition 308. In: *Marine Geology* 315–318, pp. 98–107. DOI: 10.1016/j.margeo.2012.05.001.

Elger, J., C. Berndt, L. Rüpke, S. Krastel, F. Gross, and W. H. Geissler (2018). Submarine Slope Failures Due to Pipe Structure Formation. In: *Nature Communications* 9.1, p. 715. DOI: 10.1038/s41467-018-03176-1.

Ford, J., R. Urgeles, A. Camerlenghi, and E. Gràcia (2021). Seismic Diffraction Imaging to Characterize Mass-Transport Complexes: Examples From the Gulf of Cadiz, South West Iberian Margin. In: *Journal of Geophysical Research: Solid Earth* 3. DOI: 10.1029/2020JB021474.

Frey-Martinez, J., J. Cartwright, and B. Hall (2005). 3D Seismic Interpretation of Slump Complexes: Examples from the Continental Margin of Israel. In: *Basin Research* 1, pp. 83–108. DOI: 10.1111/j.1365-2117.2005.00255.x.

Frey-Martinez, J., J. Cartwright, and D. James (2006). Frontally Confined versus Frontally Emergent Submarine Landslides: A 3D Seismic Characterisation. In: *Marine and Petroleum Geology* 5, pp. 585–604. DOI: 10.1016/j.marpetgeo.2006.04.002.

Gatter, R., M. Clare, J. Kuhlmann, and K. Huhn (2021). Characterisation of Weak Layers, Physical Controls on their Global Distribution and their Role in Submarine Landslide Formation. In: *Earth-Science Reviews* 223, p. 103845. DOI: 10.1016/j.earscirev.2021.103845.

Gee, M., R. Gawthorpe, and S. Friedmann (2006). Triggering and Evolution of a Giant Submarine Landslide, Offshore Angola, Revealed by 3D Seismic Stratigraphy and Geomorphology. In: *Journal of Sedimentary Research* 76.1, pp. 9–19. DOI: 10.2110/jsr.2006.02.

Gutowski, M., J. Malgorn, and M. Vardy (2015). "3D Sub-Bottom Profiling—High Resolution 3D Imaging of Shallow Subsurface Structures and Buried Objects". In: *OCEANS 2015-Genova*. IEEE, pp. 1–7. DOI: 10.1109/oceans-genova.2015.7271468.

Haflidason, H., H. P. Sejrup, A. Nygård, J. Mienert, P. Bryn, R. Lien, C. F. Forsberg, K. Berg, and D. Masson (2004). The Storegga Slide: Architecture, Geometry and Slide Development. In: *Marine Geology* 1-4, pp. 201–234. DOI: 10.1016/j.margeo.2004.10.007.

Hampton, M. A., H. J. Lee, and J. Locat (1996). Submarine Landslides. In: *Reviews of Geophysics* 34.1, pp. 33–59. DOI: 10.1029/95RG03287.

Harbitz, C. B., F. Løvholt, and H. Bungum (2014). Submarine Landslide Tsunamis: How Extreme and How Likely? In: *Natural Hazards* 3, pp. 1341–1374. DOI: 10.1007/s11069-013-0681-3.

Hasegawa, H. and H. Kanamori (1987). Source Mechanism of the Magnitude 7.2 Grand Banks Earthquake of November 1929: Double Couple or Submarine Landslide? In: *Bulletin of the seismological Society of America* 77.6, pp. 1984–2004. DOI: 10.1785/BSSA0770061984.

Heezen, B. C., D. Ericson, and M. Ewing (1954). Further Evidence for a Turbidity Current following the 1929 Grand Banks Earthquake. In: *Deep Sea Research (1953)* 1.4, pp. 193–202. DOI: 10.1016/0146-6313(54)90001-5.

Helbig, K. (1983). Seismic Impedance. In: *First Break* 1.3.

HERMESIONE (2009). *Cruise Report BIO Hesperides Research cruise HERMESIONE*. Antoni M. Calafat and Miquel Canals: University of Barcelona, Spain; Institut National de Recherche Halieutique, Morocco; Consejo Superior de Investigaciones Científicas, Spain: Gibraltar Strait – Western Mediterranean (Cartagena – Cartagena) 15th September – 9th October 2009: Hotspot Ecosystem Research on Europe's

Deep-Ocean Margins (HERMES), Hotspot Ecosystem Research and Man's Impact on European Seas (HERMIONE), and Ocean Tracking Network (OTN).

Imbo, Y., M. De Batist, M. Canals, M. Prieto, and J. Baraza (2003). The Gebra Slide: a Submarine Slide on the Trinity Peninsula Margin, Antarctica. In: *Marine Geology* 193.3-4, pp. 235–252. DOI: 10.1016/S0025-3227(02)00664-3.

Jackson, C. A.-L. (2011). Three-Dimensional Seismic Analysis of Megaclast Deformation within a Mass Transport Deposit; Implications for Debris Flow Kinematics. In: *Geology* 3, pp. 203–206. DOI: 10.1130/G31767.1.

Kaminski, P., T. Sager, J. Grabe, and M. Urlaub (2021). A New Methodology to Assess the Potential of Conjectural Trigger Mechanisms of Submarine Landslides Exemplified by Marine Gas Occurrence on the Balearic Promontory. In: *Engineering Geology*, p. 106446. DOI: 10.1016/j.enggeo.2021.106446.

Kearey, P., M. Brooks, and I. Hill (2002). *An Introduction to Geophysical Exploration*. Vol. 4. John Wiley and Sons.

Krastel, S., W. Li, M. Urlaub, A. Georgiopoulou, R. B. Wynn, T. Schwenk, C. Stevenson, and P. Feldens (2019). Mass Wasting along the NW African Continental Margin. In: *Geological Society, London, Special Publications* 1, pp. 151–167. DOI: 10.1144/SP477.36.

Kühn, M., J. Karstens, C. Berndt, and S. F. Watt (2021). Seismic Reconstruction of Seafloor Sediment Deformation during Volcanic Debris Avalanche Emplacement Offshore Sakar, Papua New Guinea. In: *Marine Geology*, p. 106563. DOI: 10.1016/j.margeo.2021.106563.

Kvalstad, T. J., F. Nadim, A. M. Kaynia, K. H. Mokkelbost, and P. Bryn (2005). Soil Conditions and Slope Stability in the Ormen Lange Area. In: *Marine and Petroleum Geology* 1-2, pp. 299–310. DOI: 10.1016/j.marpetgeo.2004.10.021.

Lackey, J., G. Moore, and M. Strasser (2018). Three-Dimensional Mapping and Kinematic Characterization of Mass Transport Deposits along the Outer Kumano Basin and Nankai Accretionary Wedge, Southwest Japan. In: *Progress in Earth and Planetary Science* 1, p. 65. DOI: 10.1186/s40645-018-0223-4.

Lafuerza, S., N. Sultan, M. Canals, G. Lastras, A. Cattaneo, J. Frigola, S. Costa, and C. Berndt (2012). Failure Mechanisms of Ana Slide from Geotechnical Evidence, Eivissa Channel, Western Mediterranean Sea. In: *Marine Geology*, pp. 1–21. DOI: 10.1016/j.margeo.2012.02.010.

Lastras, G., M. Canals, D. Amblas, J. Frigola, R. Urgeles, A. Calafat, and J. Acosta (2007). Slope Instability along the Northeastern Iberian and Balearic Continental Margins. In: *Geologica Acta: An International Earth Science Journal* 5.1, pp. 35–48.

Lastras, G., M. Canals, D. Amblas, M. Ivanov, B. Dennielou, L. Droz, A. Akhmetzhanov, and TTR-14 Leg 3 Shipboard Scientific Party (2006). Eivissa Slides, Western Mediterranean Sea: Morphology and Processes. In: *Geo-Marine Letters* 4, pp. 225–233. DOI: 10.1007/s00367-006-0032-4.

Lastras, G., M. Canals, R. Urgeles, J. E. Hughes-Clarke, and J. Acosta (2004). Shallow Slides and Pockmark Swarms in the Eivissa Channel, Western Mediterranean Sea. In: *Sedimentology* 4, pp. 837–850. DOI: 10.1111/j.1365-3091.2004.00654.x.

Lindberg, B., J. Laberg, and T. Vorren (2004). The Nyk Slide—Morphology, Progression, and Age of a Partly Buried Submarine Slide Offshore Northern Norway. In: *Marine Geology* 213.1-4, pp. 277–289. DOI: 10.1016/j.margeo.2004.10.010.

Locat, J., S. Leroueil, A. Locat, and H. Lee (2014). "Weak layers: Their Definition and Classification from a Geotechnical Perspective". In: *Submarine mass movements and their consequences: 6th international symposium*. Springer, pp. 3–12. DOI: 10.1007/978-3-319-00972-8_1.

Løvholt, F., I. Schulten, D. Mosher, C. Harbitz, and S. Krastel (2019). Modelling the 1929 Grand Banks Slump and Landslide Tsunami. In: *Geological Society, London, Special Publications* 477.1, pp. 315–331. DOI: 10.1144/SP477.2.

Lykousis, V., G. Roussakis, M. Alexandri, P. Pavlakis, and I. Papoulia (2002). Sliding and Regional Slope Stability in Active Margins: North Aegean Trough (Mediterranean). In: *Marine Geology* 186.3-4, pp. 281–298. DOI: 10.1016/S0025-3227(02)00269-4.

Masson, D., A. Watts, M. Gee, R. Urgeles, N. Mitchell, T. Le Bas, and M. Canals (2002). Slope failures on the flanks of the western Canary Islands. In: *Earth-Science Reviews* 57.1-2, pp. 1–35. DOI: 10.1016/S0012-8252(01)00069-1.

Miramontes, E., N. Sultan, S. Garziglia, G. Jouet, E. Pelleter, and A. Cattaneo (2018). Altered Volcanic Deposits as Basal Failure Surfaces of Submarine Landslides. In: *Geology* 46.7, pp. 663–666. DOI: 10.1130/G40268.1.

Mitchum, R., P. R. Vail, and S. Thompson III (1977). Seismic stratigraphy and global changes of sea level: Part 2. The depositional sequence as a basic unit for stratigraphic analysis: Section 2. Application of seismic reflection configuration to stratigraphic interpretation. In: *Subject Group: Seismic Stratigraphy, Sequence Stratigraphy*.

Moscardelli, L. and L. Wood (2008). New Classification System for Mass Transport Complexes in Offshore Trinidad. In: *Basin Research* 20.1, pp. 73–98. DOI: 10.1111/j.1365-2117.2007.00340.x.

— (2015). Morphometry of Mass-Transport Deposits as a Predictive Tool. In: *Geological Society of America Bulletin*, B31221.1. DOI: 10.1130/B31221.1.

Müller, C., B. Milkereit, T. Bohlen, and F. Theilen (2002). Towards High-Resolution 3D Marine Seismic Surveying using Boomer Sources. In: *Geophysical Prospecting* 50.5, pp. 517–526. DOI: 10.1046/j.1365-2478.2002.00335.x.

Müller, C., S. Wuelz, and S. Kalmring (2013). High-resolution 3D marine seismic investigation of Hedeby Harbour, Germany. In: *International Journal of Nautical Archaeology* 42.2, pp. 326–336. DOI: 10.1111/1095-9270.12011.

Nugraha, H. D., C. A.-L. Jackson, H. D. Johnson, D. M. Hodgson, and M. A. Clare (2022). Extreme Erosion by Submarine Slides. In: *Geology* 50.10, pp. 1130–1134. DOI: 10.1130/G50164.1.

Ochoa, D., F. J. Sierro, J. Lofi, A. Maillard, J.-A. Flores, and M. Suarez (2015). Synchronous Onset of the Messinian Evaporite Precipitation: First Mediterranean Offshore Evidence. In: *Earth and Planetary Science Letters* 427, pp. 112–124. DOI: 10.1016/j.epsl.2015.06.059.

Omira, R., M. Baptista, R. Quartau, R. Ramalho, J. Kim, I. Ramalho, and A. Rodrigues (2022). How Hazardous Are Tsunamis Triggered by Small-Scale Mass-Wasting Events on Volcanic Islands? New Insights from Madeira – NE Atlantic. In: *Earth and Planetary Science Letters* 578, p. 117333. DOI: 10.1016/j.epsl.2021.117333.

Panieri, G., A. Camerlenghi, I. Cacho, C. S. Cervera, M. Canals, S. Lafuerza, and G. Herrera (2012). Tracing Seafloor Methane Emissions with Benthic Foraminifera: Results from the Ana Submarine Landslide (Eivissa Channel, Western Mediterranean Sea). In: *Marine Geology*, pp. 97–112. DOI: 10.1016/j.margeo.2011.11.005.

Principaud, M., T. Mulder, H. Gillet, and J. Borgomano (2015). Large-Scale Carbonate Submarine Mass-Wasting along the Northwestern Slope of the Great Bahama Bank (Bahamas): Morphology, Architecture, and Mechanisms. In: *Sedimentary Geology* 317, pp. 27–42. DOI: 10.1016/j.sedgeo.2014.10.008.

Raad, F. (2022). "Balearic Promontory Architecture and History during the Formation of the Mediterranean Salt Giant". PhD thesis. Université Montpellier. URL: https://theses.hal.science/tel-03844128/.

Riedel, M., J.-J. Bahk, N. Scholz, B.-J. Ryu, D.-G. Yoo, W. Kim, and G. Kim (2012). Mass-transport Deposits and Gas Hydrate Occurrences in the Ulleung Basin, East Sea – Part 2: Gas Hydrate Content and Fracture-Induced Anisotropy. In: *Marine and Petroleum Geology* 35.1, pp. 75–90. DOI: 10.1016/j.marpetgeo.2012.03.005.

Sammartini, M., J. Moernaut, A. Kopf, S. Stegmann, S. Fabbri, F. Anselmetti, and M. Strasser (2021). Propagation of Frontally Confined Subaqueous Landslides: Insights from Combining Geophysical, Sedimentological, and Geotechnical Analysis. In: *Sedimentary Geology* 416, p. 105877. DOI: 10.1016/j.sedgeo.2021.105877.

Shan, Z., H. Wu, W. Ni, M. Sun, K. Wang, L. Zhao, Y. Lou, A. Liu, W. Xie, X. Zheng, et al. (2022). Recent Technological and Methodological Advances for the Investigation of Submarine Landslides. In: *Journal of Marine Science and Engineering* 10.11, p. 1728. DOI: 10.3390/jmse10111728.

Sheriff, R. E. and L. P. Geldart (1995). *Exploration Seismology*. Cambridge University Press.

Shin, J., J. Ha, J.-H. Chun, and I.-K. Um (2022). Field application of 3D CHIRP for Geological Surveys of Shallow Coastal Regions. In: *Marine Geophysical Research* 43.2, p. 13. DOI: 10.1007/s11001-022-09477-x.

Steventon, M. J., C. A.-L. Jackson, D. M. Hodgson, and H. D. Johnson (2019). Strain Analysis of a Seismically Imaged Mass-transport Complex, Offshore Uruguay. In: *Basin Research* 3, pp. 600–620. DOI: 10.1111/bre.12337.

Sultan, N., P. Cochonat, M. Canals, A. Cattaneo, B. Dennielou, H. Haflidason, J. Laberg, D. Long, J. Mienert, F. Trincardi, R. Urgeles, T. Vorren, and C. Wilson (2004). Triggering Mechanisms of Slope Instability Processes and Sediment Failures on Continental Margins: A Geotechnical Approach. In: *Marine Geology* 213.1-4, pp. 291–321. DOI: 10.1016/j.margeo.2004.10.011.

Sun, Q., T. M. Alves, X. Lu, C. Chen, and X. Xie (2018). True Volumes of Slope Failure Estimated From a Quaternary Mass-Transport Deposit in the Northern South China Sea. In: *Geophysical Research Letters* 6, pp. 2642–2651. DOI: 10.1002/2017GL076484.

Talling, P., M. Clare, M. Urlaub, E. Pope, J. Hunt, and S. Watt (2014). Large Submarine Landslides on Continental Slopes: Geohazards, Methane Release, and Climate Change. In: *Oceanography* 27.2, pp. 32–45. DOI: 10.5670/oceanog.2014.38.

Tang, Q., J. Geersen, A. Düring, D. Unverricht, J. Schneider von Deimling, K.-F. Lenz, W. Li, and S. Krastel (2022). Sequence of Multiple Slope Failures in the Headwall Area of the Giant Sahara Slide Complex at the NW African Continental Margin. In: *Geochemistry, Geophysics, Geosystems* 23.7. DOI: 10.1029/2021GC010283.

Urlaub, M., P. J. Talling, A. Zervos, and D. Masson (2015). What Causes Large Submarine Landslides on Low Gradient ($< 2°$) Continental Slopes with Slow (~ 0.15 m/Kyr) Sediment Accumulation?: Large submarine landslides on low gradients. In: *Journal of Geophysical Research: Solid Earth* 10, pp. 6722–6739. DOI: 10.1002/2015JB012347.

Urlaub, M., A. Zervos, P. J. Talling, D. G. Masson, and C. I. Clayton (2012). "How Do $\sim 2°$ Slopes Fail in Areas of Slow Sedimentation? A Sensitivity Study on the Influence of Accumulation Rate and Permeability on Submarine Slope Stability". In: *Submarine Mass Movements and Their Consequences*. Ed. by Y. Yamada, K. Kawamura, K. Ikehara, Y. Ogawa, R. Urgeles, D. Mosher, J. Chaytor, and M. Strasser. Dordrecht: Springer Netherlands, pp. 277–287. DOI: 10.1007/978-94-007-2162-3_25.

Völker, D. J. (2010). A Simple and Efficient GIS Tool for Volume Calculations of Submarine Landslides. In: *Geo-Marine Letters* 5, pp. 541–547. DOI: 10.1007/s00367-009-0176-0.

Webster, J. M., N. P. George, R. J. Beaman, J. Hill, A. Puga-Bernabeu, G. Hinestrosa, E. A. Abbey, and J. J. Daniell (2016). Submarine Landslides on the Great Barrier Reef Shelf Edge and Upper Slope: A Mechanism for Generating Tsunamis on the North-East Australian Coast? In: *Marine Geology* 371, pp. 120–129. DOI: 10.1016/j.margeo.2015.11.008.

Wilson, C. K., D. Long, and J. Bulat (2004). The Morphology, Setting and Processes of the Afen Slide. In: *Marine Geology* 213.1–4, pp. 149–167. DOI: 10.1016/j.margeo.2004.10.005.

3 Development and Emplacement of Ana Slide, Eivissa Channel, Western Mediterranean Sea

Sager, T. F.[1*], Urlaub, M.[1], Kaminski, P.[2], Papenberg, C.[1], Lastras, G.[3], Canals, M.[3], Berndt, C.[1]

Geochemistry, Geophysics, Geosystems (G^3) (2022)
https://doi.org/10.1029/2022GC010469

[1] GEOMAR Helmholtz Centre for Ocean Research Kiel, Kiel, Germany

[2] Institute of Geotechnical Engineering & Construction Management, Hamburg University of Technology (TUHH), Hamburg, Germany

[3] CRG Marine Geoscience, Department of Earth and Ocean Dynamics, University of Barcelona, Barcelona, Spain

[*] Corresponding Author: tsager@geomar.de

Published online November 15th, 2022 in Geochemistry, Geophysics, Geosystems (G^3); Received May 19th, 2022; Accepted November 5th, 2022.

We thank Antonio Cattaneo (IFREMER, Brest - France), Jonathan Ford (OGS, Trieste - Italy) and an anonymous reviewer for their constructive criticism and invaluable insightful comments on this paper during peer reviewing.

Abstract

Submarine landslides can destroy seafloor infrastructures and generate devastating tsunamis. In spite of decades of research into the functioning of submarine landslides there are still numerous open questions, in particular how different phases of sliding influence each other. Here, we re-analyze Ana Slide—a relatively small (<1 km^3) landslide offshore the Balearic Islands, which is unique in the published literature because it is completely imaged by high-resolution 3D reflection seismic data. Ana Slide comprises three domains: (a) a source area that is almost completely evacuated with evidence of headscarp retrogression, (b) an adjacent downslope translational domain representing a by-pass zone for the material that was mobilized in the source area, and (c) the deposit formed by the mobilized material, which accumulated downslope in a sink area and deformed slope sediment. Isochron maps show deep chaotic seismic units underneath the thickest deposits. We infer that the rapid deposition of the landslide material deformed the underlying sediments. A thin stratified sediment unit between three lobes suggests that Ana Slide evolved in two failure stages separated by several tens of thousands of years. This illustrates the problem of over-estimating the volume of mobilized material and under-estimating the complexity even of relatively simple slope failures without high-quality 3D reflection seismic data.

Plain Language Summary

We investigate a submarine landslide in the Balearic Islands off Spain. The aim is to find out how such landslides work. This study is special because it can draw on a unique data set: the complete imaging of this landslide with high quality reflection seismic data. We find that previous studies have over-estimated the volume of the mobilized material because deformed sediments below the landslide were also counted, and that the slide actually consisted of two individual slope failures that occurred at the same place but in distinct episodes separated by some tends of thousands of years. Together these results show that there is a large risk of overestimating landslide-related tsunami hazards when this kind of reflection seismic data is not available.

Key points:

- Ana Slide is completely covered by 3D reflection seismic data and its kinematic development is addressed.
- Large parts of the volume previously interpreted as landslide material was deformed *in-situ*.
- Ana Slide developed during two separate phases that involved likely significantly smaller volumes of material than previously proposed.

3.1 Introduction

Submarine slope failures are widespread phenomena on continental margins and around ocean islands. They are often several orders of magnitude larger than their terrestrial counterparts (Varnes, 1978) and can generate devastating tsunamis that are able to inundate surrounding coastal areas while threatening infrastructure (Bondevik et al., 2005; Farrell, 1984; Haugen et al., 2005; Løvholt et al., 2017; Prior et al., 1984; Varnes, 1978). As an example a tsunami with runup heights of 8 m in western Denmark has been interpreted to have been generated by the Storegga Slide offshore Norway (Fruergaard et al., 2015).

Large-scale mass-transport deposits (MTDs) resulting from submarine slope failures have been described in many areas for example, offshore Norway (e.g., Bryn et al., 2005; Bugge et al., 1987; Haflidason et al., 2004; Kvalstad et al., 2005), in the Eastern Mediterranean Sea (Frey-Martinez et al., 2006; Frey-Martinez et al., 2005), in the Gulf of Mexico (Sawyer et al., 2009), and off the coast of North-west Africa (Krastel et al., 2019). Submarine slope failures mobilize large amounts of sediment from the continental margins toward the deep ocean and thus represent an important sediment transport mechanism (Huehnerbach, Masson, et al., 2004). For comparison, the volume of material involved in the Storegga Slide has been determined at around $2,400 - 3,200$ km^3 (Haflidason et al., 2005), which greatly exceeds the volume of material involved, for instance, in the collapse of Mount St. Helens, which was estimated at around 2.8 km^3 (Voight et al., 1983).

Alongside the volume of material involved in slope failures and the runout velocity, the development of a slope failure determines its tsunamigenic potential (Harbitz et al., 2014; Lenz et al., 2018; Masson et al., 2006). For example, a multi-stage failure with long time periods in between individual stages is less tsunamigenic than a single event failure of the same mass (Harbitz et al., 2014). For assessing the tsunamigenic potential of a landslide, and thus the hazard it might represent, it is therefore essential to understand its detailed kinematic development and if possible, assess the volume of mobilized material.

Clare et al., 2019 reveal that ambiguity exists in the sound and consistent identification of morphometric parameters for submarine landslides. Whereas the length of evacuational and depositional zones, and the average slope angles are important input variables in predictive models for tsunamigenic potential of submarine landslides, errors in the identification of those tsunami source parameters may directly propagate into modeling results. Further, the retrogression of the headscarp needs to be addressed as it could indicate that the slope failure developed during several stages.

Previous studies based on bathymetric and 2D reflection seismic imagery provide valuable insights into landslide evolution (e.g., Barrett et al., 2020; Lenz et al., 2018). However, these data do not provide the three-dimensional structure of the entire submarine landslide. Therefore, a detailed analysis of various characteristics in and around submarine landslide deposits that are key to understanding emplacement processes, such as deformation of internal

structure, distribution and size of transported blocks, erosion of underlying strata, or reconstruction of paleo-morphology has rarely been possible due to the lack of high-quality 3D reflection seismic data. Nonetheless, important work has been published on emplacement processes (e.g., Lenz et al., 2018; Steventon et al., 2019); deformation mechanisms (e.g., Ogata et al., 2014; Sobiesiak et al., 2018); transported blocks (e.g., Alves and Cartwright, 2009); erosive processes (e.g., Nugraha et al., 2020; Ogata et al., 2014; Sobiesiak et al., 2018); and reconstruction of the paleo seafloor morphology (e.g., Völker, 2010).

In this study, we use very-high resolution multibeam bathymetric and high-quality 3D reflection seismic reflection data, and re-processed high-quality 2D quality reflection seismic profiles that completely cover a small submarine landslide, named Ana Slide, located within the Eivissa Channel, Western Mediterranean Sea. Our objectives are to establish a relative chronology and reconstruct the kinematic development of Ana Slide. Our aim is to ameliorate current understanding on emplacement processes of submarine landslides, making use of the unique observational data base of Ana Slide.

3.2 Terminology

In this study, we use the term failure to describe the active process that translates or mobilizes landslide material from a source to a sink area. The resulting deposit is defined as the mass transport deposit (MTD) of Ana Slide. We refrain from the use of the classic terms of the "headwall" and "toe" domains. Although they correlate with the evacuational source and accumulational sink areas, they provide no information about kinematic processes involved in the emplacement and development of failure. Therefore, we use the terms "source" and "sink area" instead. While the source area can be identified from the upward deviation of contour-lines inside a landslide scar, the sink area will show downwards deviating contour-lines with respect to those of the surrounding seafloor. We also use the term by-pass zone to describe the transitional area in between the source and sink areas, where neither sediment has been removed nor added.

In addition, while the term MTD has previously been used to refer to all material involved in the slope failure (e.g., Bull et al., 2009; Frey-Martinez et al., 2005; Frey-Martinez et al., 2006; Lackey et al., 2018; Nugraha et al., 2020; Sobiesiak et al., 2016; Sobiesiak et al., 2018; Jackson, 2011), we further distinguish between "landslide material" and "affected slope sediment." The former describes material that was actively incorporated and mobilized during failure. The latter describes material that per se was not part of the landslide but experienced *in-situ* deformation immediately below mobilized landslide material.

By assuming that a slope failure did not change sedimentation patterns within the vicinity of a MTD, the top surface of a MTD is recognized as the boundary between relatively conformal reflections and chaotic/disrupted seismic facies within the MTD below (Bull et al., 2009).

The lower boundary with conformal seismic reflectors below is delimited by the "base of deformation" surface previously referred to as the "slip plane" or "glide plane" (Lastras et al., 2004). We use the term "basal shear surface" to describe the interface between mobilized landslide material from affected slope sediment below. In this study we expand on the classical usage of "seismic stratigraphy" (Mitchum et al., 1977). In addition to seismic reflectors having a chronological significance that bound seismic units, we introduce several sub-units bound by the same seismic reflectors that reflect for instance *in-situ* deformation of parts of the unit.

3.3 Geological Background and Previous Studies

The Eivissa Channel is located at the western end of the Balearic Promontory (Figure 3.1). It includes the islands of Eivissa (Ibiza) and Formentera, Mallorca, and Menorca, from west to east. The Promontory is the north-eastern prolongation of the Betic Range that extends along the southern Iberian Peninsula (Maillard and Mauffret, 2013; Mauffret et al., 2001). The regional structural framework is controlled by strong compressive activity that initiated in the Late Oligocene. Contraction was completed during the Serravalian and since then the Balearic Promontory has experienced extension (Maillard and Mauffret, 2013). Hence, the Promontory is located in a complex setting with successive compression and extension phases, though at present it shows relatively little tectonic activity (sensu del Valle et al., 2016).

From short 3 – 6 m long gravity cores, local sediments in the Eivissa Channel are identified as carbonate-rich ($\sim$ 50% $CaCO_3$) silty clays ($\sim$ 60% clay and $\sim$ 30% silt) with biogenic sands ($\sim$ 10%) with limited organic content (TOC <0.5%) (Lafuerza et al., 2012; Panieri et al., 2012). Siliciclastic input into the Eivissa Channel is limited, clayey, and originates from rivers such as the Ebro, Turia and Júcar on the Iberian Peninsula, north-west of the study area (Panieri et al., 2012). Hence, low accumulation rate, fine-grained hemipelagic carbonate-rich sedimentation dominates the study area (Canals and Ballesteros, 1997).

Previous studies evaluated failures within the Eivissa Channel by means of geophysical data sets (Berndt et al., 2012; Lastras et al., 2004; Lastras et al., 2006), gravity cores (Panieri et al., 2012) and in combination with geotechnical CPTu measurements (Lafuerza et al., 2012). Lastras et al., 2004; Lastras et al., 2006 identified three additional MTDs north of Ana Slide called Joan, Nuna, and Jersi from south to north (Figure 3.1). Ana Slide is located at water depths between 630 m to the east and 790 m to the west (Figure 3.2). It has a maximum length from east to west of 4.1 km with a headscarp height of $\sim$ 30 m while the average slope angle is $\sim 2^{\circ}$ (Figure 3.2).

In 2006, the RSS Charles Darwin Cruise 178 acquired high-resolution bathymetric and 3D seismic reflection data. From these, a buried slope failure — pre-Ana Slide — was mapped in detail around 30 – 40 ms travel time below Ana Slide (Berndt et al., 2012). While pre-Ana

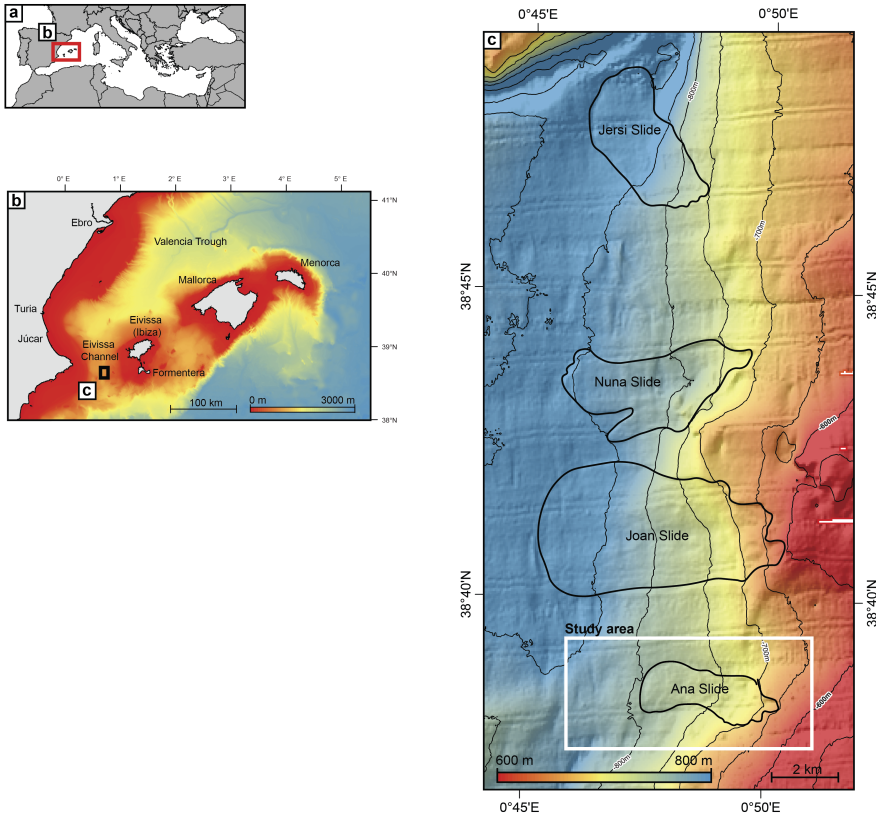

Figure 3.1: (a) Overview map of the Western Mediterranean Sea showing the location of the Balearic Promontory (BP). The red box indicates the location of panel b. (b) General bathymetric map of the Balearic Promontory. Data from the "Global multi-resolution topography synthesis" (Ryan, 2009). The black box indicates the location of panel c. (c) Bathymetric map of the eastern slopes of the Eivissa Channel showing the outlines of Jersi, Nuna, Joan, and Ana Slides. Bathymetric data from the BIG'95 survey. The white box indicates the location of the study area (Figure 3.2).

Slide extends around 1.4 km westwards of Ana Slide the shape and location of the headscarps are very similar (Figure 3.2).

Lastras et al., 2004 propose that fluid overpressure indicated by the presence of fluid escape structures in the vicinity of Ana Slide and mechanically weak layers are the main controlling factors for slope failures along the eastern slope of the Eivissa Channel. In addition, they indicate that failures throughout the Eivissa Channel possibly occurred simultaneously as they share the same seismic horizon—the "slip plane"—as their basal shear surfaces. The study by Lafuerza et al., 2012 corroborates this by geotechnical tests on Kullenberg piston core samples and *in-situ* CPTu measurements, while adding that failure required the presence of gas in the substrate. Cattaneo et al., 2011, using AMS radiocarbon dating, planktonic foraminiferal assemblages, and correlation with regional oxygen isotope curves, suggest an age of $\sim$ 61.5 ka. B.P. for Ana Slide. Berndt et al., 2012 propose, from the analysis of a 3D reflection seismic data, that both slides were caused by changes of pore pressure as indicated by the spatial relation between pre-Ana and Ana Slide and by evidence for gas and fluid migration. Panieri et al., 2012, based on δ13C benthic foraminifera records, show that methane was released from the seabed before and during the failure of Ana Slide.

Although these previous studies regard the physiography and potential triggering, the internal architecture of Ana Slide and its complete kinematic development has yet to be addressed from analysis of 3D reflection seismic data. Hence, within this study, the kinematic development of Ana Slide is presented, which lends itself as a natural laboratory for more extensive landslides that are not fully covered by bathymetric or reflection seismic data.

3.4 Data and Methodology

The 3D reflection seismic data were acquired with the P-Cable system of the National Oceanographic Centre, Southampton, UK during cruise CD178 in 2006 onboard the RRS Charles Darwin alongside a high-resolution bathymetric grid (Berndt et al., 2012). Additional bathymetric data acquired during cruise BIG'95 in 1995 onboard R/V Hespérides (50 m grid spacing) are also considered (Figure 3.1c) (Lastras et al., 2004).

The P-Cable system consisted of two paravanes and a central buoy, spanning a perpendicular cable. From this cable we towed eleven 12.5 m-long single-channel Teledyne streamers (Berndt et al., 2012). The seismic source consisted of four 40 in^3 Bolt 600B airguns spaced 0.75 m apart, towed at a depth of 1.5 m about 20 m behind the vessel. The processing steps for the 3D reflection seismic data included frequency filtering (35 – 350 Hz) before a 3D Stolt time migration with a migration velocity of 1500 m/s was applied (Berndt et al., 2012). The data have an inline and crossline spacing of 10 m. Given the high frequency of the 3D reflection seismic data the vertical seismic resolution, defined as 1/4 of the dominant wavelength, is approximately 5 – 6 m immediately beneath the seafloor ($Vp = 1500$ m/s). The data are displayed in the way that a downward increase in acoustic impedance is represented by a red-blue-red wavelet (e.g., Figure 3.3).

For bathymetric analysis we used the ArcGIS (ArcMAP) 10.6 software. Interpretation of the reflection seismic data and further data integration was carried out in IHS KingdomSuite 2018/2020. We calculated the Smoothed Dip of Maximum Similarity attribute on the SFR reflector from the RockSolid Attributes to map lateral discontinuities.

3.4.1 Additional Seismic Processing

For this study, we re-analyzed the 3D reflection seismic data because they are affected by receiver ghosts (e.g., Figure 3.7) and identified the cables that were affected by receiver ghosts. These receiver ghosts were generated by varying streamer depths during seismic acquisition as the perpendicular cable apparently sagged between the paravanes and the central buoy. Streamers close to the paravanes and the central buoy show little receiver ghosts. For the detailed analysis we extracted only the 2D profiles along the streamers that were not affected by the receiver ghost. Obviously, this higher resolution was bought at the expense of incomplete coverage. A visual comparison between profiles from the 3D

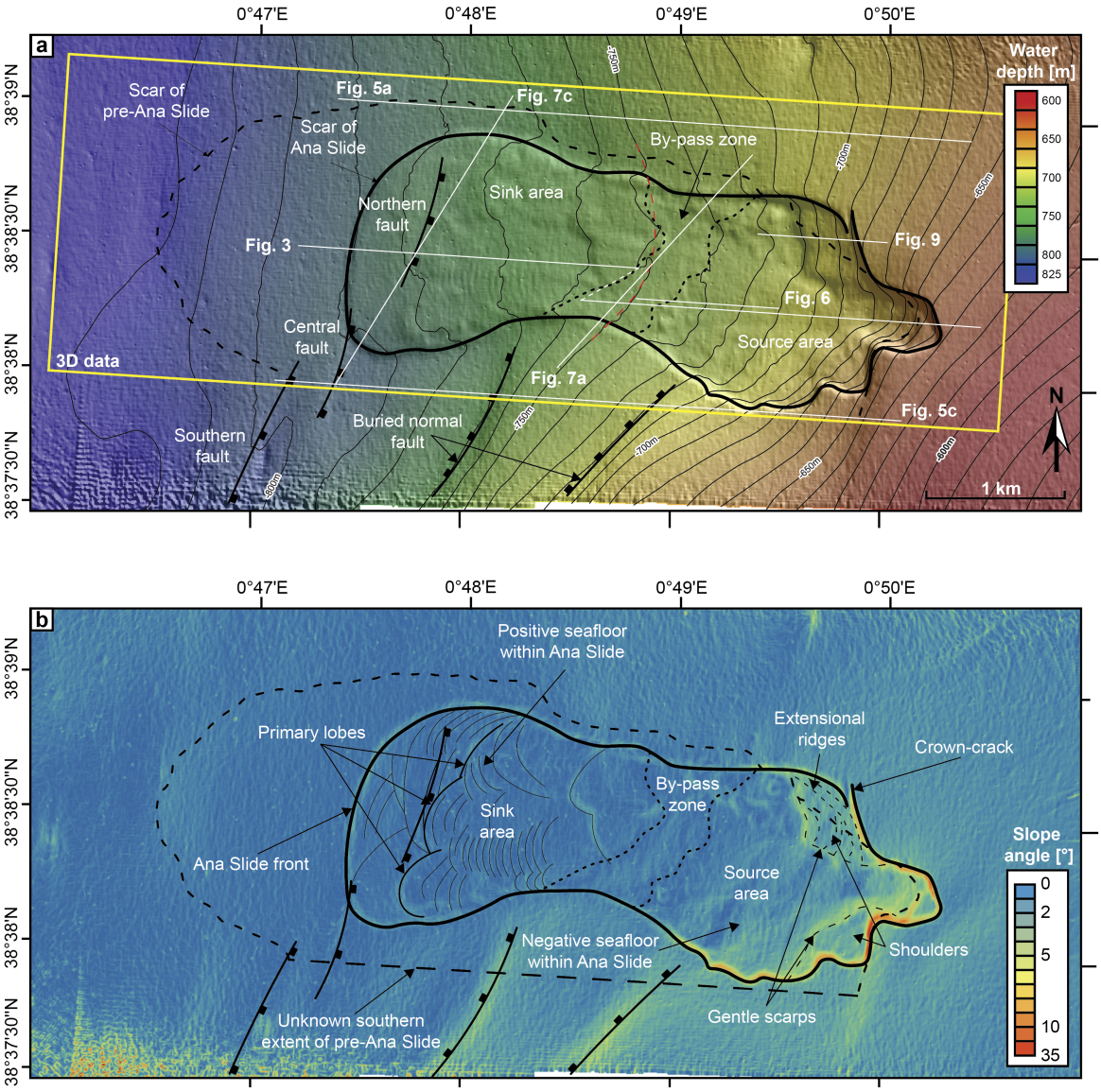

Figure 3.2: (a) Detailed bathymetric map of the study area with 10 m contour-line spacing. Ana Slide is outlined by a solid black line, while the outline of pre-Ana Slide is highlighted by a stippled black line. The location of reflection seismic profiles in subsequent figures is shown with solid white lines. Inside Ana Slide, the 750 m contour-line corresponds to those interpolated from outside Ana Slide (stippled red line). Several seafloor offsetting features are located south off and below the downslope part of Ana Slide. (b) Slope gradient map of the study area. Kinematic features are highlighted. The seafloor is gentle outside and north of Ana Slide while toward the south the seafloor displays several offsetting features.

data and re-processed 2D profiles is provided in Figures S6–S11 of Supporting Information S1 and location of profiles (S5). In the figures we normally present the single-channel 2D reflection seismic profiles extracted from inlines unaffected by the receiver ghost, while plan view maps of key seismic horizons and seismic attributes are derived from the binned 3D reflection seismic data set which is partly affected by receiver ghosts (Table S1 in Supporting Information S1). The extracted 2D profiles are frequency bandpass filtered and burst noise

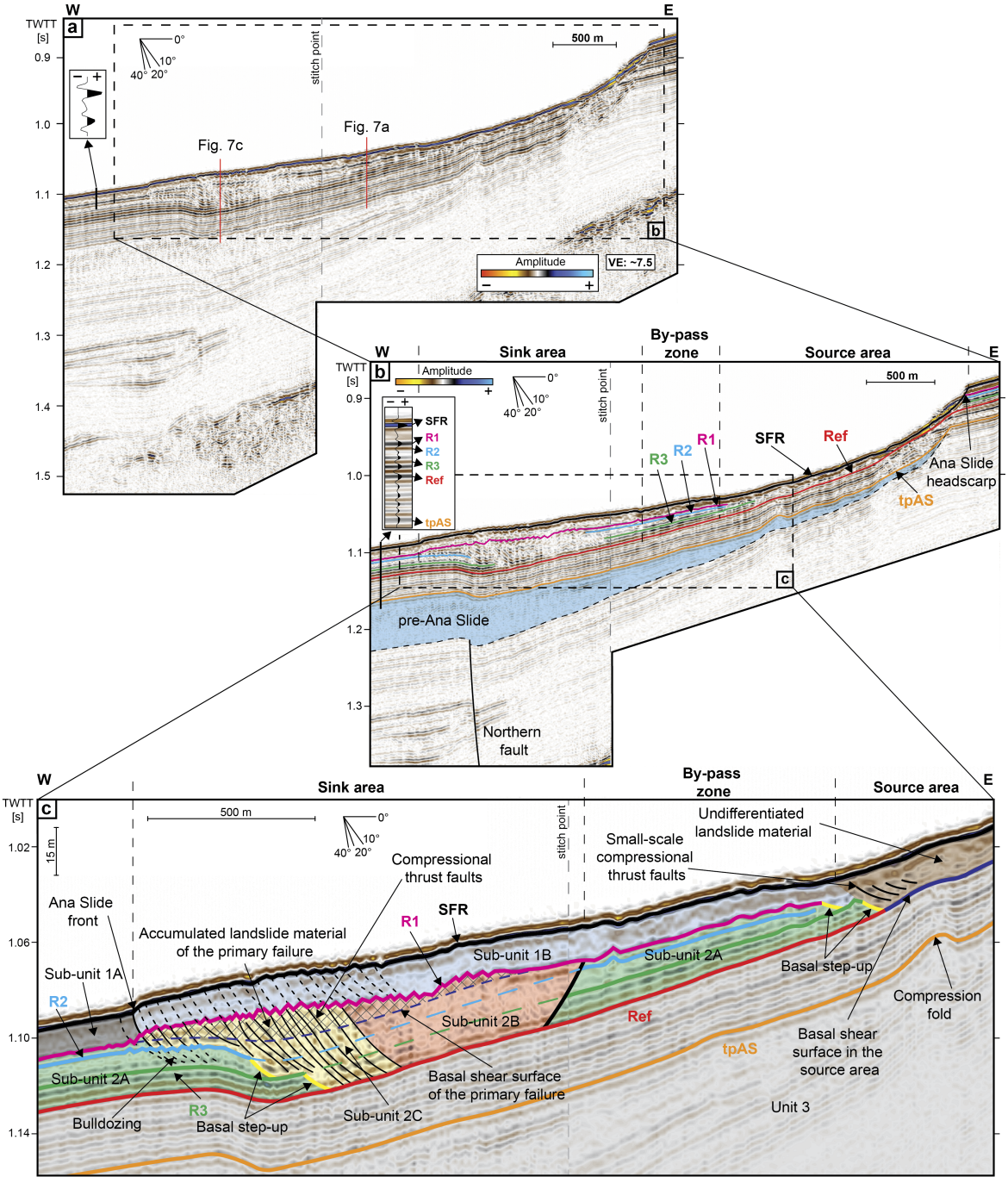

Figure 3.3: (a) Uninterpreted stitched reflection seismic profile (re-processed 2D data) through Ana Slide (Figure 3.2). The combination of two profiles shows the Ana Slide represented along-strike through the source and sink areas. (b) Close-up of Ana Slide with interpretation of key seismic reflectors: SFR, R1, R2, R3, Ref, and tpAS. (c) Sketch of seismic units. Sub-units involved in Ana Slide are 2B, 2C, 1B, and undifferentiated landslide material. Sub-units 2A and 1A characterize un-affected slope sediments outside the scar of Ana Slide. A compression fold that affects tpAS is located toward the east at depth while the basal shear surface inside the source area is represented by Ref. A visual comparison of the 3D and 2D reflection seismic profiles is presented in Figures 3.16 to 3.21 of Supporting Information S1.

attenuated. These data were binned, NMO-corrected, and stacked. Finally, a Stolt migration with seismic velocities of 1520 m/s was applied.

The receiver ghosts affect the entire traces in the 3D reflection seismic data set. As they only occur on individual streamers that are too deep below the surface, they align with the ship track. This makes their identification fairly easy in map view as they appear as stripes on attribute map. These have not been used for interpretation. For depth conversion of Ref and R1 we used seismic velocities of 1500 m/s and volume calculation was performed inside the sink area.

The *"Smoothed Dip of Maximum Similarity"* attribute is derived from a similarity attribute. First semblance between adjacent traces is calculated for a moving window. Then, the dip is calculated for the maximum semblance direction, and this is smoothed spatially. The Smoothed Dip of Maximum Similarity attribute is able to highlight the depositional environment and detect faults. These faults are representative of compressional ridges, extensional normal faults, ridges, and the front of Ana Slide that are characterized as structural elements namely faults.

3.5 Results

3.5.1 Morphology of Ana Slide

Ana Slide is located on the eastern slopes of Eivissa Channel (Figure 1). The surrounding seafloor is gently inclined from east to west and relatively smooth immediately north of Ana Slide while several seafloor offsetting features are located along its southern vicinity (Figure 3.2). The upslope scar of Ana Slide referred to as the headscarp is cauliflower shaped meaning that it consists of several smaller headscarp sections upslope. The landslide is 1.5 km wide from north to south. The headscarp forms two distinct "shoulders," with the southern shoulder being steeper than the northern one. These shoulders, in turn, have gentle scarps (<10°) located some hundreds of meters downslope (Figure 3.2). Around 1.5 km downslope of the headscarp, the sidewalls form a narrow, approximately 1.1 km wide corridor with irregular seafloor morphology.

The frontal break of slope that marks the downslope-most extent of Ana Slide opens to around 1.5 km width. In this study we refer to it as the "front of Ana Slide." Inside this lower part we identify three primary lobes located around 300 – 500 m upslope of the front of Ana Slide. The primary lobes are visible in the slope map as minor (2–4°) concave downslope breaks of slope and show numerous pressure ridges (Figure 3.2). These ridges align approximately parallel to the front of Ana Slide. In the northern downslope part, Ana Slide is around 5 m higher with respect to the surrounding seafloor outside the scar of Ana Slide while this difference is less significant in the southern downslope part.

3.5.2 3D seismic Interpretation

For the analysis of the kinematic development of Ana Slide we mapped five key seismic reflectors (Figure 3.3). These were mapped in both the 3D and 2D reflection seismic data and used accordingly to the data presented.

Reference Reflector (Ref)

The high-amplitude positive regional Reference (Ref) reflector (marked in red) is present throughout the study area (Figure 3.3). Inside the scar of Ana Slide it correlates with the apparent slip plane reflector identified by (Lastras et al., 2004). This reflector is the shallowest undisturbed stratigraphic reflector throughout Ana Slide. While in some places, such as the upslope eastern part of the slide, it indeed represents the slip plane, in other areas it is overlain by undisturbed and disturbed reflections. Thus, it is an important reference surface for the further discussion of the slide's thickness variations.

R3 and R2 Reflectors

The moderate-amplitude negative R3 and R2 (marked in green and light-blue) are mapped around 10 and 20 ms above Ref (Figure 3.3). Within the upslope part both reflectors are absent to around 1.5 km downslope of the easternmost headscarp. The lateral extent of R3 is limited to a small circular region with a diameter of around 500 m located within the central lower part approximately 900 m upslope of the front of Ana Slide (Figure 3.4). In contrast, R2 extends around 300 – 500 m upslope of the front of Ana Slide. In profile, R3 is irregular while R2 exhibits a strong hummocky appearance toward the front of Ana Slide (Figure 3.3) while both R2 and R3 have a congruent upslope extent.

R1 Reflector

R1 reflector (marked in pink) is the first high-amplitude positive reflector beneath the Seafloor (SFR) reflector (Figure 3.3). It is absent within the upslope part of the landslide to around 1.5 km downslope of the headscarp. The upslope limit of R1 is congruent with that of R2 and R3 and parallel with Ref for around 500 m downslope. It appears irregular within the lower area, while outside the scar of Ana Slide reflections are continuous and parallel with R3, R2, and Ref.

Seafloor and Ana Slide top Reflector (SFR)

The very-high-amplitude positive Seafloor reflector (SFR) (marked in black) represents the seafloor and the assumed top Ana Slide reflector since they cannot be distinguished due to

limited vertical resolution (Figure 3.3). Hemipelagic sediment deposited after the Ana Slide failure that was identified in sediment cores (2.5 m) by (Cattaneo et al., 2011) and (Lafuerza et al., 2012) is, consequently, included.

Top pre-Ana Slide Reflector (tpAS)

The top pre-Ana Slide (tpAS) reflector (marked in orange) is the upper reflector of pre-Ana Slide (Figure 3.3). It separates chaotic reflections below, which correspond to material of pre-Ana Slide with conformal reflections above up to 40 ms below Ref.

3.5.3 Seismic units

Within this study, we define three seismic units according to their seismic facies, relation to Ana Slide, and lateral extent bound by reflectors. These seismic units are sub-divided into several sub-units: 2A, 2B, 2C, 1A, and 1B. Throughout the study area such as immediately west of Ana Slide (Figure 3.3) the reflectors that bound these units are conformally arranged and highlight that sedimentation was relatively steady since before the emplacement of pre-Ana Slide Panieri et al., 2012. Nonetheless, these sediments have probably been deposited at an unsteady pace in response to eustatic or climatic changes throughout the Quaternary but were relatively unaffected by other processes such as contour-currents.

Unit 1

This unit appears between R1 and SFR (Figure 3.3) and was mapped from the re-processed 2D reflection seismic data. The isochron map of Unit 1 is presented in Figure 3.4a. Unit 1 is sub-divided into sub-units 1A and 1B. Sub-unit 1A is located outside the scar of Ana Slide and consists of conformal and continuous reflectors arranged in a slight downslope thickening configuration (Figure 3.4a). Sub-unit 1B is made of moderate-amplitude, highly irregular and disrupted reflections within the scar of Ana Slide. Unit 1 is absent within the upslope part of Ana Slide, while it is composed of slope sediment that was present within the lower part and landslide material that accumulated during the secondary failure. The isochron map of Unit 1 shows distinct ridges orientated sub-parallel toward the front of Ana Slide (Figure 3.4a).

Unit 2

This unit occurs between Ref and R1 (Figure 3.3c) and was mapped from the 3D reflection seismic data. The isochron map of Unit 2 is presented in Figure 3.4b. Unit 2 is sub-divided into three sub-units. Sub-unit 2A, formed by high-amplitude continuous parallel seismic reflections located primarily outside the scar of Ana Slide in a downslope thickening

configuration (Figure 3.4b). Sub-unit 2A is present within the scar of Ana Slide in an area around 500 m downslope of the upslope limits of R3, R2 and R1 (Figure 3.4b). Inside the scar of Ana Slide Sub-unit 2B generally describes chaotic seismic facies with lower-amplitude, highly disrupted reflectors, while Sub-unit 2C displays semi-continuous, moderately higher-amplitude disrupted reflectors. The lateral extent of these sub-units is sketched in Figures 4a–4c and the isochron map of Unit 2 is shown in Figure 3.4b. Unit 2 is thickest in the downslope part of Ana Slide about 300 – 500 m upslope of the front of Ana Slide. Outside the scar of Ana Slide, the thickness increases linearly in downslope direction.

Unit 3

This unit is located below Ref (Figure 3.3). It includes the interval between pre-Ana and Ana Slide, material of pre-Ana Slide, and all material below. For instance, between Ref and tpAS reflections are conformal and characterize a steady hemipelagic depositional environment.

Undifferentiated Landslide Material

This unit occurs above Ref and around 1.5 km downslope of the headscarp (Figure 3.3). It characterizes disrupted, lower-amplitude seismic reflections. This unit could not clearly be associated with Sub-unit 1B, 2B or 2C. It represents material that was involved in Ana Slide that cannot be distinguished conclusively.

3.5.4 Faults and Crown-Cracks

Several faults are identified within the study area from both bathymetry and reflection seismic data (Figure 2). These are primarily located along the southern vicinity of Ana Slide (Figures 5c and 5d). There are two faults that dip down-slope that is, westwards, and three faults that dip eastwards. All strike in NNE-SSW direction. Two of the three eastwards inclined faults are covered by reflection seismic data (Figure 3.2). These three faults characterize an en-echelon fault system of unknown southwards extent that terminates to the north below the downslope part of Ana Slide. In addition, a crown-crack exists immediately upslope north-east of the headscarp that detaches northwards. Within Ana Slide, numerous small-scale compressional thrust faults terminate from Ref up to R1 (e.g., Figures 3.3 and 3.6). Some thrust faults located around 500 m upslope of the front of Ana Slide reach SFR (e.g., Figure 3.3). Upslope the extents of R2 and R3 small-scale compressional thrust faults are identified in profile (Figure 3.6).

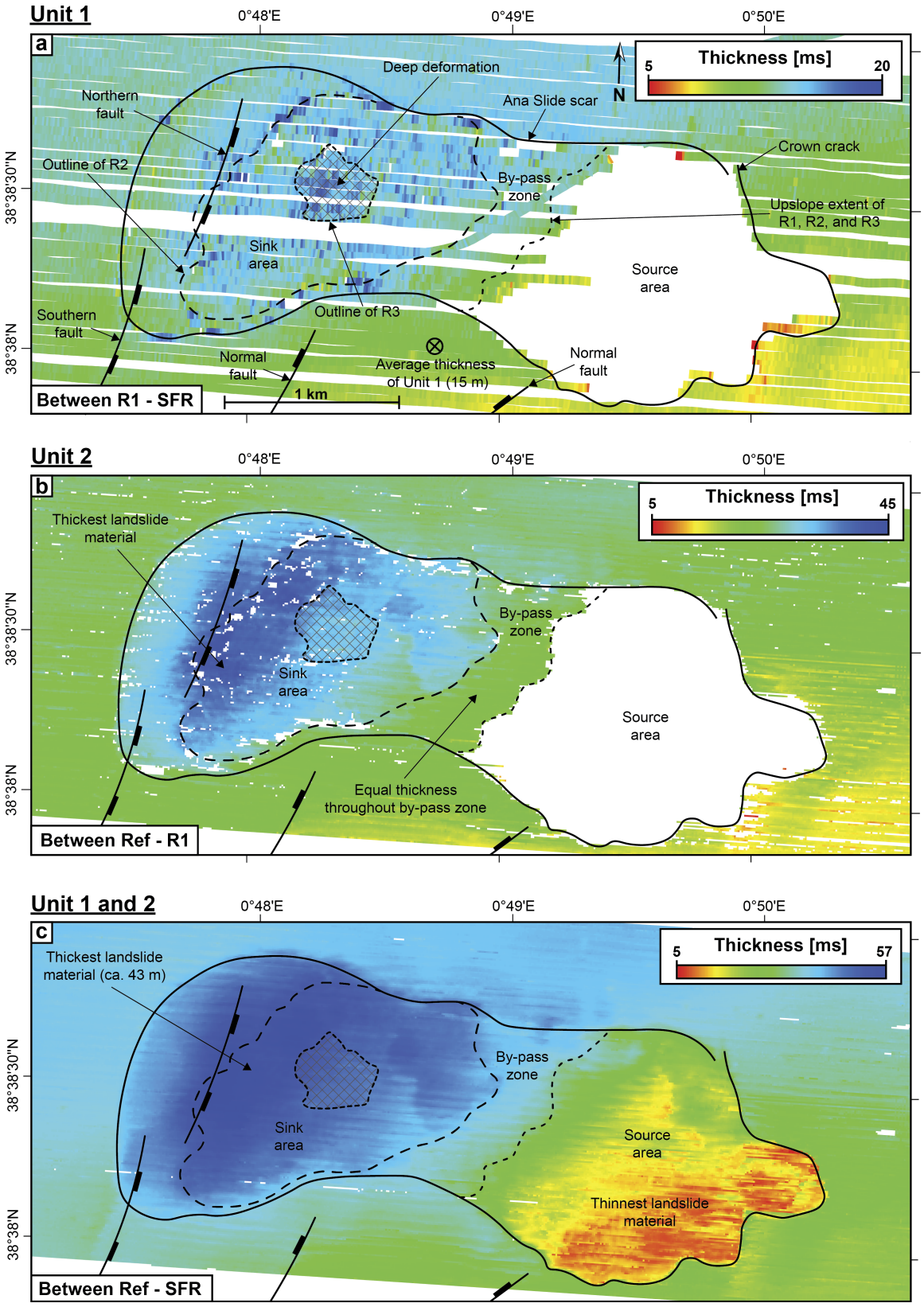

Figure 3.4: (Caption on next page.)

Figure 3.4: (Figure on previous page). Isochore maps of units 1 and 2. (a) Thickness of material between R1—SFR that represents Unit 1 (re-processed 2D data). "Average thickness of Unit 1" is approximately 15 m using a seismic velocity of 1500 m/s for depth conversion. Ref is absent inside the source area and no isochore map was calculated inside this area. (b) Thickness of material between Ref—R1 that represents Unit 2 (3D data). Receiver ghosts are introduced into the 3D reflection seismic data from varying streamer depth during seismic acquisition. The thickest landslide material is located within the central sink area immediately upslope of the northern fault with in-situ deformation located some hundreds of meters upslope of thickest landslide material. Ref is absent inside the source area and no isochore map was calculated inside this area. (c) Thickness of material between Ref—SFR represents both units 1 and 2 (3D data). The southern, central, and eastern source area are significantly thinner than the area along the north-eastern headscarp. Material is thickest (ca. 43 m) within the central and along the northern sink area and upslope of the northern fault.

3.5.5 MTD Kinematic Domains

Source Area

By comparing the shape and orientation of the present-day contour lines with those interpolated from outside the scar of Ana Slide and into the slide area (Figure 3.2), the evacuational source area is defined by the downwards excursion of present-day bathymetric contours (representing loss of material). This area extends around $1.5km$ downslope of the easternmost headscarp and is congruent with the upslope limits of R3, R2, and R1 (Figures 3.3 and 3.4). Within the source area, the thickness of Ana Slide is defined by the interval between Ref and SFR or units 1 and 2 and here the source area thickness is significantly thinner compared to outside the scar of Ana Slide and thus the source area was not completely evacuated. Immediately upslope of the by-pass zone the remaining land- slide material experienced shortening, as evidenced by small-scale compressional thrust faults (e.g., Figure 3.6).

The isochron map of Ref—SFR is thickest in the western part of the source area and thinnest in the south-eastern part (Figure 3.4c). In particular, on the northern shoulder, the interval between Ref-SFR is almost twice as thick as on the southern shoulder.

Transitional Domain or "By-Pass Zone"

For Ana Slide the bathymetry shows no significant deviation from the 750 m contour line where the scar of Ana Slide narrows (Figure 3.2) that we define as the transitional domain or more accurate for this study the by-pass zone. It indicates either that no material has been added or removed by the landslide, or that the removed material has been replaced by material coming from the source area with no thickness variation. The zone representing the by-pass zone extends over a downslope distance of about 500 m from approximately 700 to 800 m water depth and coincides with the narrowing of the scar of Ana Slide. The upslope extent of the by-pass zone coincides with the upslope termination of R3, R2 and R1 (Figures 3.4a – c, and 3.6b).

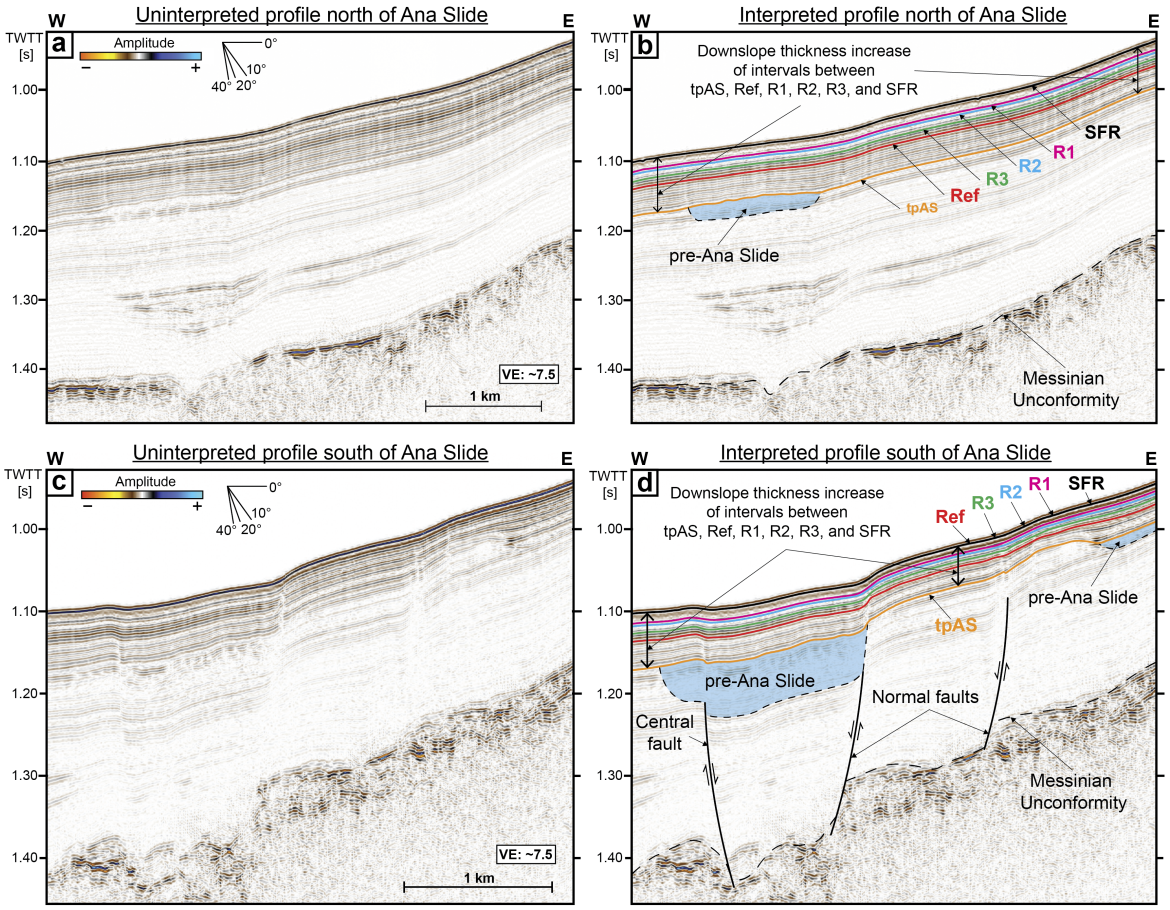

Figure 3.5: (a) Un-interpreted profile (re-processed 2D data) north of Ana Slide (see location in Figure 3.2). (b) Interpreted profile (re-processed 2D data) north of Ana Slide. The intervals between SFR, R1, R2, R3 and Ref thickens in downslope direction representing Unit 2 (Ref-R1) and Unit 1 (R1-SFR). (c) Un-interpreted profile (re-processed 2D data) south of Ana Slide (see location in Figure 3.2). (d) Interpreted profile (re-processed 2D data) south of Ana Slide. The intervals between SFR, R1, R2, R3, and Ref thickens in downslope direction representing Unit 2 (Ref-R1) and Unit 1 (R1-SFR) but are locally controlled by the recent activity of normal faults and the central fault. A visual comparison of the 3D and 2D reflection seismic profiles is presented in Figures 3.16 – 3.21 of Supporting Information S1.

The reflection seismic data provide insight into the kinematics of the by-pass zone. Seismic coherent reflections of Sub-unit 2A above Ref up to R1 (Figure 3.3) continue uninterrupted out of the scar of Ana Slide (Figures 3.7a and b). The isochron maps between Ref—R1, R1—SFR, and Ref—SFR show equal thickness throughout the by-pass zone and the surrounding areas toward the north and south (Figure 3.4). These observations suggest that the by-pass zone is intact in its entirety and that it was not moved at depth between Ref and R1. We would expect to see at least some disruption of the seismic reflections if the by-pass zone had been translated, moved, or affected by the mobilization of landslide material below R1 and therefore the by-pass zone not been part of the failure process.

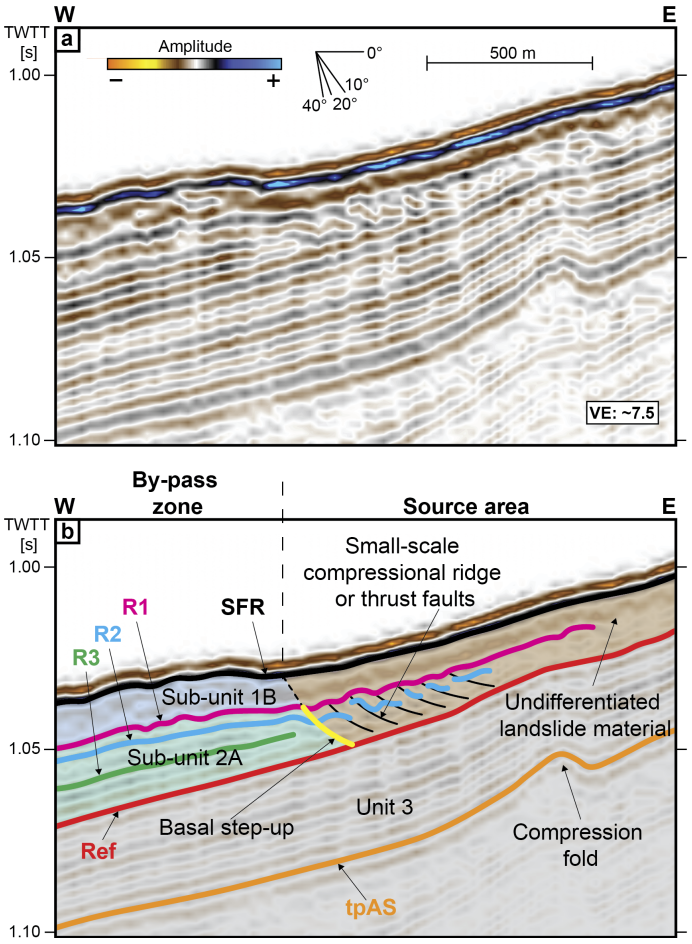

Figure 3.6: (a) Un-interpreted profile (re-processed 2D data) through the by-pass zone (see location in Figure 3.2). (b) Interpreted profile showing small-scale compressional ridges that are located within undifferentiated landslide material immediately upslope of the by-pass zone. A basal step-up exists downslope of the small-scale compressional ridges and material that composes the by-pass zone. A visual comparison of the 3D and 2D reflection seismic profiles is presented in Figures 3.16 to 3.21 of Supporting Information S1.

Sink Area

In the sink area Ref marks the lowest stratigraphic level of observed deformation. Within the sink area the *in-situ* deformation zone is marked by the lateral extent of R3 (Figure 3.4). Toward the front of Ana Slide *in-situ* deformation steps up stratigraphically from Ref to R3, R2, and R1 (Figure 3.3).

The isochron map of Ref—SFR shows thickness variations throughout the sink area (Figure 3.4c). The maximum thickness of 57 ms TWTT (ca. 43 m) occurs around 300 – 500 m upslope of the front of Ana Slide. The isochron map shows a depositional center immediately east of the northern fault that extends toward the northern scar of Ana Slide within the sink area (Figures 3.4b and c). From there, thickness in the interval between Ref—SFR and Ref— R1 decreases gradually to the south and east. The volume of Sub-unit 2B and 2C meaning the material involved in landsliding inside the sink area is 0.058 km^3.

3.6 Discussion

3.6.1 Chronology of Ana Slide

Reflection seismic data allow constraining the relative temporal development of the failure of Ana Slide, the timing of which is poorly constrained in terms of absolute dates (e.g., Cattaneo et al., 2011). The lateral continuity of reflectors and the constant thickness of units outside the scar of Ana Slide indicate that units 1, 2, and 3 have been deposited by relatively steady hemipelagic sedimentation and only within Ana Slide are they reworked by gravity processes (e.g., Figures 3.3, 3.4c, and 3.5). Of these, the failure of Ana Slide involved units 1 and 2.

Unit 1 shows slight thickness variations toward the west and immediately north of Ana Slide (Figure 3.4a). Within the source area, though barely present, Unit 1 is partly represented by undifferentiated landslide material. Inside the scar of Ana Slide Unit 1 is thicker within the sink area compared to outside of it. We thus infer that material of Sub-unit 1A was evacuated from the source area, mobilized on R1 through the by-pass zone and deposited within the sink area, forming parts of Sub-unit 1B. Hence, Sub-Unit 1B is the sum of *in-situ* Sub-Unit 1A and failed and mobilized Sub-Unit 1A (originating from the source area).

Sub-unit 1B lies above material that was previously deposited within the sink area (Figures 3b, 3c, 7c, and 7d) and R1 separates it from the underlying sediments. This previously deposited material relates to Unit 2 located between Ref and R1 that is significantly thickened toward the central sink area immediately upslope of the northern fault (Figure 3.4b). In addition, R1 has a strongly irregular appearance in the sink area (Figures 3.3b and c), which we interpret to represent the top surface of an earlier stage of failure. Hence, Sub-unit 1B depicts a failure that is stratigraphically separated from underlying material beneath R1. The fact that (a) Unit 1 has constant thickness between R1 and SFR outside the scar of Ana Slide, (b) Unit 1 is practically absent in the source area, and (c) R1 separates Unit 1 and Unit 2, indicates that landslide material of sub-units 2B and 2C must have moved prior to deposition and failure of Unit 1. Hence, contrarily to the interpretation of Lastras et al., 2004, Ana Slide comprises two failure events. These are separated in time by the period it took to deposit Unit 1. We call these two events the "primary failure" and the "secondary failure".

Based on a 2 – 3 m thick post-failure drape, Cattaneo et al., 2011 inferred that Ana Slide occurred approximately 61.5 ka B.P. Following our interpretation, this age corresponds to the occurrence time of the secondary failure. The age proposed by (Cattaneo et al., 2011) assumes an average sedimentation rate of around 5 cm/ka for the study area. From the reflection seismic data, we infer an average thickness of Unit 1 of about 15 m, using seismic velocities of 1500 m/s (Figure 3.4a). Assuming no change in sedimentation rate, this would result in a time-lag between the primary and secondary failure of approximately 300 ka. This is a very rough estimate because it is likely that sedimentation rates throughout the

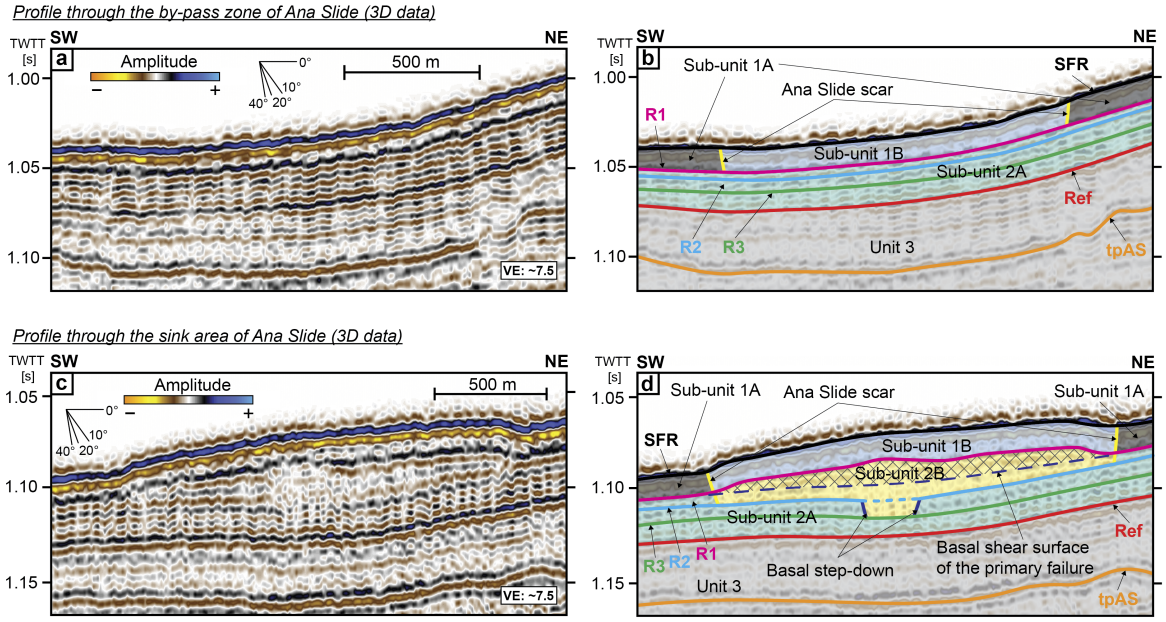

Figure 3.7: Transect profiles through the by-pass zone and sink area of Ana Slide. (a) Uninterpreted transect profile (3D reflection seismic data) through the by-pass zone of Ana Slide (see location in Figures 3.2 and 3.3). 3D reflection seismic profiles on crosslines show receiver ghost as continuous irregularities throughout both profiles (a and c). (b) Interpreted transect profile through the by-pass zone of Ana Slide. Material of Sub-unit 1B is located above un-affected and in-situ slope sediment of Sub-Unit 2a. The outline and scar of Ana Slide is highlighted by solid yellow lines. Note the lack of thickness variation within Ana Slide of units 1 and 2 compared to outside of Ana Slide. (c) Uninterpreted transect profile (3D reflection seismic data) through the sink area of Ana Slide (see location in Figures 3.2 and 3.3). (d) Interpreted transect profile through the sink area of Ana Slide. Material of Sub-unit 2B is significantly thickened within the sink area and extends into material of Sub-unit 2A below. The hatched area represents accumulated landslide material within the sink area. Here, material inside Ana Slide is significantly thickened compared to outside of Ana Slide between Ref and SFR namely by the thickness of Sub-unit 2B.

Eivissa Channel varied due to sea-level oscillations during the late-Quaternary linked to climate variability (Hodge et al., 2008; Tuccimei et al., 2007) and that the seismic velocities are poorly constrained for the study area with the exception of velocities measured from a shallow gravity core (Lafuerza et al., 2012) (Figure 3.2).

3.6.2 Headscarp Retrogression During the Primary and Secondary Failures

The headscarp of Ana Slide is characterized by multiple smaller headscarps linked with "shoulders" in the northern and southern source area (Figure 3.2). The slide plane steps up stratigraphically forming terraces. Each of these terraces has its own headscarp and the shape of the overall headscarp is comprised of these individual segments resulting in a cauliflower-shape, which has been shown as typical morphology for retrogressive landslide behavior (Micallef et al., 2008). The observation of at least two shoulders therefore suggests that the present-day head- scarp of Ana Slide formed by multiple failures and retrogression. In addition, the relative position and size of the Ana Slide headscarp segments suggest

that the failures associated with retrogression involved smaller amounts of material during successive failure. It is not possible to relate individual headscarp segments to the primary and secondary failures discussed above.

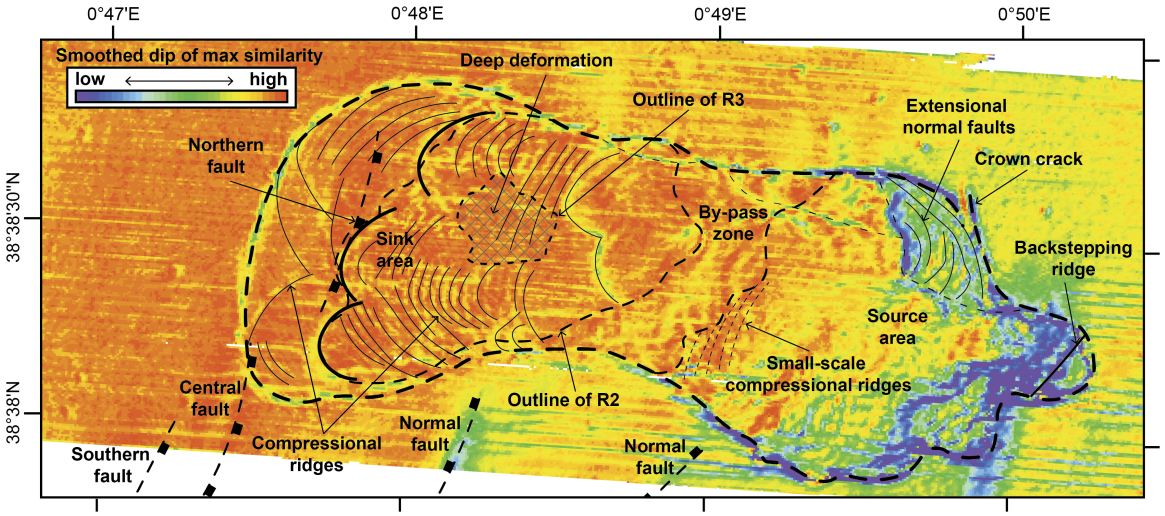

Figure 3.8: Seismic attribute map calculated on SFR (*Smoothed Dip of Maximum Similarity* — RockSolid Attributes from the 3D reflection seismic data). Kinematic features such as extensional ridges within the limited mobilized material within the northern source area, small-scale compressional ridges immediately upslope of the by-pass zone, and numerous compressional ridges throughout the sink area are highlighted. The backstepping ridge indicates easternmost headscarp retrogression during the secondary failure (Figure 3.10).

We observe a crown-crack along the northern headscarp of Ana Slide (Figure 3.2). Here within the northern source the slope gradient is gentler compared to that within the central and southern source areas (Figure 3.2). Crown-cracks have been described to form as a result of extensional stresses related to upslope propagating retrogressive failures (Frey-Martinez et al., 2005; Varnes, 1978). We therefore interpret that this crown-crack was generated by latest headscarp retrogression, because material within the northern source area immediately downslope of the present-day headscarp was mobilized a limited distance downslope during the secondary failure (Figure 3.9). Consequently, the crown-crack also developed during this stage as one of the latest features. Ultimately, the crown-crack is the expression of retrogression that was unable to propagate further upslope probably controlled by the gentler slope gradient within the northern source area.

3.6.3 Evolution and Emplacement of the Primary Failure

Unit 2 is thicker than Unit 1 (Figure 3.3) and the isochore map of both units shows a thinner central and southern source area (Figure 3.4c). This indicates the location from where most landslide material was evacuated as Unit 2 is thinned inside the scar of Ana Slide compared to outside of it, thus representing evacuation from the source area. Throughout the by-pass zone landslide material was neither added nor removed during the primary failure. The main accumulation features, that is, the three primary lobes, are located around 300

– 500 m upslope of the front of Ana Slide (Figures 3.2 and 3.8). Thus, landslide material mainly accumulated within the central sink area. This probably happened during the earliest part of the primary failure because landslide material did not reach all the way to the front of Ana Slide as documented by the location of thick material of Unit 2 immediately upslope of the northern fault (Figure 3.4c). During a later part of the primary failure, landslide material reached the northern sink area, constrained by the positive topographic relief along the northern lateral margin (Figures 3.2, 3.7c, and d) and orientation of the northern primary lobe further toward the west-north-west compared to the central primary lobe that is orientated more toward the west. The southern primary lobe formed at the latest part of the primary failure, as the central sink area was already infilled by previously accumulated landslide material. During the secondary failure landslide material ran out within the whole sink area, as shown by compressional ridges in the isochore map of Unit 1, which are located sub-parallel to and reach the front of Ana Slide (Figure 3.4a). If these compressional ridges where exclusively generated during the secondary failure or were also affected by the post-failure seafloor after the primary failure is unclear.

3.6.4 Evolution and Emplacement of the Secondary Failure

The difference in thickness of Unit 1 between inside and outside the scar of Ana Slide is less significant within the sink area compared to Unit 2 (Figure 3.4a). In addition, Unit 1 is generally thinner throughout the study area compared to Unit 2 (Figure 3.3). Hence, the secondary failure involved relatively small amounts of landslide material compared to the primary failure. Compressional ridges observed in Unit 1 are located sub-parallel to and reach the front of Ana Slide and characterize one overall orientation of movement of landslide material during the secondary failure (Figure 3.4a). During this, landslide material was fully mobilized throughout the by-pass zone above R1 as the thickness of Sub-unit 1B in this area equals that of Sub-unit 1A outside the scar of Ana Slide. Thus, neither accumulation nor deposition of landslide material occurred in the by-pass zone during the secondary failure. In addition, the headscarp retrogressed the farthest eastwards, that is, some hundred meters upslope of the location of the steepest slope gradient within the easternmost headscarp (Figure 3.3). The shoulders and the eastern-most headscarp outline consequently smaller areas while the backstepping ridge marks the location of the latest retrogression (Figure 3.8). Compared to the primary failure with the extensive evacuation of landslide material from the source area, less extensive evacuation from the source area occurred during the secondary failure. Further, undifferentiated landslide material represents both ponded material from the primary and secondary failures.

Material located between Ref and SFR immediately downslope of the head- scarp within the northern source area shows small-scale extensional ridges linked to small-scale normal faults (Figure 3.9). This material was initially linked to Sub-unit 2A, but it was not mobilized during the primary failure. This material occurs within the northern source area at present and

thus also remained *in-situ* during the primary failure. After the primary failure hemipelagic sedimentation deposited Unit 1 between R1 and SFR. During the secondary failure material of Unit 1 was evacuated from the northern source area and the headscarp retrogressed to the location of the present-day headscarp (Figure 3.10c). Since inherent material of Unit 2 at this location shows small-scale extensional ridges but was not fully evacuated, we interpret this material to have experienced limited downslope mobilization during the secondary failure. In addition, this material changed apparent stratigraphic identity from being part of Unit 2 to material of Sub-unit 1B because it was affected first during the secondary failure.

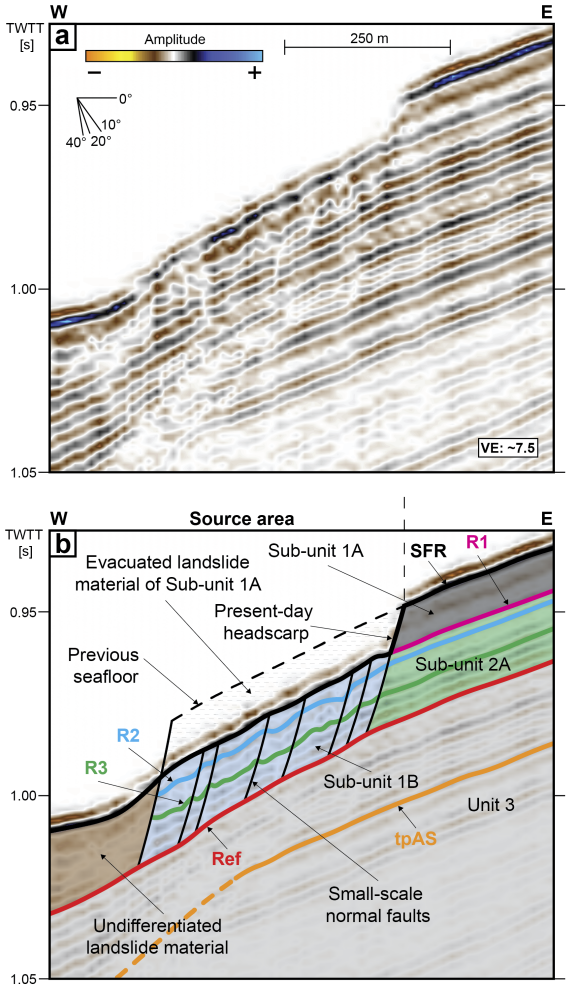

Figure 3.9: Caption on next page.

Figure 3.9: (Figure on previous page.) (a) Uninterpreted profile (re-processed 2D data) through the northern source area (see location in Figure 3.2). (b) Interpreted profile showing (re-processing 2D data) showing material formerly of Sub-unit 2A (light blue) previously in-situ and un-affected. This material changed apparent stratigraphic identify during the secondary failure with the general of small-scale extensional normal faults that terminate at depth above Ref. These small-scale extensional normal faults document that the material of Sub-unit 1B (formerly Sub-Unit 2A) was deformed in-situ by the evacuation of landslide material of Sub-unit 1A above. A visual comparison of the 3D and 2D reflection seismic profiles is presented in Figures 3.16 to 3.21 of Supporting Information S1.

3.6.5 Structural and Morphological Controls on Landslide Emplacement

The emplacement of Ana Slide encompasses the active processes of evacuation, mobilization, and accumulation of landslide material. A small amount of material represented by the "undifferentiated landslide material" ponded upslope against the by-pass zone. This material was unable to step up and above R1 and the by-pass zone that acted as an obstacle to the downslope propagation of landslide material. Also, undifferentiated landslide material partly remained at this position during the primary and secondary failures but if the small-scale thrust faults were generated mainly during primary or secondary failure is inconclusive (Figure 3.6). The largest part of the landslide material mobilized during both failures stepped up and over by-pass zone and accumulated within the sink area (Figures 3.3c and 3.4b).

Moernaut and De Batist, 2011 propose that when a failure is able to overrun an obstacle and emerges frontally, the source area will evacuate in an unconfined manner. The failing landslide material will accelerate gaining kinematic energy and will be able to empty the source area of landslide material. As the primary failure of Ana Slide involved larger amounts of material than the secondary failure this may be an explanation as to why the secondary failure left some material ponded against the by-pass zone. The small-scale compressional thrust faults within the undifferentiated landslide material might thus have been created during the primary failure, similar to compressional thrusts faults toward the front of submarine landslide as the movement experiences basal step-up. Alternatively, during the secondary failure deformational processes during the by-pass of landslide material occurred. Similar ponding also occurred at the northern fault, which acted as another obstacle against the downslope propagation of landslide material within the central sink area (Figure 3.4b). This fault generated a local basin upslope of its location, which was infilled by landslide material from the primary failure. The infill smoothed the seafloor morphology and therefore landslide material mobilized during the secondary failure could have more easily ran out within the sink area and have reached all the way toward the front of Ana Slide. The northern fault acted as a controlling mechanism to the emplacement of Ana Slide and as an obstacle to the downslope propagation of mobilized landslide material mainly during the primary failure. This means that the seafloor was already affected by the central and northern faults prior to the primary failure. Hence, accumulated landslide material mainly of the primary failure is located NE-SW above the northern fault.

Strongly imprinted on tpAS, there exists a compression fold at tpAS immediately toward the west of the by-pass zone (Figures 3.3 and 3.6). The small-scale compressional thrusts faults were likely created by the interplay of frontal emergence of both stages of failure from Ref toward R1 between the source and by-pass zone and from a morphological jump for the downslope propagation of failure controlled by the compression fold during the primary and secondary failure.

Although landslide material accumulated primarily around 300 – 500 m upslope of the front of Ana Slide and upslope of the northern fault (Figures 3.4b, and c, and 3.8), compressional ridges are located at depth toward the front of Ana Slide (Figure 3.3c). This is observed between R3 and R2 and immediately below R1 (Figure 3.3). These compressional ridges were presumably generated by landslide material from the primary failure that bulldozed inherently un-affected slope sediment because the amount of landslide material was significantly larger during the primary than the secondary failure. Furthermore, the compressional ridges are located at depth below R1 that constituted the seafloor at the time of the primary failure and are thus the result of bulldozing landslide material into the footwall of the northern fault.

Figure 3.10: (Figure on next page.) Interpretative development sketch of Ana Slide. (a) Early stage of primary failure (ca. 300 ka.). The central and northern primary lobes are formed within the sink area that are sourced by material evacuated from the central and southern source area. These primary lobes relate to retrogression of secondary headscarps inside the eastern source area. In-situ deformation is induced around 300 – 500 m upslope of the northern fault inside the sink area. (b) Consecutive headscarp retrogression during the late stage of the primary failure (at 300 ka.). This process presumably evacuated more landslide material from the source area and generated the southern primary lobe within the southern sink area with generation of compressional ridges throughout the sink area. (c) Limited mobilization of material within the northern source area (ca. 65 ka.). The easternmost headscarp is generated by retrogression upslope of the backstepping ridge. Landslide material ran out within the whole sink area and generated compressional ridges sub-parallel with the front of Ana Slide. Small-scale compressional ridges were generated upslope of the by-pass zone linked to a structural control. (d) Compilation of kinematic features observed from the bathymetry, and slope gradient and seismic attribute map (at 65 ka. (present-day)) (Figure 3.9).

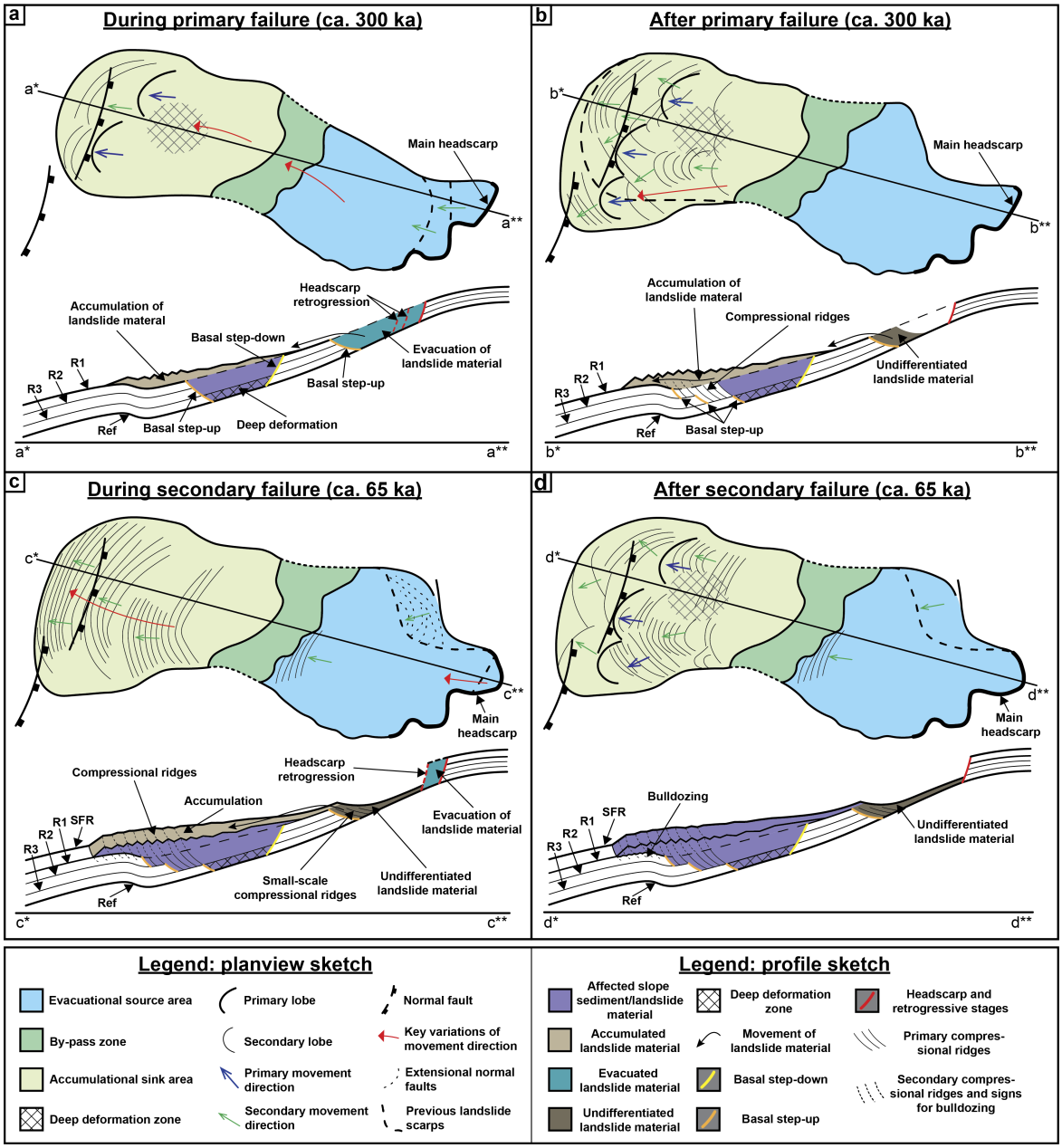

Figure 3.10: (Caption on previous page.)

3.6.6 Causal Factors Between Fault Activity and Landsliding

The southern, central, and northern faults represent slope anti-thetic normal faults of unknown origin (Figures 3.3, 3.5c, and d). These faults modified the seafloor in the study area prior to the occurrence of Ana Slide. The faults could have acted as fluid conduits that resulted in gas-charging of the shallow sub-surface. Gas-charging may reduce the frictional resistance of sediments, thus acting as a pre-conditioning to slope failure (e.g., Kaminski et al., 2021). Seismogenic fault activity might have acted as a trigger mechanism. However, the role of the faults in both pre-conditioning and triggering remains inconclusive.

3.6.7 Identification of the Basal Shear Surfaces

Classic models for landslides describe one common basal shear surface through the source area, translational domain and sink area with possible upslope secondary basal shear surfaces created during retrogression (e.g., Bull et al., 2009; Frey-Martinez et al., 2005; Frey-Martinez et al., 2006). This does not hold true for Ana Slide because two basal shear surfaces existed inside the sink area for the primary and the late-stage failures. Within the source area, the basal shear surface followed Ref toward the by-pass zone. Throughout the by-pass zone, the basal shear surface of the primary failure stepped up and over *in-situ* and un-affected material and thus followed the seafloor at the time of failure (Figures 3.3, 3.10a, and b). Within the sink area during the primary failure the basal shear surface was located at the seafloor (represented by R1 outside the scar of Ana Slide) while the base of deformation reached to depth of Ref (Figure 3.3). It is not easily discernible in the reflection seismic data, but the basal shear surface in the sink area during the primary failure must have been located within sub-units 2B and 2C (Figure 3.3c) as these units are significantly thicker than Sub-unit 2A (Figures 3.3c and 3.4b). During the secondary failure the basal shear surface inside the source area was located above Ref inside undifferentiated landslide material (Figures 3.3 and 3.10c). While we cannot conclusively constrain the identity of undifferentiated landslide material within the source area, landslide material of the secondary failure was certainly mobilized above Ref and stepped up and over *in-situ* and unaffected slope sediment of the by-pass zone. Inside the by-pass zone and into the sink area the basal shear surface at the time of the secondary failure was located between R1 and SFR (Figure 3.10c).

Both the primary and secondary failures of Ana Slide were frontally emergent inside the source area because they stepped up toward the seafloor (R1) immediately upslope of the by-pass zone at the time of their respective occurrences (Figures 3.10a and c). Inside the sink area landslide material ran up against un-affected slope sediment downslope and thus both the primary and secondary failures were frontally confined within the sink area.

3.6.8 In-Situ Deformation Beneath Landslide Deposit

In recent years, a new consensus arose from studies of (Sobiesiak et al., 2016; Sobiesiak et al., 2018) distinguishing a set of basal interactions, that is, basal erosion, liquefaction and substrate deformation. These authors proposed that, in principle, basal interaction of some form might occur within the substrate beneath an overriding mass of landslide material. On the seismic scale (5–50 m) these deformational processes produce cryptic reflections that appear as low-amplitude transparent to chaotic seismic facies (e.g., Ford et al., 2021).

For Ana Slide, the basal shear surface of the primary failure is identified to have been located at the depth of R1 parallel to Ref inside sub-units 2B and 2C (stippled dark blue line in Figure 3.3c). Consequently, sub-units 2B and 2C involve material that respectively experienced apparent high and moderate degrees of deformation assuming that the increasingly chaotic

seismic character corresponds to increasing *in-situ* deformation (Figure 3.3) while leaving the by-pass zone un-affected.

During the primary failure of Ana Slide landslide material mainly reached the central sink area upslope of the northern fault (Figure 3.4b). Accumulated landslide material was rapidly deposited within the sink area and able to load un-affected slope sediment. Sun and Alves, 2020 show that MTDs generally have lower water content, porosity and permeability compared to background hemipelagic sediments. The rapid deposition of this relatively low water content, porosity, and permeability landslide material during the primary failure could have induced overpressure within hemipelagic sediments immediately beneath. This then acted as a "sealing lid" and loaded the seafloor and slope sediment of Unit 2A that change stratigraphic identify to Sub-Unit 2B and 2C. Low-amplitude seismic facies in Sub-unit 2B could be related to discontinuous reflectors due to some small-scale disturbance and interruptions of sediment layering because rapidly deposited landslide material prevented the vertical dissipation of excess pore pressure. The observation that the location of *in-situ* deformation is congruent with the location of thickest landslide deposits involved during the primary failure supports this hypothesis. A similar process has been suggested by Lenz et al., 2018 offshore Oregon, where rapidly deposited sedimentary blocks induced *in-situ* deformation within the immediate substrate. Deformation in Ana Slide possibly was further facilitated by the presence of fluids and gas as proposed by Berndt et al., 2012 in the overburden immediately above and east of the northern fault along Ref. The location of *in-situ* deformation within the sink area could thus be linked with deformation that only occurred some hundred meters upslope of the northern fault. The extent of *in-situ* deformation furthermore coincides with the fluid and gas migration vertically along the northern fault and horizontally along Ref approximately to the downslope extent of the by-pass zone (Figure 3.4).

Alternatively, the accumulating landslide material sheared the substrate below the interpreted basal shear surface down to Ref (Figure 3.3). Similar processes have been described for debris avalanches from a volcanic island in Papua New Guinea (Kühn et al., 2021). Since the by-pass zone has not been part of Ana Slide and remained un-affected during the primary and secondary failures shearing would also have deformed material within the by-pass zone beneath R1 and down to Ref. Hence, shearing of overriding landslide material seems improbable to explain the observed deformation.

It is, however, questionable if the process of loading is solely responsible for the observed deformation. Ultimately, we are unable to differentiate the loading from the shearing hypothesis, as they may have acted at the same time. Landslides develop dynamically over large distances, and several factors and processes may be responsible for kinematic features, with both processes acting concomitantly.

3.6.9 Implications for the Development and Emplacement of Submarine Landslides

Our detailed analysis of Ana Slide reveals emplacement processes differing from those previously suggested, most often based on bathymetry and 2D reflection seismic data. Lastras et al., 2004 interpreted the by-pass zone to be comprised of rotated intact blocks and the *in-situ* sediment deformation in the sink area as part of Ana Slide. Consequently, the estimated landslide volume was much larger compared to the model we propose, in which the deformed and affected slope sediment inside the sink area was not per se part of landslide material of Ana Slide. Furthermore, Ana Slide was interpreted as an exemplary frontally confined landslide. In contrast, we show that it is a mixed system. In the following, we use the example of Ana Slide (imaged in its entirety) to identify potential pitfalls when analyzing emplacement processes of submarine landslides that are only partly imaged.

3.6.9.1 Intact Blocks

Stratified and non-disturbed areas in reflection seismic profiles within submarine landslides are a common observation and are usually referred to as "intact blocks" (e.g., Bull et al., 2009). It is only with 3D reflection seismic data covering the whole landslide that we were able to identify that the by-pass zone (interpreted as an intact block previously) was not part of the landslide but remained entirely un-affected. Consequently, caution must be taken when areas with conformal stratigraphic layering are identified within the landslide as these may represent *in-situ* and un-affected slope sediment instead of mobilized blocks. Furthermore, the fact that previously identified blocks inside a MTD may represent *in-situ* slope sediment greatly depends on their location and kinematics within the MTD (e.g., Bull et al., 2009). Ultimately, the MTD term is kinematically problematic, as it infers that the material was moved and involved by the failure.

3.6.9.2 Deformation of Underlying Sediment

We suggest that the deposition of landslide material is able to deform a thick interval underneath. This highlights the potential of deformational processes observed for Ana Slide to penetrate deep into the subsurface (Figure 3.3). It is important to note that affected and deformed slope sediment within the sink area may not represent actual MTD material and should not be attributed to the actual volume of material mobilized during the landslide.

3.6.9.3 Complex Failure

The scar of Ana Slide includes a wide source area with additional upslope retrogressing headscarps, a narrow by-pass zone, and a wide lobe-shaped sink area (Figure 3.2). Such a

geometry might indicate a relatively "simple" failure and emplacement process, in which the one age obtained through sampling represents the approximate timing of this landslide. However, our detailed analysis shows that Ana Slide involved multiple failure stages and complex emplacement processes, pointing to an overall complex behavior that likely is reproduced in other submarine landslides.

3.6.9.4 Landslide Volumes

The volume of Ana Slide inferred from the volume of material accumulated inside the sink area is around 0.058 km^3 (+/<10 %) calculated between Ref and R1. This volume is significantly smaller than that calculated by Lastras et al., 2004 of 0.14 km^3 and does likely not represent the tsunamigenic material but much *in-situ* deformation that does not add to the tsunamigenic potential of Ana Slide. It is worth acknowledging that the slide volume is not the only important parameter controlling the tsunamigenic potential of a submarine landslide. It could be even with a smaller volume, if it undergoes higher acceleration, that it induces could induce a similar magnitude tsunami compared with larger lower acceleration landslides.

3.7 Conclusions

Our detailed examination of a high-resolution 3D seismic data set covering an entire submarine landslide (Ana Slide) reveals important new insights into the kinematic development of this landslide. Ana Slide is the result of two main stages of failure: a more voluminous primary failure and a smaller secondary failure separated by a time-lag of several hundreds of thousands of years. Both the primary and secondary failure were frontally emergent from the source areas and frontally confined in the sink area. A by-pass zone consisting of undisturbed *in-situ* slope sediment separates the source and the sink areas. Sediments underneath the deposit of Ana Slide show evidence for deformation, which was likely caused by rapid loading of the seafloor by the deposit. Both the by-pass zone and *in-situ* deformation had previously been accounted as landslide material. Consequently, these previous studies overestimated the volume and therewith the tsunamigenic potential of Ana Slide. If similar processes of emplacement and *in-situ* deformation below a basal shear surface deep into the subsurface are at play for other submarine landslides remains speculative but such processes are not inconceivable for frontally emergent landslides.

Acknowledgments

The 3D reflection seismic data was acquired as part of the EC-funded HERMIONE project (ref. 226354-HERMIONE). Also, the Spanish CONSOLIDER-INGENIO 2010 "GRAC-

CIE" project (ref. CSD2007 – 00067) contributed to this research. We thank the master and the crew of RRS Charles Darwin who facilitated data acquisition during voyage 178, and Frode Eriksen of VBPR, Oslo for technical support on the same cruise. IHS Markit provided academic licenses for KingdomSuite and Schlumberger for OMEGA. This study was supported by the DFG (Deutsche Forschungsgemeinschaft) Verbundprojekt UR 226/3 – 1 and GR 1024/35 – 1 by MU, Juergen Grabe of the TUHH, Hamburg, Germany, and CB. MC and GL acknowledge support from a Grups de Recerca Consolidats (excellence research groups) Grant to GRC Geociències Marines (ref. 2017 SGR 315) by the Government of Catalonia.

Author Contributions

Conceptualization: TFS, MU, CB; Data curation: CP, GL, MC, CB; Formal analysis: TFS, GL, MC, CB; Funding acquisition: MU, CB; Investigation: TFS; Methodology: TFS, CB; Project administration: MU, CB; Resources: TFS; Software: CP; Visualization: TFS has produced all figures (Figures 1 to 10).

Data availability statement

2D and 3D reflection seismic data used for integrated seismic interpretation of Ana Slide presented in this study are available at World Data Centre Pangaea: `https://doi.org/10.1594/PANGAEA.943506` (3D reflection seismic data); `https://doi.org/10.1594/PANGAEA.943523` (2D re-processed reflection seismic data).

References

Alves, T. M. and J. A. Cartwright (2009). Volume Balance of a Submarine Landslide in the Espírito Santo Basin, Offshore Brazil: Quantifying Seafloor Erosion, Sediment Accumulation and Depletion. In: *Earth and Planetary Science Letters* 3-4, pp. 572–580. DOI: 10.1016/j.epsl.2009.10.020.

Barrett, R., E. Lebas, R. Ramalho, I. Klaucke, S. Kutterolf, A. Klügel, K. Lindhorst, F. Gross, and S. Krastel (2020). Revisiting the Tsunamigenic Volcanic Flank Collapse of Fogo Island in the Cape Verdes, Offshore West Africa. In: *Geological Society, London, Special Publications* 1, pp. 13–26. DOI: 10.1144/SP500-2019-187.

Berndt, C., S. Costa, M. Canals, A. Camerlenghi, B. de Mol, and M. Saunders (2012). Repeated Slope Failure Linked to Fluid Migration: The Ana Submarine Landslide Complex, Eivissa Channel, Western Mediterranean Sea. In: *Earth and Planetary Science Letters*, pp. 65–74. DOI: 10.1016/j.epsl.2011.11.045.

Bondevik, S., F. Løvholt, C. Harbitz, J. Mangerud, A. Dawson, and J. Inge Svendsen (2005). The Storegga Slide Tsunami – Comparing Field Observations with Numerical Simulations. In: *Marine and Petroleum Geology* 1-2, pp. 195–208. DOI: 10.1016/j.marpetgeo.2004.10.003.

Bryn, P., K. Berg, C. F. Forsberg, A. Solheim, and T. J. Kvalstad (2005). Explaining the Storegga Slide. In: *Marine and Petroleum Geology* 22.1-2, pp. 11–19. DOI: 10.1016/j.marpetgeo.2004.12.003.

Bugge, T., S. Befring, R. H. Belderson, T. Eidvin, E. Jansen, N. H. Kenyon, H. Holtedahl, and H. P. Sejrup (1987). A Giant Three-Stage Submarine Slide off Norway. In: *Geo-Marine Letters* 4, pp. 191–198. DOI: 10.1007/BF02242771.

Bull, S., J. Cartwright, and M. Huuse (2009). A Review of Kinematic Indicators from Mass-Transport Complexes Using 3D Seismic Data. In: *Marine and Petroleum Geology* 7, pp. 1132–1151. DOI: 10.1016/j.marpetgeo.2008.09.011.

Canals, M. and E. Ballesteros (1997). Production of Carbonate Particles by Phytobenthic Communities on the Mallorca-Menorca Shelf, Northwestern Mediterranean Sea. In: *Deep Sea Research Part II: Topical Studies in Oceanography* 3-4, pp. 611–629. DOI: 10.1016/S0967-0645(96)00095-1.

Cattaneo, A., D. Minisini, A. Asioli, M. Canals, G. Lastras, A. Remia, N. Sultan, and M. Taviani (2011). Age Constraints and Sediment Properties of Ana Slide (Balearic Sea, Western Mediterranean) and Implications on Age Dating of Submarine Landslides. In: EGU 2011 - Abstract. DOI: 10.1007/978-90-481-3071-9_42.

Clare, M., J. Chaytor, O. Dabson, D. Gamboa, A. Georgiopoulou, H. Eady, J. Hunt, C. Jackson, O. Katz, S. Krastel, R. Le0n, A. Micallef, J. Moernaut, R. Moriconi, L. Moscardelli, C. Müller, A. Normandeau, M. Patacci, M. Steventon, M. Urlaub, D. Völker, L. Wood, and Z. Jobe (2019). A Consistent Global Approach for the Morphometric Characterization of Subaqueous Landslides. In: *Geological Society, London, Special Publications* 1, pp. 455–477. DOI: 10.1144/SP477.15.

del Valle, L., L. Gómez-Pujol, J. J. Fornós, A. Timar-Gabor, V. Anechitei–Deacu, and F. Pomar (2016). Middle to Late Pleistocene Dunefields in Rocky Coast Settings at Cala Xuclar (Eivissa, Western Mediterranean): Recognition, Architecture and Luminescence Chronology. In: *Quaternary International*, pp. 4–13. DOI: 10.1016/j.quaint.2016.01.050.

Farrell, S. (1984). A Dislocation Model Applied to Slump Structures, Ainsa Basin, South Central Pyrenees. In: *Journal of Structural Geology* 6, pp. 727–736. DOI: 10.1016/0191-8141(84)90012-9.

Ford, J., R. Urgeles, A. Camerlenghi, and E. Gràcia (2021). Seismic Diffraction Imaging to Characterize Mass-Transport Complexes: Examples From the Gulf of Cadiz, South West Iberian Margin. In: *Journal of Geophysical Research: Solid Earth* 3. DOI: 10.1029/2020JB021474.

Frey-Martinez, J., J. Cartwright, and B. Hall (2005). 3D Seismic Interpretation of Slump Complexes: Examples from the Continental Margin of Israel. In: *Basin Research* 1, pp. 83–108. DOI: 10.1111/j.1365-2117.2005.00255.x.

Frey-Martinez, J., J. Cartwright, and D. James (2006). Frontally Confined versus Frontally Emergent Submarine Landslides: A 3D Seismic Characterisation. In: *Marine and Petroleum Geology* 5, pp. 585–604. DOI: 10.1016/j.marpetgeo.2006.04.002.

Fruergaard, M., S. Piasecki, P. Johannessen, N. Noe-Nygaard, T. Andersen, M. Pejrup, and L. Nielsen (2015). Tsunami Propagation over a Wide, Shallow Continental Shelf Caused by the Storegga Slide, Southeastern North Sea, Denmark. In: *Geology*, G37151.1. DOI: 10.1130/G37151.1.

Haflidason, H., R. Lien, H. P. Sejrup, C. F. Forsberg, and P. Bryn (2005). The Dating and Morphometry of the Storegga Slide. In: *Marine and Petroleum Geology* 1-2, pp. 123–136. DOI: doi.org/10.1016/j.marpetgeo.2004.10.008.

Haflidason, H., H. P. Sejrup, A. Nygård, J. Mienert, P. Bryn, R. Lien, C. F. Forsberg, K. Berg, and D. Masson (2004). The Storegga Slide: Architecture, Geometry and Slide Development. In: *Marine Geology* 1-4, pp. 201–234. DOI: 10.1016/j.margeo.2004.10.007.

Harbitz, C. B., F. Løvholt, and H. Bungum (2014). Submarine Landslide Tsunamis: How Extreme and How Likely? In: *Natural Hazards* 3, pp. 1341–1374. DOI: 10.1007/s11069-013-0681-3.

Haugen, K. B., F. Løvholt, and C. B. Harbitz (2005). Fundamental Mechanisms for Tsunami Generation by Submarine Mass Flows in Idealised Geometries. In: *Marine and Petroleum Geology* 1-2, pp. 209–217. DOI: 10.1016/j.marpetgeo.2004.10.016.

Hodge, E. J., D. A. Richards, P. L. Smart, A. Ginés, and D. P. Mattey (2008). Sub-Millennial Climate Shifts in the Western Mediterranean during the Last Glacial Period Recorded in a Speleothem from Mallorca, Spain. In: *Journal of Quaternary Science* 8, pp. 713–718. DOI: 10.1002/jqs.1198.

Huehnerbach, V., D. Masson, et al. (2004). Landslides in the North Atlantic and Its Adjacent Seas: An Analysis of Their Morphology, Setting and Behaviour. In: *Marine Geology* 1-4, pp. 343–362. DOI: doi.org/10.1016/j.margeo.2004.10.013.

Jackson, C. A.-L. (2011). Three-Dimensional Seismic Analysis of Megaclast Deformation within a Mass Transport Deposit; Implications for Debris Flow Kinematics. In: *Geology* 3, pp. 203–206. DOI: 10.1130/G31767.1.

Kaminski, P., T. Sager, J. Grabe, and M. Urlaub (2021). A New Methodology to Assess the Potential of Conjectural Trigger Mechanisms of Submarine Landslides Exemplified by Marine Gas Occurrence on the Balearic Promontory. In: *Engineering Geology*, p. 106446. DOI: 10.1016/j.enggeo.2021.106446.

Krastel, S., W. Li, M. Urlaub, A. Georgiopoulou, R. B. Wynn, T. Schwenk, C. Stevenson, and P. Feldens (2019). Mass Wasting along the NW African Continental Margin. In: *Geological Society, London, Special Publications* 1, pp. 151–167. DOI: 10.1144/SP477.36.

Kühn, M., J. Karstens, C. Berndt, and S. F. Watt (2021). Seismic Reconstruction of Seafloor Sediment Deformation during Volcanic Debris Avalanche Emplacement Offshore Sakar, Papua New Guinea. In: *Marine Geology*, p. 106563. DOI: 10.1016/j.margeo.2021.106563.

Kvalstad, T. J., F. Nadim, A. M. Kaynia, K. H. Mokkelbost, and P. Bryn (2005). Soil Conditions and Slope Stability in the Ormen Lange Area. In: *Marine and Petroleum Geology* 1-2, pp. 299–310. DOI: 10.1016/j.marpetgeo.2004.10.021.

Lackey, J., G. Moore, and M. Strasser (2018). Three-Dimensional Mapping and Kinematic Characterization of Mass Transport Deposits along the Outer Kumano Basin and Nankai Accretionary Wedge, Southwest Japan. In: *Progress in Earth and Planetary Science* 1, p. 65. DOI: 10.1186/s40645-018-0223-4.

Lafuerza, S., N. Sultan, M. Canals, G. Lastras, A. Cattaneo, J. Frigola, S. Costa, and C. Berndt (2012). Failure Mechanisms of Ana Slide from Geotechnical Evidence, Eivissa Channel, Western Mediterranean Sea. In: *Marine Geology*, pp. 1–21. DOI: 10.1016/j.margeo.2012.02.010.

Lastras, G., M. Canals, D. Amblas, M. Ivanov, B. Dennielou, L. Droz, A. Akhmetzhanov, and TTR-14 Leg 3 Shipboard Scientific Party (2006). Eivissa Slides, Western Mediterranean Sea: Morphology and Processes. In: *Geo-Marine Letters* 4, pp. 225–233. DOI: 10.1007/s00367-006-0032-4.

Lastras, G., M. Canals, R. Urgeles, J. E. Hughes-Clarke, and J. Acosta (2004). Shallow Slides and Pockmark Swarms in the Eivissa Channel, Western Mediterranean Sea. In: *Sedimentology* 4, pp. 837–850. DOI: 10.1111/j.1365-3091.2004.00654.x.

Lenz, B., D. Sawyer, B. Phrampus, K. Davenport, and A. Long (2018). Seismic Imaging of Seafloor Deformation Induced by Impact from Large Submarine Landslide Blocks, Offshore Oregon. In: *Geosciences* 1, p. 10. DOI: 10.3390/geosciences9010010.

Løvholt, F., S. Bondevik, J. S. Laberg, J. Kim, and N. Boylan (2017). Some Giant Submarine Landslides Do Not Produce Large Tsunamis: Giant Landslide Tsunamis. In: *Geophysical Research Letters* 16, pp. 8463–8472. DOI: 10.1002/2017GL074062.

Maillard, A. and A. Mauffret (2013). Structure and Present-Day Compression in the Offshore Area between Alicante and Ibiza Island (Eastern Iberian Margin). In: *Tectonophysics*, pp. 116–130. DOI: 10.1016/j.tecto.2011.07.007.

Masson, D., C. Harbitz, R. Wynn, G. Pedersen, and F. Løvholt (2006). Submarine Landslides: Processes, Triggers and Hazard Prediction. In: *Philosophical Transactions of the Royal Society A: Mathematical, Physical and Engineering Sciences* 1845, pp. 2009–2039. DOI: 10.1098/rsta.2006.1810.

Mauffret, A., B. Durand de Grossouvre, A. Tadeu Dos Reis, C. Gorini, and A. Nercessian (2001). Structural Geometry in the Eastern Pyrenees and Western Gulf of Lion (Western Mediterranean). In: *Journal of Structural Geology* 11, pp. 1701–1726. DOI: 10.1016/S0191-8141(01)00025-6.

Micallef, A., C. Berndt, D. G. Masson, and D. A. Stow (2008). Scale Invariant Characteristics of the Storegga Slide and Implications for Large-Scale Submarine Mass Movements. In: *Marine Geology* 1-2, pp. 46–60. DOI: 10.1016/j.margeo.2007.08.003.

Mitchum, R., P. R. Vail, and S. Thompson III (1977). Seismic stratigraphy and global changes of sea level: Part 2. The depositional sequence as a basic unit for stratigraphic analysis: Section 2. Application of seismic reflection configuration to stratigraphic interpretation. In: *Subject Group: Seismic Stratigraphy, Sequence Stratigraphy.*

Moernaut, J. and M. De Batist (2011). Frontal Emplacement and Mobility of Sublacustrine Landslides: Results from Morphometric and Seismostratigraphic Analysis. In: *Marine Geology* 1-4, pp. 29–45. DOI: 10.1016/j.margeo.2011.05.001.

Nugraha, H. D., C. A.-L. Jackson, H. D. Johnson, and D. M. Hodgson (2020). Lateral Variability in Strain along the Toewall of a Mass Transport Deposit: A Case Study from the Makassar Strait, Offshore Indonesia. In: *Journal of the Geological Society* 6, pp. 1261–1279. DOI: 10.1144/jgs2020-071.

Ogata, K., J. Mountjoy, G. Pini, A. Festa, and R. Tinterri (2014). Shear Zone Liquefaction in Mass Transport Deposit Emplacement: A Multi-Scale Integration of Seismic Reflection and Outcrop Data. In: *Marine Geology*, pp. 50–64. DOI: 10.1016/j.margeo.2014.05.001.

Panieri, G., A. Camerlenghi, I. Cacho, C. S. Cervera, M. Canals, S. Lafuerza, and G. Herrera (2012). Tracing Seafloor Methane Emissions with Benthic Foraminifera: Results from the Ana Submarine Landslide (Eivissa Channel, Western Mediterranean Sea). In: *Marine Geology*, pp. 97–112. DOI: 10.1016/j.margeo.2011.11.005.

Prior, D. B., B. D. Bornhold, and M. W. Johns (1984). Depositional Characteristics of a Submarine Debris Flow. In: *The Journal of Geology* 6, pp. 707–727. DOI: 10.1086/628907.

Ryan, W. B. F. (2009). Decoding the Mediterranean Salinity Crisis. In: *Sedimentology* 1, pp. 95–136. DOI: 10.1111/j.1365-3091.2008.01031.x.

Sawyer, D. E., P. B. Flemings, B. Dugan, and J. T. Germaine (2009). Retrogressive Failures Recorded in Mass Transport Deposits in the Ursa Basin, Northern Gulf of Mexico. In: *Journal of Geophysical Research* B10, B10102. DOI: 10.1029/2008JB006159.

Sobiesiak, M. S., B. Kneller, G. I. Alsop, and J. P. Milana (2016). Internal Deformation and Kinematic Indicators within a Tripartite Mass Transport Deposit, NW Argentina. In: *Sedimentary Geology*, pp. 364–381. DOI: 10.1016/j.sedgeo.2016.04.006.

Sobiesiak, M. S., B. Kneller, G. I. Alsop, and J. P. Milana (2018). Styles of Basal Interaction beneath Mass Transport Deposits. In: *Marine and Petroleum Geology*, pp. 629–639. DOI: 10.1016/j.marpetgeo.2018.08.028.

Steventon, M. J., C. A.-L. Jackson, D. M. Hodgson, and H. D. Johnson (2019). Strain Analysis of a Seismically Imaged Mass-transport Complex, Offshore Uruguay. In: *Basin Research* 3, pp. 600–620. DOI: 10.1111/bre.12337.

Sun, Q. and T. M. Alves (2020). Petrophysics of Fine-Grained Mass-Transport Deposits: A Critical Review. In: *Journal of Asian Earth Sciences*, p. 104291. DOI: 10.1016/j.jseaes.2020.104291.

Tuccimei, P., J. J. Fornos, A. Gines, J. Gines, F. Gracia, and M. Mucedda (2007). Sea Level Change at Capo Caccia (NW Sardinia) and Mallorca (Balearic Islands) during Oxygen Isotope Substage 5e, Based on Th/U Datings of Phreatic Overgrowths on Speleothems. In: *Geomorfologia Litoral i Quaternari. Homenatge a Joan Cuerda Barcelo. Monografies de la Societat d'Historia Natural de les Balears* 14, 121e136.

Varnes, D. J. (1978). Slope Movement Types and Processes. In: *Special Report*, pp. 11–33.

Voight, B., R. Janda, H. Glicken, and P. Douglass (1983). Nature and Mechanics of the Mount St Helens Rockslide-Avalanche of 18 May 1980. In: *Geotechnique* 3, pp. 243–273. DOI: doi.org/10.1680/geot.1983.33.3.243.

Völker, D. J. (2010). A Simple and Efficient GIS Tool for Volume Calculations of Submarine Landslides. In: *Geo-Marine Letters* 5, pp. 541–547. DOI: 10.1007/s00367-009-0176-0.

Supporting Information: Development and Emplacement of Ana Slide, Eivissa Channel, Western Mediterranean Sea

Sager, T. F.[1*], Urlaub, M.[1], Kaminski, P.[2], Papenberg, C.[1], Lastras, G.[3], Canals, M.[3], Berndt, C.[1]

Geochemistry, Geophysics, Geosystems (G^3) (2022)
https://doi.org/10.1029/2022GC010469

[1] GEOMAR Helmholtz Centre for Ocean Research Kiel, Kiel, Germany

[2] Institute of Geotechnical Engineering & Construction Management, Hamburg University of Technology (TUHH), Hamburg, Germany

[3] CRG Marine Geoscience, Department of Earth and Ocean Dynamics, University of Barcelona, Barcelona, Spain

[*] Corresponding Author: (tsager@geomar.de)

Contents of this file

Here we present and discuss the workflow for re-processing of 3D reflection seismic data to improve data quality for the shallow subsurface used for the detailed analysis of Ana Slide, located in the Eivissa Channel, western Mediterranean Seas. The reasoning behind the re-processing is discussed (Fig. 3.11 - 3.14) and a visual comparison between both data is provided (Fig. 3.15 - 3.21). The main article presents several profiles that all are part of the re-processed 2D reflection seismic profile, while transects through the by-pass zone and sink area were extracted from the 3D reflection seismic data and a 2D profile through the by-pass zone is presented (Fig. 3.22). A TOPAS profile through Ana Slide is presented (Fig. 3.23) and the key horizons (reflectors Ref, R3, R2, R1, and SFR) used for isochron map calculation are presented from the 3D and 2D reflection seismic data (Fig. 3.24 - 3.29).

Introduction

In this supplementary material we provide detailed information about the seismic data that ultimately necessitated re-processing of the raw data. The data is available upon request under:

`https://doi.org/10.1594/PANGAEA.943506` - 3D reflection seismic data;

`https://doi.org/10.1594/PANGAEA.943523` - 2D re-processed reflection seismic data.

Information about profiles that are presented in the article are given in Table 3.1:

Figure reference (article)	**Figure reference (supplementary material)**	**Data type presented in article**	**2D re-processed profile name**	**3D data inline**
Fig. 3 – left side un-interpreted	Supple. Fig. 9	2D re-processed data	Channel01_ line09	Inline L98
Fig. 3 – right side un-interpreted	Supple. Fig. 7	2D re-processed data	Channel01_ line29	Inline L72
Fig. 5a – un-interpreted	Supple. Fig. 6	2D re-processed data	Channel01_ line83	Inline L03
Fig. 5c – un-interpreted	Supple. Fig. 11	2D re-processed data	Channel01_ line07	Inline L202
Fig. 6a – un-interpreted	Supple. Fig. 8	2D re-processed data	Channel01_ line25	Inline L77
Fig. 9a – un-interpreted	Supple. Fig. 10	2D re-processed data	Channel01_ line67	Inline L127

Table 3.1: Profiles shown in the article are presented in full size in this supplementary material. Location of both the 3D and 2D re-processed reflection profiles are provided in figure 1. The names of 2D re-processed and 3D reflection seismic profiles are correlated and presented in Figures 3.12, 3.13, 3.14, 3.15, 3.16, 3.17.

3D processing workflow

The data have been frequency-filtered (Bandpass min – 35 and 350 – max Hz), binned and migration with water velocity (1500 m/s). During seismic analysis of the 3D data, we identified heavy source-receiver ghosts on inlines that necessitated re-processing. In the article, horizon and attribute maps were picked from the 3D data and isochron maps were calculated from these, while all profile except those that transect the by-pass and sink area use the 2D re-processed reflection seismic profiles.

2D re-processing workflow and pre-requisite information

Here we provide additional information about the re-processing workflow presented in the article:

The data have been frequency-filtered (Ormsby Bandpass 18/42/250/500 Hz) and de-spiked to attenuate noise bursts (sliding Alpha Trim 11-trace mean filter in common receiver gather trim factor 66). The individual channels were binned onto a crooked line with a bin size of 12.5 m. Before stacking a normal move-out was applied with 1520 m/s below seafloor and 1512 m/s above (levitus). The stack was post-migrated using the Stolt method with

a constant velocity of 1520 m/s approximating the average seismic velocities in the upper most sediment.

The single channel 3D data was significantly affected by varying ghost signatures (Figure 3.11) due to the deep sagging of streamer sections. During acquisition, 12 single channel streamers were towed perpendicular to the inline vessel track attached to a cross-cable. This cable sagged to varying water depths leading to different ghost interference patterns from channel to channel (Figure 3.13, left panel). To compensate the varying streamer depths, the two lobes (primary and receiver ghost, Figure 3.12) of the seafloor reflection were picked to approximate the streamer depth for each shot and each channel. Subsequently, the data was statically corrected (Figure 3.13). Standard de-ghosting, e.g., applied in the fk domain, could not be applied due to the absence of move-out (single channel data!). We decided to process and interpret individual lines to minimize 'smearing' by combining heavily ghosted signals with assumed 'good' signals.

The average frequency content for each channel is shown in Figure 3.14, displaying the ghost signature affecting the signal frequency by its so-called ghost-notch.

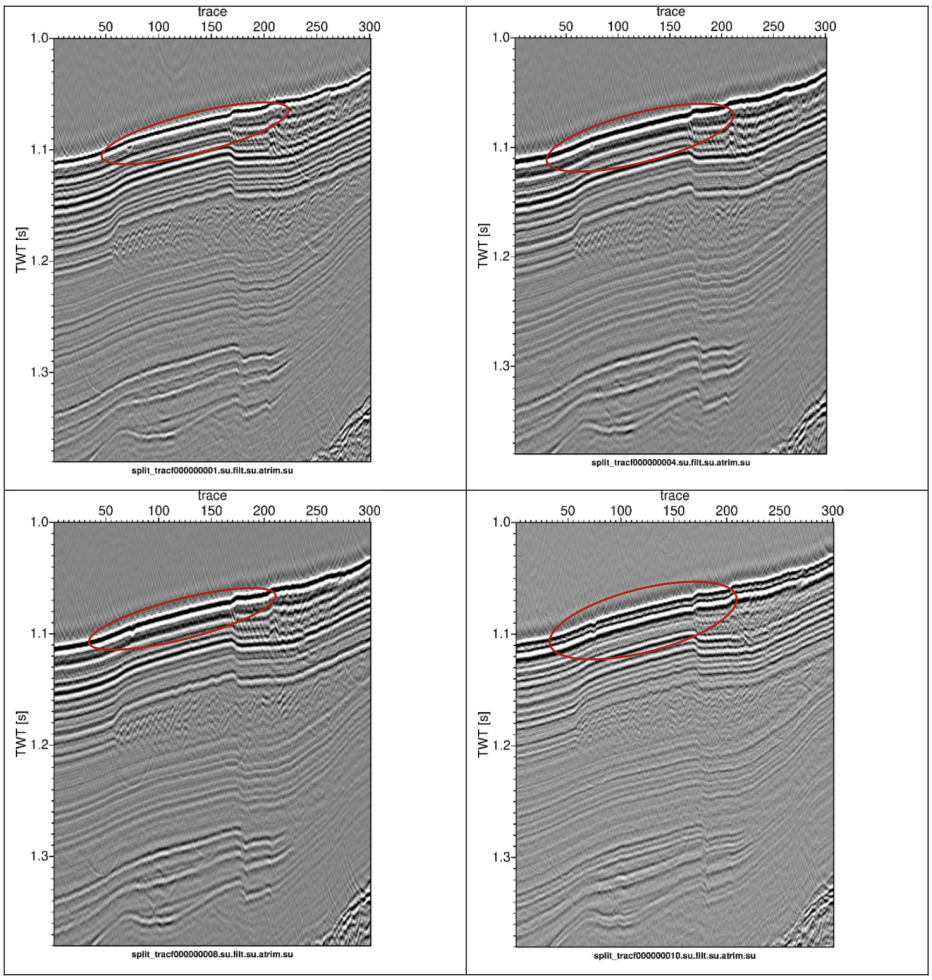

Figure 3.11: Channel 1, 4, 8 and 10 of same section – signal broadening in channel 4 and 8 – and even total separation to double seafloor (and double phases below) in channel 12!

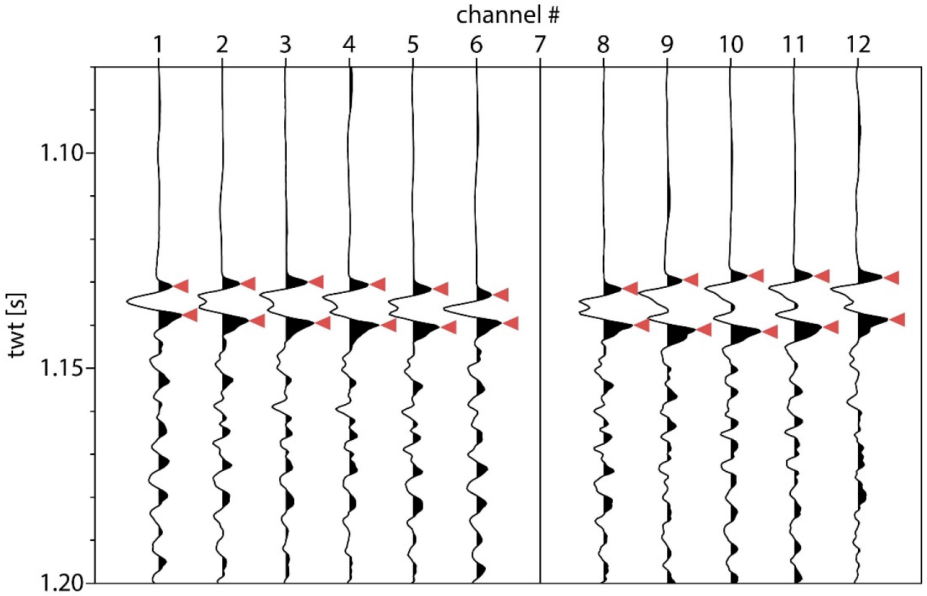

Figure 3.12: Seafloor reflection of a single shot; channels 3-4 and 9-11: heavy receiver ghost as both wavelets are fully separated, channels 2,5,8 and 12: moderate receiver ghost as both wavelets are partially separated, channels 1 and 6: 'tuned' receiver ghost as both wavelets are concomitant. Red arrows mark the automated pick pairs at the peak of both lobes to approximate the streamer depths.

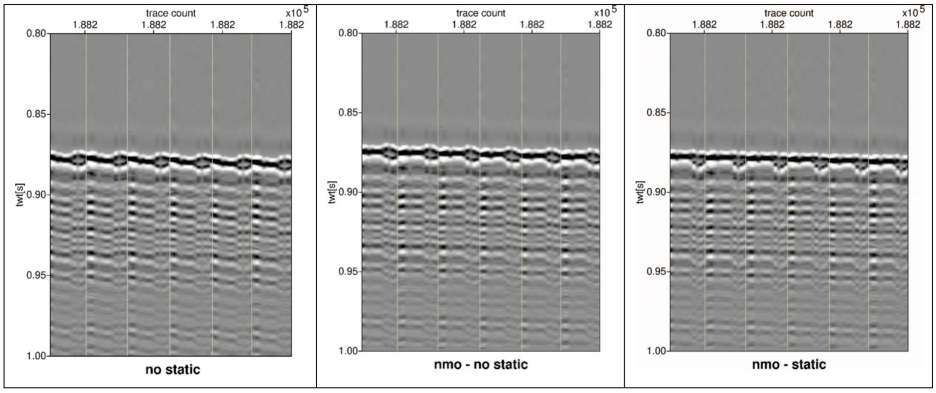

Figure 3.13: Shot-gathers, shot-sorted 3D single channel data. Shots are separated by vertical yellow lines. The sagged cross-cable generates a seafloor-reflection coming 'too early' on sagged channels and creating a ghost signal detached from the primary signal in the worst case (here channel 7-10). After NMO and streamer depth correction, the primary signal is aligned (flat), whereas the ghost signal remains unaffected.

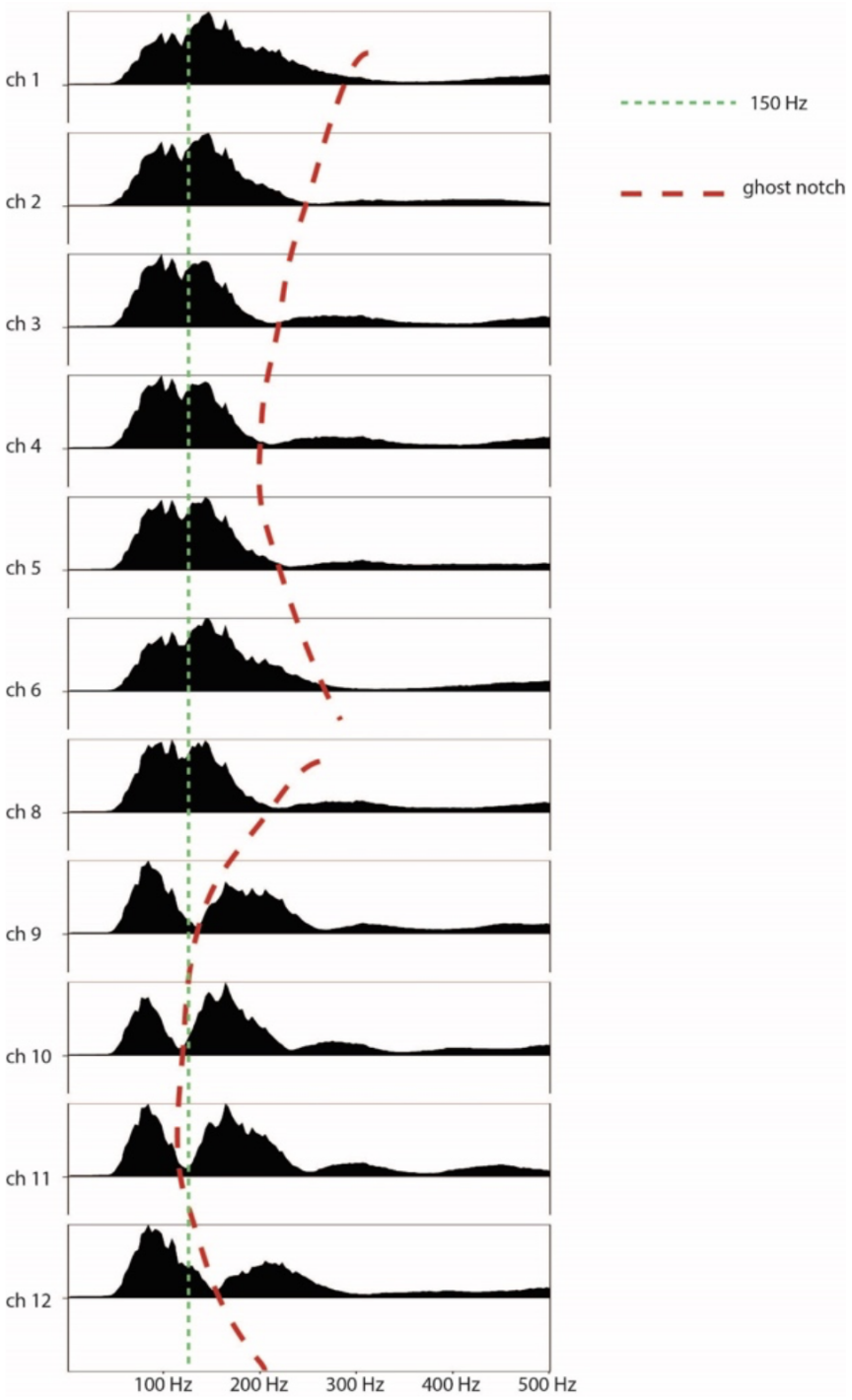

Figure 3.14: Average frequency content for each channel, displaying the ghost signature affecting the signal frequency by its so-called ghost-notch (stippled red line).

Visual Comparison

To validate the re-processing of the raw data, we show a visual comparison between the 3D reflection seismic and 2D re-processed reflection seismic profiles. Although no automatic gain control (AGC) was calculated for the 2D re-processed profiles, deep reflections that relate with the Messinian Unconformity (Berndt et al., 2012) observed at a depth of 1.2 – 1.5 s TWTT throughout the study area are clearly visible and constitute the strongest amplitude reflections, also larger than the first seafloor reflection. The frequency content and overall visual quality of shallow reflections is significantly increased and landslide internal features such as chaotic, disrupted, and transparent seismic facies are more clearly imaged. The names of 2D and 3D profiles are indicated (Figure 3.16 - 3.21 and Tab. 3.1) . In addition, we show a transect through the by-pass zone from the 2D re-processed data (Figure 3.22).

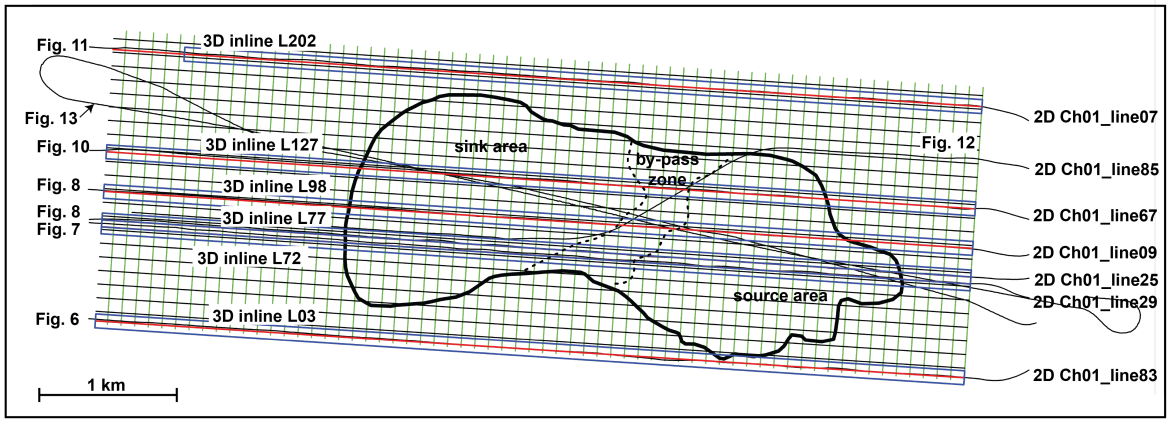

Figure 3.15: Location of profiles of 3D and 2D re-processed reflection seismic data for comparison of shallow subsurface data quality. Comparison figures are presented from south to north (Fig. 3.16, 3.21) and a 2D re-processed profile through the by-pass zone is presented (Fig. 3.22). A TOPAS profile (previously presented by Lastras et al., 2004) is shown in Figure 3.23.

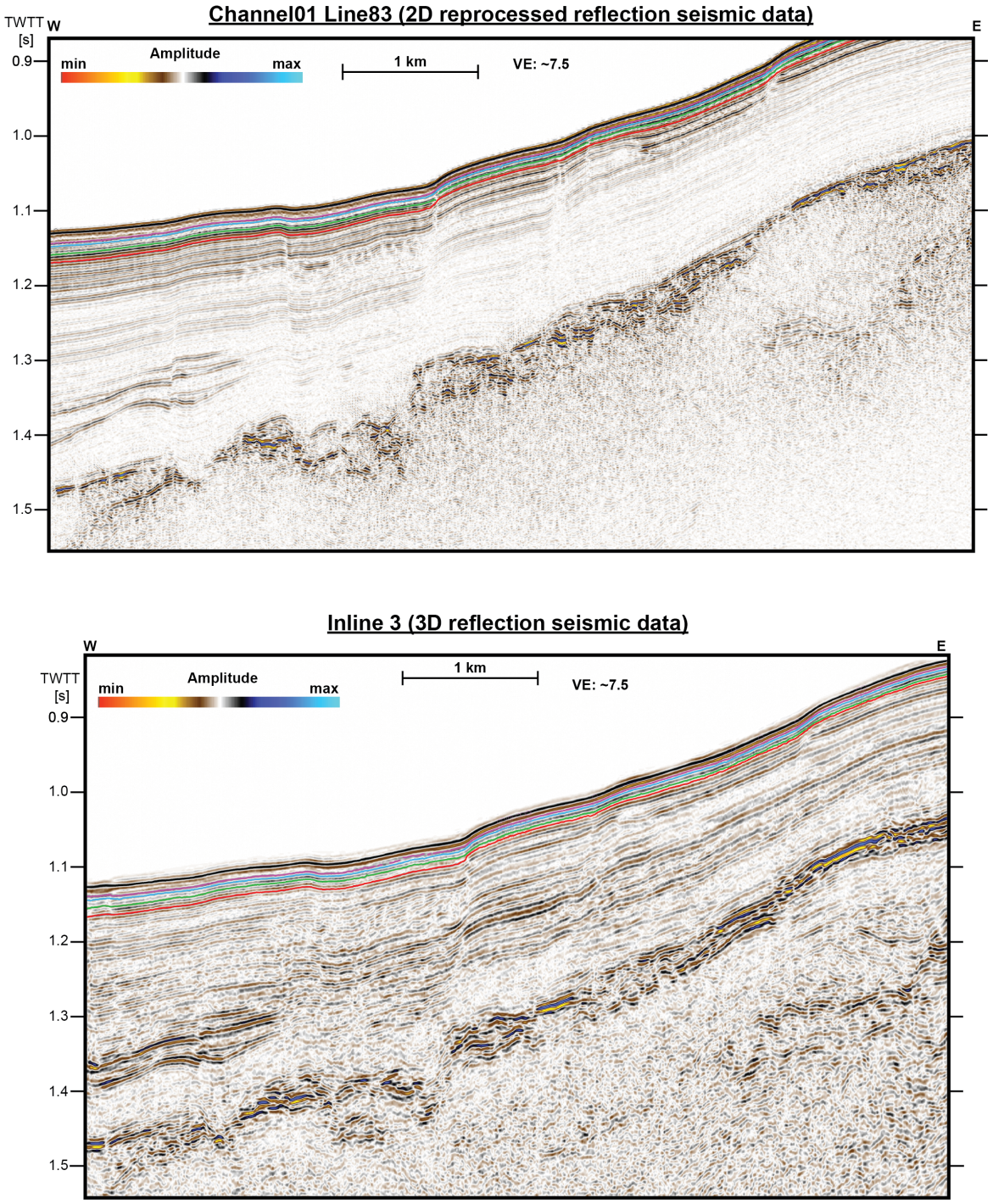

Figure 3.16: Profiles from south of Ana Slide. Data quality is markedly increased of the 2D reflection seismic data (top figure). In the article the 2D re-processed reflection seismic profile is presented in Figure 3.15a.

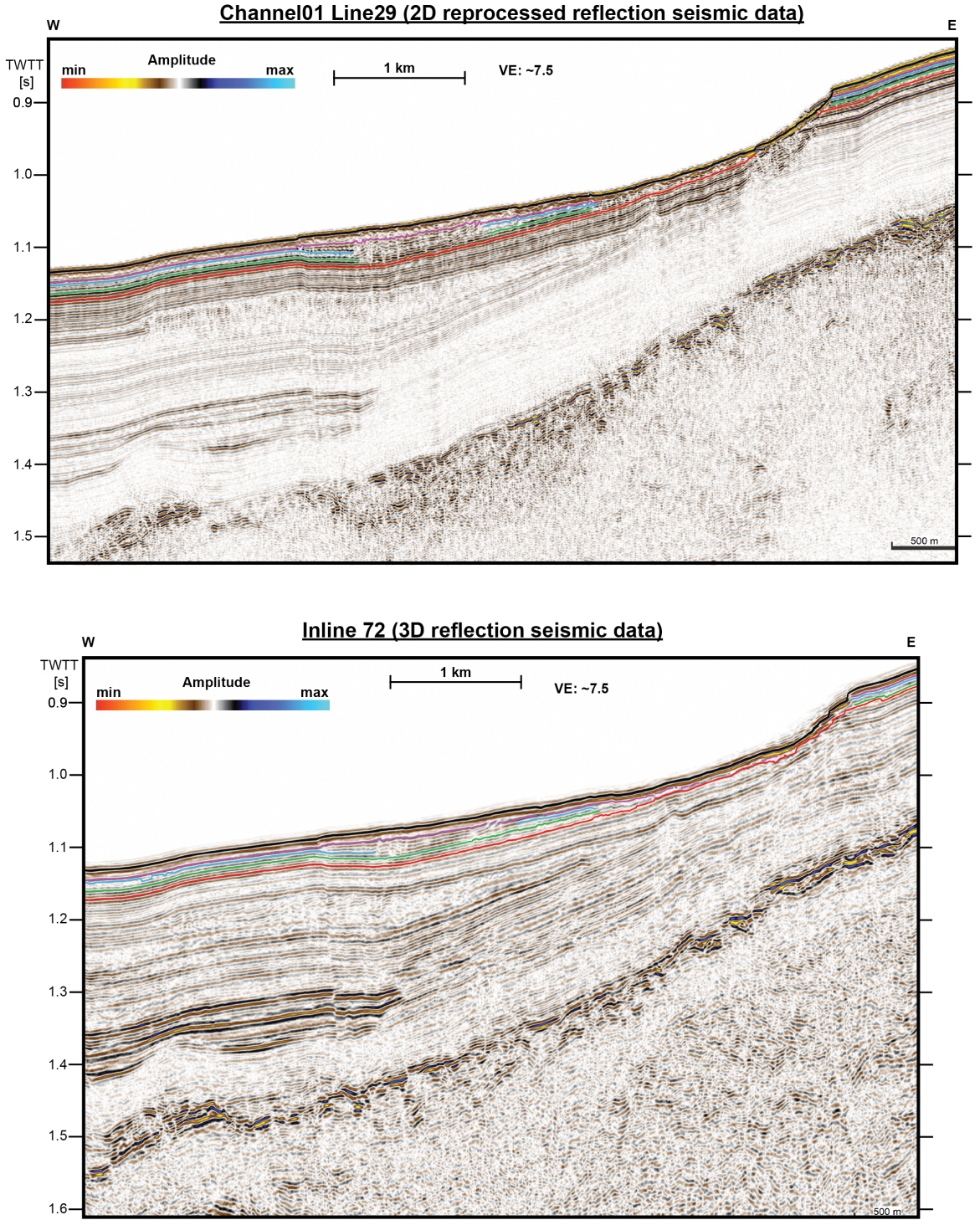

Figure 3.17: Profiles crossing the southern Ana Slide. Data quality is markedly increased of the 2D reflection seismic data (top figure). In the article the 2D re-processed reflection seismic profile is presented in Figure 3.13 (right side of the stitched profile).

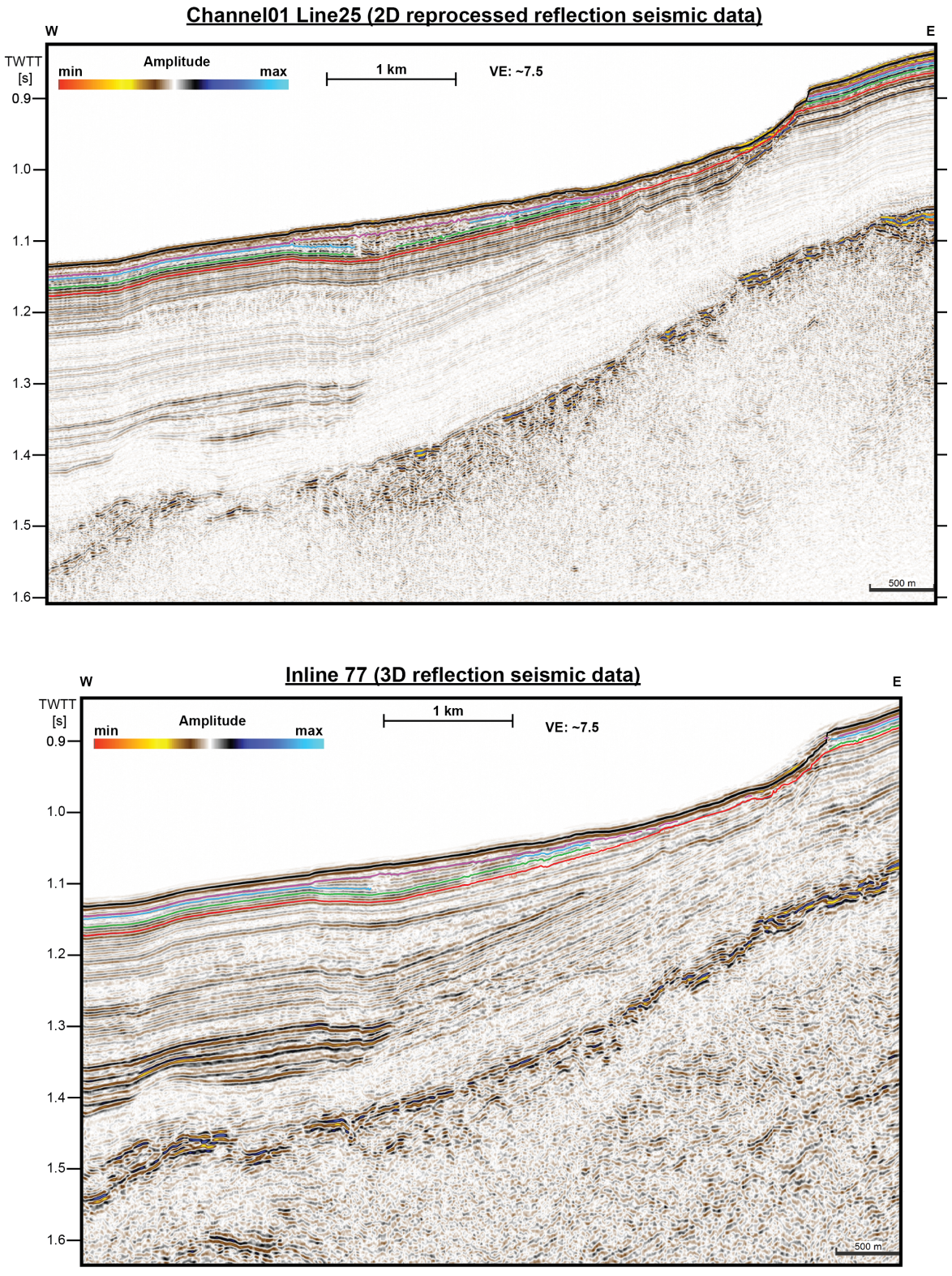

Figure 3.18: Profiles from south of Ana Slide. Data quality is markedly increased of the 2D reflection seismic data (top figure). In the article the 2D re-processed reflection seismic profile is presented in Figure 3.16a.

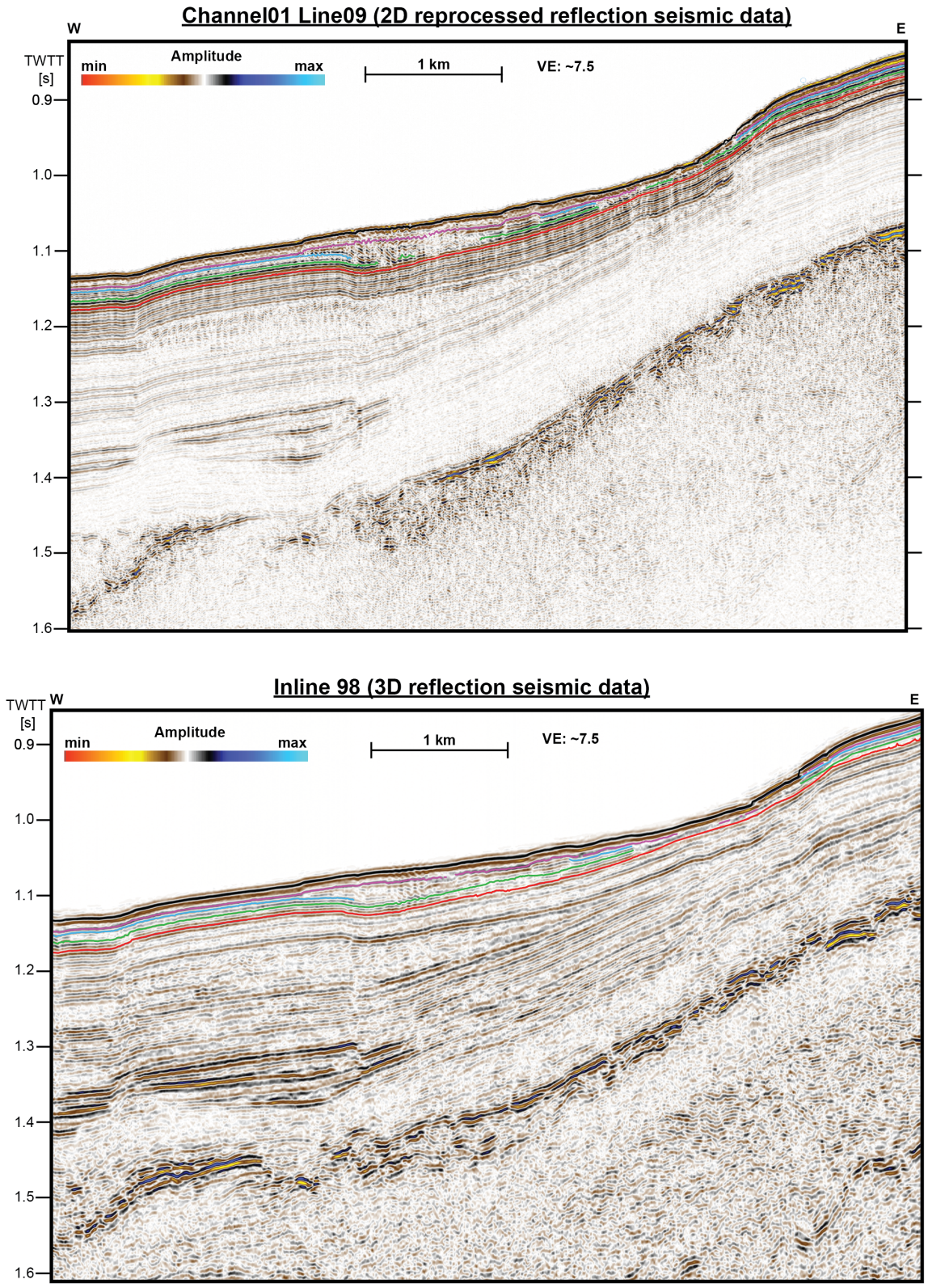

Figure 3.19: Profiles from the middle of Ana Slide. Data quality is markedly increased of the 2D reflection seismic data (top figure). In the article the 2D re-processed reflection seismic profile is presented in Figure 3.13 (left side of the stitched profile).

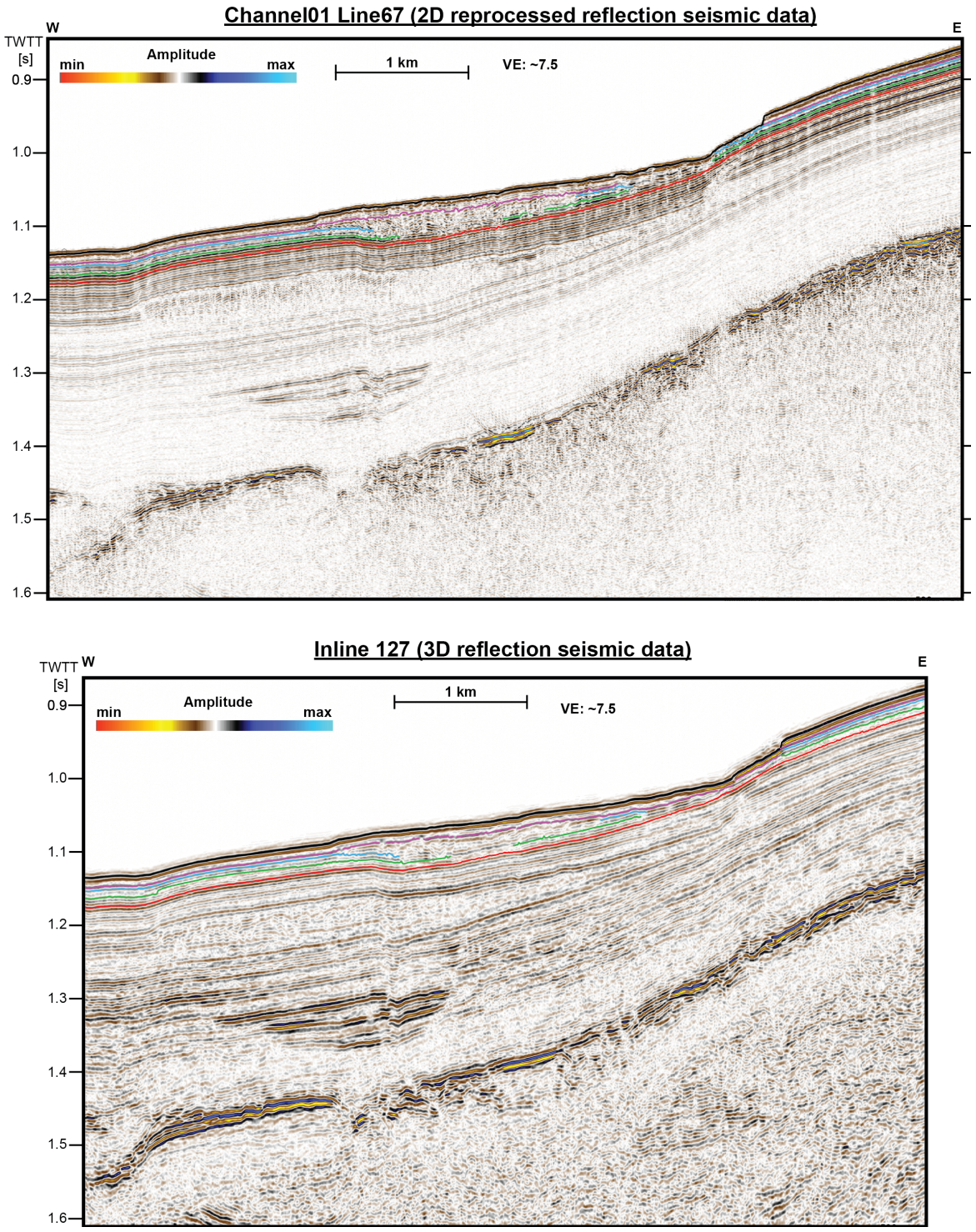

Figure 3.20: Profiles from the northern Ana Slide. Data quality is markedly increased of the 2D reflection seismic data (top figure). In the article the 2D re-processed reflection seismic profile is presented in Figure 3.19a.

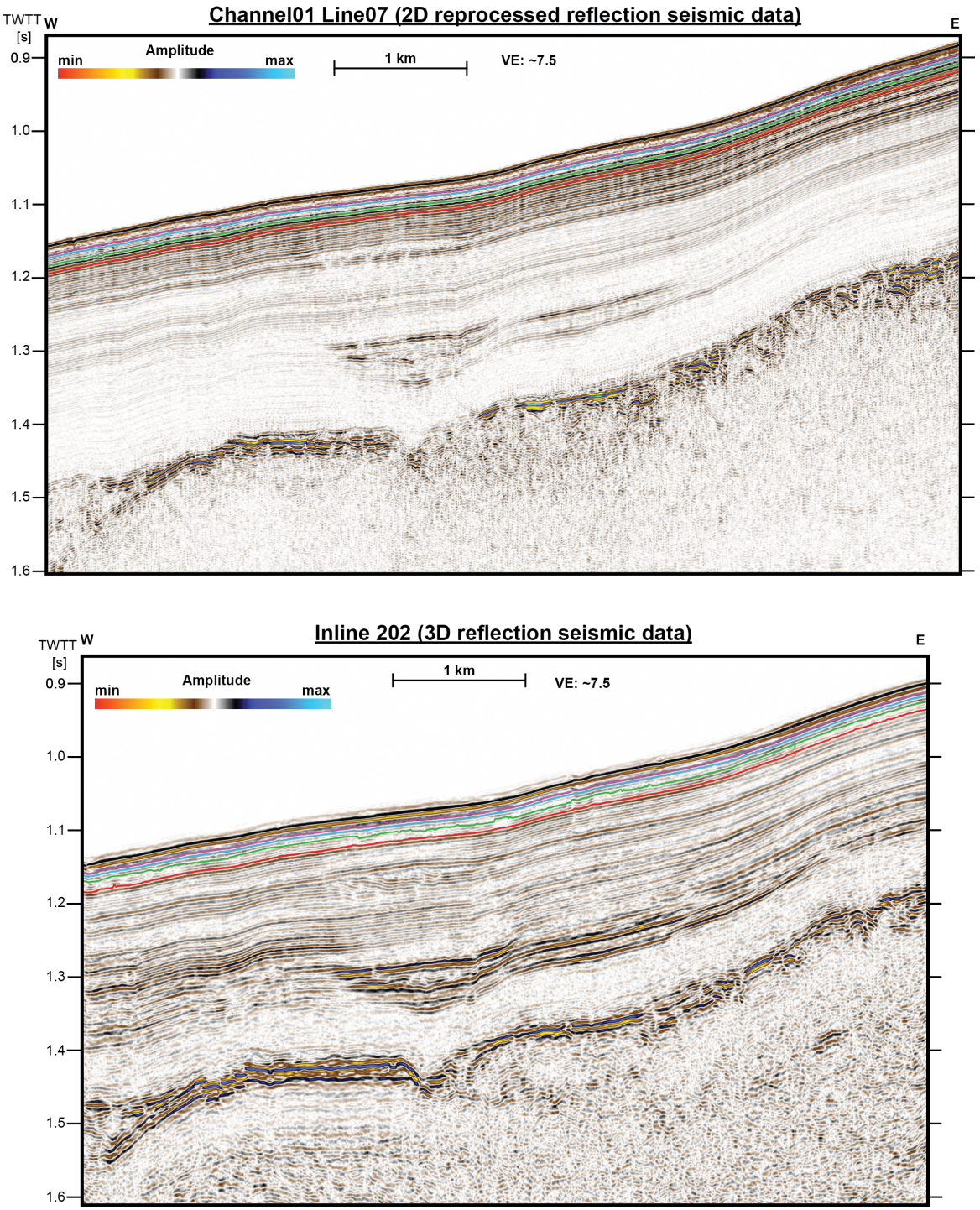

Figure 3.21: Profiles from north of Ana Slide. Data quality is markedly increased of the 2D reflection seismic data (top figure). In the article the 2D re-processed reflection seismic profile is presented in Figure 3.5c.

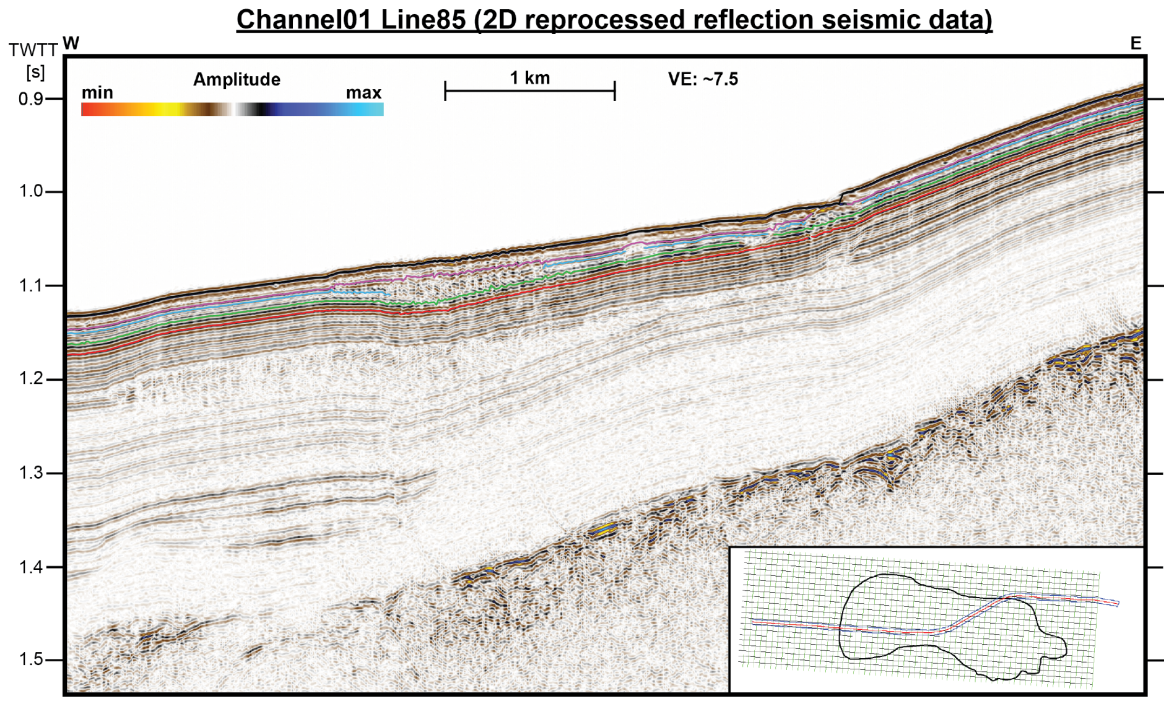

Figure 3.22: Profiles through the by-pass zone of Ana Slide. Data quality is markedly increased of the 2D reflection seismic data (top figure). This profile is representative of Figure 3.17a in the main article.

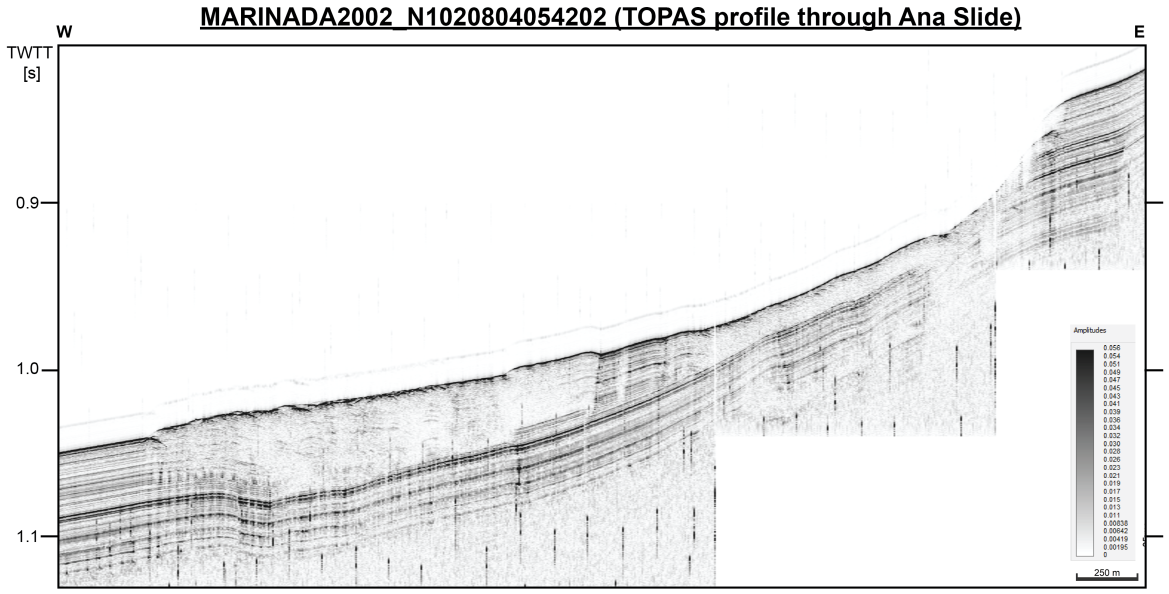

Figure 3.23: TOPAS profile through Ana Slide (presented by Lastras et al., 2004. This figure shows no clear sedimentary drape on top of landslide material inside the sink area (towards the west) but outside of Ana Slide (west) and inside the by-pass zone that correlates with stratigraphic layering in the middle of the figure.

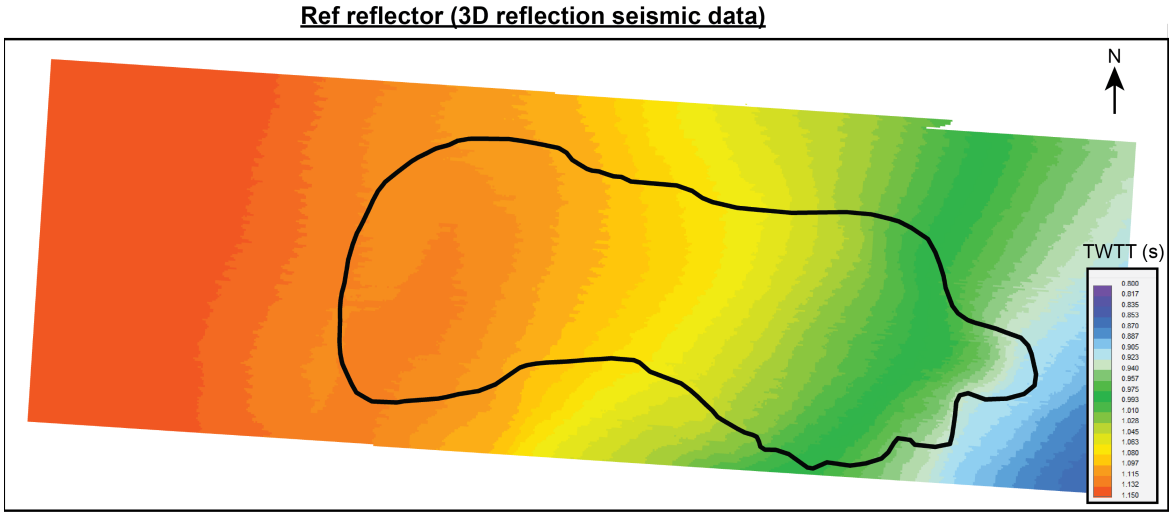

Figure 3.24: TWTT (s) map of the Ref reflector (mapped from the 3D reflection seismic data).

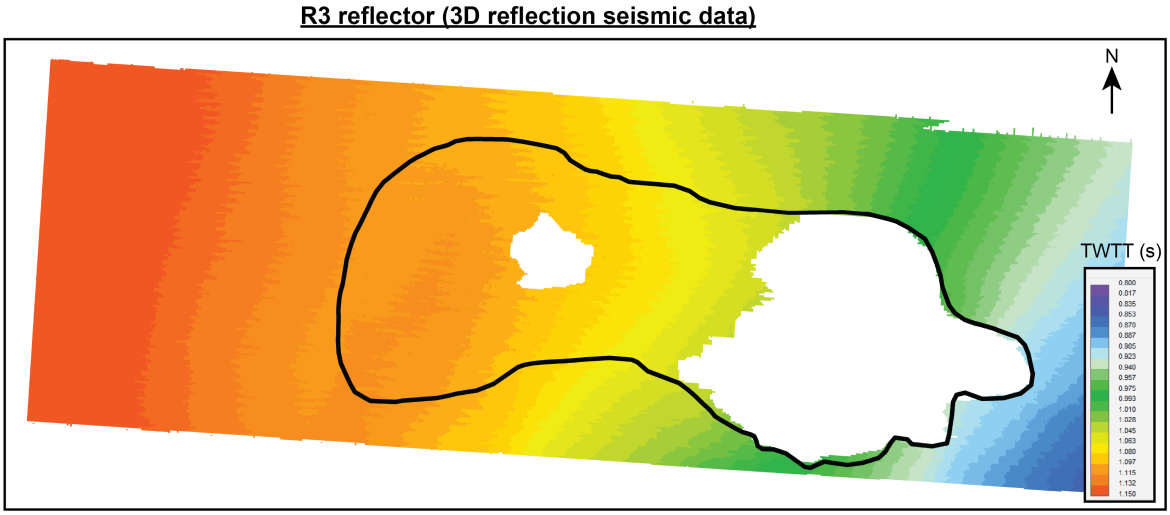

Figure 3.25: TWTT (s) map of the R3 Reflector (mapped from the 3D reflection seismic data).

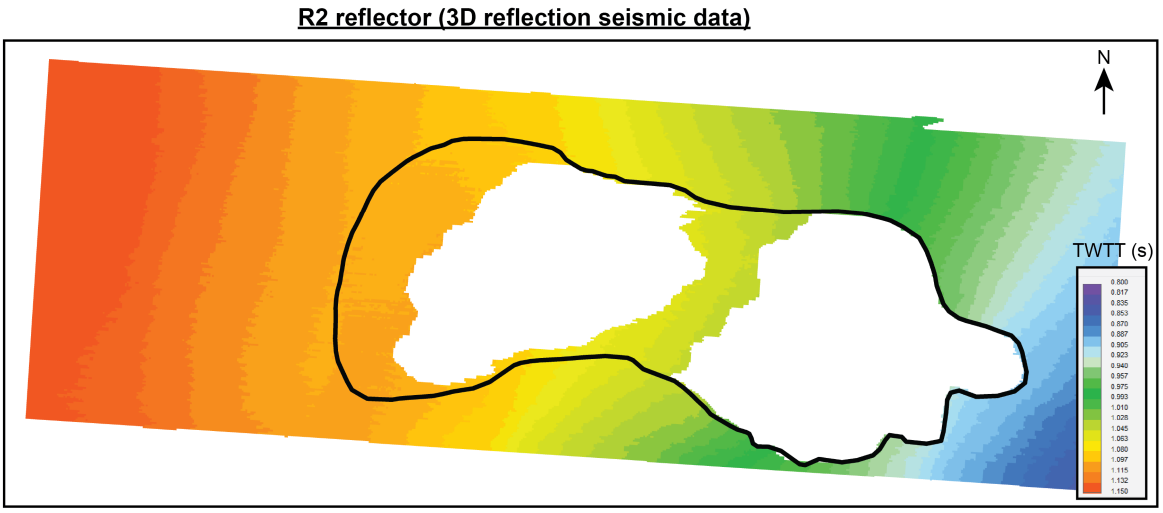

Figure 3.26: TWTT (s) map of the R2 reflector (mapped from the 3D reflection seismic data).

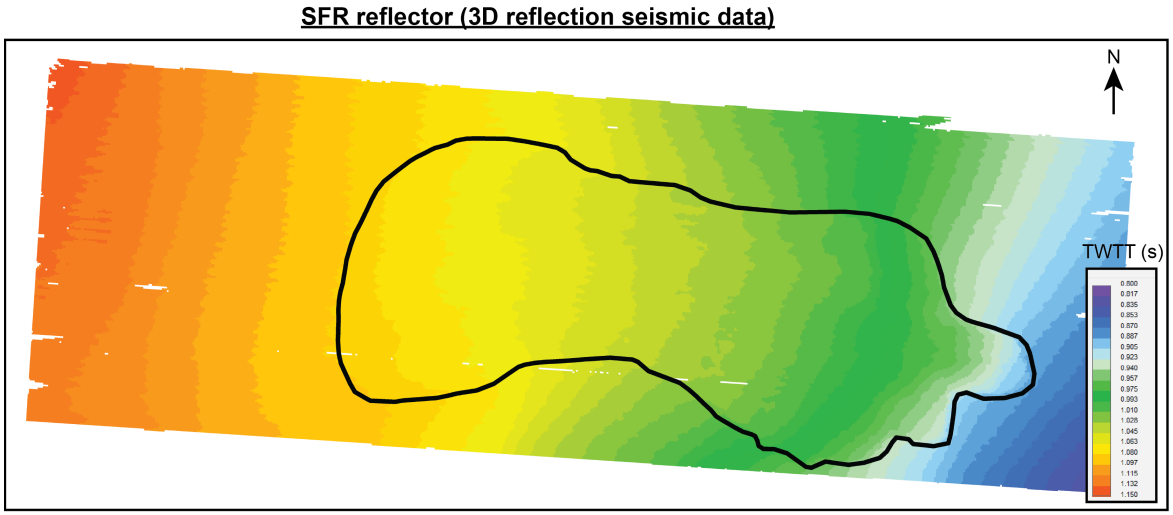

Figure 3.27: TWTT (s) map of the SFR reflector (mapped from the 3D reflection seismic data)

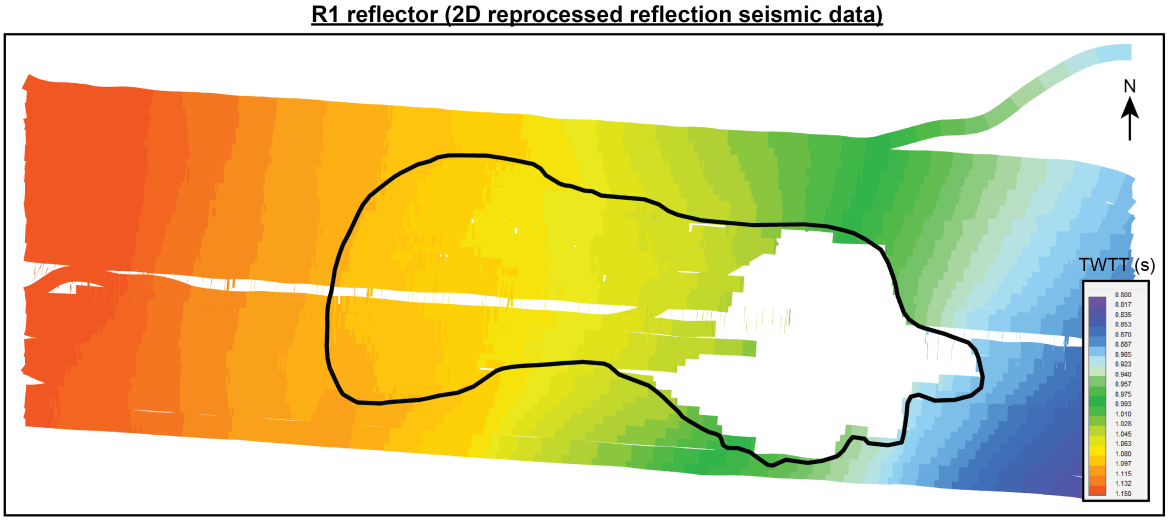

Figure 3.28: TWTT (s) map of the R1 reflector (mapped from the re-processed 2D reflection seismic data).

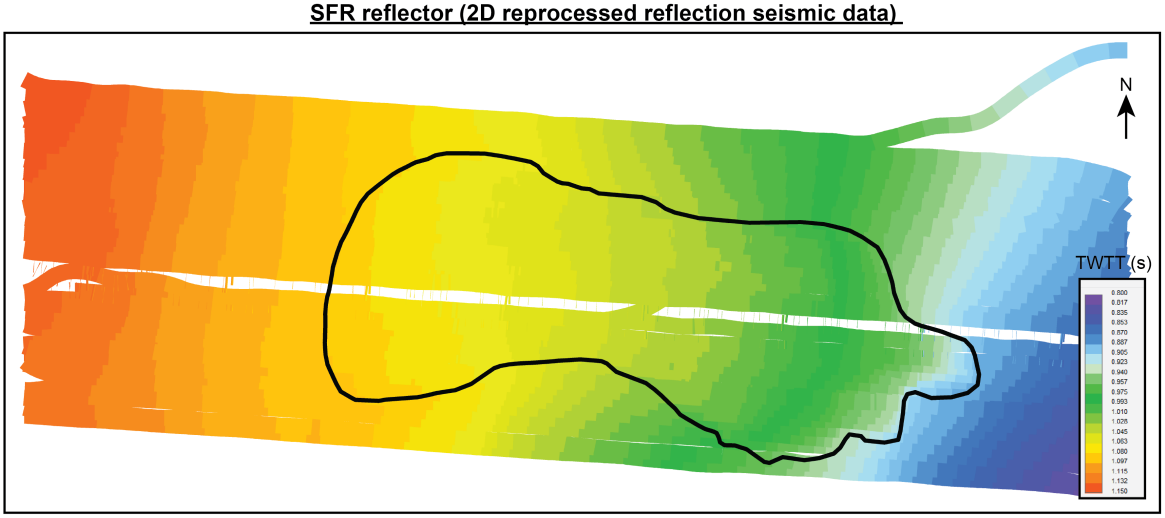

Figure 3.29: TWTT (s) map of the SFR reflector (mapped from the re-processed 2D reflection seismic data).

References

Berndt, C., S. Costa, M. Canals, A. Camerlenghi, B. de Mol, and M. Saunders (2012). Repeated Slope Failure Linked to Fluid Migration: The Ana Submarine Landslide Complex, Eivissa Channel, Western Mediterranean Sea. In: *Earth and Planetary Science Letters*, pp. 65–74. DOI: 10.1016/j.epsl.2011.11.045.

Lastras, G., M. Canals, R. Urgeles, J. E. Hughes-Clarke, and J. Acosta (2004). Shallow Slides and Pockmark Swarms in the Eivissa Channel, Western Mediterranean Sea. In: *Sedimentology* 4, pp. 837–850. DOI: 10.1111/j.1365-3091.2004.00654.x.

4 Assessment of Submarine Landslide Volume

Sager, Thore F.[1*], Urlaub, Morelia[1], Berndt, Christian[1]

re-submitted to Geo-Marine Letters (GML)

[1] GEOMAR Helmholtz Centre for Ocean Research Kiel, Kiel, Germany

[*] Corresponding Author: tsager@geomar.de

We thank an anonymous reviewer and Dave R. Tappin for comments on a previous version of this manuscript previously submitted to GML (Submission ID: 59f81609-8b2d-4f9a-ade2-754a030e5ffa).

Abstract

Submarine landslides pose major geohazards as they can destroy seafloor infrastructure such as communication cables and cause tsunamis. The volume of material displaced with the landslide is one factor that determines its hazard and is typically estimated using bathymetric and/or seismic data. Here, we review methods to determine the initial failed volume based on a well-constrained case study, the Ana Slide, a small slope failure in the Eivissa Channel off the eastern Iberian Peninsula. We find that not only the availability and quality of data but also the emplacement mechanism determine the quality of the volume estimation. In general, the volume estimation based on comparison of modern and reconstructed pre-failure seafloor topographies yields conservative, yet most robust volumes. In contrast, volume estimated from seismic data may be prone to excessive overestimation if no detailed constraints on the nature of the chaotic, transparent, or disrupted seismic facies commonly used to identify landslide material are available.

Keywords *volume assessment, pre-failure seafloor reconstruction, landslide volume, emplacement mechanism*

4.1 Introduction

Submarine landslides are a serious geohazard to coastal populations worldwide (Bondevik et al., 2005; Haugen et al., 2005; Løvholt et al., 2017; Prior et al., 1984; Talling et al., 2014; Watt et al., 2012; Synolakis et al., 2002). Slope failure can destroy offshore infrastructure such as platforms and telecommunication cables (e.g., Løvholt et al., 2019; Vanneste et al., 2014) and release large quantities of methane and other greenhouse gases from the seafloor (e.g., Maslin et al., 2004). While the record of slope failure-generate tsunamis is mainly limited to their deposits on land (e.g., Bondevik et al., 2005; Bondevik et al., 1997; Fruergaard et al., 2015), mass-transport deposits (MTDs) are widespread features on the ocean floor (e.g., Camerlenghi et al., 2010; Gatter et al., 2021; Moscardelli and Wood, 2015). The inclination of the seafloor, water depth, duration of the slide event, its acceleration, related landslide mechanisms, run-out velocity, the timing between multiple stages of failure, the volume of mobilized material, and its density and cohesion are all factors that control the impact of a landslide (e.g., Harbitz et al., 2014; Murty, 2003). Constraining these factors requires seafloor samples and age datings that are rarely available. Some factors, such as the acceleration and propagation velocity cannot be quantified at all from MTDs. While the landslide mechanism is one of the most important factors for the generation of tsunamis (e.g., Synolakis et al., 2002), this is difficult to quantify. However, the volume of a submarine landslide can be estimated relatively easily from bathymetry and/or a few seismic lines. Volume in a landslide is not a constant as it may change during the evolution of the landslide. The volume of the deposit may exceed the initial failed volume because of processes like basal erosion and entrainment (e.g., Watt et al., 2012; Sobiesiak et al., 2018). On the other hand, the deposit

may be distributed over large areas by highly mobile sediment flows (Talling et al., 2007), which can escape the resolution of mapping and imaging systems. Here, we focus particularly on the initial failed volume of a landslide as it is one of the key input parameters for tsunami models (e.g., Murty, 2003; Iglesias et al., 2012).

There are various ways to estimate the volume of submarine landslides from bathymetric or reflection seismic data. McAdoo et al. (2000) measured the area of the source area (A) and height of the headscarp (H) from bathymetric data to estimate the evacuated volume through volume $= \frac{1}{2} A H$. On the contrary, Völker (2010) estimated the evacuated volume by subtracting a pre-failure seafloor that was reconstructed by fitting slope functions into the landslide scar from the present-day seafloor. Here, a negative volume in the source area provides an estimate of the initial failed volume and a positive volume in the sink area provides an estimate of the deposited and accumulated volume. Wilson et al. (2004) calculated the volume of a debris lobe from measures of its depth or thickness (D), width (W), and length (L) through the relationship of volume $= \frac{1}{6} \pi D W L$. For landslides that are imaged from sub-seafloor sediment echo-sounder profiles or 2D and 3D reflection seismic data, the average thickness of chaotic, transparent, and disrupted seismic facies representing the mobilized material can be measured and multiplied by the landslide area. This provides the 'bulk volume' of material involved in and affected by the landslide referred to as Vd by Nugraha et al. (2022) that accumulated inside the sink area. This method was used by Lastras et al. (2004) to estimate the landslide volume or total affected volume of Ana Slide, located in the Eivissa Channel, western Mediterranean Sea. These authors used the average thickness of Ana Slide at 23 m inside the landslide scar (with an area of 6 km^2) to propose a volume or Vd (sensu Nugraha et al., 2022) of 0.14 km^3.

This study aims to determine the most suitable and robust approach to determine this initial failed volume, in particular in the absence of extensive coverage of reflection seismic data and geological sampling. This is done for the Ana Slide in the Eivissa Channel located in the western Mediterranean Sea, for which the landslide structure, as well as the development, emplacement, evacuation, and accumulation processes, are known in the greatest detail. Ana Slide is entirely covered by high-resolution 3D reflection seismic data. Both the detailed knowledge and complete coverage of seismic data allow us to determine its volume with low uncertainties.

4.2 Emplacement of Ana Slide

Ana Slide is a relatively small landslide located on the eastern slopes of the Eivissa Channel, western Mediterranean Sea between 635 and 790 m water depth (Berndt et al., 2012; Lastras et al., 2004; Lastras et al., 2006; Sager et al., 2022) (Figure 4.1b). Beneath Ana Slide the pre-Ana Slide was previously identified by Lastras et al. (2004) and mapped by Berndt et al. (2012) and Sager et al. (2022) with a congruent headscarp toward the east while the

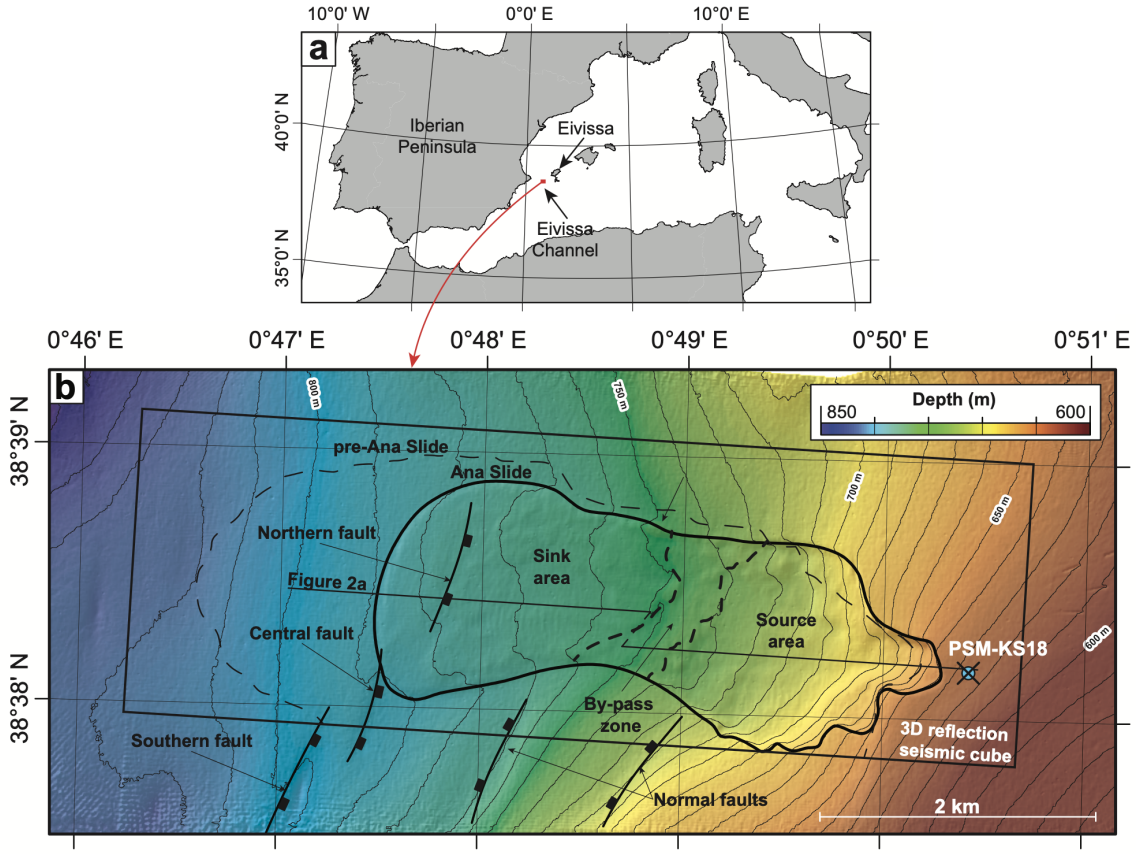

Figure 4.1: a) Regional map of the western Mediterranean Sea showing the study area in the Eivissa Channel located on the Balearic Promontory between the Iberian Peninsula and the island of Eivissa. **b)** Hillshaded bathymetry map of Ana Slide at water depths between 635 and 790 m. The southern, central, and northern faults comprise a local seafloor antithetic en-echelon fault system that controlled the development of Ana Slide (Sager et al., 2022). The location of Kullenberg gravity core PSM-KS18 is indicated by a blue symbol (0° 50.453' E 38° 38.184' N) presented by Lafuerza et al. (2012). Landslide material involved in Ana Slide was evacuated from the source area and accumulated inside the sink area.

pre-Ana Slide extends around 1.5 km further toward the west (Figure 4.1b). We take the interpretation of development and emplacement processes of Ana Slide presented by Sager et al. (2022). These authors use high-resolution bathymetry, 3D reflection seismic data and re-processed 2D reflection seismic profiles that completely cover this landslide. Sager et al. (2022) show that Ana Slide developed during two stages referred to as the primary (300 ka) and secondary failures (61.5 ka after Cattaneo et al., 2011). The primary failure involved slope material located between the basal shear surface represented by the reference reflector Ref and the sub-reflector R1 (Sager et al., 2022) (Figure 4.2a and b). The landslide material emerged frontally, travelled across a 500 m long by-pass zone, and accumulated above the pre-failure seafloor at the time of the primary failure represented by the 'pre-failure R1 reflector' inside the sink area as the 'actual deposit of the primary failure' (Figure 4.2a and b). The accumulation of this deposit induced in situ deformation of the underlying sediments reaching a depth of up to 30 m below the pre-failure R1 reflector throughout

the sink area that marked the seafloor during the primary failure (Figure 4.2f). Landslide material mobilized during the primary failure accumulated inside the sink area and attained a thickness of approximately 15 m. The secondary failure involved slope material between R1 and SFR. It was much smaller and is not seismically resolved even in high-resolution seismic data ($\sim$ 5 m vertical resolution, Sager et al., 2022).

For this study, the primary and secondary failures of Ana Slide are combined as the seismic data do not allow to distinguish the secondary failure deposit from the seafloor reflection (Figure 4.2b). Consequently, the top reflector of Ana Slide referred to as SFR corresponds to the occurrence of the secondary failure.

Submarine landslides can generally be defined as those that are frontally confined or frontally emergent (Frey-Martinez et al., 2006). A confined landslide experiences restricted downslope translation above a basal shear surface at depth and it is unable to emerge frontally onto the seafloor, whereas an unconfined landslide can emerge frontally onto the seafloor and propagate freely above the seafloor leaving the source area entirely evacuated. On the one hand side landslide material is mobilized and evacuated from a source area where it leaves a void space between the pre-failure and present-day seafloor. On the other hand, this landslide material accumulates inside the sink area and if the landslide is frontally emergent this landslide material may propagate further downslope as a turbidity current and lay down a debris flow or turbidite deposit over a large area (e.g., Lastras et al., 2002). Ana Slide describes a mixed system landslide. The primary failure developed as frontally emergent while the secondary failure developed more like a frontally confined slope failure. A fraction of the mobilized landslide material was able to overcome frontal confinement and emerge onto the seafloor. The other part of the mobilized material remained ponded inside the source area defined as 'undifferentiated landslide material' by Sager et al. (2022) (Figure 4.2b).

4.2.1 Tectonic setting of the Ana Slide area

Sager et al. (2022) and Berndt et al. (2012) identified several faults inside the extent of the 3D reflection seismic data (Figure 4.1b). Three of these, the southern, central, and northern faults are located beneath the sink area of Ana Slide and further south of it. These faults characterize an en-echelon fault system that strikes SSW and NNE and extends into the 3D reflection seismic data from the south with an unknown extent. This fault system dips in the opposite direction compared to the seafloor and therefore is termed 'seafloor antithetic' in this study. Primarily the northern but also the central fault affected the seafloor morphology before the primary failure of Ana Slide by vertical fault movement (Sager et al., 2022).

4.2.2 Depositional environment in the Eivissa Channel

Eivissa Channel received a limited input of terrestrial sediments from rivers on the Iberian Peninsula including the Ebro, Turia, and Jucar and there are no permanent rivers on the Balearic Islands (Lafuerza et al., 2012; Lastras et al., 2004; Panieri et al., 2012). Steady hemipelagic sedimentation with the deposition of fine-grained water-rich marine clays enriched in calcareous nano fossils generated well-stratified seafloor sub-parallel reflectors and there exists no evidence for strong bottom currents or contourites (e.g., Lastras et al., 2004). In profile, the thickness of the interval between reflector Ref and SFR increases in the downslope direction toward the west with increasing water depth (Sager et al., 2022, their Figure 4c) generating predictable thicknesses of these stratigraphic intervals.

4.3 Data

This study uses bathymetric data and 3D reflection seismic data acquired with the P-Cable system of the National Oceanographic Centre (NOC) in Southampton, UK equipped with two sleeve guns and 11 streamers during cruise 178 onboard RSS Charles Darwin in 2006 (CD178). Data were processed including time migration with water velocity (1500 m s^{-1}). For further information about acquisition and processing workflows, the reader is referred to Berndt et al. (2012) and Sager et al. (2022). The bathymetric data have a horizontal resolution of 5 m (5 x 5 m grid size) while the 3D reflection seismic data have a vertical resolution of 5 – 6 m and a horizontal resolution of 10 – 15 m (Berndt et al., 2012). The 2D reflection seismic profile presented in Figure 4.2a shows a re-processed profile presented previously by Sager et al. (2022).

4.4 Methods for volume estimation of submarine landslides through pre-failure seafloor reconstructions

Volume calculations of evacuated and accumulated landslide material of Ana Slide are performed in Kingdom Suite using the Volumetric tool that uses one bounding polygon and two depth-converted grids in meters depth (calculated from horizons in seconds two-way travel time or seconds TWTT). For depth conversion of seismic horizons, a seismic velocity of 1500 m s^{-1} is used. This velocity is consistent with seismic velocity measurements from the shallow 8 m long Kullenberg gravity core PSM-KS18 (0° 50.453' E 38° 38.184' N) presented by Lafuerza et al. (2012) obtained during the PRISM cruise with the R/V L'Atalante in 2007 led by IFREMER, France. The 3D reflection seismic data are presented in the time domain (seconds TWTT) and volumes are calculated in the upper 50 m beneath the seafloor. Sediments are water-rich (Lafuerza et al., 2012; Lastras et al., 2004; Panieri et al., 2012) and seismic P-wave velocities of such sediments typically vary between 1500 to 1640 m s^{-1}

(Hamilton, 1979). Thus, a seismic velocity of 1500 m s^{-1} is appropriate to use for depth conversion of seismic reflectors Ref and SFR and the reconstructed pre-failure seafloors for the source and sink areas.

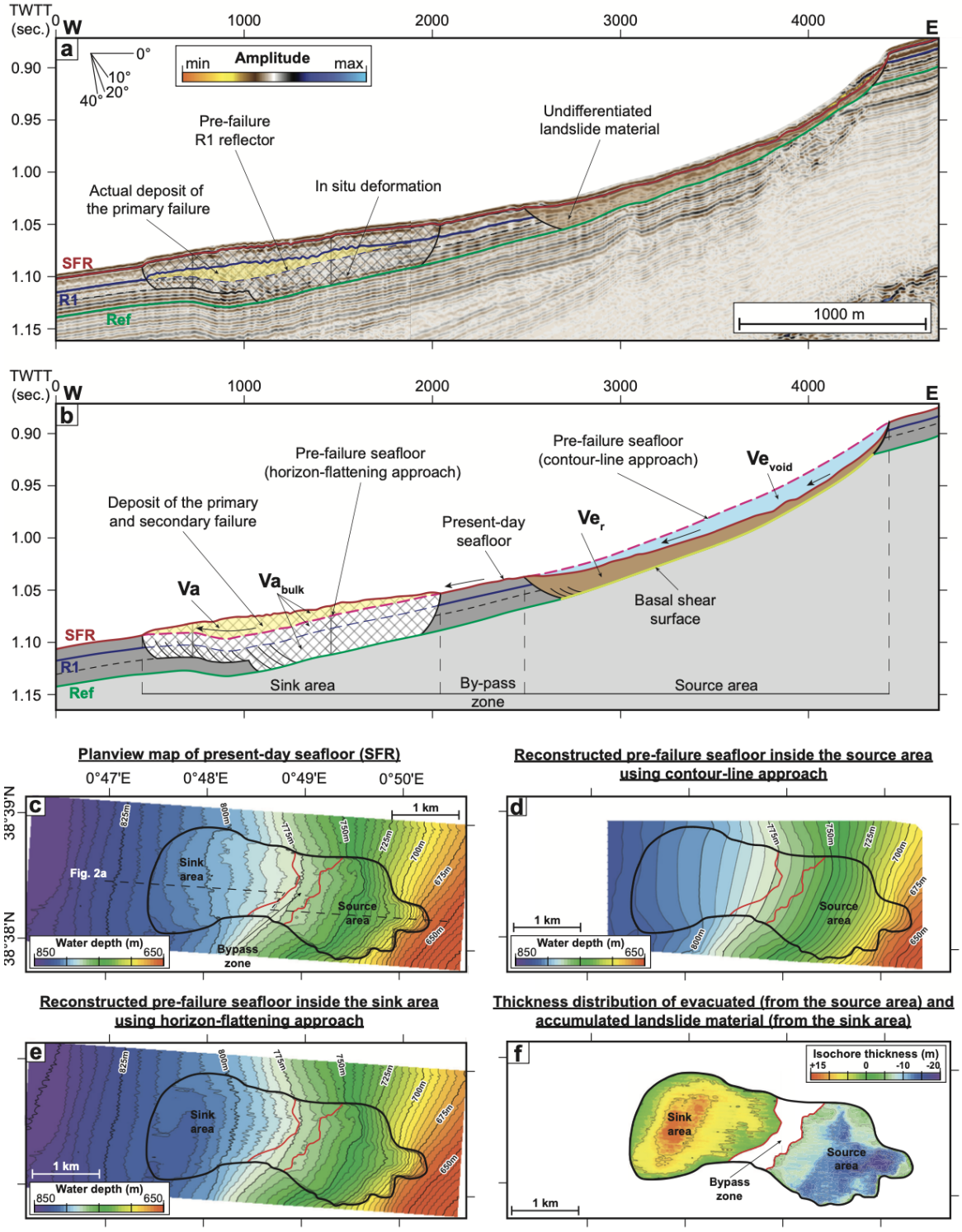

Figure 4.2: (Caption on next page.)

Figure 4.2: (Previous page.) **a)** Uninterpreted 2D reflection seismic profile (Channel 01 – Line 37) of Ana Slide (see Figure 4.1) previously presented by Sager et al. (2022). Landslide reflectors Ref (green), R1 (blue), and SFR (red) are highlighted. **b)** Interpreted profile of Ana Slide showing several volumes related to Ana Slide: Va describes accumulated landslide material inside the sink area above the pre-failure seafloor. Ve_rrepresents mobilized landslide material (of the primary and secondary failures) which was unable to overcome frontal confinement and ponded downslope inside the source area. Va_{bulk} represents all affected and involved landslide material and slope sediment, while Va represents the volume of actually accumulated landslide material above the pre-failure seafloor inside the sink area. **c)** Plan-view map of the present-day seafloor SFR reflector mapped from the 3D reflection seismic data. **d)** Reconstructed pre-failure seafloor using the contour-line approach used for volume estimation of Ve_{void} inside the source area. **e)** Reconstructed pre-failure seafloor using the horizon-flattening approach for volume estimation of Va inside the sink area. **f)** Thickness distribution of the reconstructed pre-failure seafloors inside the source (using the contour-line approach) and sink area (using the horizon-flattening approach) and the present-day seafloor SFR. A vertical thickness of up to 20 m of landslide material (Ve_{void}) was evacuated from the source area, while a thickness of up to 15 m of accumulated landslide material (Va) was added to the sink area.

In this study, three horizontal bounding polygons are defined: the source area that covers an area of 1.9 km^2, the by-pass zone with an area of 0.45 km^2, and the sink area covering an area of 2.45 km^2 (Figures 4.1b and 4.2c). In total, Ana Slide covers an area of 4.8 km^2 referred to as the landslide scar.

We define several landslide volumes (Figures 4.2 and 4.3), the values of which are calculated independently and with different approaches:

Apparent evacuated volume (Ve_{void}) the void space in the source area. Ve_{void} is calculated following the approach of Völker (2010) where the volume of evacuated landslide material is calculated by comparing the present-day with the reconstructed pre-failure seafloors (e.g., Omira et al., 2022; Sun et al., 2018; Webster et al., 2016). The pre-failure seafloor of the source area of Ana Slide is reconstructed by manually interpolating the course of local and regional contour lines from outside the landslide scar into the inside of it (Figure 4.2a and b). To test the sensitivity of the applied pre-failure seafloor reconstructions, we reconstructed the seafloor inside the source area assuming a simple yet unlikely realistic pre-failure seafloor morphology (referred to as the straight-line approach hereafter). This was done by reconstructing straight pre-failure contour lines between the intersection of the landslide scar with local 10 m contour lines (Figure 4.5). The resulting calculated volume of evacuated landslide material from the source area serves as the maximum value for Ve_{void}.

Remaining volume (Ve_r) the volume of 'undifferentiated landslide material' (sensu Sager et al., 2022) that remained inside and was mobilized but did not leave the source area of Ana Slide. It is calculated from the 3D reflection seismic data and represents the difference between the present-day seafloor (SFR) and the basal shear surface (Ref) in the source area.

Turbidite volume (Vt) the volume of material which potentially was transported into the deeper basin and out of the study area by turbidity currents. This material accumulated over a potentially vast area approaching zero thickness. With the available geophysical data limited to the proximal area of Ana Slide, it is impossible to determine whether a turbidity

current was caused nor to estimate the volume of the turbidite deposit because of the lack of appropriate distal geological sampling. In the following, we, therefore, assume Vt = 0 for Ana Slide.

Evacuated volume (Ve) the initially failed volume. It is the sum of Ve_{void}, Ve_r, and Vt (if a turbidite deposit was generated in the distal part):

$Ve = Ve_{void} + Ve_r + Vt.$

Bulk accumulated volume (Va_{bulk}) chaotic, transparent, and disrupted seismic facies representing mobilized and affected landslide material and slope sediment. This volume is calculated from 3D reflection seismic data between the present-day seafloor and Ref in the sink area. This volume is referred to as volume deposited Vd by Nugraha et al. (2022).

Accumulated volume (Va) the amount of material that accumulated above the pre-failure seafloor and the present-day seafloor SFR inside the sink area. It represents the difference between the apparent evacuated volume of Ve_{void} and the volume of a potential turbidite deposit and therefore:

$Va = Ve_{void} - Vt.$

The approach of Völker (2010) could be used to estimate Va. However, for Ana Slide, the morphology of the sink area was modified by a local seafloor antithetic en-echelon fault system before the failure occurrence of Ana Slide (and the primary failure) (Sager et al., 2022). Thus, the pre-failure seafloor inside the sink area cannot be reconstructed using the contour-line approach previously used for the source area. Therefore, to account for vertical fault movement in the pre-failure seafloor reconstruction, the predictable thickness of sedimentary sequences (between Ref and SFR) throughout the study area is used to constrain the course of the pre-failure seafloor inside the sink area (Figure 4.2b and e). For the horizon-flattening approach, first reflectors Ref and SFR are picked in the 3D reflection seismic data. Then, reflector SFR is removed from inside the sink area. For pre-failure seafloor reconstruction, reflector Ref is horizontally flattened and SFR is reconstructed inside the sink area using the predictable thickness of the stratigraphic sequence between reflectors Ref and SFR by manually picking straight lines that represent this thickness between the upslope and downslope extent of the source area on individual inlines (the workflow is presented in Figure 4.6). After reconstruction is completed, reflector Ref is de-flattened with the resulting reconstructed pre-failure seafloor accounting for vertical tectonic movement of the seafloor antithetic en-echelon fault system with activity before failure occurrence of the primary failure of Ana Slide (Sager et al., 2022). The resulting surface is called the 'pre-failure seafloor following the horizon-flattening approach' (Figure 4.2b and e).

4.4.1 Uncertainties of volume estimations

General uncertainties for volume estimation are related to reflection seismic data such as unknown seismic velocities, lateral changes in seismic velocities, and reflector picking errors

(related to the vertical seismic resolution). Additional uncertainties unique to Ana Slide are related to the localization of bounding polygons of the source and sink areas related to the horizontal resolution of reflection seismic data and those related to issues with ghost artefacts in the 3D reflection seismic data previously discussed by Sager et al. (2022). Overall, the picking errors are small for 3D reflection seismic data (< 5 % of the total volume) and the uncertainty due to unknown seismic velocity is small for the uppermost sediments (< 5 %), while the uncertainty related to polygons of the source and sink areas is neglectable (< 2 %).

Dugan (2012) and Sun and Alves (2020) demonstrate that MTD material has higher density and lower porosity compared to background sediment, which would impact the seismic velocity of the landslide interval. A comparison of several cores inside and outside the landslide area shows that no notable differences in P-wave velocities in background sediment and MTD exist, at least in the upper 8 m (Lafuerza et al., 2012). Therefore, we assume no uncertainties resulting from lateral variations in seismic velocities.

The above uncertainties affect the different volume estimations in distinct ways. In sum, the above uncertainties of the volume estimation of Ana Slide add up to 12 %. Uncertainties related to the approach to pre-failure seafloor reconstruction are significantly larger but difficult to quantify in percentages (Table 4.1).

Volume assessment of Ana Slide assumes that slope failure occurred at once. From the analysis of the development and emplacement processes of Ana Slide (Sager et al., 2022), it is known that it developed during two overall stages of failure separated by around 240 ka. Because of limited vertical seismic resolution (5 m), it is not possible to identify the boundary between the two, which would be needed to differentiate between the individual volumes. Hence, despite better knowledge, we have to consider both as one and therefore Ve given here overestimates the initial failed volume for the main (primary) failure.

4.5 Results from volume assessments of Ana Slide

The amount of evacuated landslide material that remained inside the source area of Ana Slide called Ve_r is 0.024 km^3 (Table 4.1a). Together with the volume of Ve_{void} of 0.016 km^3 (Table 4.1b), the amount of all mobilized and involved landslide material from inside the source area called Ve is calculated by:

$Ve = Ve_{void} + Ve_r +$ (Vt), thus 0.016 km^3 + 0.024 km^3 = 0.040 km^3 (Table 4.1b and d).

The amount of material that was transported and deposited as a turbidite Vt could not be determined and is assumed to be zero.

The amount of bulk accumulated landslide material inside the sink area Va_{bulk} is 0.084 km^3 (Table 4.1c). This volume refers to both the amount of actually accumulated landslide material Va of 0.016 km^3 above the pre-failure seafloor reconstructed using the horizon-flattening

	Name	Upper surface (depth-converted horizons)	Lower surface (depth-converted horizons)	Bounding polygon	Areal extent (km^2)	Volume (km^3)
a	**Ve_r**	present-day seafloor (SFR)	reference reflector (Ref)	source area	1.90	0.024
b	**Ve_{void}**	reconstructed pre-failure seafloor using the contour-line approach	present-day seafloor (SFR)	source area	1.90	0.016
	Ve	Ve_r+ Ve_{void} Ve_r+ Va				0.040 0.040
c	**Va_{bulk}**	present-day seafloor (SFR)	reference reflector (Ref)	sink area	2.45	0.084
d	**Va**	present-day seafloor (SFR)	reconstructed pre-failure seafloor using the horizon-flattening approach	sink area	2.45	0.016
e	**Ve_{void}** (straight-line approach)	reconstructed pre-failure seafloor using the straight-line approach	present-day seafloor (SFR)	source area	1.90	0.027
f	**Va** (straight-line approach)	present-day seafloor (SFR)	reconstructed pre-failure seafloor using the straight-line approach	sink area	2.45	0.006

Table 4.1: Results from volume assessment of Ana Slide. Names of volumes calculated, and bounding surfaces are presented. The volume of Ve_{void} (evacuated volume from the source area) and Va (volume accumulated above the pre-failure seafloor inside the sink area) is the same at 0.016 km^3 (b and d).

approach (Table 4.1d), and the slope sediment deformed in situ between the reconstructed seafloor using the horizon-flattening approach and Ref inside the sink area. Va corresponds to Ve_{void} through (Vt is assumed to be zero):

Va = Ve_{void} – Vt, thus 0.016 km^3 = 0.016 km^3, and therefore Va = Ve_{void} for Ana Slide.

From the simple yet unrealistic pre-failure seafloor reconstruction using the straight-line approach applied inside the landslide scar of Ana Slide, we have estimated the amounts of Ve_{void} (straight-line approach) between the reconstructed and present-day seafloors inside the source area at 0.027 km^3 (Table 4.1e). The amount of Va estimated between the pre-failure seafloor using the straight-line approach for pre-failure seafloor reconstruction and the present-day seafloor inside the sink area yields a volume of 0.006 km^3 for Va (Table 4.1f).

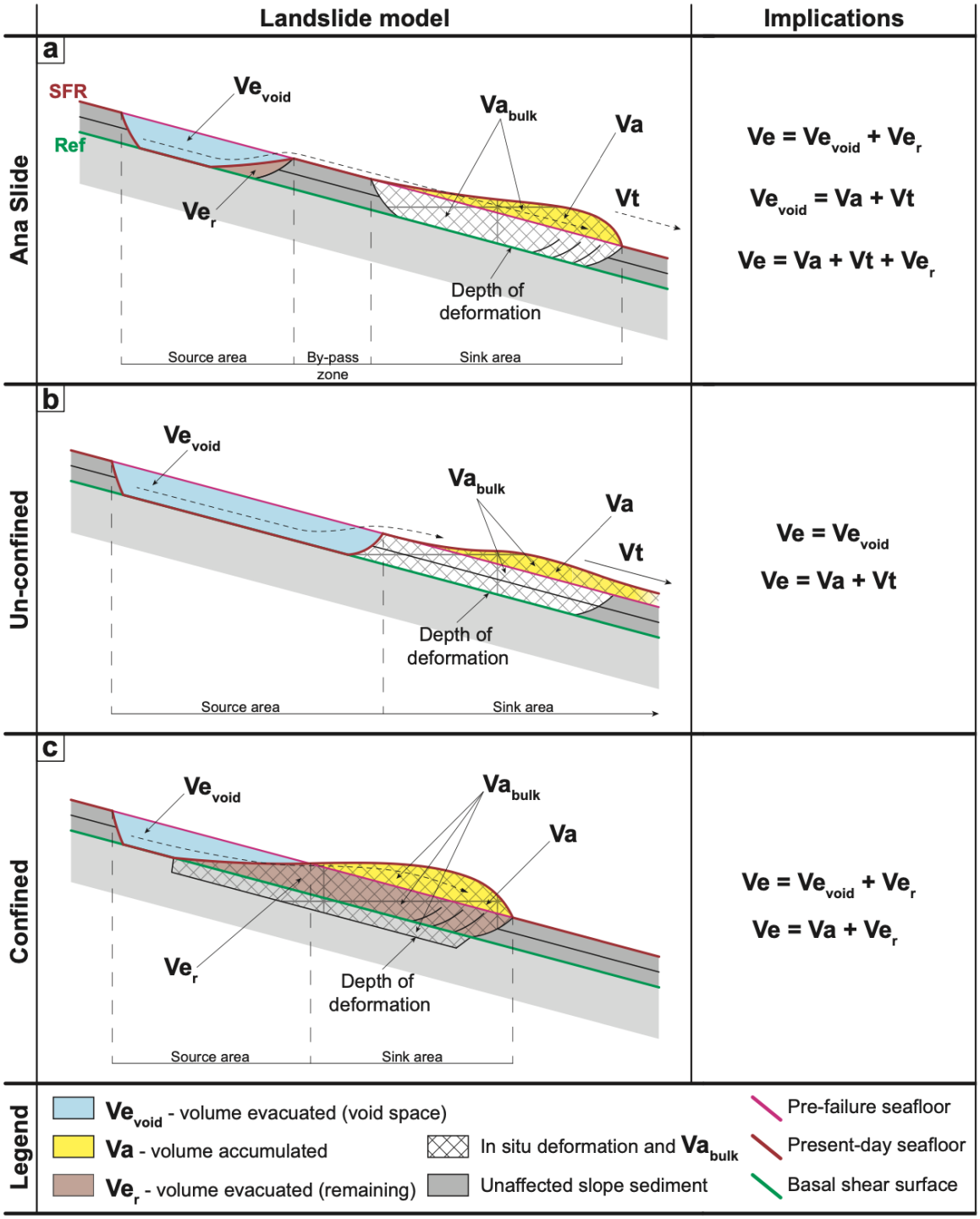

Figure 4.3: Conceptual models for assessing submarine landslide volume using unconfined and confined slope failure end members. **a)** Model of Ana Slide, with frontal emergence of landslide material above slope sediment that comprises the by-pass zone (in profile) and in situ deformation to a depth of Ref inside the sink area beneath the pre-failure seafloor. **b)** Model of an unconfined landslide with free propagation of landslide material over the seafloor inside of the extensively evacuated source area. **c)** Model of a confined landslide with restricted propagation of landslide material inside the sink area and limited evacuation of the source area.

4.6 Discussion

4.6.1 Ana Slide volume assessment

The initial failed volume of Ana Slide Ve is the sum of the actually evacuated volume Ve_{void} from the source area and the volume of the remaining material Ve_r inside the source area (Figure 4.3a). Furthermore, Ve can also be expressed as the sum of Ve_{void} and the volume of accumulated landslide material in the sink area Va. For Ana Slide both approaches result in Ve of 0.040 km^3 and thus are consistent. This suggests that the Ana Slide did not generate a turbidity current, because otherwise Ve estimated from Ve_{void} and Ve_r should exceed the Ve estimated from Va and Ve_r.

The volume of Va_{bulk} at 0.084 km^3 (Table 4.1c) is more than twice as large as Ve. Because of the previously detailed investigations for Ana Slide by Sager et al. (2022), we know the reason for this discrepancy. The deposit of Ana Slide induced in situ deformation that penetrated to a depth of reflector Ref in the sink area so that this deformed slope sediment appears chaotic, transparent, or disrupted in the reflection seismic data. However, the sediment beneath the deposit inside the sink area is not related to the initial failed volume mobilized from the source area Ve as the sediment deformed in situ and only very limited displacement or transport occurred above reflector Ref inside the sink area of Ana Slide (sensu Lastras et al., 2004). Hence, volume estimation based on seismic data considering seismically chaotic facies without further constraints on its origin would overestimate the initial failed volume of Ana Slide by more than 200 %.

To obtain the initial failed volume Ve, Ve_r and either Ve_{void} or Va need to be known. While Ve_{void} (and Va) can be estimated from bathymetry data alone, for example through comparing the modern and pre-failure seafloors, Ve_r can only be identified and quantified using sub-seafloor reflection seismic data. If no reflection seismic data had been available for Ana Slide, only Ve_{void} could have been estimated. This would have underestimated the initial failed volume by 40 % (because Ve = 0.040 km^3 while Ve_{void} = 0.016 km^3).

The value of Ve_{void} using the straight-line approach represents the upper limit of Ve_{void} because more realistic pre-failure seafloor reconstructions will estimate a smaller volume of Ve_{void}, and contour lines will diverge further upslope following the local and regional trends (Figure 1b and S1). The maximum Ve_{void} is thus 0.027 km^3, which exceeds the actual value of Ve_{void} of 0.016 km^3 by far. Similarly, the amount of Va estimated using the straight-line approach represents the lower limit of Va because more realistic contour lines will again diverge further upslope than those reconstructed with this approach. This value is much lower than Va estimated from the 'realistic' seafloor reconstruction.

Ana Slide is known to have formed during two stages of failure (Sager et al., 2022). The volume of the secondary failure is ignored because the thickness of accumulated landslide material is below the vertical seismic resolution. Nevertheless, the potential volume of a deposit resulting from the secondary failure that uniformly covers the entire sink area assuming

a thickness of 4 m which is just below the vertical seismic resolution of 5 m would have a volume of < 0.010 km^3, hence about a fourth of the volume of Ve at 0.040 km^3 (Table 4.1).

4.6.2 Volume assessment of unconfined and confined submarine landslides

In this section, we generalize our findings for Ana Slide. For the discussion, it is useful to categorize submarine landslides according to their emplacement mechanisms. Here, we distinguish between two endmembers following the terminology and definition by Frey-Martinez et al. (2006) – confined and unconfined types.

In the unconfined case, the source area is fully evacuated and devoid of landslide material, therefore Ve = $\mathrm{Ve_{void}}$ (Figure 4.3b). Ve can also be estimated by adding Va and Vt. Consequently, to assess the volume of unconfined submarine landslides, bathymetric data are ideal to estimate the volumes of $\mathrm{Ve_{void}}$ (and potentially Va) by comparing the modern and pre-failure seafloor topographies. Here, any post-slide modifications of the seafloor by external factors, such as tectonic movement or bottom currents, need to be excluded. The bathymetry-based approach will yield more robust values for Ve than approaches based on single profiles of sub-seafloor reflection seismic data. First, it is possible to cover the entire landslide area. Second, estimates for Ve and Va can be made and compared for additional quality control assuming that Ve = Va, here called volume balance between the source and sink areas and under this assumption, Va should not exceed Ve. Third, when using sub-seafloor reflection seismic data, a potential flaw could be introduced by estimating $\mathrm{Va_{bulk}}$ instead of Va. This is because the internals of a submarine landslide may be imaged as chaotic, disrupted, or transparent seismic facies. Sediments that were disturbed through internal deformation for example by rapid loading (e.g., Sager et al., 2022) or shearing induced by passing landslide material (e.g., Sobiesiak et al., 2018) also display as chaotic, disrupted, or transparent seismic facies. Hence, seismic facies of Va and $\mathrm{Va_{bulk}}$ are similar if not identical and therefore it is difficult if not impossible to distinguish material that moved, was translated, or was deformed in situ. This is problematic because $\mathrm{Va_{bulk}}$ may largely exceed Ve (and Va).

In the case of a confined landslide (Figure 4.3c), the initial failed volume of Ve equals the sum of $\mathrm{Ve_{void}}$ and $\mathrm{Ve_r}$, where $\mathrm{Ve_r} >> \mathrm{Ve_{void}}$. In this case, it is impossible to differentiate between $\mathrm{Ve_r}$ and Va. The amount of $\mathrm{Ve_r}$ can be calculated between the present-day seafloor and the basal shear surface and thus this approach requires sub-seafloor reflection seismic data. Using only bathymetric data to determine $\mathrm{Ve_{void}}$ will underestimate the initial failed volume by the value of $\mathrm{Ve_r}$ ($\mathrm{Ve} = \mathrm{Ve_{void}} + \mathrm{Ve_r}$). In the analysis of reflection seismic data, care must be taken in the identification of the basal shear surface. There is a risk to end up estimating $\mathrm{Va_{bulk}}$ instead of Va because of the reasons outlined above.

4.6.3 How to determine the initially failed volume of submarine landslides?

Based on the above considerations we here provide a framework and recommendations for assessing the initial failed volume of submarine landslides taking into account available data and emplacement mechanism (Figure 4.4). The framework applies only to landslide scars outcropping at the seafloor in areas, which have not experienced modification of the seafloor since the occurrence of the landslide. Hence, vertical tectonic movement, deposition by sediment transport processes, or ocean currents must be excluded, or these influences need to be accounted for in the pre-failure seafloor reconstruction. For instance, this is demonstrated by the horizon-flattening approach applied for pre-failure seafloor reconstruction performed inside the sink area of Ana Slide.

First, the pre-failure seafloor must be reconstructed using bathymetric data. Then, this reconstructed pre-failure seafloor may act as the upper surface in calculating Ve_{void} inside the source area using the present-day seafloor as the lower surface. Va is calculated between the present-day and reconstructed pre-failure seafloor inside the sink area. Now, the suggested workflow deviates according to the emplacement mode (unconfined or confined).

In the case the given submarine landslide developed as frontally unconfined (left branch in Fig. 4.4) it is beneficial to have seismic data covering the source area so that the amount of remaining landslide material (Ve_r) can be calculated in order to estimate the complete initial failed volume by $Ve = Ve_{void} + Ve_r$. Ve can also be estimated from Ve = Va + Vt. In the case no reflection seismic data are available, the rule that $Ve_{void} >= Va$ can serve as an additional constraint. Va cannot be larger than Ve_{void} because the material deposited in the sink area (estimated based on bathymetry) cannot exceed what was evacuated from the source area while Va can decrease if landslide material is transported as a turbidity current (Vt). If this condition, nevertheless, is not fulfilled one should revise the pre-failure seafloor reconstruction until the condition is fulfilled. In both cases, if reflection seismic data are available or not, it is robust to calculate Ve_{void} inside the sink area, because it either represents the amount of initial failed landslide material and represents the amount of Va, or the pre-failure seafloor reconstruction is incorrect assuming that no turbidite transported landslide material (not resolvable in the bathymetric data) and that no erosion and incorporation of seafloor sediment occurred.

In the case the given submarine landslide developed as frontally confined (right branch in Fig. 4.4), if reflection seismic data are available, the amount of all landslide material involved in or affected by the slope failure can be calculated as the bulk accumulated volume Va_{bulk}. For frontally confined submarine landslides the amount of Va_{bulk} is equal to Ve only in the case where no deep deformation has occurred. In that case, Va_{bulk} is larger than Ve. Ve_{void} underestimates Ve because the source area is only partly evacuated. In case no sub-seafloor reflection seismic data is available, the only means to approximate the initial failed volume of a submarine landslide is by Ve_{void} and Va, both of which will underestimate Ve.

In case the given landslide developed as a mixed system placed kinematically between the unconfined and confined case, or if the emplacement mode is unknown, we suggest estimating Ve_{void} and Va. If the amount of landslide material transported and deposited as a turbidite is neglectable, the amount of Ve_{void} and Va should be the same (Ve_{void} = Va). If Ve_r is unknown, one should consider that Ve_{void} and Va likely underestimate Ve by the unknown amount of Ve_r.

We showed that for Ana Slide, Va_{bulk} based on seismic data overestimates Ve by more than 200 % whereas estimating Ve from Ve_{void} and/or Va based on bathymetry data alone underestimates Ve by 40 %. Due to the risk of excessive overestimation, we suggest that the Ve = Ve_{void} + Ve_r approach should always be preferred over the Va_{bulk} approach, even if Ve_r is unknown.

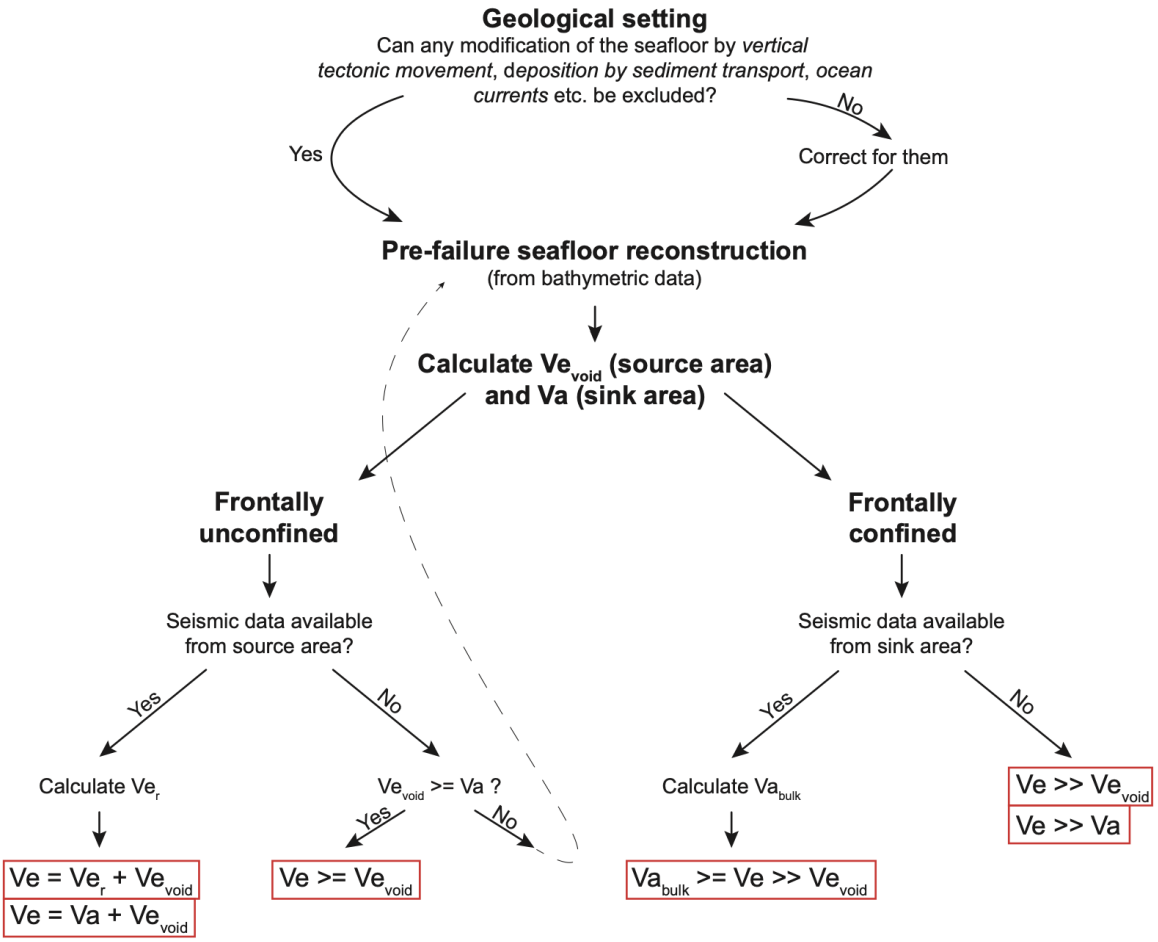

Figure 4.4: Workflow for assessing submarine landslide volumes.

4.6.4 Limitations and assumption of submarine landslide volume assessments

Estimation of Ve relies on the approach to pre-failure seafloor reconstruction. This may be challenging for submarine landslides in morphologically complex settings and pre-failure seafloor reconstruction might require a certain degree of subjectivity. For instance, the seafloor morphology of the source area before the failure of Ana Slide may have been influenced by the earlier pre-Ana Slide source area (Berndt et al., 2012; Sager et al., 2022). It is clear that Ve and Ve_{void} must be equal or larger than Va (if Vt > zero). This constraint can help assess the quality of the seafloor reconstruction at least in one direction.

Volume estimation based on bathymetry and pre-failure seafloor reconstructions also relies on the assumption that the seafloor has not changed significantly since the occurrence of the landslide. Any modifications of the seafloor, for instance by vertical tectonic movements, erosion, deposition by sediment transport, or ocean currents will result in wrong volume estimates. Another assumption is that the volume has been evacuated during one event. If the volume was evacuated during multiple stages with significant time gaps in between, for instance, the potential hazard will likely be overestimated, although controlled by many other factors such as landslide mechanisms, angle of the slide, water depth, density and cohesion of the landslide material, duration of the slide event, its acceleration, and run-out velocity (e.g., Harbitz et al., 2014).

Va is prone to underestimation because the resolution of bathymetric data and reflection seismic data is typically too low to resolve thin and far travelled turbidites approaching zero thickness in the distal parts, making a clear distinction between Va and Vt difficult.

Recent studies have shown that processes of basal erosion and incorporation of seafloor material can lead to a significant increase in Va (Sobiesiak et al., 2018; Nugraha et al., 2022), but this volume does not represent the volume of initial failed landslide material Ve. The deposit in the sink area might therefore not be a good representation and therefore we advocate to consider Ve, Ve_r, and Ve_{void} to estimate the initial failed volume.

4.7 Conclusions

In the absence of extensive geological, geotechnical, and age data, the hazard of submarine landslides is oftentimes assessed from their volume. Amongst the landslide mechanism, which is difficult to quantify, the initial failed volume is an important factor in tsunami simulations (Murty, 2003), for the estimation of which we identify the most robust method. It is not only the data type and quantity that controls the quality of the volume estimation but also the landslide‘s emplacement mechanism. If no seismic data from the source area of the landslide is available, the initial failed landslide volume Ve can reliably be determined only for frontally unconfined landslides. For unconfined or mixed systems, this approach will underestimate the true initial failed volume because the amount of landslide material that was mobilized but

remained inside the source area is neglected. Seismic data is required to estimate the volume of landslide material that remained inside the source area. If such data is not available, we find that the most robust approximation for the initial failed volume of an unconfined or mixed-system submarine landslide also is to determine the amount of evacuated landslide material between the pre-failure and present-day seafloors inside the source area from the void space between both surfaces using bathymetric data.

The initial failed volume has previously been estimated using the seismically identified deposit (Va_{bulk}). It is important to acknowledge that this may be prone to extreme overestimation (more than 200 % in this case) because of in situ deformation of sediments underlying the pre-failure seafloor in the sink area that may result from rapid deposition or shearing of the accumulating landslide deposits. When estimating the volume from the amount of seismically chaotic, transparent, or disrupted seismic facies, we advocate for balancing this against the initial failed volume estimated from bathymetric data, which yields a more conservative estimate.

Acknowledgements

This work is part of the Deutsche Forschungsgemeinschaft (DFG) – funded the TRISCO project (UR 226/3-1) under which Thore F. Sager was employed. We thank Jürgen Grabe (Institute of Geotechnical Engineering & Construction Management, Hamburg University of Technology (TUHH), Hamburg, Germany) for supporting funding acquisition. Many thanks are given to the master and the crew of RRS Charles Darwin who facilitated data acquisition during voyage 178, and Frode Eriksen of VBPR, Oslo for technical support on the same cruise. IHS Markit and Schlumberger provided academic licenses for Kingdom Suite and OMEGA, respectively. We would like to thank an anonymous reviewer and David Tappin (BGS) for reviews and suggestions to improve an earlier version of the manuscript.

Funding (not applicable for MU and CB)

The research leading to these results received funding from Deutsche Forschungsgemeinschaft (DFG) – TRISCO project under Grant Agreement number UR 226/3-1.

Conflicts of Interest/Competing Interests

The authors have no relevant financial or non-financial interests to disclose. These authors have no competing interests to declare that are relevant to the content of this article.

Availability of Data and Material

The 3D reflection seismic data from Ana Slide analyzed in the current study are available at the World Data Centre Pangaea repository (`https://doi.pangaea.de/10.1594/PANGAEA.943506`), the 2D reflection seismic data are available under (`https://doi.pangaea.de/10.1594/PANGAEA.943523`), and the multibeam bathymetry data of the study area are available under (`https://doi.pangaea.de/10.1594/PANGAEA.953762`).

Code Availability

Not applicable.

Author Contribution

Conceptualization: TFS, MU, CB; Methodology: TFS; Formal analysis and investigation: TFS; Writing original draft preparation: TFS; Writing – review and editing: TFS, MU, CB; Funding acquisition: MU, CB; Resources: CB; Supervision: MU, CB. Visualization: TFS has produced all figures (Figures 1 to 4). All authors reviewed the manuscript.

Code Availability

Additional Declarations for Articles in Life Science Journals that Report the Results of Studies Involving Humans and/or Animals (not applicable)

Ethics Approval

Not applicable.

Consent to Participate

Not applicable.

Consent for publication

Not applicable.

References

Berndt, C., S. Costa, M. Canals, A. Camerlenghi, B. de Mol, and M. Saunders (2012). Repeated Slope Failure Linked to Fluid Migration: The Ana Submarine Landslide Complex, Eivissa Channel, Western Mediterranean Sea. In: *Earth and Planetary Science Letters*, pp. 65–74. DOI: 10.1016/j.epsl.2011.11.045.

Bondevik, S., F. Løvholt, C. Harbitz, J. Mangerud, A. Dawson, and J. Inge Svendsen (2005). The Storegga Slide Tsunami – Comparing Field Observations with Numerical Simulations. In: *Marine and Petroleum Geology* 1-2, pp. 195–208. DOI: 10.1016/j.marpetgeo.2004.10.003.

Bondevik, S., J. I. Svendsen, and J. Mangerud (1997). Tsunami sedimentary facies deposited by the Storegga tsunami in shallow marine basins and coastal lakes, western Norway. In: *Sedimentology* 44.6, pp. 1115–1131. DOI: 10.1046/j.1365-3091.1997.d01-63.x.

Camerlenghi, A., R. Urgeles, and L. Fantoni (2010). "A Database on Submarine Landslides of the Mediterranean Sea". In: *Submarine Mass Movements and Their Consequences*. Ed. by D. C. Mosher, R. C. Shipp, L. Moscardelli, J. D. Chaytor, C. D. P. Baxter, H. J. Lee, and R. Urgeles. Dordrecht: Springer Netherlands, pp. 503–513. DOI: 10.1007/978-90-481-3071-9_41.

Cattaneo, A., D. Minisini, A. Asioli, M. Canals, G. Lastras, A. Remia, N. Sultan, and M. Taviani (2011). Age Constraints and Sediment Properties of Ana Slide (Balearic Sea, Western Mediterranean) and Implications on Age Dating of Submarine Landslides. In: EGU 2011 - Abstract. DOI: 10.1007/978-90-481-3071-9_42.

Dugan, B. (2012). "A Review of Overpressure, Flow Focusing, and Slope Failure". In: *Submarine Mass Movements and Their Consequences*. Ed. by Y. Yamada, K. Kawamura, K. Ikehara, Y. Ogawa, R. Urgeles, D. Mosher, J. Chaytor, and M. Strasser. Dordrecht: Springer Netherlands, pp. 267–276. DOI: 10.1007/978-94-007-2162-3_24.

Frey-Martinez, J., J. Cartwright, and D. James (2006). Frontally Confined versus Frontally Emergent Submarine Landslides: A 3D Seismic Characterisation. In: *Marine and Petroleum Geology* 5, pp. 585–604. DOI: 10.1016/j.marpetgeo.2006.04.002.

Fruergaard, M., S. Piasecki, P. Johannessen, N. Noe-Nygaard, T. Andersen, M. Pejrup, and L. Nielsen (2015). Tsunami Propagation over a Wide, Shallow Continental Shelf Caused by the Storegga Slide, Southeastern North Sea, Denmark. In: *Geology*, G37151.1. DOI: 10.1130/G37151.1.

Gatter, R., M. Clare, J. Kuhlmann, and K. Huhn (2021). Characterisation of Weak Layers, Physical Controls on their Global Distribution and their Role in Submarine Landslide Formation. In: *Earth-Science Reviews* 223, p. 103845. DOI: 10.1016/j.earscirev.2021.103845.

Hamilton, E. L. (1979). Sound Velocity Gradients in Marine Sediments. In: *The Journal of the Acoustical Society of America* 65.4, pp. 909–922. DOI: 10.1121/1.382594.

Harbitz, C. B., F. Løvholt, and H. Bungum (2014). Submarine Landslide Tsunamis: How Extreme and How Likely? In: *Natural Hazards* 3, pp. 1341–1374. DOI: 10.1007/s11069-013-0681-3.

Haugen, K. B., F. Løvholt, and C. B. Harbitz (2005). Fundamental Mechanisms for Tsunami Generation by Submarine Mass Flows in Idealised Geometries. In: *Marine and Petroleum Geology* 1-2, pp. 209–217. DOI: 10.1016/j.marpetgeo.2004.10.016.

Iglesias, O., G. Lastras, M. Canals, M. Olabarrieta, M. González, Í. Aniel-Quiroga, L. Otero, R. Durán, D. Amblas, J. L. Casamor, E. Tahchi, S. Tinti, and B. De Mol (2012). The BIG'95 Submarine Landslide–Generated Tsunami: A Numerical Simulation. In: *The Journal of Geology* 120.1, pp. 31–48. DOI: 10.1086/662718.

Lafuerza, S., N. Sultan, M. Canals, G. Lastras, A. Cattaneo, J. Frigola, S. Costa, and C. Berndt (2012). Failure Mechanisms of Ana Slide from Geotechnical Evidence, Eivissa Channel, Western Mediterranean Sea. In: *Marine Geology*, pp. 1–21. DOI: 10.1016/j.margeo.2012.02.010.

Lastras, G., M. Canals, D. Amblas, M. Ivanov, B. Dennielou, L. Droz, A. Akhmetzhanov, and TTR-14 Leg 3 Shipboard Scientific Party (2006). Eivissa Slides, Western Mediterranean Sea: Morphology and Processes. In: *Geo-Marine Letters* 4, pp. 225–233. DOI: 10.1007/s00367-006-0032-4.

Lastras, G., M. Canals, J. Hughes-Clarke, A. Moreno, M. De Batist, D. Masson, and P. Cochonat (2002). Seafloor Imagery from the BIG'95 Debris Flow, Western Mediterranean. In: *Geology* 30.10, p. 871. DOI: 10.1130/0091-7613(2002)030<0871:SIFTBD>2.0.CO;2.

Lastras, G., M. Canals, R. Urgeles, J. E. Hughes-Clarke, and J. Acosta (2004). Shallow Slides and Pockmark Swarms in the Eivissa Channel, Western Mediterranean Sea. In: *Sedimentology* 4, pp. 837–850. DOI: 10.1111/j.1365-3091.2004.00654.x.

Løvholt, F., S. Bondevik, J. S. Laberg, J. Kim, and N. Boylan (2017). Some Giant Submarine Landslides Do Not Produce Large Tsunamis: Giant Landslide Tsunamis. In: *Geophysical Research Letters* 16, pp. 8463–8472. DOI: 10.1002/2017GL074062.

Løvholt, F., I. Schulten, D. Mosher, C. Harbitz, and S. Krastel (2019). Modelling the 1929 Grand Banks Slump and Landslide Tsunami. In: *Geological Society, London, Special Publications* 477.1, pp. 315–331. DOI: 10.1144/SP477.2.

Maslin, M., M. Owen, S. Day, and D. Long (2004). Linking Continental-Slope Failures and Climate Change: Testing the Clathrate Gun Hypothesis. In: *Geology* 32.1, p. 53. DOI: 10.1130/G20114.1.

McAdoo, B., L. Pratson, and D. Orange (2000). Submarine Landslide Geomorphology, US Continental Slope. In: *Marine Geology* 169.1-2, pp. 103–136. DOI: 10.1016/S0025-3227(00)00050-5.

Moscardelli, L. and L. Wood (2015). Morphometry of Mass-Transport Deposits as a Predictive Tool. In: *Geological Society of America Bulletin*, B31221.1. DOI: 10.1130/B31221.1.

Murty, T. S. (2003). Tsunami Wave Height Dependence on Landslide Volume. In: *Pure and Applied Geophysics* 160.10-11, pp. 2147–2153. DOI: 10.1007/s00024-003-2423-z.

Nugraha, H. D., C. A.-L. Jackson, H. D. Johnson, D. M. Hodgson, and M. A. Clare (2022). Extreme Erosion by Submarine Slides. In: *Geology* 50.10, pp. 1130–1134. DOI: 10.1130/G50164.1.

Omira, R., M. Baptista, R. Quartau, R. Ramalho, J. Kim, I. Ramalho, and A. Rodrigues (2022). How Hazardous Are Tsunamis Triggered by Small-Scale Mass-Wasting Events on Volcanic Islands? New Insights from Madeira – NE Atlantic. In: *Earth and Planetary Science Letters* 578, p. 117333. DOI: 10.1016/j.epsl.2021.117333.

Panieri, G., A. Camerlenghi, I. Cacho, C. S. Cervera, M. Canals, S. Lafuerza, and G. Herrera (2012). Tracing Seafloor Methane Emissions with Benthic Foraminifera: Results from the Ana Submarine Landslide (Eivissa Channel, Western Mediterranean Sea). In: *Marine Geology*, pp. 97–112. DOI: 10.1016/j.margeo.2011.11.005.

Prior, D. B., B. D. Bornhold, and M. W. Johns (1984). Depositional Characteristics of a Submarine Debris Flow. In: *The Journal of Geology* 6, pp. 707–727. DOI: 10.1086/628907.

Sager, T. F., M. Urlaub, P. Kaminski, C. Papenberg, G. Lastras, M. Canals, and C. Berndt (2022). Development and Emplacement of Ana Slide, Eivissa Channel, Western Mediterranean Sea. In: *Geochemistry, Geophysics, Geosystems*. DOI: 10.1029/2022GC010469.

Sobiesiak, M. S., B. Kneller, G. I. Alsop, and J. P. Milana (2018). Styles of Basal Interaction beneath Mass Transport Deposits. In: *Marine and Petroleum Geology*, pp. 629–639. DOI: 10.1016/j.marpetgeo.2018.08.028.

Sun, Q. and T. M. Alves (2020). Petrophysics of Fine-Grained Mass-Transport Deposits: A Critical Review. In: *Journal of Asian Earth Sciences*, p. 104291. DOI: 10.1016/j.jseaes.2020.104291.

Sun, Q., T. M. Alves, X. Lu, C. Chen, and X. Xie (2018). True Volumes of Slope Failure Estimated From a Quaternary Mass-Transport Deposit in the Northern South China Sea. In: *Geophysical Research Letters* 6, pp. 2642–2651. DOI: 10.1002/2017GL076484.

Synolakis, C. E., J.-P. Bardet, J. C. Borrero, H. L. Davies, E. A. Okal, E. A. Silver, S. Sweet, and D. R. Tappin (2002). The slump origin of the 1998 Papua New Guinea tsunami. In: *Proceedings of the Royal Society of London. Series A: Mathematical, Physical and Engineering Sciences* 458.2020, pp. 763–789. DOI: 10.1098/rspa.2001.0915.

Talling, P., M. Clare, M. Urlaub, E. Pope, J. Hunt, and S. Watt (2014). Large Submarine Landslides on Continental Slopes: Geohazards, Methane Release, and Climate Change. In: *Oceanography* 27.2, pp. 32–45. DOI: 10.5670/oceanog.2014.38.

Talling, P., R. B. Wynn, D. G. Masson, M. Frenz, B. T. Cronin, R. Schiebel, A. M. Akhmetzhanov, S. Dallmeier-Tiessen, S. Benetti, P. P. E. Weaver, A. Georgiopoulou, C. Zuehlsdorff, and L. A. Amy (2007). Onset of Submarine Debris Flow Deposition Far from Original Giant Landslide. In: *Nature* 450.7169, pp. 541–544. DOI: 10.1038/nature06313.

Vanneste, M., N. Sultan, S. Garziglia, C. F. Forsberg, and J.-S. L'Heureux (2014). Seafloor instabilities and sediment deformation processes: The need for integrated, multi-disciplinary investigations. In: *Marine Geology* 352, pp. 183–214. DOI: 10.1016/j.margeo.2014.01.005.

Völker, D. J. (2010). A Simple and Efficient GIS Tool for Volume Calculations of Submarine Landslides. In: *Geo-Marine Letters* 5, pp. 541–547. DOI: 10.1007/s00367-009-0176-0.

Watt, S., P. Talling, M. Vardy, D. Masson, T. Henstock, V. Hühnerbach, T. Minshull, M. Urlaub, E. Lebas, A. Le Friant, C. Berndt, G. Crutchley, and J. Karstens (2012). Widespread and Progressive Seafloor-Sediment Failure Following Volcanic Debris Avalanche Emplacement: Landslide Dynamics and Timing Offshore Montserrat, Lesser Antilles. In: *Marine Geology* 323–325, pp. 69–94. DOI: 10.1016/j.margeo.2012.08.002.

Webster, J. M., N. P. George, R. J. Beaman, J. Hill, A. Puga-Bernabeu, G. Hinestrosa, E. A. Abbey, and J. J. Daniell (2016). Submarine Landslides on the Great Barrier Reef Shelf Edge and Upper Slope: A Mechanism for Generating Tsunamis on the North-East Australian Coast? In: *Marine Geology* 371, pp. 120–129. DOI: 10.1016/j.margeo.2015.11.008.

Wilson, C. K., D. Long, and J. Bulat (2004). The Morphology, Setting and Processes of the Afen Slide. In: *Marine Geology* 213.1–4, pp. 149–167. DOI: 10.1016/j.margeo.2004.10.005.

Supporting Information: Assessment of Submarine Landslide Volume

Sager, T. F.[1*], Urlaub, M.[1], Berndt, C.[1]

re-submitted to Geo-Marine Letters (GML)

[1] GEOMAR Helmholtz Centre for Ocean Research Kiel, Kiel, Germany

[*] Corresponding Author: tsager@geomar.de

We thank an anonymous reviewer and Dave R. Tappin for comments on a previous version of this manuscript previously submitted to GML (Submission ID: 59f81609-8b2d-4f9a-ade2-754a030e5ffa).

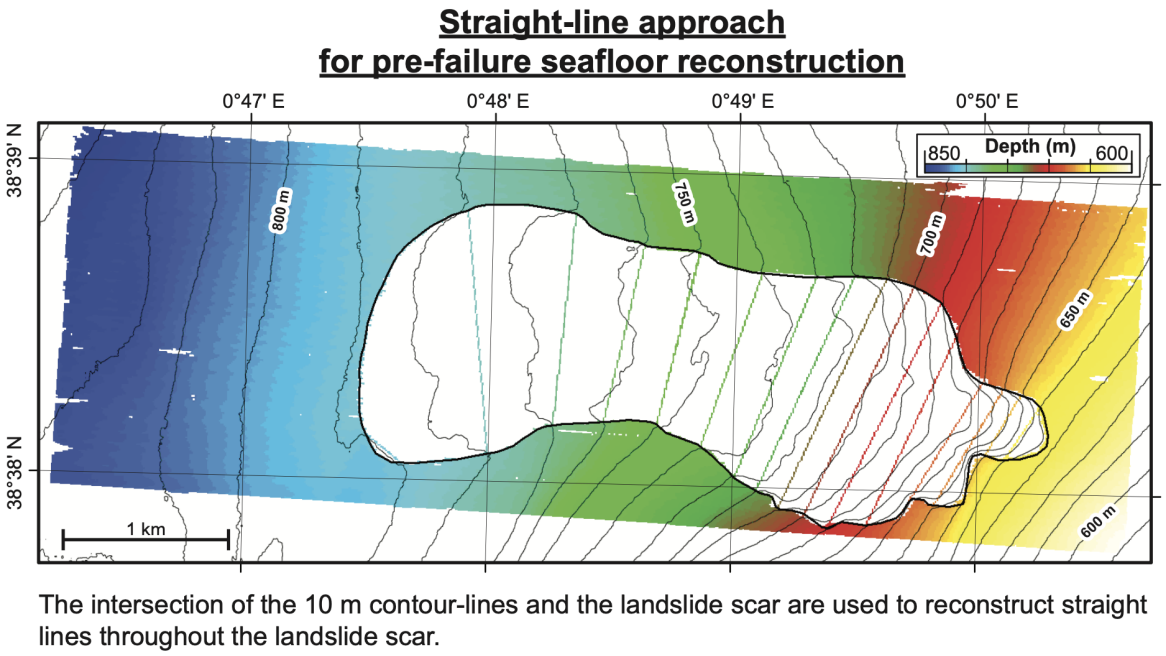

Figure 4.5: 'Straight-line ' pre-failure seafloor reconstruction approach.

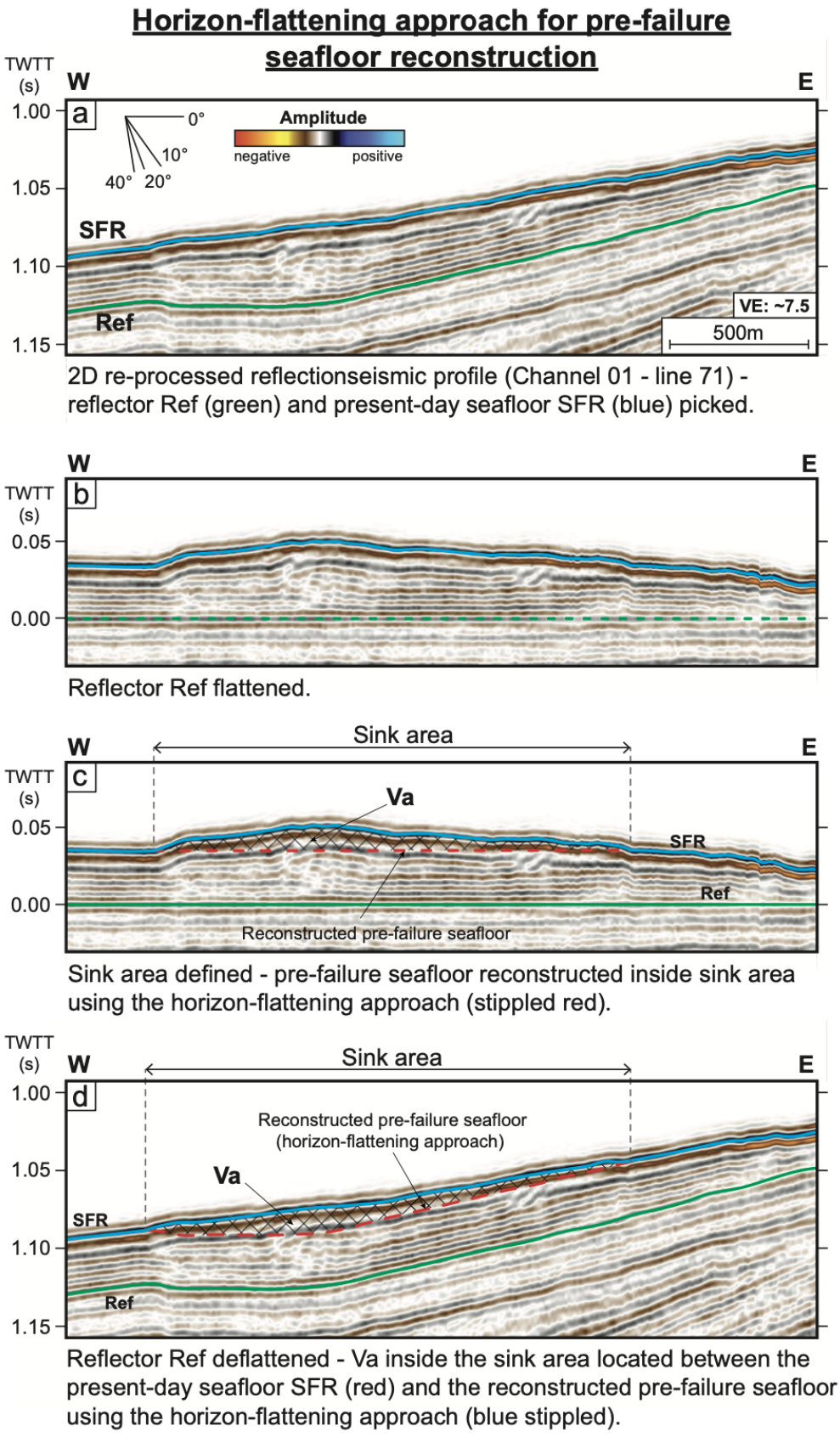

Figure 4.6: 'Horizon-flattening' pre-failure seafloor reconstruction approach.

5 Destabilizing Factors for Submarine Landslides in the Eivissa Channel, Western Mediterranean Sea

Sager, T. F.[1*], Urlaub, M.[1], Kaminski, P.[2], Lastras, G.[3], Canals, M.[3], Berndt, C.[1]

This version of the manuscript is submitted to Geochemistry, Geophysics, Geosystems (G^3) on the 5th of June 2023

[1] GEOMAR Helmholtz Centre for Ocean Research Kiel, Kiel, Germany

[2] Institute of Geotechnical Engineering & Construction Management, Hamburg University of Technology (TUHH), Hamburg, Germany

[3] Department of Earth and Ocean Dynamics, CRG Marine Geosciences, University of Barcelona, Barcelona, Spain

[*] Corresponding Author: tsager@geomar.de

Abstract

Submarine landslides can destroy offshore installations and generate tsunamis with the potential to inundate coastal areas. Here, we re-evaluate submarine landslide occurrences in the Eivissa Channel, Western Mediterranean Sea, from the analysis of geophysical data and draw upon conclusions from previous studies. A common slide plane for four slides in the Eivissa Channel indicates that changes in the sedimentation history have created an inherently unstable slope that is prone to failure. The position of the slides concerning the Messinian evaporites facies rules out direct and indirect controls of the Messinian on the observed slope failures. This is supported by the absence of compressional structures at the toe of the slopes. The data show that the southernmost of the slides, i.e., the Ana Slide Complex, has been active repeatedly. This may be due to the presence of gas in the sediments in this region. Repeated slope failures cannot be documented for the slides further north, but this may be due to sparser data coverage. Variations in landslide deposit thicknesses next to normal faults document continuous tectonic activity suggesting that fault activity was a potential trigger for the landslides.

Plain Language Summary

We investigate four submarine landslides off the coast of the Iberian Peninsula and the island of Ibiza. The aim of this study is to understand the causes of these landslides. We use existing and new geophysical data and identify a link between slope failure and tectonic activity of small local faults. These faults moved around the time at which the landslides occurred and controlled the vertical migration of gas and water. Movement of the faults and the presence of gas could have made the slope unstable. Beneath the southern-most landslide an additional landslide is found, which suggests that local tectonic activity and gas migration might be a recurrent process.

Key Points

- Landslides in the Eivissa Channel are located above small faults that show signs of past fluid migration.
- Their geomorphometrical similarity suggests identical failure mechanisms.
- Local tectonic activity and fluid migration might be a recurrent driver of landslides in the Eivissa Channel.

5.1 Introduction

Submarine landslides can destroy offshore infrastructure and pose a significant risk to coastal populations through tsunami generation (e.g., Bondevik et al., 2005; Haugen et al., 2005; Løvholt et al., 2017; Prior et al., 1984). The active process of slope failure has rarely been observed (e.g., Shan et al., 2022). Thus, knowledge about development and emplacement processes of slope failures is derived from seafloor morphology and resulting deposits called mass transport deposits (MTDs). These are imaged from geophysical methods such as multibeam bathymetry, sub-bottom echo-sounding, side-scan sonar, or 2D and 3D reflection seismic data (e.g., Frey-Martinez et al., 2005; Frey-Martinez et al., 2006; Gee et al., 2006; Gee et al., 2007; Hampton et al., 1996; Huvenne et al., 2002; Imbo et al., 2003; Wilson et al., 2004) and seldomly sampled in-situ by cores (Gatter et al., 2020; Lafuerza et al., 2012; Miramontes et al., 2018) or wells (Sawyer and Hodelka, 2016; Sun and Alves, 2020; Urlaub et al., 2018).

Destabilizing factors of submarine slopes are affected, for instance by the local physiography, geological setting, environmental stresses, and the depositional environment (e.g., Hampton et al., 1996). Furthermore, local tectonics, fluid and gas migration, and geotechnical properties of the slope sediments influence slope stability. Large landslides on gentle slopes can accommodate slope failure along laterally extensive 'weak layers' that appear in thick fine-grained sedimentary sequences (e.g., Gatter et al., 2021; Haflidason et al., 2004; Hjelstuen et al., 2007; Lindberg et al., 2004; Locat et al., 2014; Masson et al., 2006). While a weak layer represents a prime pre-conditioning factor for submarine slope failure, earthquakes and related peak ground accelerations (PGAs) are regarded as the ultimate triggering mechanism for many submarine landslides (e.g., Bryn et al., 2005; Gee et al., 2006; Laberg and Vorren, 2000; Lackey et al., 2018; Lastras et al., 2004).

To better understand the processes that inherently control and those that ultimately trigger slope failure, first the development and emplacement processes that govern them need to be addressed. This information could then potentially point toward pre-conditioning factors and triggering mechanisms previously at play. This was achieved for a relatively small landslide on the eastern slope of the Eivissa Channel, Western Mediterranean Sea (Figure 5.1), called Ana Slide (Berndt et al., 2012; Lastras et al., 2004; Lastras et al., 2006) (Figure 5.2). Development and emplacement processes of Ana Slide were interpreted by (Sager et al., 2022). This landslide is the southernmost one in a set of four landslides on the eastern slopes of the Eivissa Channel, the other three are known as Joan, Nuna, and Jersi slides from south to north (Lastras et al., 2004). In addition, a buried landslide was imaged in seismic reflection data beneath Ana Slide, called pre-Ana Slide (Berndt et al., 2012). The pre-Ana and Ana slides form the Ana Slide Complex.

This study aims to re-evaluate the causes for submarine slope failures on the eastern slope of the Eivissa Channel, Western Mediterranean Sea, in light of significant advances over the past two decades both regarding the fundamental reasons for slope destabilization and

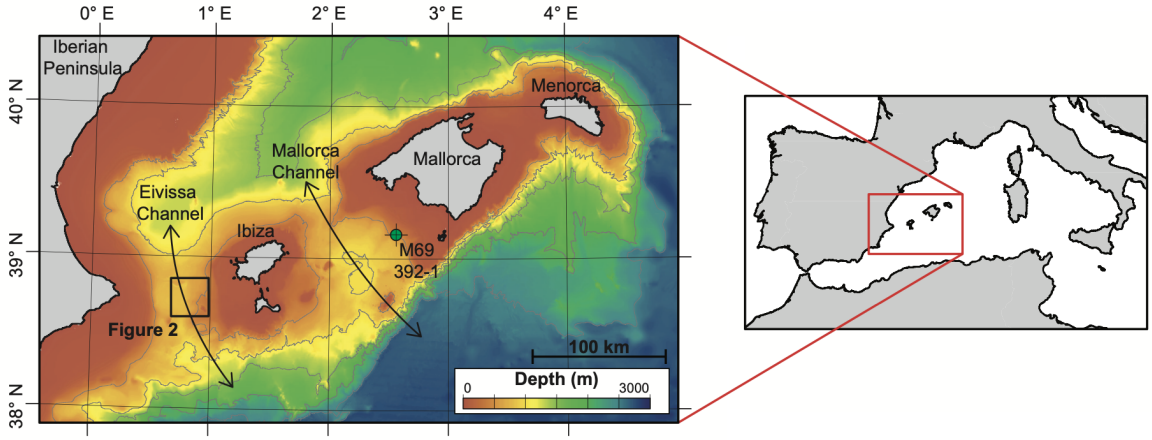

Figure 5.1: Bathymetry map of the Balearic Promontory located in the Western Mediterranean Sea (EMODnet, 2023). Isobath contours are 500 m. The study area (Figure 5.2) is located inside the Eivissa Channel between Eivissa and the Iberian Peninsula. Gravity core M69 392 – 1 (green symbol at 39° 09.397' N 2° 33.800' E) is located in the Mallorca Channel southwest off Mallorca. The black curved arrows mark the Eivissa Channel between the Iberian Peninsula and Eivissa and the Mallorca Channel between Eivissa and Mallorca.

new information on the geological setting of this area through several previous studies. In particular, we here investigate local tectonic activity concerning landslide timing, detailed geomorphometry, and internal structure under consideration of the revised emplacement mechanism of Ana Slide (Sager et al., 2022) for all landslides in the Eivissa Channel.

5.2 Geological setting of the Eivissa Channel

The Eivissa Channel is located at the western end of the Balearic Promontory that comprises the islands of Eivissa (*Ibiza* in Spanish), Formentera, Mallorca, and Menorca in the Western Mediterranean Sea (Figure 5.1). This promontory is around 350 km long from northeast to southwest, 100 – 150 km wide, and 1000 – 2000 m high with respect to the surrounding seafloor (Acosta et al., 2001a; Acosta et al., 2001b). The Eivissa Channel located between the island of Eivissa, and the Iberian Peninsula is characterized by a saddle-like structure with a maximum water depth of more than 900 m immediately south of the Xabia Seamount (Figure 5.2). Toward the southwest, the Balearic Promontory connects to the Betic Range along the southern Iberian Peninsula (Maillard and Mauffret, 2013; Mauffret et al., 1995). Toward the southeast, this promontory is limited by the Emile Baudot Escarpment (Acosta et al., 2001b). Nowadays, isolated earthquakes with magnitudes of 4 – 5 occur at shallow depths (0 – 50 km) inside the Eivissa Channel while earthquakes with magnitudes of Mw $<$ 5 occur frequently along the Betic System to the southwest and along the Algerian Margin to the south (IGN, 2023).

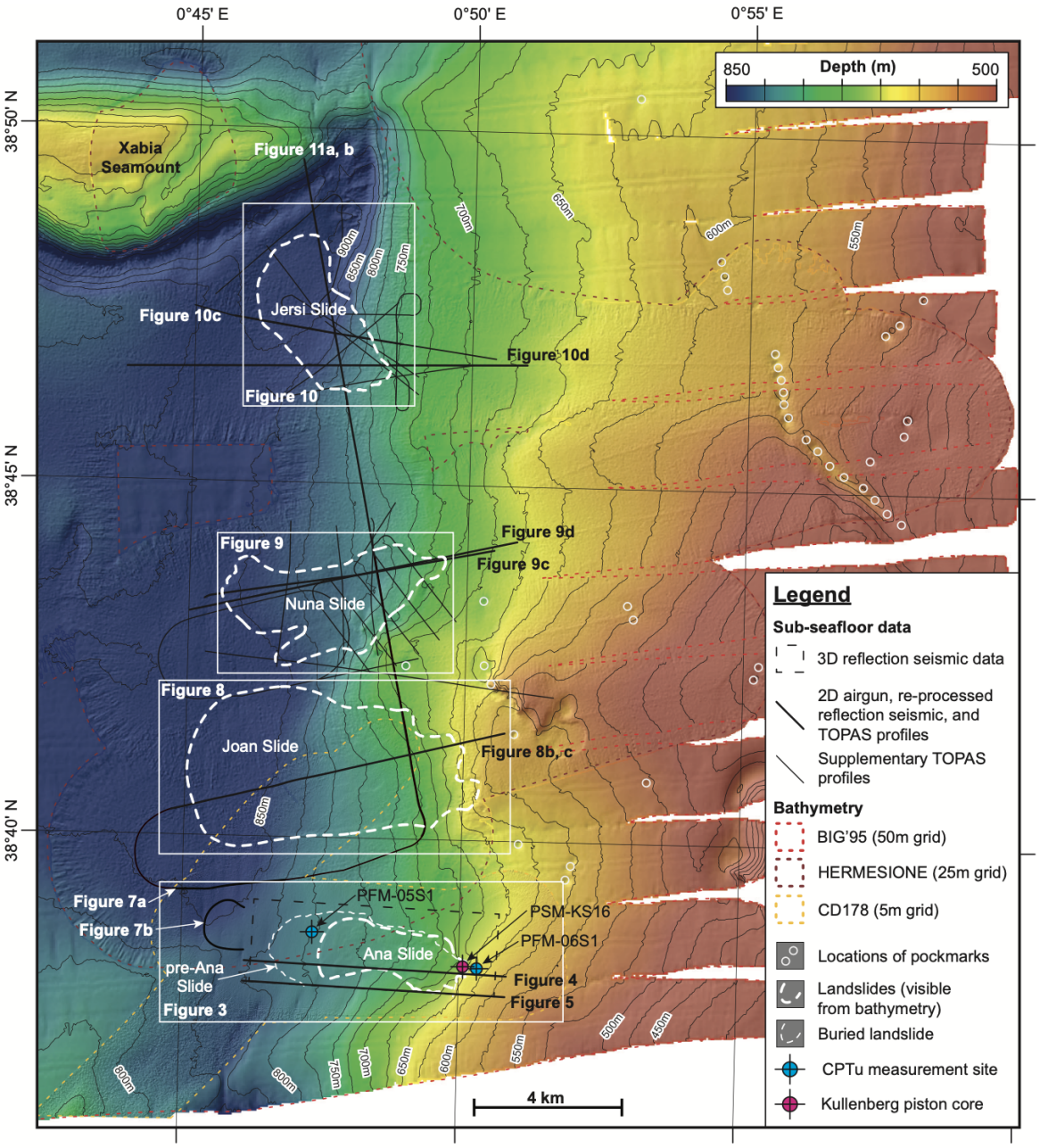

Figure 5.2: Hillshaded multibeam bathymetry map (acquired during cruises BIG'95, HERMESIONE, and CD178) of the eastern slopes of the Eivissa Channel, location in Figure 5.1. Ana, Joan, Nuna, and Jersi slides have seafloor expression and are located at water depths from 610 to 905 m. Beneath Ana Slide, the pre-Ana Slide has a congruent headscarp and extends around 1.5 km farther westward downslope. CPTu measurement sites in blue symbols (PFM-06S1: 38° 38.160' N 0° 50.382' E and PFM-05S1: 38° 38.651' N 0° 47.356' E from Lafuerza et al. (2012)) and Kullenberg piston core locations (PSM-KS16: 38° 38.219' N 0° 50.139' E from Lafuerza et al. (2012) and Panieri et al. (2012)) in red symbol. The location of pockmarks (white rings) is taken from Lastras et al. (2004). The location of TOPAS profiles, airgun profiles, re-processed 2D reflection seismic profiles, and the extent of the 3D reflection seismic data are highlighted by black lines.

5.2.1 Gas in the Eivissa Channel

There are multiple indicators for active gas seepage as well as the occurrence of free gas in the sub-seafloor of the Eivissa Channel. Multibeam bathymetry data and side-scan sonar imagery revealed several pockmarks at water depth ranging from 500 – 700 m in between the landslide scars (e.g., Acosta et al., 2001b; Lastras et al., 2004) (Figure 5.2). Berndt et al. (2012) showed the distribution of free gas in the sediments underlying the Ana Slide Complex using 3D reflection seismic data and indicate amplitude anomalies referred to as 'gas clouds' to be located around 150 – 200 m beneath the seafloor. A potential source for gas in the Balearic Promontory has previously been attributed to a deep thermogenic source (Acosta et al., 2001b).

Panieri et al. (2012) analyzed sediment core PSM-KS16 (38° 38.219' N 0° 50.139' E) located inside the upper Ana Slide scar at a water depth of 672 m for biostratigraphy, benthic foraminifera assemblages, carbon and oxygen stable isotope composition, and sedimentary structures to identify possible methane emissions from the seafloor. The authors conclude that the pre-landslide sediments have been subject to pervasive methane emissions for several thousands of years before the Ana Slide slope failure occurred. Then, during and after the occurrence of Ana Slide approximately 61.5 ka ago, methane emission continued, decreased, and ceased during the last deglaciation and the Holocene. No geophysical evidence for gas hydrates exists in the Eivissa Channel such as bottom-simulating reflectors (BSRs) (sensu Berndt et al., 2004). Local conditions of very salty waters (Camerlenghi et al., 2023), relatively high bottom water temperatures close to 13°C (Lafuerza et al., 2012), and relatively high geothermal gradients (compared to the eastern Mediterranean Sea; e.g., Praeg et al., 2008), inhibited gas hydrate formation in the past (Camerlenghi et al., 2023; Praeg et al., 2011)

5.2.2 Messinian evaporites

During the Messinian Salinity Crisis that occurred 5.96 – 5.33 Ma ago (Duggen et al., 2003; Krijgsman et al., 1999), the closure of the Gibraltar Strait through a combination of tectonic and glacio-eustatic processes isolated the Mediterranean Sea from the Atlantic Ocean (Gargani and Rigollet, 2007; Krijgsman et al., 1999). This closure in combination with high evaporation rates and limited fluvial influx caused the sea-level of the Mediterranean Sea to fall 2500 m (Gargani and Rigollet, 2007; Ryan, 1976) during three main stages (Roveri et al., 2014). Through evaporation, salinity steadily increased with initial gypsum precipitation at 200 m water depth beneath the sea-level at the onset of the Messinian Salinity Crisis (Ochoa et al., 2015). This was followed by mature precipitation products such as anhydrite (e.g., Roveri et al., 2008) and highly mature precipitation and deposition of halite in the deep basins of the Mediterranean Sea. In the eastern Mediterranean Sea, these thick evaporites acted as detachment surfaces for later raft tectonics of whole slope sequences (e.g., Roveri

et al., 2014), while mobile evaporites generated complex geological structures in the Algerian Basin (e.g., Blondel et al., 2022), south of the Balearic Promontory, and in the distal parts of the Rhone Delta in the Gulf of Lions north of the Balearic Promontory (e.g., Reis et al., 2005).

From the analysis of reflection seismic profiles, Driussi et al. (2015) and Ochoa et al. (2015) showed the extent of sedimentary units related to the Messinian Salinity Crisis in the Balearic Promontory (Figure 5.13). These authors interpret shallow areas around the Balearic Promontory to represent margin erosional surfaces because no Messinian depositional units are present. These areas were exposed immediately after the sea-level drop at the onset of the Messinian Salinity Crisis. In the deeper parts of the Eivissa and Mallorca channels (Figure 5.13) erosional products from the margin's erosional surface were deposited (Driussi et al., 2015; Ochoa et al., 2015). These authors call the Messinian unit beneath landslides on the eastern slopes of the Eivissa Channel the 'bedded unit' (BU) that corresponds to erosional products derived from the margin's erosional surface for which a precise chronostratigraphic control is lacking.

5.2.3 Terminology, local tectonic setting, and stratigraphy

Throughout this study, we use landslide terminology defined for Ana Slide by Sager et al. (2022). This includes, for instance, the 'source area' from where landslide material was initially evacuated and the 'sink area' where this landslide material ultimately accumulated. Furthermore, the outline of a landslide is called the landslide scar while the latest stage of upslope retrogression created the present-day upslope headscarp (Figure 5.3). Sager et al. (2022) mapped several seafloor syn- and antithetic normal faults reaching the seafloor in the study area of the Ana Slide Complex (Figures 5.3, 5.4, and 5.5). There are two seafloor synthetic normal faults located south of Ana Slide (labelled 'normal fault' in Figure 5.3). Beneath the Ana Slide Complex, three seafloor antithetic en-echelon normal faults were mapped. These comprise a fault system with an unknown extent to the south with the northern fault terminating beneath the sink areas of the Ana Slide Complex. The seafloor antithetic en-echelon fault system strikes from SSW to NNE and comprises the southern, central, and northern faults (Figures 5.3, 5.4, and 5.5).

Sager et al. (2022) present a stratigraphic framework for the study area of Ana Slide based on the interpretation of 3D and re-processed 2D reflection seismic data. Several seismic reflectors were picked that bound seismic units. Seismic reflectors used in this study are the top pre-Ana Slide – tpAS, reference – Ref, sub-reflector R1, and the seafloor reflector – SFR (Figures 5.4 and 5.5). Reflectors bpAS – tpAS bound the pre-Ana Slide Unit, the Interval Unit is bound by tpAS – Ref, and the Ana Slide Unit is located between Ref and SFR. Previously, Lastras et al. (2004) introduced Ref as their 'slip plane' reflector present throughout the study area of the Eivissa Channel.

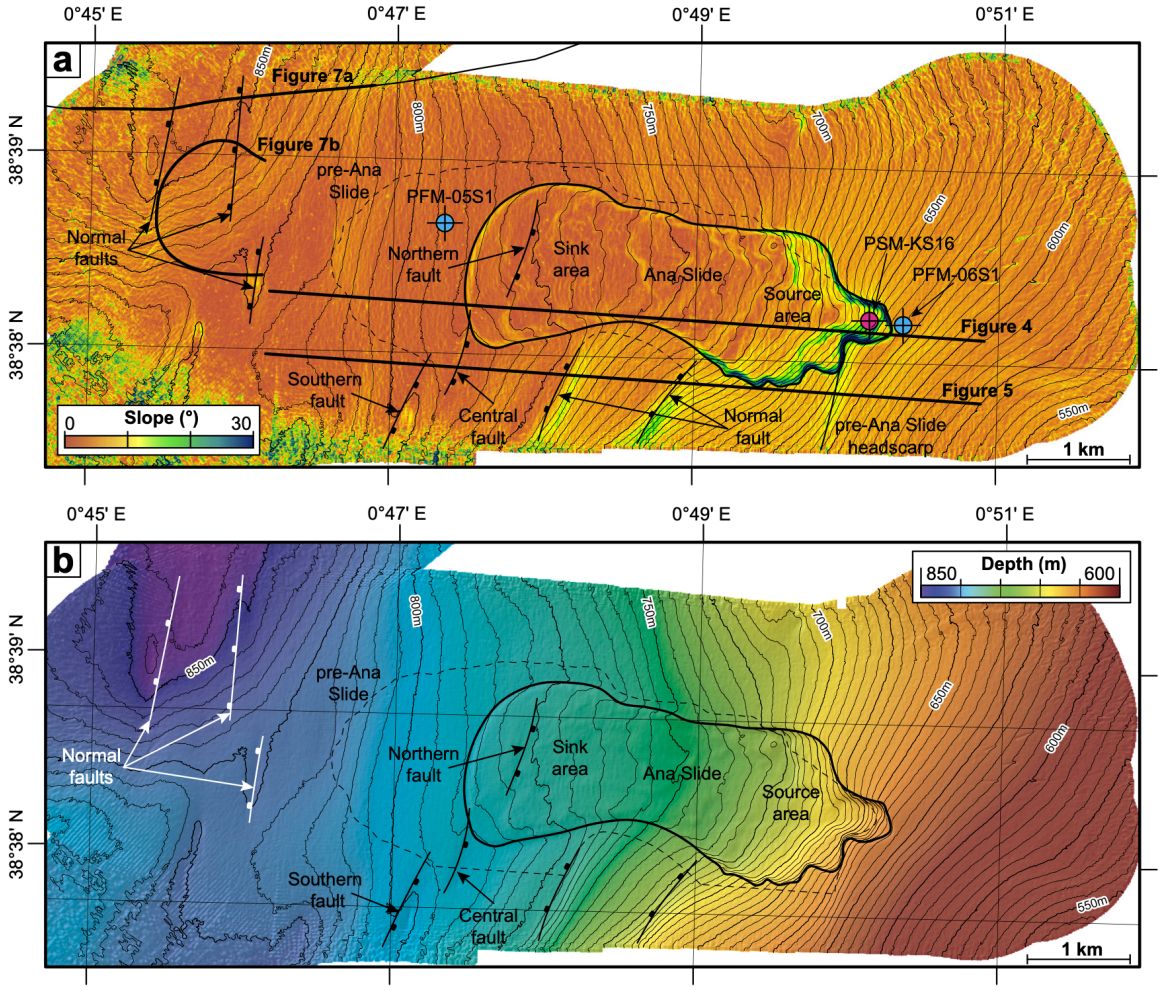

Figure 5.3: a) Slope gradient map of Ana Slide. Several faults are located beneath, south of, and west of Ana Slide (modified from Berndt et al., 2012). Locations of CPTu measurement sites (PFM-06S1: 38° 38.160' N 0° 50.382' E and PFM-05S1: 38° 38.651' N 0° 47.356' E from Lafuerza et al., 2012) are highlighted by blue symbols. Kullenberg piston core location (PSM-KS16: 38° 38.219' N 0° 50.139' E from Lafuerza et al. (2012) and Panieri et al. (2012)) indicated by the red symbol. The southern, central, and northern faults comprise the seafloor antithetic en-echelon fault system. The pre-Ana Slide extends around 1.5 km west of Ana Slide. **b)** Hillshaded bathymetry map of Ana Slide.

From the analysis of 3D reflection seismic data, Berndt et al. (2012) mapped several reflectors related to the Messinian Salinity. In the seismic data this event created a very-high amplitude reflector between 1.00 and 1.50 s TWTT here referred to as the Messinian Unconformity reflector (e.g., Figures 5.4 and 5.5).

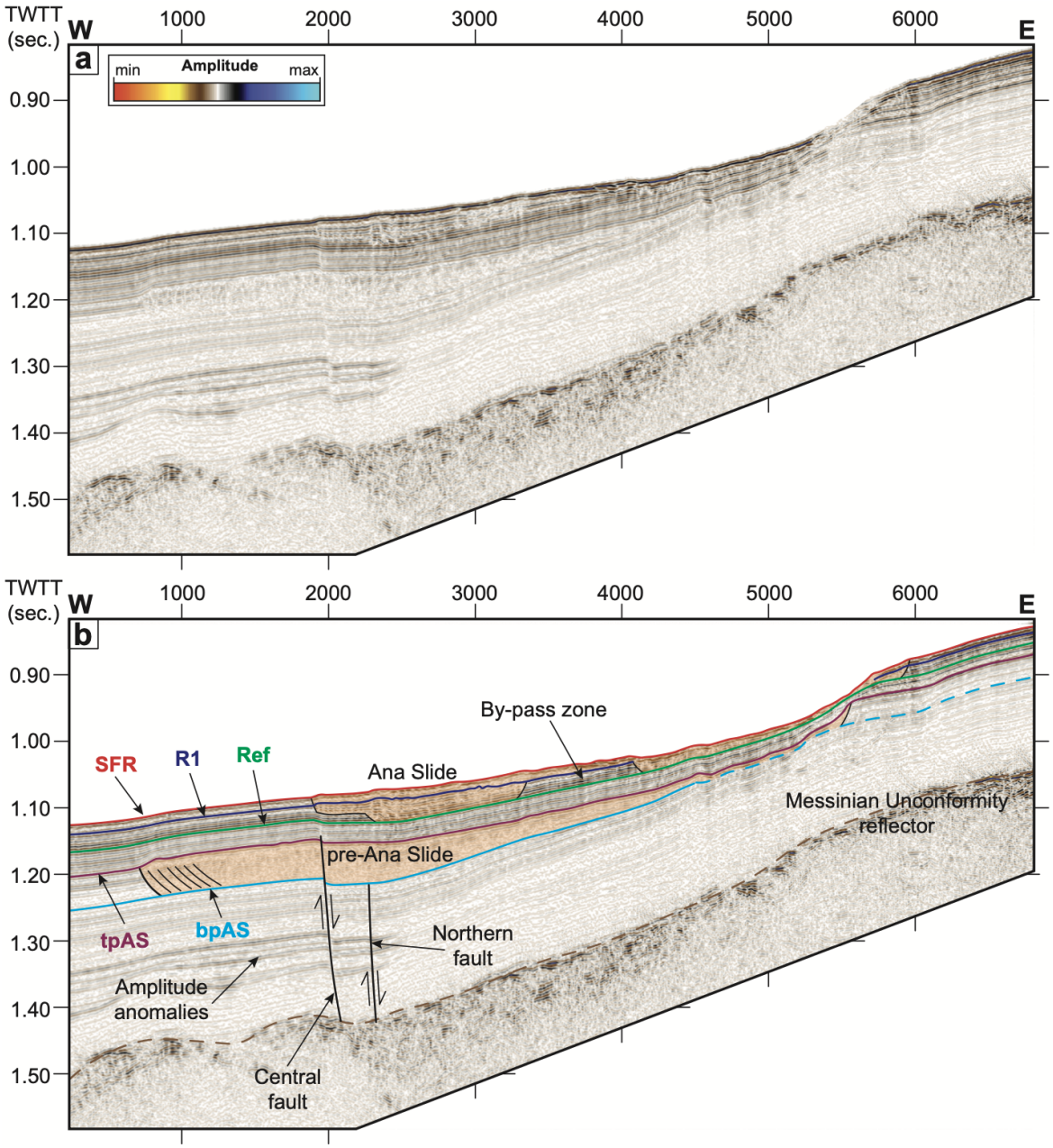

Figure 5.4: a) Uninterpreted re-processed 2D reflection seismic profile (Channel 1 – Line 37) through Ana Slide (location in Figure 5.2 and 5.3) from Sager et al. (2022). **b)** Interpreted profile with the northern and central faults that are part of the seafloor antithetic en-echelon fault system (Figure 5.3) that controlled the development and emplacement of Ana Slide Sager et al. (2022). Seismic reflectors at the base of pre-Ana Slide (bpAS), top of pre-Ana Slide (tpAS), Ref, R1, and the present-day seafloor (SFR). Vertical thicknesses between seismic reflectors, for instance between Ref and SFR (Ana Slide Unit) increase with increasing water depth toward the west.

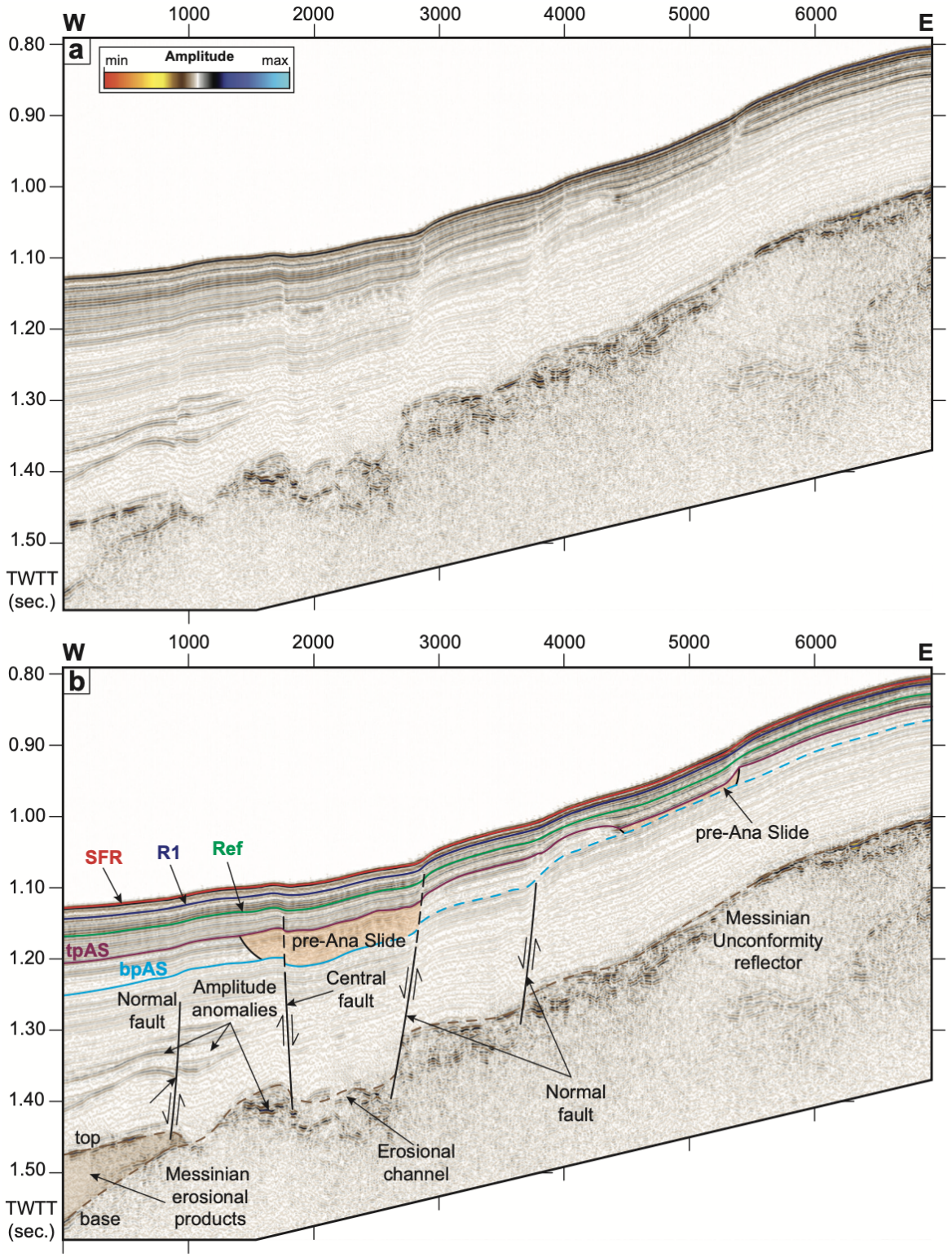

Figure 5.5: a) Uninterpreted re-processed 2D reflection seismic profile (Channel 1 – Line 83) through Ana Slide (location in Figures 5.2 and 5.3) from Sager et al. (2022). **b)** The interpreted profile shows three seafloor synthetic normal faults located south of Ana Slide and further toward the west and the central fault that is part of the seafloor antithetic en-echelon fault system (Sager et al., 2022). The central fault and the normal fault to the east created a graben-like structure that is rooted in the Messinian Unconformity reflector. Thickness between bpAS, tpAS, Ref, R1, and SFR increases with increasing water depth.

5.2.4 Characteristics and morphology of submarine landslides in the Eivissa Channel

Landslides in the Eivissa Channel are imaged from multibeam bathymetry maps, TOPAS, airgun and re-processed 2D and 3D reflection seismic data (Berndt et al., 2012; Lastras et al., 2004; Lastras et al., 2006; Sager et al., 2022) (Figure 5.2). In particular, Ana Slide has been the focus of several studies that performed geotechnical CPTu measurements, numerical modelling, foraminiferal, and reflection seismic data analysis (Berndt et al., 2012; Cattaneo et al., 2011; Lafuerza et al., 2012; Lastras et al., 2004; Lastras et al., 2006; Panieri et al., 2012; Sager et al., 2022). In the following, we provide an overview of the main results and hypotheses of previous studies for the destabilization, pre-conditioning and triggering for slope failures in the Eivissa Channel, Western Mediterranean Sea.

Ana, Joan, Nuna, and Jersi slides are located at a water depth between 610 and 905 m (Lastras et al., 2004; Lastras et al., 2006; Lastras et al., 2007) (Table 5.1) within distances of 20 km from each other (Figure 5.2). Their headscarps are not coincident with the location of the maximum slope gradient which is located some hundreds of meters downslope and, therefore, Lastras et al. (2006) concluded that the four landslides developed retrogressively and initial slope failure began at the location of maximum slope gradient.

Based on TOPAS profiles Lastras et al. (2004) showed that Ana, Joan, Nuna, and Jersi slides share the same basal shear surface referred to as the slip plane (called reflector Ref in this study) (e.g., Figures 5.4 and 5.5). The authors concluded that the basal shear surface must represent a geo-mechanical layer of weakness that controlled slope failure in the Eivissa Channel. Furthermore, because all landslides 'occupy the same stratigraphic position and share the same slip horizon', the authors suggest that this 'could indicate that they occurred simultaneously following a common triggering mechanism'.

5.2.5 Development and emplacement of Ana Slide

Sager et al. (2022) present the detailed development of Ana Slide from the analysis of multibeam bathymetry maps, 3D reflection seismic data, and re-processed 2D reflection seismic profiles. Ana Slide developed during two overall stages called the larger 'primary' and the much smaller 'secondary' failure that comprises sediments between Ref and R1 reflectors and between R1 and SFR reflectors, respectively (Sager et al., 2022, their Figure 3c) (Figures 5.4 and 5.5). These stages of failure comprise several additional smaller failures likely generated by retrogressive failure that generated a dissected headscarp (e.g., Figure 5.3).

During the primary failure, slope sediment located inside the source area was evacuated along the basal shear surface represented by reflector Ref (Sager et al., 2022, their Figure 3c) (Figure 5.4). Around 1.5 km downslope of the headscarp this mobilized landslide material emerged frontally above unaffected sediment representing the 'by-pass zone'. Landslide material then accumulated inside the sink area attaining a thickness of approximately 15 m,

which represents the main Ana Slide MTD. Its rapid deposition likely deformed slope in-situ sediment immediately underneath down to reflector Ref at a depth of 30 m inside the sink area.

During the secondary failure, sediment deposited after the primary failure with a thickness of approximately 15 m was again evacuated from the source area above reflector Ref (Figure 5.4). Mobilized landslide material again emerged frontally up and over the by-pass zone (in profile). From the analysis of magnetic susceptibility measurements of gravity cores, Cattaneo et al. (2011) showed that Ana Slide occurred around 61.5 ka ago. Based on sediment thickness and sedimentation rates, Sager et al. (2022) estimated a time-lag between the primary and secondary failures of the Ana Slide Complex of approximately 300 ka. Thus, both failures are separated by approximately 240 ka.

The study by Panieri et al. (2012) documents methane seepage before and during the failure of Ana Slide. From the analysis of Ana Slide performed by Sager et al. (2022) this places methane seepage to have occurred before and after the failure of Ana Slide which represents the time of the secondary failure meaning that methane seepage occurred around 61.5 ka ago. There is nevertheless no control if methane seepage occurred similarly before or immediately after the occurrence of the primary failure of Ana Slide around 300 ka ago.

5.2.6 Hypotheses for pre-conditioning factors and trigger mechanisms of Ana Slide

Lastras et al. (2004) discuss potential pre-conditioning factors for submarine slope failure in the Eivissa Channel from the evidence that all landslides occurred above the same seismic reflector the 'slip plane' or Ref. They, therefore, conclude that this reflector must represent a mechanically weak layer. In addition, the apparent weakness of this layer could have been enhanced by the escape of fluids sourced from pockmarks that are observed throughout the Eivissa Channel (Figure 5.2). Fluid sourced from these pockmarks may have generated increased pore pressure in the shallow sub-seafloor that could have decreased slope stability. In addition, these pockmarks could have represented a bedding discontinuity that may have reduced the shear resistance along this weak layer which could have promoted slope failure at the locations of maximum slope angles. Lastras et al. (2004), furthermore, highlight that acoustic wipe-out zones, for instance beneath Ana Slide, support the hypothesis of an origin for slope instability by fluid escape. In the area northeast of Ana Slide Lastras et al. (2004) and Lastras et al. (2006) suggested the location of pockmarks but there are no signs for deep roots of these in the reflection seismic data. Furthermore, the 'acoustic wipe-out'-zone in (Lastras et al., 2004; Lastras et al., 2006) (their Figure 4b) does not appear to correlate with a deep-rooted pockmark from the 3D reflection seismic data that outlines the headscarps of pre-Ana and Ana slides.

Lafuerza et al. (2012) used results from CPTu measurements and geotechnical laboratory tests on sediment cores from Ana Slide (Figures 5.2 and 5.3) as input to slope stability back

analyses. They concluded that excess pore pressure by gas exsolution and expansion along reflector Ref at the time of Ana Slide (secondary failure around 61.5 ka) did not generate high overpressures that reduce the effective stress. Yet, gas accumulated at the base of reflector Ref and subsequent expansion may explain the occurrence of Ana Slide (Figures 5.4 and 5.5). Furthermore, they suggested that a very close and moderate to strong earthquake (i.e., Mw $\geq$ 5) may have triggered Ana Slide and the historical records do not contradict this hypothesis (IGN, 2023).

Berndt et al. (2012) showed the distribution of free gas in the sediments underlying the Ana Slide Complex and active gas migration pathways using 3D reflection seismic data. The similar sizes of pre-Ana and Ana slides and the almost congruent location of the headscarps suggest that similar processes governed both landslides potentially pointing toward similar destabilizing factors. No direct indicators for overpressure exist such as 'seismic flat spots at the base of the gas accumulations' (Berndt et al., 2012). There is no clear vertical connection between high-amplitude reflections, for instance along local faults (the seafloor antithetic en-echelon fault system). This 'suggests that pore-pressures are not significantly increased at least at present' (Berndt et al., 2012). Based on previous evidence from Lastras et al. (2004), Berndt et al. (2012) suggest that the failure of pre-Ana and Ana slides were controlled by changes in pore pressure. A possible driver for the increased pore pressure could be the exsolution of gas during times of lowered sea-level. Since there are no signs of rapid deposition, the sediment overburden had little control on the pressure regime. Instead, this was controlled by lowering the sea-level. As presented in this study, pre-Ana and Ana slides are located above a local en-echelon fault system. While pre-Ana Slide developed completely above the central and northern faults, Ana Slide developed mainly upslope the northern fault.

Finally, Kaminski et al. (2021) attempted to quantify the impact of free gas on the stability of the Eivissa Channel slope using a constitutive model describing the mechanical behavior of gas-charged fine-grained sediments. Their results demonstrate that a disturbed soil structure as a consequence of former gas occurrence decreases overall slope stability. However, even in saturated conditions, slopes are inherently stable, and gas-induced soil disturbance can only be regarded as a pre-conditioning factor and not as a triggering mechanism for slope failures in the Balearic Promontory. This study and the previous study of Ana Slide by Sager et al. (2022) provide detailed accounts of local tectonic, depositional, and morphological features. Using new and updated observations, previous studies of pre-conditioning factors and potential triggering mechanisms must be revised.

5.3 Data and methodology

5.3.1 Data

This study uses multibeam bathymetry maps, sub-bottom echo-sounding, and 2D and 3D reflection seismic data from submarine landslides on the eastern slope of the Eivissa Channel, Western Mediterranean Sea (Figure 5.2). The EM 12 swath bathymetry maps (13 kHz, 81 beams) acquired during the BIG'95 (1995) and MARINADA (2002) cruises with the R/V Hespérides yield a horizontal resolution of 50 m. During the EUROLEON (2007) and HERMESIONE (2009) cruises the EM 120 system acquired higher quality multibeam bathymetry maps of submarine landslides in the Eivissa Channel were acquired with horizontal resolutions of 20 and 25 m, respectively. TOPAS 2D reflection seismic profiles were acquired with the PS018 system during the MARINADA, EUROLEON, and HERMESIONE cruises. During the latter cruise also airgun 2D reflection seismic profiles were acquired using an array of two 40 in^3 BOLT guns with a shooting rate of 5 s, and a GeoResources Geosense 24 streamer recording one channel with an active section of 25 m. The 3D reflection seismic data of the Ana Slide was acquired during cruise CD178 Berndt et al. (2012) and used in the interpretation of Ana Slide and re-processed by Sager et al. (2022) into 2D reflection seismic profiles.

5.3.2 Methodology

Here, we use seismic interpretation performed in IHS Kingdom Suite to map reflectors from the 3D reflection seismic data and re-processed 2D profiles of the Ana Slide Complex (reprocessing using OMEGA by Schlumberger) (Sager et al., 2022, and their supplementary material). Observations are tied with TOPAS and airgun profiles throughout the Eivissa Channel. Furthermore, analysis of multibeam bathymetry maps allows the seafloor expression of features observed in sub-seafloor data to be delimited.

We provide geomorphometric parameters for submarine landslides in the Eivissa Channel (Table 5.1). These include parameters previously presented by Lastras et al. (2007), Lastras et al. (2006), and Lastras et al. (2004) such as the water depth of the headscarps (d_{min}) and landslide fronts (d_{max}) and the drop height between both (H), the distance between the headscarp and the landslide fronts referred to as the length (L), the maximum width of the landslide scar measured perpendicular to the length (W), and the areal extent of the landslide scar (A). Maximum deposit thickness (t_{max}) is derived from the depth of deformation represented by reflector Ref beneath the seafloor reflector (SFR) inside the sink area for Ana, Joan, Nuna, and Jersi slides (Figures 5.4 and 5.8 to 5.11) through depth conversion (using a seismic velocity of 1500 m s^{-1}).

5.3.2.1 Local tectonic activity

The activity of the seafloor antithetic en-echelon fault system beneath pre-Ana and Ana slides is examined from reflection seismic profiles and isochore thickness maps by the apparent thickening and thinning relative to the mean stratigraphic unit thickness of the pre-Ana Slide, Interval, and Ana Slide units outside and inside the landslide scars (e.g., Figure 5.6). In planview, isochore thickness maps can provide information about emplacement and failure processes from the relative thickening or thinning or past morphological influences of stratigraphic units (Sager et al., 2022). In the case no landslide modified the seafloor morphology, steady background sedimentation would deposit a stratigraphic unit with a homogenous thickness inside an area if no external processes influenced the depositional environment. If a landslide occurred in this area, deposition after the failure would show an imprint of the previous seafloor morphology and thus thickness variation of post-landslide stratigraphic units will document the previous seafloor morphology and potentially external factors that influenced deposition. Relative thinning observed in an isochore map inside the landslide scar indicates the source area, while relative thickening indicates the sink area (Sager et al., 2022, their Figure 4c).

5.3.2.2 Observations of in-situ deformation

In reflection seismic data in-situ deformation results in chaotic, transparent, or disrupted seismic facies (e.g., Ford et al., 2021; Lenz et al., 2018; Posamentier and Martinsen, 2011; Sobiesiak et al., 2018). While it is difficult to distinguish between the style and the exact amount of deformation, the seismic facies can provide information, for instance about the susceptibility of slope sediment to deform and the penetration depth of deformation.

Figure 5.6: (Figure on next page.) **a)** Interpreted re-processed 2D reflection seismic profile (Channel 1 – Line 37 location in Figures 5.2 and 5.3) shows the base pre-Ana Slide (bpAS), top pre-Ana Slide (tpAS), Ref, R1, and seafloor (SFR) reflectors. **b)** Isochore thickness map in milliseconds (ms) two-way travel time (TWTT) of the pre-Ana Slide unit (tpAS – bpAS) extracted from 3D reflection seismic data. Unit thickness increases immediately upslope of the central and northern faults and inside the sink area of pre-Ana Slide. **c)** Isochore thickness map (ms TWTT) of the Interval Unit (tpAS – Ref). Sedimentation after the pre-Ana Slide commenced, and sediment unit thickens in the north of the former pre-Ana Slide and immediately west of it. Decreased thickness observed west of the central fault. **d)** Isochore thickness map (ms TWTT) of the Ana Slide Unit (Ref – SFR) (previously presented by Sager et al., 2022, their Figure 4c). Thickness increases immediately upslope of the northern fault in the sink area of Ana Slide, with thinning observed inside the source area. Thickness increases with increasing water depth toward the west between Ref and SFR.

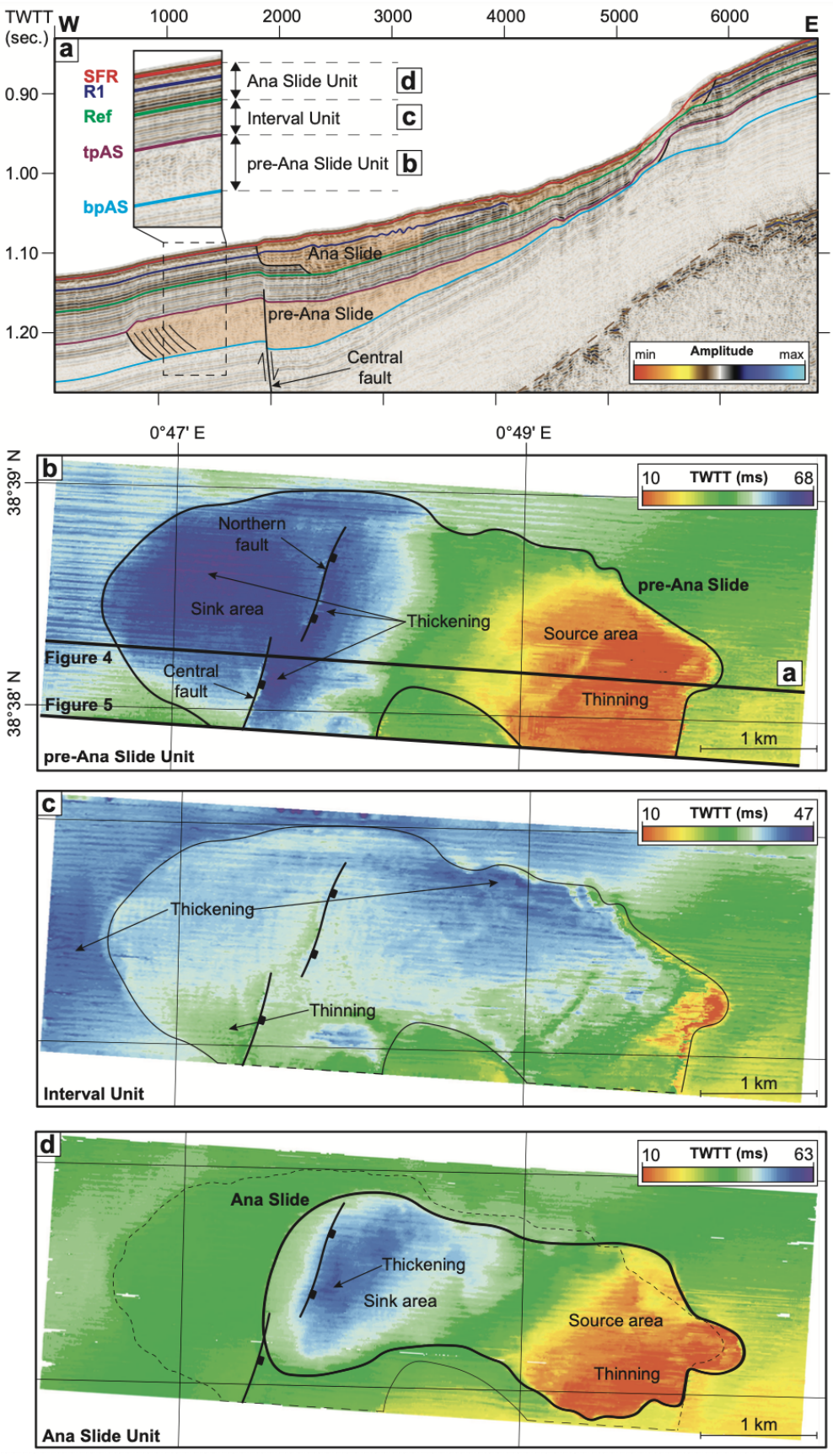

Figure 5.6: (Caption on previous page.)

5.3.2.3 Age determination of landslides

We determine the age of the pre-Ana Slide from the extrapolation of average sedimentation rates and the depth of tpAS that marks the timing of the pre-Ana Slide. The average sedimentation rate is assumed to be relatively steady inside the study area at 5 cm ka^{-1} following Cattaneo et al. (2011) and Sager et al. (2022). From the depth conversion of reflectors using a seismic velocity of 1500 m s^{-1} (Lafuerza et al., 2012) we then calculate the age that corresponds to the time of initial deposition after slope failure.

Calculations of the average sedimentation rates are related to uncertainties such as variability in lateral sedimentation rates and likely changes in sedimentation rates controlled by climatic variability (Sager et al., 2022). Furthermore, the depth conversion of sedimentary thicknesses is affected by the vertical resolution of the reflection seismic data with significant uncertainty and imprecise seismic velocities used for depth conversion. Altogether, we approximately evaluate the uncertainty of age determination to be about ± 20 %.

5.4 Results

	Water depth of head-scarp (m)	Water depth of land-slide front (m)	Drop height (m)	Length (km)	Width (km)	Area (km^2)	Maximum thickness of affected landslide material (m)			
	d_{min}	d_{max}	H	L	W	A	t_{max}	ratio: L/W	ratio: H/L	ratio: t_{max}/L_{max}
Ana	635	790	155	4.1	1.1	4.8	39	3.73	0.038	0.0095
Joan	610	860	250	7.7	4	23.6	52.5	1.93	0.033	0.0068
Nuna	705	855	150	5.9	2.2	10.2	45	2.68	0.025	0.0076
Jersi	750	905	155	4.5	2.1	8.1	41.25	2.14	0.034	0.0092
pre-Ana	-	-	-	5.3	2.1	8.5	48.75	2.52	-	0.0092

Table 5.1: Geomorphometric table of submarine landslides in the Eivissa Channel. Parameters are defined after Clare et al. (2019). Values of d_{min}, d_{max}, A, and t_{max} were previously presented by Lastras et al. (2004), Lastras et al. (2006), and Lastras et al. (2007).

5.4.1 Geomorphometry of landslides

Here, we provide geomorphometric parameters for submarine landslides in the Eivissa Channel (Table 5.1). Some of these were previously published by Lastras et al. (2004), Lastras et al. (2006), and Lastras et al. (2007). The minimum water depth of landslides (d_{min}) or the depth of the headscarps in the Eivissa Channel decreases from 610 m for Ana Slide in the south to 750 m for Jersi Slide in the north (Figure 5.2 and Table 5.1). The drop heights of Ana, Nuna, and Jersi slides are around 150 m while Joan Slide shows a drop height of

250 m. This larger drop height correlates with an increase in the length, width, and area of Joan Slide as for instance, the H/L ratio is similar for all landslides (0.025 – 0.038). The maximum thickness of affected landslide material ranges between 39 – 52.5 m and correlates with the overall length of the landslides represented by the L/W ratio of 1.93 for Joan Slide and 2.68 for Nuna Slide although Ana Slide shows an increased L/W ratio of 3.73. Similar L/W ratios were measured for landslides on the Great Bahama Banks in the range of 2 – 2.86 (Principaud et al., 2015) which is similar to the range measured for the studied landslides here (1.93 – 2.68). The t_{max}/L ratio of Joan Slide is slightly decreased (0.068) compared to the other landslides that range between 0.076 – 0.095.

5.4.2 Internal structure of landslides

In-situ deformation of slope sediment is characterized by chaotic, transparent, and disrupted seismic facies at depth (Figures 5.4 and 5.8 to 5.11). Here, the depth to which in-situ deformation penetrated is called 'depth of deformation'. Because detailed knowledge of development and emplacement processes were known only for Ana Slide, we adopt the notion that chaotic, transparent, and disrupted seismic facies characterize in-situ deformed and affected slope sediment within the sink areas of Joan, Nuna, and Jersi slides (Figures 5.8, 5.9, and 5.10). For all these landslides, the depth of deformation is confined to reflector Ref.

5.4.3 Reconstructing fault activity

5.4.3.1 Ana Slide Complex

The isochore thickness map of the pre-Ana Slide Unit is bound between tpAS and bpAS (Figure 5.6b) and shows thickening immediately east of the central and northern faults. Furthermore, thickness increases west of the faults. The Interval Unit bound between reflectors tpAS and Ref (Figure 5.6c) shows thickening toward the west of the pre-Ana Slide landslide front and in the northern source area. Thickness decreases immediately east of the central and northern faults and increases west of the central fault. The Ana Slide Unit bound between reflectors Ref and SFR (Figure 5.6d) shows a thickness increase immediately east of the northern fault while Ana Slide propagated around 300 – 500 m further downslope toward the west (Sager et al., 2022). This position aligns with the central fault's northern prolongation.

The 3D seismic data extend around 500 m to the west of the pre-Ana Slide scar while the re-processed 2D reflection seismic profile previously presented by Sager et al. (2022) shows the sub-seafloor in the turns of the vessel up to 1.5 km west of the extent of the 3D cube (Figure 5.3). This data was subsequently included in the re-processing (Figure 5.7b) and new profiles were correlated with TOPAS profiles from between Ana and Joan slides (Figure 5.7a). These shallow profiles show two seafloor synthetic normal faults at the toe of the slope

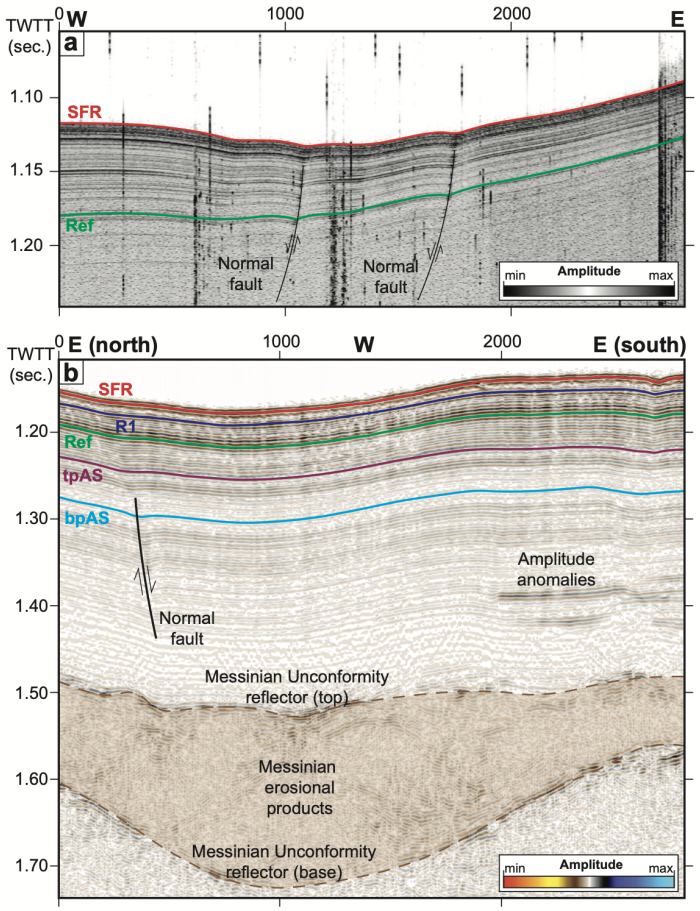

Figure 5.7: a) TOPAS profile (Figure 5.2). Two seafloor-synthetic normal faults terminate beneath the seafloor with seafloor expression (Figure 5.3). **b)** Re-processed 2D reflection seismic profile (Channel 1 – Line 20) west of the Ana Slide Complex after Sager et al. (2022). The normal faults on the left in b correspond to the normal faults on the right side of a with the location presented in Figure 5.3.

toward the deepest part of the Eivissa Channel that are sub-parallel with the en-echelon fault system beneath the Ana Slide Complex (Figure 5.3). The eastern fault in Figure 5.7a that recently affected the seafloor morphology at shallow depth (Figure 5.3) corresponds to the 'normal fault' shown in Figure 5.7b at depth beneath the seafloor.

5.4.3.2 Joan Slide

Joan Slide is imaged by TOPAS profiles acquired in parallel with airgun profiles. These cross the landslide from east to west and show a change in the inclination of reflector Ref that represents the 'Joan Slide normal fault' about 1.5 km downslope of the headscarp (Figure 5.8a, b). This fault is also imaged in the regional NS profile (Figure 5.11) where it appears in the southern source area along with amplitude anomalies. This fault appears in the slope gradient map with NNW to SSE orientation that extends for at least 1 km outside the Joan Slide scar toward the south (Figure 5.8a). In the airgun profile slight amplitude anomalies

are observed immediately west of the landslide around 1.45 s TWTT (Figure 5.8c) and west of the Joan Slide normal fault beneath the source area.

5.4.3.3 Nuna Slide

TOPAS profiles from the Nuna Slide (Figure 5.9c) show the thickening of the landslide unit bounded by reflectors Ref and SFR around 3 km downslope of the headscarp (Figure 5.9a) that is not evident in the slope gradient map (Figure 5.9b). The location of this thickening coincides with the 'Nuna Slide normal fault' that terminates on the Messinian Unconformity reflector at depth and aligns with a vertical feature at the Messinian Unconformity reflector at a depth of 1.25 s TWTT (Figure 5.9d). An additional normal fault located around 1 km toward the east also terminates above the feature. Because of limited seismic penetration beneath the Messinian Unconformity reflector, we cannot exclude that these faults have displaced Messinian Units beneath. The seismic facies of the Nuna Slide Unit changes from chaotic to disrupted east of the faults to almost completely transparent to the west of it (Figure 5.9c).

5.4.3.4 Jersi Slide

We calculate the thickness of the Jersi Slide Unit bound by reflectors Ref and SFR from several TOPAS profiles (Figure 5.2). The upslope source area of Jersi Slide is thinned toward the southeast while the thickest area is located immediately to the west (Figure 5.10a). No faults have been identified beneath or close to Jersi Slide on TOPAS profiles and no seafloor features of faults were observed in the slope gradient map (Figure 5.10b, c). Nonetheless, the airgun profile (Figure 5.10d) images a deep normal fault that terminates along the Messinian Unconformity reflector and shows amplitude anomalies on the hanging wall side in the west while seismic amplitudes are low on the footwall side toward the east. Furthermore, immediately beneath Jersi Slide, the Messinian Unconformity reflector shows high-amplitude anomalies.

Figure 5.8: (Figure on next page.) **a)** Slope gradient map of Joan Slide. The TOPAS profile (b) and the airgun profile (sub-figure c) were collected in parallel and are highlighted by the thick black line. Around 1.5 km downslope of the headscarp we observe a seafloor feature from SSE to NNW labelled 'Joan Slide normal fault'. **b)** TOPAS profile of Joan Slide. The Joan Slide normal fault is located around 1.5 km downslope of the headscarp. In-situ deformation in the sink area down to reflector Ref (limited penetration depth). **c)** Airgun profile of Joan Slide. The fault observed from the slope gradient map (a) and TOPAS profile (b) terminates toward the Messinian Unconformity reflector. In-situ deformation is observed to have penetrated to depths of reflector Ref inside the sink area.

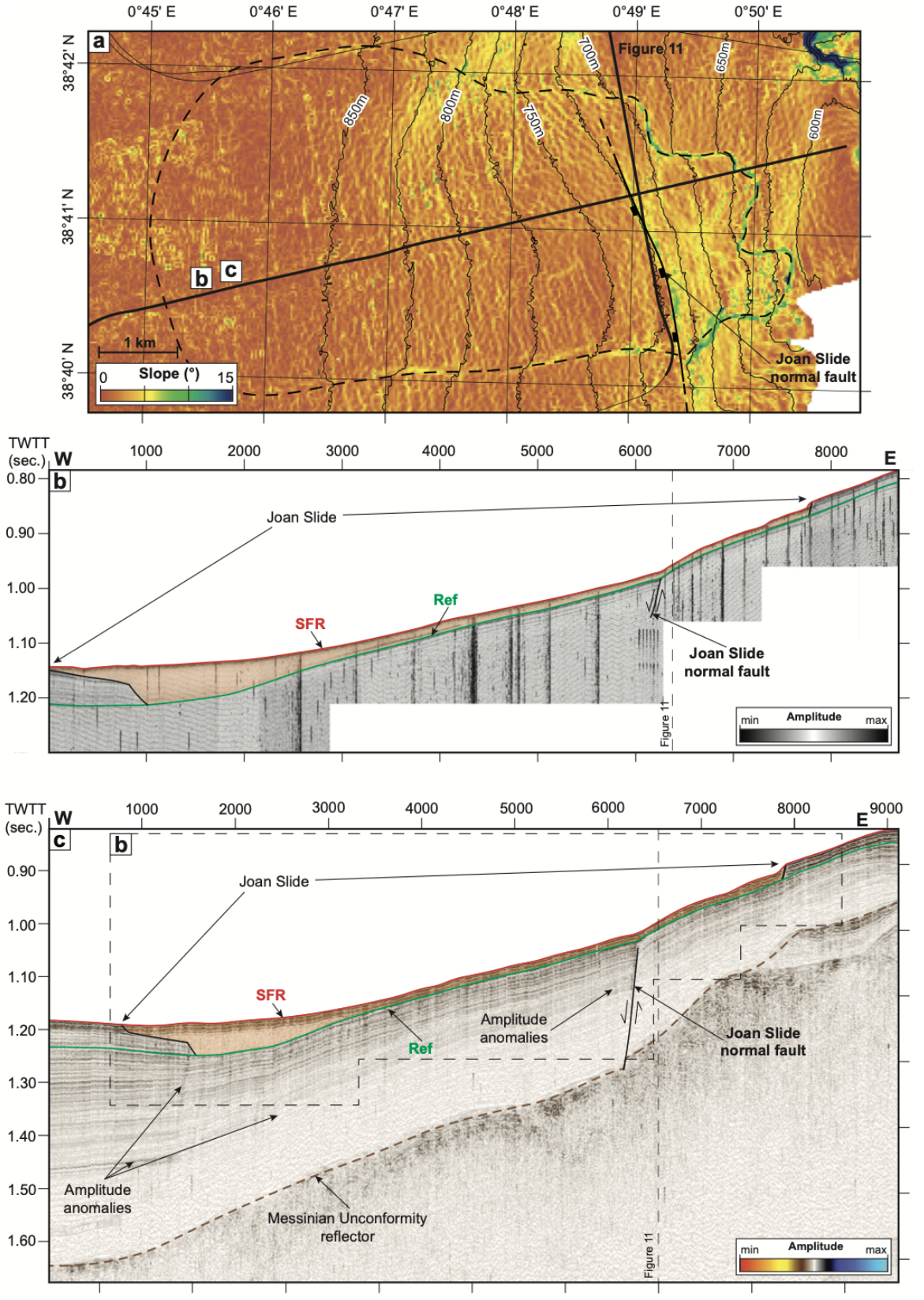

Figure 5.8: (Caption on previous page.)

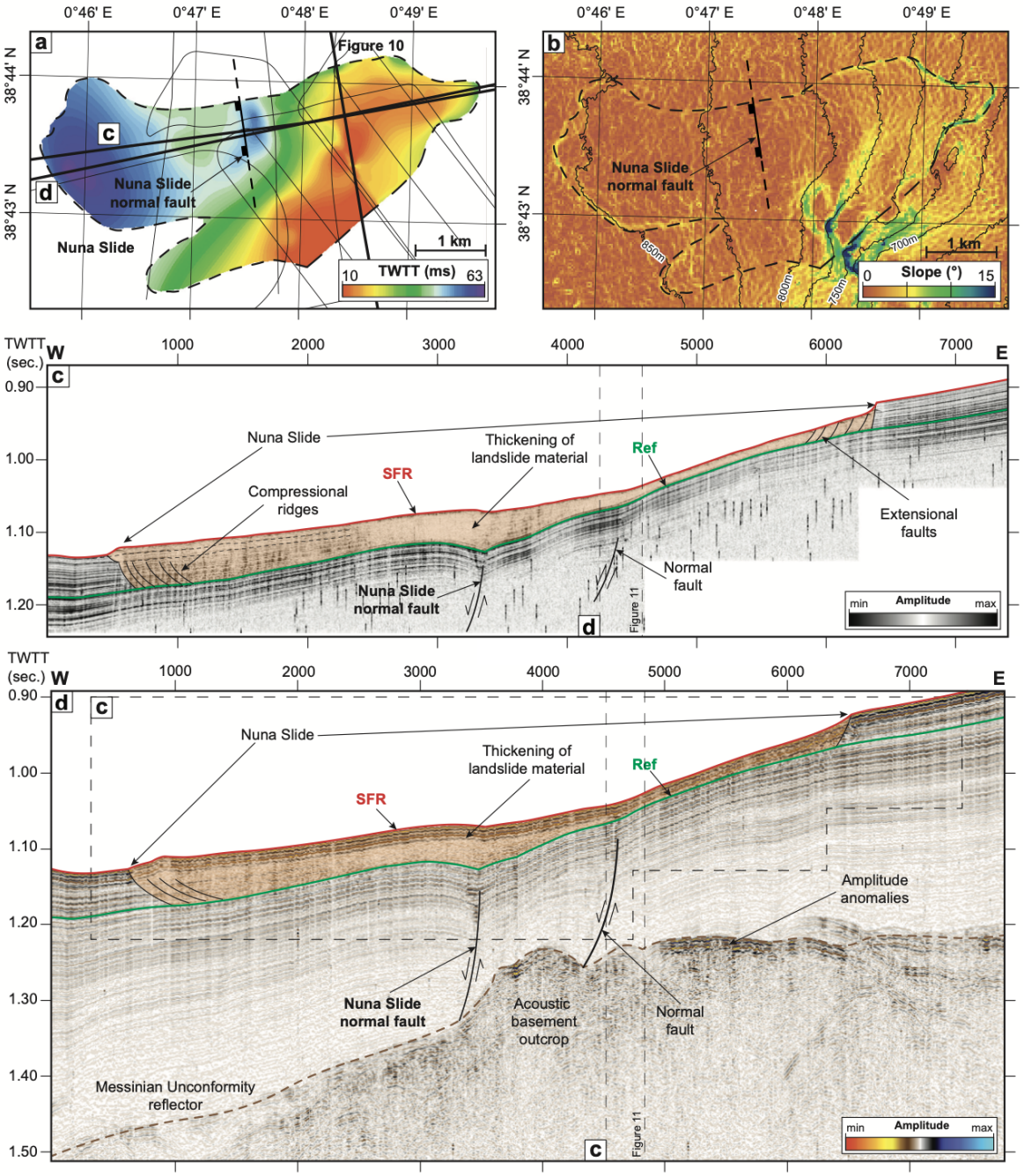

Figure 5.9: a) Isochore thickness map of the Nuna Slide (Ref – SFR) calculated from TOPAS profiles (thick and narrow black lines). The location of the 'Nuna Slide normal fault' is perpendicular to TOPAS and airgun profiles (c and d) with unknown northern and southern extents. Thickness increases in the center of the Nuna Slide. **b)** Slope gradient map of Nuna Slide. **c)** TOPAS profile across Nuna Slide shows the Nuna Slide normal fault that offsets reflector Ref. Around 1 km east of it another fault appears to offset reflector Ref. **d)** Airgun seismic profile shows that these two faults terminate at least above the Messinian Unconformity reflector

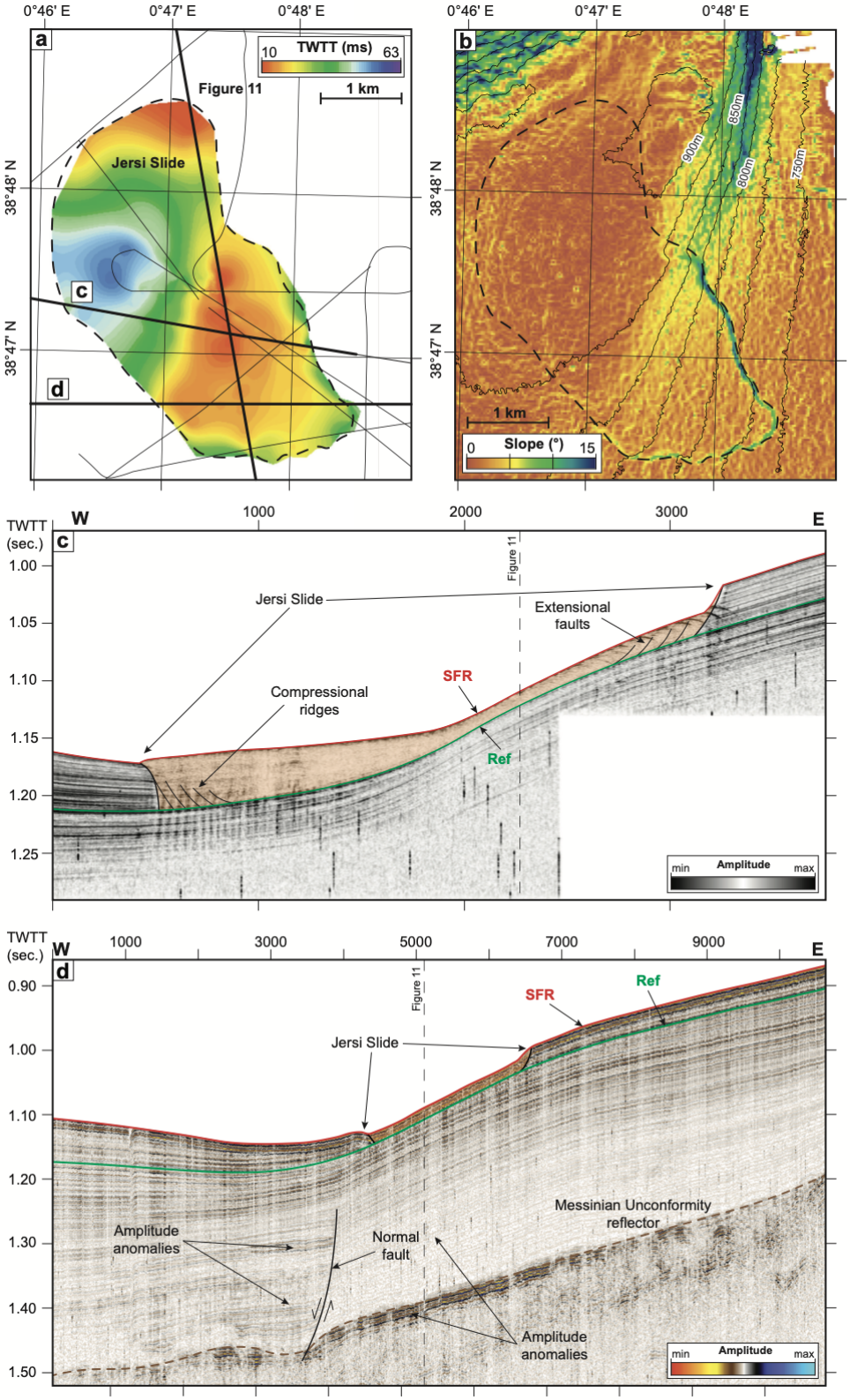

Figure 5.10: a) Isochore thickness map of Jersi Slide (Ref – SFR) calculated from TOPAS profiles (thick and narrow black lines). Thickness increases downslope in Jersi Slide while the landslide moved further toward the northwest and north. **b)** Slope gradient map of Jersi Slide. **c)** TOPAS profile of Jersi Slide. **d)** Airgun profile of Jersi Slide. Amplitude anomalies beneath Jersi Slide along the Messinian Unconformity reflector. A normal fault terminates at the Messinian unconformity reflector with amplitude anomalies on the hanging wall side toward the west.

5.4.4 Repeated slope failure in the Eivissa Channel

From the analysis of 3D and re-processed 2D reflection seismic data, repeated slope failure occurrence in the Eivissa Channel is confined to the Ana Slide Complex, where the younger Ana Slide overlies the previous pre-Ana Slide (Figures 5.4 and 5.5). From TOPAS and airgun profiles, no buried landslides are identified beneath Joan (Figure 5.8), Nuna (Figure 5.9), and Jersi slides (Figure 5.10). Nonetheless, from the limited coverage of reflection seismic profiles from the Eivissa Channel, we cannot conclusively dismiss the potential existence of additional buried slope failures that are not located beneath previous landslides.

The tpAS reflector marks the occurrence of the pre-Ana Slide (Figures 5.4 and 5.5). The depth-conversion of tpAS locates it 70.5 m beneath the R1 reflector, which marks the timing of the pre-Ana Slide. Thus, using an average sedimentation rate of 5 cm ka^{-1} (Sager et al., 2022), the pre-Ana Slide occurred around 1.41 Ma ± 282 ka ago. This age is highly speculative and refers to the latest stage of failure of pre-Ana Slide but yields a rough estimate of the overall timings of repeated slope failures of the Ana Slide Complex.

5.4.5 Sedimentary features

We observe increasing thickness of stratigraphic units from east to west in TOPAS profiles imaging the eastern slopes of the Eivissa Channel (e.g., Figures 5.8, 5.9, and 5.10). Furthermore, the isochore thickness maps of the pre-Ana, the Interval, and the Ana Slide Units show that the thickness increases similarly for the three units in the downslope direction outside the landslide scars (Figure 5.6). TOPAS profiles that cross Joan, Nuna, and Jersi slides from east to west show that the unit bound by reflectors Ref and SFR, respectively, called Joan, Nuna, and Jersi Slide units is significantly thinner compared to the area between Jersi and Nuna slides, for instance between Jersi and Nuna slides, for instance Figure 5.11a and b. Furthermore, thickness is significantly increased between Jersi and Nuna slides, compared to a deeper area immediately north of Jersi Slide.

5.5 Discussion

Ana, Joan, Nuna, and Jersi slides on the eastern slopes of the Eivissa Channel have similar lengths, widths, drop heights, occurred in similar water depths, and have similar headscarp shapes (Lastras et al., 2004; Lastras et al., 2006; Lastras et al., 2007). They share the same basal shear surface (Lastras et al., 2004) represented by reflector Ref and show the same depth of deformation that indicate equivalent geo-mechanical properties. These similarities could suggest a common failure process, which must be one that acted over the entire study area. Here, we discuss factors that affect slope stability and evaluate associated processes, which may have contributed to the destabilization of parts of the eastern slope of the Eivissa Channel. Here, we address and re-evaluate previous hypotheses of pre-conditioning factors

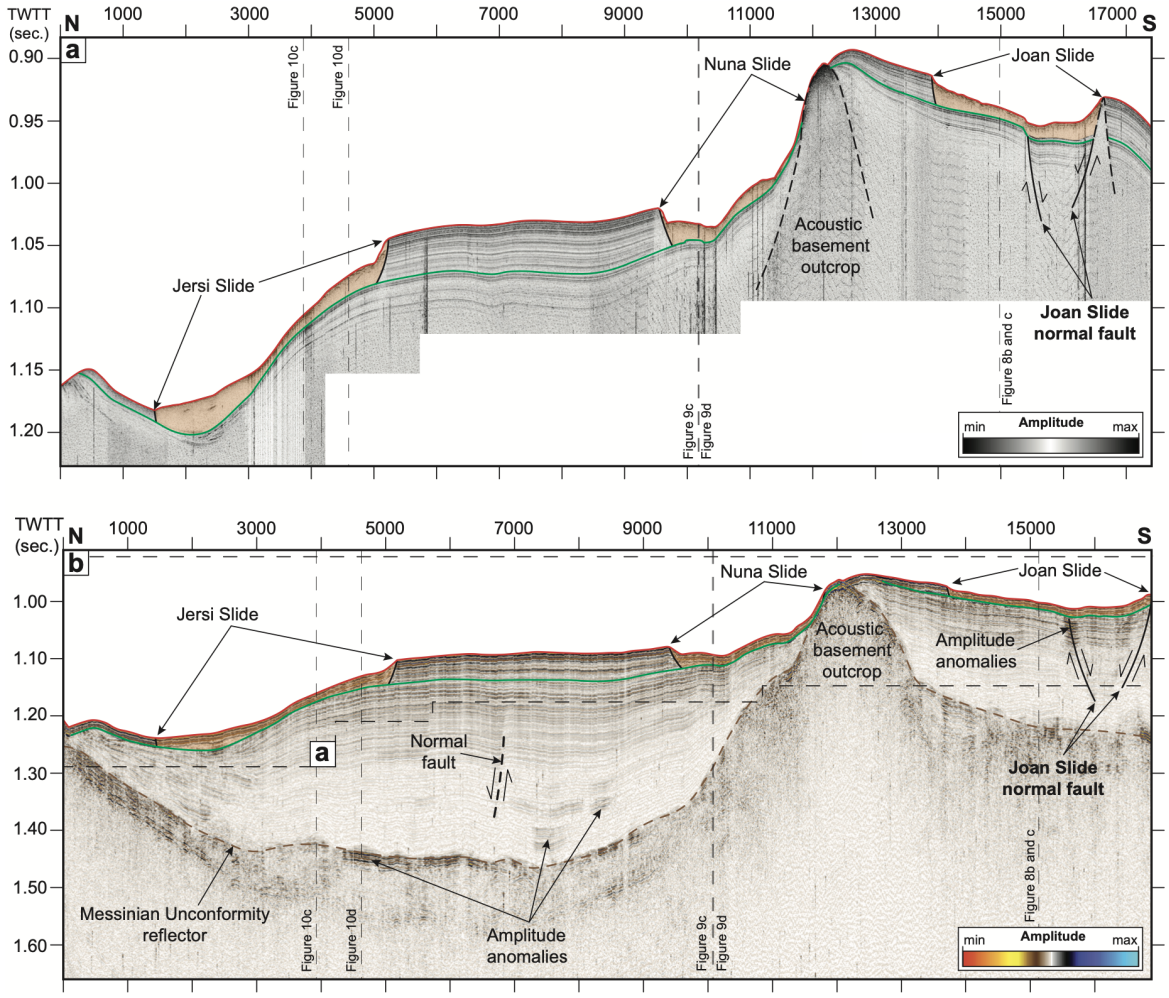

Figure 5.11: a) TOPAS profile across Joan, Nuna, and Jersi slides (this profile was acquired in parallel with the airgun profiles in b). South of Nuna Slide, the 'acoustic basemap outcrop' reaches the seafloor. Stratigraphic thickness between reflectors Ref and SFR increases between Nuna and Jersi slides. **b)** The airgun profile images the Messinian Unconformity reflector.

and triggering mechanisms of submarine landslide occurrence in the Eivissa Channel. We present them in the light of recent findings and discuss them regarding our new observations.

5.5.1 Sedimentation history

The eastern slope of the Eivissa Channel consists of well-stratified, carbonate-rich fine sediments (e.g., Panieri et al., 2012) (e.g., Figures 5.4 and 5.11). The depositional stratigraphic layers, in which the landslides occurred (between reflector Ref and SFR) extend along the slope and stratigraphic thickness generally increases with increasing water depth. Hence, the depositional environment has been the same all over the study area in time and space. Yet, the depositional history can be an important agent in the stability of the slope. Rapid deposition of low permeable and highly compressible sediment can prevent drainage of excess pore fluid and thereby lead to a build-up of excess pore pressure. Lafuerza et al. (2012)

measured compression indices ranging between 0.19 and 0.36 and a mean friction angle of 28° on sediments recovered by piston coring from the Ana Slide area. Based on grain size distribution from Ana Slide measured by Lafuerza et al. (2012) it can be assumed that the permeability of pre-slide material is similar to those measured from the Mallorca Channel that yield permeabilities of 10^{-8} m s^{-1} at low effective stresses (Kaminski et al., 2021). The consolidation parameters are thus not extreme, and along with a relatively low sedimentation rate of about 5 cm ka^{-1} (Sager et al., 2022), sediment deposition and consolidation are unlikely to generate excess pore pressures that significantly impact slope stability on low-angle slopes (Urlaub et al., 2015).

The nature of the weak layer represented by reflector Ref that marks the basal shear surface inside the source areas and the depth of deformation inside the sink areas of landslides in the Eivissa Channel is unknown because no in-situ samples exist. Yet, given that it coincides with a prominent high-amplitude seismic reflector (Figures 5.4, 5.5 and 5.8 to 5.11), its large spatial extent, and the fact that it follows the general stratigraphy (and is not a BSR), we suggest a link between sedimentation history and slope failures. Since this stratigraphic unit (between reflector Ref and SFR) above the weak layer easily deforms when loaded (Sager et al., 2022), we infer that the entire sediment package is weak, rather than a thin isolated layer that accommodated sliding, as it is oftentimes suggested for submarine landslides on low-angle slopes (Gatter et al., 2021; Locat et al., 2014) (see Figures 5.3a, 5.8a, 5.9b and 5.10b). Reasons for the occurrence of a mechanical interface include: (i) erosion of overlying material, (ii) change in the depositional environment with deposition of stronger and weak materials, or (iii) change in the sediment source. In the case of erosion, an increase in the over-consolidation ratio would be expected. In contrast, consolidation tests show a general decrease in the over-consolidation ratio with depth (Lafuerza et al., 2012). The seismic data do not provide any evidence for a change in the depositional environment and thus, Lafuerza et al. (2012) accounted the increased OCR to inter-particle bonding and cementation processes.

Inside the Eivissa Channel, normal faults are observed beneath the landslides (Figures 5.4, 5.5 and 5.8 to 5.10), which extend down to the Messinian Unconformity reflector. It is not possible to observe these faults deeper in the seismic data which indicates either that seismic imaging below the Messinian is imperfect or that the faults detach along the Messinian deposits. However, raft tectonics (or thin-skinned tectonics) above a detachment layer will create extensional features upslope and shortening at the toe of the slope (Acosta et al., 2004; Brun and Fort, 2011; Stewart, 1999; Duval et al., 1992). The observation of upslope extensional faults beneath the landslides in the Eivissa Channel fits this scenario, but extensional faults also exist in the deepest part of the survey area at a water depth of 850 m between Ana and Joan slides (Figures 5.3 and 5.7). Because the extent of mobile precipitation products is limited to the deep basins outside the Balearic Promontory and extensional faults are observed at the toe of the slopes inside the Eivissa Channel we conclude that gravitational

processes along an evaporite detachment do not play a role in the formation of the Eivissa Channel landslides.

5.5.2 Inherent changes in the sediment's physical properties

Here, we discuss processes that could have negatively affected slope stability during burial and consolidation. Decreases in frictional resistance could result from a lowering of the effective stress or from changes in the structure of the sediment. Sediments in the Eivissa Channel were deposited under relatively steady conditions (Panieri et al., 2012; Sager et al., 2022). There is no evidence for erosion that could have led to a decrease in effective stress. Furthermore, there is no evidence of episodes of rapid deposition prior to or after the four landslides, such as by other landslides, which could have caused excess pore pressures and decreases in effective stress away from the overburden.

Free gas may lead to excess pore pressure when total pressure decreases as gas bubbles expand. Lafuerza et al. (2012) suggested this process as the main cause of excess pore pressure and slope failure. This hypothesis was also based on the age of Ana Slide, at the time dated to 61.5 ka, postdating the sea-level low stand of Marine Isotopic Stage (MIS) 4 (70.5 to 65 ka ago). We know now that this age corresponds to the timing of the secondary failure and that the primary failure of Ana Slide is significantly older at around 300 ka (Sager et al., 2022). The uncertainties regarding the age of the main failure are too large to reliably link the timing of Ana Slide to a specific sea-level stand, and occurrence during MIS 6 or 8 cannot be excluded. Repeated failure in response to sea-level falls is thus possible (e.g., Talling et al., 2014). Nevertheless, the driver for instability in the Eivissa Channel cannot be a purely cyclic one because there is a mismatch between the global sea-level with multiple short periods of rapid sea-level fall in the past 300 ka and just two slope failure events.

Geotechnical experiments have shown that free gas in fine-grained soils modifies the internal grain structure and the internal friction with possible negative impacts on its shear strength (see Kaminski et al., 2020, for a summary). Kaminski et al. (2021) conducted a back analysis of Ana Slide under consideration of reduced shear strength due to gas-induced soil structure disturbance. The authors concluded that gas-induced soil structure disturbance weakens the slope but not to the extent of triggering slope failures.

The CPTu measurements do not indicate a change in mechanical properties, at least for a static measurement such as CPTu (Lafuerza et al., 2012). CPTu measurements inside the source area of Ana Slide penetrated the basal shear surface represented by reflector Ref and Lafuerza et al. (2012) report a sharp increase in cone resistance and sleeve friction immediately above. Therefore, the variations observed above reflector Ref inside the source area likely resulted from the failure process and mobilization of landslide material, and do not represent the pre-failure state.

5.5.3 Local external factors

The seafloor antithetic en-echelon fault system beneath the Ana Slide Complex shows activity prior to the pre-Ana and Ana Slide failures and no activity in the period between the two landslides (Figures 5.6 and 5.12). This is evident from the 3D reflection seismic data covering Ana Slide (Figures 5.4 and 5.5). Hence, there appears to be a temporal correlation between the episodic activity of the local seafloor antithetic en-echelon fault system and the occurrence of landslides (pre-Ana and Ana slides). Local faults are also present immediately beneath Nuna and Joan slides (Figures 5.8 and 5.9). A link between local fault activity and these other landslides may be possible but cannot be confirmed due to the lack of extensive 3D reflection seismic data. If seismicity had a role in the destabilization can neither be confirmed nor discarded as a potential triggering mechanism due to the lack of historical earthquake records.

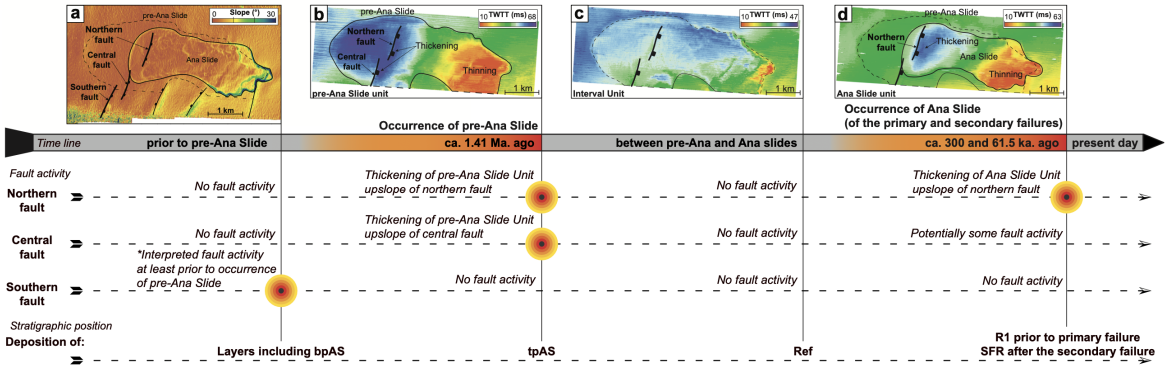

Figure 5.12: Activity plot of slope failure occurrence and tectonic activity of the Ana Slide Complex. Sub-figure **a** shows a slope gradient map of Ana Slide that highlights the location of the southern, central, and northern faults. Subsequently, sub-figure **b** shows fault activity on the central and northern faults prior to pre-Ana Slide that influenced the stratigraphy beneath bpAS. After pre-Ana Slide, sedimentation commenced and deposited slope sediment between reflectors tpAS and Ref (**c**). The Ana Slide unit in **d** shows thickening primarily above the northern faults thus the northern fault was primarily active prior to slope failure. Fault activity plotted with approximate timings of pre-Ana and Ana slides.

There are several ways, in which the activity and re-activity of local faults could have affected slope stability in the Eivissa Channel. First, owing to the specific geometry of this seafloor antithetic en-echelon fault system, the downward movement of the hanging wall side to the east will lead to an increase in the slope angle of the upslope area (Figures 5.4 and 5.5). This leads to higher shear stresses that thus negatively impact slope stability. Slope geometry has been found to have a larger impact on stability than, for example, an altered soil structure due to former gas occurrence (Kaminski et al., 2021) and differences in sediment properties (Miramontes et al., 2018). The observation that the headscarps of the four landslides are located around 300 m upslope of the location of the steepest slope (sensu Lastras et al., 2004) further supports the importance of slope geometry.

Second, if the faults ruptured seismically, horizontal accelerations increased shear stresses in the slopes nearby. Lafuerza et al. (2012) discussed the magnitude of such an earthquake to

generate a local PGA of 0.24 g that relates to an Mw = 5 in an epicentral distance of 1 km or a larger event with 7 ≥ Mw ≥ 5 at an epicentral distance of ≤ 15 km (IGN, 2023). From the analysis of reflection seismic data with an effective penetration depth of just above one second (Berndt et al., 2012) no large faults were observed. Thus, the small size of faults observed and limited vertical offset will not result in a seismically significant earthquake to simultaneously trigger all four landslides in the Eivissa Channel.

Third, faults provide vertical pathways for fluid and gas, and fault rupture can enhance fluid flow (e.g., Geersen et al., 2016). Berndt et al. (2012) and Lafuerza et al. (2012) suggest fluids including gas to have migrated upward beneath the Ana Slide Complex, thus decreasing the shear strength of sediments at the basal shear surface of the Ana Slide represented by reflector Ref. This process could have occurred in connection to the activity and re-activity of the en-echelon fault system (Figures 5.6 and 5.12). The timing of faults and the successive failures of pre-Ana Slide over the central and northern faults with the Ana Slide propagating over the northern fault (and central fault) furthermore suggests that vertical fluid flow may have repeated through the reactivation of the en-echelon fault system. While we cannot single out the factor(s) that led to slope failure, a connection between fault activity and failure seems evident.

5.5.4 Far-field external factors

The Balearic Promontory is generally devoid of large earthquakes > Mw => 4.5 (IGN, 2023) and there is no reason to suggest that seismicity has changed significantly since the landslides occurred. Large-scale earthquakes occurred for instance in the Strait of Gibraltar (e.g., 1954 Mw = 7.8 with a hypocenter in 626 km depth at 36° 59.28' N 3° 36.72' W) and in the Eivissa Channel (1975 Mw = 4.5 with a hypocenter in 33 km depth at 38° 35.22' N 0° 45.18' E) (IGN, 2023). Slope stability modelling showed that strong earthquakes at large distances alone are unlikely to have caused the Ana Slide (Lafuerza et al., 2012). Hence, far-field earthquakes have not acted as triggering mechanisms for slope failures in the Eivissa Channel unless slopes were inherently weakened by local destabilizing factors.

The occurrence of submarine landslides has often been linked to changes in global climate and sea-level (e.g., Talling et al., 2014). In the case of Ana Slide, the chronology of repeated failure, with failures occurring at around 1.41 Ma (± 282 ka), 300 ka, and 61.5 ka ago, speaks against a climatic trigger. This is because the occurrence does not directly relate to ice-age timings or prevailing processes of, for instance, Milankovitch cycles including periods of precession at 21 ka, obliquity at 41 ka, and eccentricity at 95 ka (e.g., Maslin, 2016). The fact that the occurrence rate of landslides is approximately and at least 240 ka and that slope failures occurred around 61.5 ka ago speaks against slope failures in the near future. Furthermore, the fact that the basal shear surface is represented by reflector Ref which is the basal shear surface of the primary and secondary failures of Ana Slide shows that it developed after some hundred thousand years of consolidation.

5.6 Conclusions

Previous studies have suggested sea-level lowering, gas migration, earthquakes, or a combination of these to be responsible for the occurrence of submarine landslides in the Eivissa Channel. Here, we re-evaluate these hypotheses by integrating new information on the geological setting and landslide dynamics of one of the four Eivissa Channel landslides. The sedimentary package that comprises the Ana, Joan, Nuna, and Jersi slides probably consists of intrinsically weak material that is easily deformed when loaded. This package is overlying a mechanically stronger sediment layer. The interface between both represents a change in mechanical properties and possibly also lithology. The upper layer is probably not per se weak as it displays normal shear strength values (Lafuerza et al., 2012). Given the widespread occurrence of free gas and the capability of free gas to negatively affect slope stability (Kaminski et al., 2020), we suggest that focused episodic fluid or gas flow along fault systems are agents for repeated slope failure. We here show the repeated activity of a local seafloor antithetic en-echelon faults system to correlate with repeated slope failure of pre-Ana and Ana slides. Faults observed beneath Joan and Nuna slides together with amplitude anomalies beneath Jersi Slide support this hypothesis along with a local seismic trigger. Repeated slope failure occurrences are separated by significant time periods of 61.5 ka, 300 ka, and 1.41 Ma ago (± 282 ka) making slope failure in the Eivissa Channel unlikely in the near future.

Acknowledgements

Data used in this study were acquired as part of several Spanish and EU-funded research projects, the latest being the HERMIONE project (ref. 226354-HERMIONE) of the European Community's Seventh Framework Programme (FP7/2007–2013). We thank officers, crew and technicians involved in sea-going work during BIG'95, MARINADA, EUROLEON and HERMESIONE cruises. We thank the master and the crew of RRS Charles Darwin who facilitated data acquisition during voyage 178, and Frode Eriksen of VBPR, Oslo for technical support on the same cruise. This study was supported by the DFG (Deutsche Forschungsgemeinschaft) Verbundprojekt UR 226/3-1 and GR 1024/35-1 by MU, Juergen Grabe of the TUHH, Hamburg, Germany, and CB. MC and GL acknowledge support from a Grups de Recerca Consolidats (excellence research groups) Grant to GRC Geociències Marines (ref. 2021 SGR 01195) by the Government of Catalonia. We thank Cord Papenberg (GEOMAR Helmholtz Centre for Ocean Research Kiel, Kiel, Germany) with re-processing of seismic data. IHS Markit and Schlumberger provided academic licenses for Kingdom Suite and OMEGA, respectively.

Author Contribution

Conceptualization: TFS, MU, CB; Methodology: TFS, MU, CB; Formal analysis and investigation: TFS; Writing original draft: TFS, MU, CB; Writing – review and editing: TFS, MU, PK, GL, MC, CB; Visualization: TFS has produced all figures (Figure 1 to 12); Funding acquisition: MU, CB; Data curation: GL, MC, CB; Project administration: MU, CB.

Open Research - Data Availability Statement

The 3D reflection seismic data from Ana Slide acquired during cruise 178 with RRS Charles Darwin of the study area analyzed in this study are available at the World Data Centre Pangaea repository at `https://doi.pangaea.de/10.1594/PANGAEA.943506`, the 2D reflection seismic data are available at `https://doi.pangaea.de/10.1594/PANGAEA.943523`, and the multibeam bathymetry data are available at `https://doi.pangaea.de/10.1594/PANGAEA.953762`.

References

Acosta, J., A. Muñoz, P. Herranz, C. Palomo, M. Ballesteros, M. Vaquero, and E. Uchupi (2001a). Geodynamics of the Emile Baudot Escarpment and the Balearic Promontory, Western Mediterranean. In: *Marine and Petroleum Geology* 3, pp. 349–369. DOI: 10.1016/S0264-8172(01)00003-4.

Acosta, J., M. Canals, A. Carbo, A. Munoz, R. Urgeles, A. Munoz-Martin, and E. Uchupi (2004). Sea Floor Morphology and Plio-Quaternary Sedimentary Cover of the Mallorca Channel, Balearic Islands, Western Mediterranean. In: *Marine Geology* 1-4, pp. 165–179. DOI: 10.1016/j.margeo.2004.02.008.

Acosta, J., A. Muñoz, P. Herranz, C. Palomo, M. Ballesteros, M. Vaquero, and E. Uchupi (2001b). Pockmarks in the Ibiza Channel and Western End of the Balearic Promontory (Western Mediterranean) Revealed by Multibeam Mapping. In: *Geo-Marine Letters* 21.3, pp. 123–130. DOI: 10.1007/s003670100074.

Berndt, C., S. Bünz, T. Clayton, J. Mienert, and M. Saunders (2004). Seismic Character of Bottom Simulating Reflectors: Examples from the Mid-Norwegian Margin. In: *Marine and Petroleum Geology* 6, pp. 723–733. DOI: 10.1016/j.marpetgeo.2004.02.003.

Berndt, C., S. Costa, M. Canals, A. Camerlenghi, B. de Mol, and M. Saunders (2012). Repeated Slope Failure Linked to Fluid Migration: The Ana Submarine Landslide Complex, Eivissa Channel, Western Mediterranean Sea. In: *Earth and Planetary Science Letters*, pp. 65–74. DOI: 10.1016/j.epsl.2011.11.045.

Blondel, S., M. Bellucci, S. Evans, A. Del Ben, and A. Camerlenghi (2022). Contractional Salt Deformation in a Recently Inverted Basin: Miocene to Current Salt Deformation within the Central Algerian Basin. In: *Basin Research* 34.5, pp. 1632–1654. DOI: 10.1111/bre.12673.

Bondevik, S., F. Løvholt, C. Harbitz, J. Mangerud, A. Dawson, and J. Inge Svendsen (2005). The Storegga Slide Tsunami – Comparing Field Observations with Numerical Simulations. In: *Marine and Petroleum Geology* 1-2, pp. 195–208. DOI: 10.1016/j.marpetgeo.2004.10.003.

Brun, J.-P. and X. Fort (2011). Salt Sectonics at Passive Margins: Geology versus Models. In: *Marine and Petroleum Geology* 28.6, pp. 1123–1145. DOI: 10.1016/j.marpetgeo.2011.03.004.

Bryn, P., K. Berg, C. F. Forsberg, A. Solheim, and T. J. Kvalstad (2005). Explaining the Storegga Slide. In: *Marine and Petroleum Geology* 22.1-2, pp. 11–19. DOI: 10.1016/j.marpetgeo.2004.12.003.

Camerlenghi, A., C. Corradin, U. Tinivella, M. Giustiniani, and C. Bertoni (2023). Subsurface Heat and Salts Cause Exceptionally Limited Methane Hydrate Stability in the Mediterranean Basin. In: *Geology* 51.2, pp. 162–166. DOI: 10.1130/G50426.1.

Cattaneo, A., D. Minisini, A. Asioli, M. Canals, G. Lastras, A. Remia, N. Sultan, and M. Taviani (2011). Age Constraints and Sediment Properties of Ana Slide (Balearic Sea, Western Mediterranean) and Implications on Age Dating of Submarine Landslides. In: EGU 2011 - Abstract. DOI: 10.1007/978-90-481-3071-9_42.

Clare, M., J. Chaytor, O. Dabson, D. Gamboa, A. Georgiopoulou, H. Eady, J. Hunt, C. Jackson, O. Katz, S. Krastel, R. Le0n, A. Micallef, J. Moernaut, R. Moriconi, L. Moscardelli, C. Müller, A. Normandeau, M. Patacci, M. Steventon, M. Urlaub, D. Völker, L. Wood, and Z. Jobe (2019). A Consistent Global Approach for the Morphometric Characterization of Subaqueous Landslides. In: *Geological Society, London, Special Publications* 1, pp. 455–477. DOI: 10.1144/SP477.15.

Driussi, O., A. Maillard, D. Ochoa, J. Lofi, F. Chanier, V. Gaullier, A. Briais, F. Sage, F. Sierro, and M. Garcia (2015). Messinian Salinity Crisis Deposits Widespread over the Balearic Promontory: Insights from New High-Resolution Seismic Data. In: *Marine and Petroleum Geology* 66, pp. 41–54. DOI: 10.1016/j.marpetgeo.2014.09.008.

Duggen, S., K. Hoernle, P. Van Den Bogaard, L. Ruepke, and J. Phipps Morgan (2003). Deep Roots of the Messinian Salinity Crisis. In: *Nature* 422.6932, pp. 602–606. DOI: 10.1038/nature01553.

Duval, B., C. Cramez, and M. P. A. Jackson (1992). Raft Tectonics in the Kwanza Basin, Angola. In: *Marine and Petroleum Geology*. DOI: 10.1016/0264-8172(92)90050-O.

EMODnet (2023). *EMODnet Map Viewer*. Retrieved May 24, 2023. DOI: https://emodnet.ec.europa.eu/geoviewer/?layers=&basemap=ebwbl&active=undefined&bounds=18.17250683719508,32.867292541600136,16.40442737697871,49.25531865352626&filters=.

Ford, J., R. Urgeles, A. Camerlenghi, and E. Gràcia (2021). Seismic Diffraction Imaging to Characterize Mass-Transport Complexes: Examples From the Gulf of Cadiz, South West Iberian Margin. In: *Journal of Geophysical Research: Solid Earth* 3. DOI: 10.1029/2020JB021474.

Frey-Martinez, J., J. Cartwright, and B. Hall (2005). 3D Seismic Interpretation of Slump Complexes: Examples from the Continental Margin of Israel. In: *Basin Research* 1, pp. 83–108. DOI: 10.1111/j.1365-2117.2005.00255.x.

Frey-Martinez, J., J. Cartwright, and D. James (2006). Frontally Confined versus Frontally Emergent Submarine Landslides: A 3D Seismic Characterisation. In: *Marine and Petroleum Geology* 5, pp. 585–604. DOI: 10.1016/j.marpetgeo.2006.04.002.

Gargani, J. and C. Rigollet (2007). Mediterranean Sea Level Variations during the Messinian Salinity Crisis. In: *Geophysical Research Letters* 34.10. DOI: 10.1029/2007GL029885.

Gatter, R., M. Clare, J. Kuhlmann, and K. Huhn (2021). Characterisation of Weak Layers, Physical Controls on their Global Distribution and their Role in Submarine Landslide Formation. In: *Earth-Science Reviews* 223, p. 103845. DOI: 10.1016/j.earscirev.2021.103845.

Gatter, R., M. A. Clare, J. E. Hunt, M. Watts, B. N. Madhusudhan, P. J. Talling, and K. Huhn (2020). A Multi-Disciplinary Investigation of the AFEN Slide: The Relationship between Contourites and Submarine Landslides. In: *Geological Society, London, Special Publications* 500.1, pp. 173–193. DOI: 10.1144/SP500-2019-184.

Gee, M., R. Gawthorpe, and S. Friedmann (2006). Triggering and Evolution of a Giant Submarine Landslide, Offshore Angola, Revealed by 3D Seismic Stratigraphy and Geomorphology. In: *Journal of Sedimentary Research* 76.1, pp. 9–19. DOI: 10.2110/jsr.2006.02.

Gee, M., H. Uy, J. Warren, C. Morley, and J. Lambiase (2007). The Brunei Slide: A Giant Submarine Landslide on the North West Borneo Margin Revealed by 3D Seismic Data. In: *Marine Geology* 246.1, pp. 9–23. DOI: 10.1016/j.margeo.2007.07.009.

Geersen, J., F. Scholz, P. Linke, M. Schmidt, D. Lange, J. H. Behrmann, D. Vuelker, and C. Hensen (2016). Fault Zone Controlled Seafloor Methane Seepage in the Rupture Area of the 2010 Maule Earthquake, Central Chile. In: *Geochemistry, Geophysics, Geosystems* 17.11, pp. 4802–4813. DOI: 10.1002/2016GC006498.

Haflidason, H., H. P. Sejrup, A. Nygård, J. Mienert, P. Bryn, R. Lien, C. F. Forsberg, K. Berg, and D. Masson (2004). The Storegga Slide: Architecture, Geometry and Slide Development. In: *Marine Geology* 1-4, pp. 201–234. DOI: 10.1016/j.margeo.2004.10.007.

Hampton, M. A., H. J. Lee, and J. Locat (1996). Submarine Landslides. In: *Reviews of Geophysics* 34.1, pp. 33–59. DOI: 10.1029/95RG03287.

Haugen, K. B., F. Løvholt, and C. B. Harbitz (2005). Fundamental Mechanisms for Tsunami Generation by Submarine Mass Flows in Idealised Geometries. In: *Marine and Petroleum Geology* 1-2, pp. 209–217. DOI: 10.1016/j.marpetgeo.2004.10.016.

Hjelstuen, B. O., O. Eldholm, and J. I. Faleide (2007). Recurrent Pleistocene Mega-Failures on the SW Barents Sea Margin. In: *Earth and Planetary Science Letters* 258.3-4, pp. 605–618. DOI: 10.1016/j.epsl.2007.04.025.

Huvenne, V. A. I., P. F. Croker, and J.-P. Henriet (2002). A Refreshing 3D View of an Ancient Sediment Collapse and Slope Failure. In: *Terra Nova* 14.1, pp. 33–40. DOI: 10.1046/j.1365-3121.2002.00386.x.

IGN (2023). *Instituto Geográfico Nacional - Geoportal Oficial Del Instituto Geográfico Nacioñal de Espana*. Retrieved May 24, 2023. DOI: https://www.ign.es/web/mapas-sismicidad.

Imbo, Y., M. De Batist, M. Canals, M. Prieto, and J. Baraza (2003). The Gebra Slide: a Submarine Slide on the Trinity Peninsula Margin, Antarctica. In: *Marine Geology* 193.3-4, pp. 235–252. DOI: 10.1016/S0025-3227(02)00664-3.

Kaminski, P., M. Urlaub, J. Grabe, and C. Berndt (2020). Geomechanical Behaviour of Gassy Soils and Implications for Submarine Slope Stability: A Literature Analysis. In: *Geological Society, London, Special Publications* 500.1, pp. 277–288. DOI: 10.1144/SP500-2019-149.

Kaminski, P., T. Sager, J. Grabe, and M. Urlaub (2021). A New Methodology to Assess the Potential of Conjectural Trigger Mechanisms of Submarine Landslides Exemplified by Marine Gas Occurrence on the Balearic Promontory. In: *Engineering Geology*, p. 106446. DOI: 10.1016/j.enggeo.2021.106446.

Krijgsman, W., F. J. Hilgen, I. Raffi, F. J. Sierro, and D. Wilson (1999). Chronology, Causes and Progression of the Messinian Salinity Crisis. In: *Nature* 400.6745, pp. 652–655. DOI: 10.1038/23231.

Laberg, J. and T. Vorren (2000). The Trænadjupet Slide, offshore Norway — Morphology, Evacuation and Triggering Mechanisms. In: *Marine Geology* 171.1-4, pp. 95–114. DOI: 10.1016/S0025-3227(00)00112-2.

Lackey, J., G. Moore, and M. Strasser (2018). Three-Dimensional Mapping and Kinematic Characterization of Mass Transport Deposits along the Outer Kumano Basin and Nankai Accretionary Wedge, Southwest Japan. In: *Progress in Earth and Planetary Science* 1, p. 65. DOI: 10.1186/s40645-018-0223-4.

Lafuerza, S., N. Sultan, M. Canals, G. Lastras, A. Cattaneo, J. Frigola, S. Costa, and C. Berndt (2012). Failure Mechanisms of Ana Slide from Geotechnical Evidence, Eivissa Channel, Western Mediterranean Sea. In: *Marine Geology*, pp. 1–21. DOI: 10.1016/j.margeo.2012.02.010.

Lastras, G., M. Canals, D. Amblas, J. Frigola, R. Urgeles, A. Calafat, and J. Acosta (2007). Slope Instability along the Northeastern Iberian and Balearic Continental Margins. In: *Geologica Acta: An International Earth Science Journal* 5.1, pp. 35–48.

Lastras, G., M. Canals, D. Amblas, M. Ivanov, B. Dennielou, L. Droz, A. Akhmetzhanov, and TTR-14 Leg 3 Shipboard Scientific Party (2006). Eivissa Slides, Western Mediterranean Sea: Morphology and Processes. In: *Geo-Marine Letters* 4, pp. 225–233. DOI: 10.1007/s00367-006-0032-4.

Lastras, G., M. Canals, R. Urgeles, J. E. Hughes-Clarke, and J. Acosta (2004). Shallow Slides and Pockmark Swarms in the Eivissa Channel, Western Mediterranean Sea. In: *Sedimentology* 4, pp. 837–850. DOI: 10.1111/j.1365-3091.2004.00654.x.

Lenz, B., D. Sawyer, B. Phrampus, K. Davenport, and A. Long (2018). Seismic Imaging of Seafloor Deformation Induced by Impact from Large Submarine Landslide Blocks, Offshore Oregon. In: *Geosciences* 1, p. 10. DOI: 10.3390/geosciences9010010.

Lindberg, B., J. Laberg, and T. Vorren (2004). The Nyk Slide—Morphology, Progression, and Age of a Partly Buried Submarine Slide Offshore Northern Norway. In: *Marine Geology* 213.1-4, pp. 277–289. DOI: 10.1016/j.margeo.2004.10.010.

Locat, J., S. Leroueil, A. Locat, and H. Lee (2014). "Weak layers: Their Definition and Classification from a Geotechnical Perspective". In: *Submarine mass movements and their consequences: 6th international symposium*. Springer, pp. 3–12. DOI: 10.1007/978-3-319-00972-8_1.

Løvholt, F., S. Bondevik, J. S. Laberg, J. Kim, and N. Boylan (2017). Some Giant Submarine Landslides Do Not Produce Large Tsunamis: Giant Landslide Tsunamis. In: *Geophysical Research Letters* 16, pp. 8463–8472. DOI: 10.1002/2017GL074062.

Maillard, A. and A. Mauffret (2013). Structure and Present-Day Compression in the Offshore Area between Alicante and Ibiza Island (Eastern Iberian Margin). In: *Tectonophysics*, pp. 116–130. DOI: 10.1016/j.tecto.2011.07.007.

Maslin, M. (2016). Forty Years of Linking Orbits to Ice Ages. In: *Nature* 540.7632, pp. 208–209. DOI: 10.1038/540208a.

Masson, D., C. Harbitz, R. Wynn, G. Pedersen, and F. Løvholt (2006). Submarine Landslides: Processes, Triggers and Hazard Prediction. In: *Philosophical Transactions of the Royal Society A: Mathematical, Physical and Engineering Sciences* 1845, pp. 2009–2039. DOI: 10.1098/rsta.2006.1810.

Mauffret, A., G. Pascal, A. Maillard, and C. Gorini (1995). Tectonics and Deep Structure of the North-Western Mediterranean Basin. In: *Marine and Petroleum Geology* 12.6, pp. 645–666. DOI: 10.1016/0264-8172(95)98090-R.

Miramontes, E., N. Sultan, S. Garziglia, G. Jouet, E. Pelleter, and A. Cattaneo (2018). Altered Volcanic Deposits as Basal Failure Surfaces of Submarine Landslides. In: *Geology* 46.7, pp. 663–666. DOI: 10.1130/G40268.1.

Ochoa, D., F. J. Sierro, J. Lofi, A. Maillard, J.-A. Flores, and M. Suarez (2015). Synchronous Onset of the Messinian Evaporite Precipitation: First Mediterranean Offshore Evidence. In: *Earth and Planetary Science Letters* 427, pp. 112–124. DOI: 10.1016/j.epsl.2015.06.059.

Panieri, G., A. Camerlenghi, I. Cacho, C. S. Cervera, M. Canals, S. Lafuerza, and G. Herrera (2012). Tracing Seafloor Methane Emissions with Benthic Foraminifera: Results from the Ana Submarine Landslide

(Eivissa Channel, Western Mediterranean Sea). In: *Marine Geology*, pp. 97–112. DOI: 10.1016/j.margeo.2011.11.005.

Posamentier, H. W. and O. J. Martinsen (2011). The Character and Genesis of Submarine Mass-Transport Deposits: Insights from Outcrop and 3D Seismic Data. In: DOI: 10.2110/sepmsp.096.007.

Praeg, D., R. Geletti, J. Mascle, V. Unnithan, and F. Harmegnies (2008). Geophysical Exploration for Gas Hydrates in the Mediterranean Sea and a Bottom-Simulating Reflection on the Nile Fan. In: *Proceedings of the 2008 GNGTS, Trieste, Italy*, pp. 6–8.

Praeg, D., R. Geletti, N. Wardell, V. Unnithan, J. Mascle, S. Migeon, and A. Camerlenghi (2011). "The Mediterranean Sea: a natural laboratory to study gas hydrate dynamics?" In: *7th International Conference on Gas Hydrates (ICGH 2011)*, Full–paper. DOI: hal-03315746/document.

Principaud, M., T. Mulder, H. Gillet, and J. Borgomano (2015). Large-Scale Carbonate Submarine Mass-Wasting along the Northwestern Slope of the Great Bahama Bank (Bahamas): Morphology, Architecture, and Mechanisms. In: *Sedimentary Geology* 317, pp. 27–42. DOI: 10.1016/j.sedgeo.2014.10.008.

Prior, D. B., B. D. Bornhold, and M. W. Johns (1984). Depositional Characteristics of a Submarine Debris Flow. In: *The Journal of Geology* 6, pp. 707–727. DOI: 10.1086/628907.

Reis, A. T. dos, C. Gorini, and A. Mauffret (2005). Implications of Salt-Sediment Interactions on the Architecture of the Gulf of Lions Deep-Water Sedimentary Systems — Western Mediterranean Sea. In: *Marine and Petroleum Geology* 22.6-7, pp. 713–746. DOI: 10.1016/j.marpetgeo.2005.03.006.

Roveri, M., R. Flecker, W. Krijgsman, J. Lofi, S. Lugli, V. Manzi, F. J. Sierro, A. Bertini, A. Camerlenghi, G. De Lange, et al. (2014). The Messinian Salinity Crisis: Past and Future of a Great Challenge for Marine Sciences. In: *Marine Geology* 352, pp. 25–58.

Roveri, M., S. Lugli, V. Manzi, and B. C. Schreiber (2008). The Messinian Sicilian Stratigraphy Revisited: New Insights for the Messinian Salinity Crisis. In: *Terra Nova* 20.6, pp. 483–488.

Ryan, W. B. (1976). Quantitative Evaluation of the Depth of the Western Mediterranean before, during and after the Late Miocene Salinity Crisis. In: *Sedimentology* 23.6, pp. 791–813. DOI: 10.1111/j.1365-3091.1976.tb00109.x.

Sager, T. F., M. Urlaub, P. Kaminski, C. Papenberg, G. Lastras, M. Canals, and C. Berndt (2022). Development and Emplacement of Ana Slide, Eivissa Channel, Western Mediterranean Sea. In: *Geochemistry, Geophysics, Geosystems*. DOI: 10.1029/2022GC010469.

Sawyer, D. E. and B. Hodelka (2016). "Tiny Fossils, Big Impact: The Role of Foraminifera-Enriched Condensed Section in Arresting the Movement of a Large Retrogressive Submarine Landslide in the Gulf of Mexico". In: *Submarine Mass Movements and their Consequences: 7th International Symposium*. Springer, pp. 479–486. DOI: 10.1007/978-3-319-20979-1_48.

Shan, Z., H. Wu, W. Ni, M. Sun, K. Wang, L. Zhao, Y. Lou, A. Liu, W. Xie, X. Zheng, et al. (2022). Recent Technological and Methodological Advances for the Investigation of Submarine Landslides. In: *Journal of Marine Science and Engineering* 10.11, p. 1728. DOI: 10.3390/jmse10111728.

Sobiesiak, M. S., B. Kneller, G. I. Alsop, and J. P. Milana (2018). Styles of Basal Interaction beneath Mass Transport Deposits. In: *Marine and Petroleum Geology*, pp. 629–639. DOI: 10.1016/j.marpetgeo.2018.08.028.

Stewart, S. (1999). Geometry of Thin-Skinned Tectonic Systems in Relation to Detachment Layer Thickness in Sedimentary Basins. In: *Tectonics* 18.4, pp. 719–732. DOI: 10.1029/1999TC900018.

Sun, Q. and T. M. Alves (2020). Petrophysics of Fine-Grained Mass-Transport Deposits: A Critical Review. In: *Journal of Asian Earth Sciences*, p. 104291. DOI: 10.1016/j.jseaes.2020.104291.

Talling, P., M. Clare, M. Urlaub, E. Pope, J. Hunt, and S. Watt (2014). Large Submarine Landslides on Continental Slopes: Geohazards, Methane Release, and Climate Change. In: *Oceanography* 27.2, pp. 32–45. DOI: 10.5670/oceanog.2014.38.

Urlaub, M., J. Geersen, S. Krastel, and T. Schwenk (2018). Diatom Ooze: Crucial for the Generation of Submarine Mega-Slides? In: *Geology* 4, pp. 331–334. DOI: 10.1130/G39892.1.

Urlaub, M., P. J. Talling, A. Zervos, and D. Masson (2015). What Causes Large Submarine Landslides on Low Gradient ($< 2°$) Continental Slopes with Slow (~ 0.15 m/Kyr) Sediment Accumulation?: Large submarine landslides on low gradients. In: *Journal of Geophysical Research: Solid Earth* 10, pp. 6722–6739. DOI: 10.1002/2015JB012347.

Wilson, C. K., D. Long, and J. Bulat (2004). The Morphology, Setting and Processes of the Afen Slide. In: *Marine Geology* 213.1–4, pp. 149–167. DOI: 10.1016/j.margeo.2004.10.005.

Supporting Information: Destabilizing factors for submarine landslides in the Eivissa Channel, Western Mediterranean Sea

Sager, T. F.[1*], Urlaub, M.[1], Kaminski, P. [2], Lastras, G. [3], Canals, M. [3], Berndt, C.[1]

[1] GEOMAR Helmholtz Centre for Ocean Research Kiel, Kiel, Germany

[2] Institute for Geotechnical Engineering & Construction Management, Hamburg University of Technology (TUHH), Hamburg, Germany

[3] Department of Earth and Ocean Dynamics, CRG Marine Geosciences, University of Barcelona, Barcelona, Spain

[*] Corresponding Author: (tsager@geomar.de)

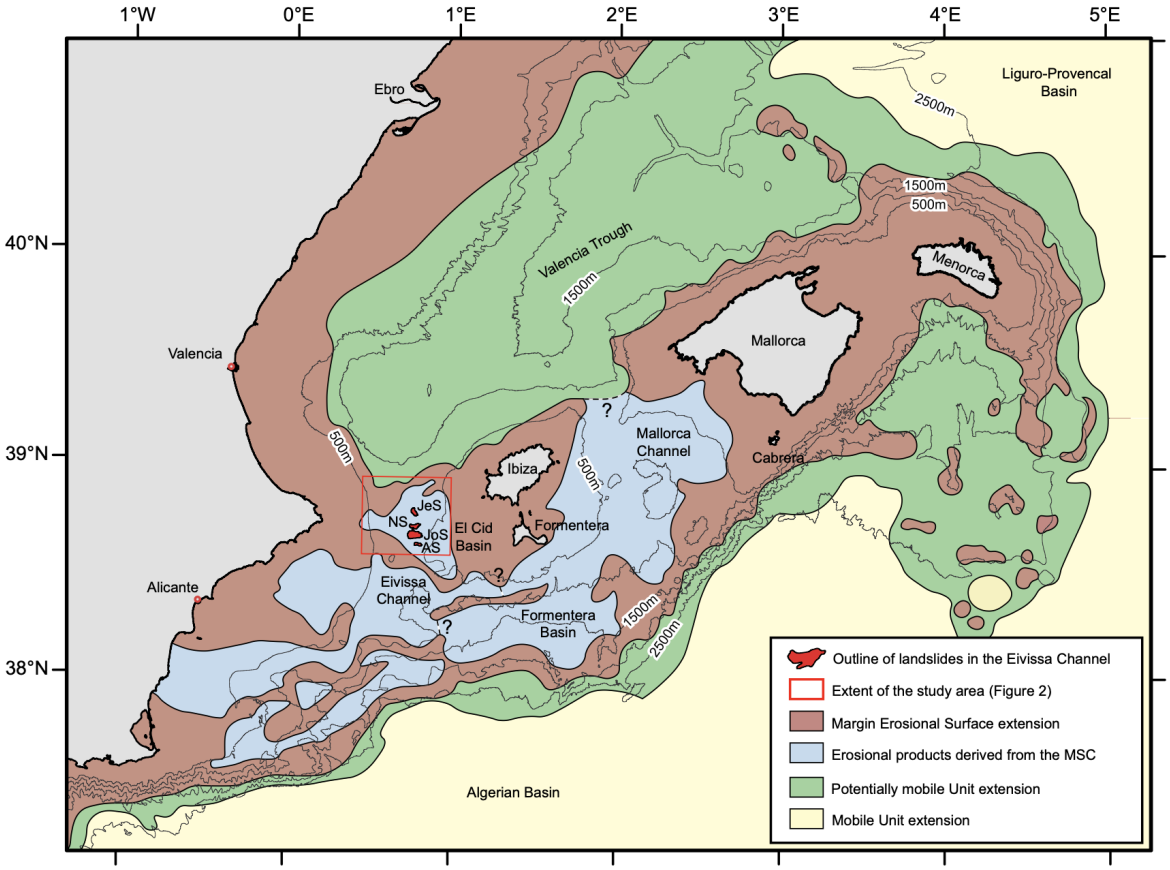

Figure 5.13: (Caption on next page.)

Figure 5.13: (Figure on previous page). Extent of Messinian Units in and around the Balearic Promontory (adapted from Driussi et al. (2015) and Ochoa et al. (2015)). The red 'Margin Erosional Surface extension' represents the extent of the Messinian Unconformity reflector without secondary erosional products above. The light blue 'Erosional product derived from the MSC' represents siliciclastic erosional products derived from the Margin Erosional Surface (called the Bedded Unit by Driussi et al., 2015). The 'Potentially mobile Unit extension' represents the extension of a potential mobile unit that is underlain by the 'Mobile Unit'. The spacing of contour lines is 500 m. Map modified from Driussi et al. (2015) and Ochoa et al. (2015).

References

Driussi, O., A. Maillard, D. Ochoa, J. Lofi, F. Chanier, V. Gaullier, A. Briais, F. Sage, F. Sierro, and M. Garcia (2015). Messinian Salinity Crisis Deposits Widespread over the Balearic Promontory: Insights from New High-Resolution Seismic Data. In: *Marine and Petroleum Geology* 66, pp. 41–54. DOI: 10.1016/j.marpetgeo.2014.09.008.

Ochoa, D., F. J. Sierro, J. Lofi, A. Maillard, J.-A. Flores, and M. Suarez (2015). Synchronous Onset of the Messinian Evaporite Precipitation: First Mediterranean Offshore Evidence. In: *Earth and Planetary Science Letters* 427, pp. 112–124. DOI: 10.1016/j.epsl.2015.06.059.

6 Conclusions and Outlook

The analysis and characterisation of submarine landslides are important to understand related geohazards and tsunami generation by identifying the destabilising factors that precondition or trigger slope failures. Furthermore, the processes of slope failures and how they interact and mix with seawater need to be understood. From the study of smaller landslides, with a presumably simpler development, processes that govern them can be analysed and understood more easily. This understanding can then be scaled up to explain how larger landslides develop and what pre-conditions or triggers them and how this relates to their tsunamigenic potential. While still in its infancy, the monitoring of active failure processes will provide insight into how landslides or their subsidiary turbidity currents interact and erode the seafloor. This has critical implications for the design of offshore seafloor installations. Similarly, geotechnical characterisation and integration with geophysical methods are increasingly needed to better constrain the instability of the seafloor for offshore platforms and wind farm design, planning, and construction.

This thesis comprises the analysis of an extensive geophysical dataset and 3D reflection seismic data that completely cover Ana Slide located in the Eivissa Channel, western Mediterranean Sea, between the Iberian Peninsula and the Eivissa Islands of Ibiza and Formentera. Knowledge from Ana Slide is extended to better constrain landslide development and emplacement processes of the similar Joan, Nuna, and Jersi slides. The novelty of this dataset allowed for cautious predictions regarding destabilising factors that controlled slope failures in the past.

6.1 Conclusions

Ana Slide is the smallest of four recent landslides in the Eivissa Channel with an area of 4.8 km^2 located at water depths between 635 - 790 m. This landslide developed during two major stages of failure called the 'primary' and 'secondary' stage, respectively. During these, several smaller landslide events occurred that successively moved landslide material from the upslope source area of evacuation into the downslope sink area of accumulation (Chapter 3). The movement of these smaller failures changed direction temporally during the development of Ana Slide. The primary failure comprised the majority of the landslide material mobilised within Ana Slide. During this stage, the downslope-most landslide front was created. Landslide material moved initially from East to West but diverged in a more

south-westerly direction following local seafloor morphology in the sink area at a later stage of failure. The morphology was previously modified by the activity of a local seafloor antithetic en echelon fault system. The location of the present-day headscarp marks the latest stage of retrogression. The present-day headscarp is around 300 m upslope from where the steepest slope was located before Ana Slide. The secondary failure occurred around 61.5 ka ago and because the primary failure occurred around 300 ka ago both stages of failure are temporally separated by approximately 240 ka.

While the tsunamigenic potential of Ana Slide has not been examined directly through modelling, the volume of actually mobilised landslide material is estimated in Chapter 4 at 0.040 km^3. This volume is smaller than previously proposed by Lastras et al., 2004 at 0.140 km^3, although these authors describe it as 'affected' material. Nonetheless, the detailed analysis of Ana Slide presented in Chapter 3 demonstrates that a better understanding of slope failure processes decreases the estimation of landslide volume. A volume of only 0.016 km^3 of fully evacuated landslide material might indicate that the tsunami hazard of Ana Slide is potentially even smaller. This is especially true considering that Ana Slide shows features of multistage retrogression from a segmented headscarp and the failure is subdivided into two separate stages of failure (the primary and secondary failures as presented in Chapter 3). Likewise, Joan, Nuna, and Jersi slides show many geomorphological similarities and signs for multistage retrogression (Lastras et al. (2004) and Chapter 5) making their tsunamigenic potential and volume likely smaller and less significant. Furthermore, all four landslides and the buried pre-Ana Slide show well-developed frontal lobes and no mobilised landslide material is observed downslope of these. This means that these landslides developed generally as frontally confined without the generation of resolvable turbidite deposit downslope the landslide fronts.

The four recent submarine landslides in the Eivissa Channel share the same stratigraphic reflector as their basal shear surface or 'glide plane' (Lastras et al., 2004) and are called the reference reflector Ref in this thesis (Chapter 3). This reflector also marks the depth of deformation of compressional ridges and chaotic seismic facies in the sink areas of Ana, Joan, Nuna, and Jersi slides. This infers that this reflector either represents a weak layer or that distinct geo-mechanical variations occur immediately above this layer. Changes in sedimentation potentially resulted in the deposition or stacking of geo-mechanically distinct layers controlled by climatic variability, changes in ocean circulations, changes in sediment fluxes from rivers on the Iberian Peninsula, or the availability of nutrients in shallow waters (Chapter 5). These factors also affect the pressure regime of a proposed weak layer to pre-condition slope failures in the Eivissa Channel that potentially were triggered by a regional mechanism of earthquake shaking. However, no undisturbed samples of the proposed weak layer exist and thus cores are needed to test these hypotheses.

Overall, the destabilising factors for the four recent submarine landslides in the Eivissa Channel are a combination of prevailing conditions and the presence of a weak layer. These developed into a basal shear surface of repeated slope failures of Ana Slide during the primary

and secondary failures. Since the weak layer is located at variable depth beneath the seafloor, it only developed instability after consolidation, during which changes in physical properties facilitated failure on the whole eastern slopes of the Eivissa Channel. Furthermore, the interplay between recurrent local fault activity observed beneath the Ana Slide Complex and potentially pulsed fluid and gas migration along this fault system indicates that submarine occurrences are controlled by local processes while the ultimate triggering mechanism was likely a far-field large-scale earthquake that simultaneously caused Ana, Joan, Nuna, and Jersi slides to fail.

In summary, the volume assessment of Ana Slide serves as a prime example that determining landslide volume requires detailed knowledge about development and emplacement processes. In the case of Ana Slide, a significant reduction in the amount of landslide material involved is proposed. The amount of landslide material involved in the landslide, here called the 'initially failed volume', is estimated to be 0.040 km^3, nearly a third from the original calculation. Even tough this, so far, can only be proved for Ana Slide, by using methods to reconstruct the pre-failure seafloor for a given landslide, in general the volume of actually mobilised landslide material can be potentially smaller than previously thought. Still much research is needed to predict and understand the underlying processes that control the tsunamigenic potential of submarine landslides. Not only the role of the landslide mechanism and the 'initially failed volume' is important but also the lithology of landslide materials, runout velocities, processes of landslide material and sea-water mixing, and the height drop between the source and sink areas (e.g., Harbitz et al., 2014).

6.2 Implications

The amount of landslide material of Ana Slide that evacuated the source area 'Ve_{void}' completely accumulated inside the sink area as 'Va'. Both volumes represent the same material with volumes of 0.016 km^3. It shows that Ana Slide is *volumetrically balanced*. Because Ana Slide is covered by 3D reflection seismic data in its entirety, the amount of the 'initially failed volume' Ve could be determined to comprise the volumes of Ve_{void} in combination with the amount of landslide material that was mobilised inside the source area but remained inside of it (Ve_r). Together these volumes represent the initially failed volume Ve of 0.040 km^3. If no reflection seismic data had been available, we could have only determined the amount of Ve_{void} from pre-failure seafloor reconstructions. Thus, volume assessment from bathymetry should serve as minimum values of the initially failed volume.

The amount and extent of chaotic, transparent, and disrupted seismic facies is an insufficient measure for the initially failed volume of submarine landslides. Instead, the void space between the reconstructed pre-failure and the present-day seafloors inside the source area provides a more robust minimum estimate referred to as Ve_{void}. Nevertheless, any volume assessment should be ideally proved using 3D reflection seismic data.

6.3 Outlook

To further study submarine landslides in the Eivissa Channel, it is recommended to compile all available geophysical data. This should articular include reflection seismic data acquired with a sparker source with a potentially high resolution during the COBAS cruise in 2004 (Lafuerza et al., 2012). This data was not incorporated to this study as it is currently not accessible. On the other hand, sediment echosounder profiles can be used to image the subseafloor covering the upper 50 m and the Messinian Unconformity reflector. Furthermore, the 3D reflection seismic data can be extend in order to cover pre-Ana Slide and the southern continuation of the seafloor antithetic en echelon fault system (Chapters 3, 4, and 5).

Additional reflection seismic data could provide critical information about the exact interaction between pre-Ana and Ana slides related to local fault reactivation of the en echelon fault system and repeated slope failures. Even though this can only be inferred at the moment, it would be possible to verify through further 3D seismic surveying. Also, fault displacement diagrams from the en echelon fault system (central and northern fault) could provide information about fault growth, as the pre-Ana Slide moved over the central and northern faults (Chapters 3 and 5), while Ana Slide propagated primarily above the northern fault (Chapter 3). Moreover,a channel that eroded into the Messinian Unconformity reflector is observed in the 3D reflection seismic data (Berndt et al., 2012) and presented in Chapters 3 and 5). A correlation between this channel and the en echelon fault system that to some degree controlled pre-Ana and Ana slides is undeniable. Therefore, closely-spaced multi-channel reflection seismic lines could provide links between the control of the local tectonic history and differential compaction of the channel fill potentially acting as a local trigger mechanism.

Besides additional reflection seismic data, long gravity cores to sample the weak layer referenced here as reflector Ref (Chapters 3, 4, and 5) could provide information about its lithology, sedimentology, and geo-mechanical properties. The maximum penetration depth of conventional gravity cores is around 30 m. The sedimentary environment inside the Eivissa Channel is assumed to have not changed since before the occurrence of pre-Ana Slide (Chapters 3 and 4). Therefore, deeper materials are assumed to be similar concerning their grain size and sediment matrix that should be readily penetrated by gravity cores. Feasible locations for gravity cores that sample the proposed weak layer are at about 100 m upslope of the headscarps of all landslides in the Eivissa Channel, inside the landslide scar where evacuated landslide material remained inside the source area, and inside the sink area where landslide material accumulated. Inside the sink area, the nature of the 'depth of the deformation layer' (sensu Chapter 5) that is represented by reflector Ref could provide valuable insight into how compressional tectonics on a microscopic scale compare with macroscopic features observed in sediment echosounder and reflection seismic profiles. In addition, gravity cores and sediment echosounder profiles from steep slope sections, such as North of Jersi or South of Ana slides could constrain the interplay between deposition and slope stability with the potential to shed light on why steep areas are less prone to failure.

New core locations can further be designed to capture lateral changes in the lithology and depositional environment within the Eivissa Channel. Cores should be taken from shallow (500 m) to deep (900 m) locations from East to West, respectively. To evaluate the influence of bottom current activity and re-deposition along the slope, cores should be obtained between local highs and lows, for example immediately South and North of Ana Slide or East-West of Nuna Slide where an acoustic basement outcrop on the seafloor is observed (HERMESIONE, 2009) (Figure 2.2 and 5.12). Overall, gravity cores should be obtained from all landslides with a focus on Ana Slide. Here, re-sampling of larger or multiple cores would allow destructive geotechnical measurements to be performed.

The results of this thesis demonstrate that studying small submarine landslides such as those in the Eivissa Channel is valuable to better understand slope failure processes on a larger scale. Nonetheless, all sampling methods and their recovery affect *in-situ* conditions, such as pressure, stress, temperature, and chemical conditions. It would be more feasible to acquire additional reflection seismic data with a focus on constraining local tectonic features and processes that influence fluid and gas migration pathways. For instance, a local fault system is identified immediately beneath the Ana Slide Complex and could have controlled local recurrent slope failure. These tectonic features were identified by sub-bottom profiler and reflection seismic data (sensu Chapters 3 and 5), yet the analysis presents more questions than answers.

The complete coverage of 3D reflection seismic data specifically targeting Ana Slide allowed for a very comprehensive analysis of development and emplacement processes. Furthermore, the detailed understanding sparked additional studies by answering the objectives outlined above.

References

Berndt, C., S. Costa, M. Canals, A. Camerlenghi, B. de Mol, and M. Saunders (2012). Repeated Slope Failure Linked to Fluid Migration: The Ana Submarine Landslide Complex, Eivissa Channel, Western Mediterranean Sea. In: *Earth and Planetary Science Letters*, pp. 65–74. DOI: 10.1016/j.epsl.2011.11.045.

Harbitz, C. B., F. Løvholt, and H. Bungum (2014). Submarine Landslide Tsunamis: How Extreme and How Likely? In: *Natural Hazards* 3, pp. 1341–1374. DOI: 10.1007/s11069-013-0681-3.

HERMESIONE (2009). *Cruise Report BIO Hesperides Research cruise HERMESIONE*. Antoni M. Calafat and Miquel Canals: University of Barcelona, Spain; Institut National de Recherche Halieutique, Morocco; Consejo Superior de Investigaciones Científicas, Spain: Gibraltar Strait – Western Mediterranean (Cartagena – Cartagena) 15th September – 9th October 2009: Hotspot Ecosystem Research on Europe's Deep-Ocean Margins (HERMES), Hotspot Ecosystem Research and Man's Impact on European Seas (HERMIONE), and Ocean Tracking Network (OTN).

Lafuerza, S., N. Sultan, M. Canals, G. Lastras, A. Cattaneo, J. Frigola, S. Costa, and C. Berndt (2012). Failure Mechanisms of Ana Slide from Geotechnical Evidence, Eivissa Channel, Western Mediterranean Sea. In: *Marine Geology*, pp. 1–21. DOI: 10.1016/j.margeo.2012.02.010.

Lastras, G., M. Canals, R. Urgeles, J. E. Hughes-Clarke, and J. Acosta (2004). Shallow Slides and Pockmark Swarms in the Eivissa Channel, Western Mediterranean Sea. In: *Sedimentology* 4, pp. 837–850. DOI: 10.1111/j.1365-3091.2004.00654.x.

List of Figures

2.1 Location of study area, western Mediterranean Sea. 11
2.2 Map of geophysical data from the Eivissa Channel. 12
2.3 2D and 3D reflection seismic data of Ana Slide. 15
2.4 Transects through Ana Slide (3D data). 16
2.5 Receiver ghost artefacts. 17
2.6 Supplement to Chapter 3: Seafloor reflection of a single shot. 18
2.7 The receiver ghost issue. 20

3.1 Basemap of the study area. 34
3.2 Bathymetric depth and slope gradient map of Ana Slide. 36
3.3 Un-interpreteted and interpreted profile through Ana Slide. 37
3.4 Time isochron maps of Unit 1, Unit 2, and Unit 1 and 2. 43
3.5 Seismic profiles north and south of Ana Slide. 44
3.6 Seismic profile of and upslope of the by-pass zone. 45
3.7 Transect profile through the by-pass zone and sink area of Ana Slide. 47
3.8 Seismic attribute map of SFR (*Smoothed Dip of Maximum Similarity*). 48
3.9 Seismic profile through the northern source area. 51
3.10 Interpretative development sketch of Ana Slide. 52
3.11 Supplement to Chapter 3: Trace separation between channel 1, 4, 8 and 10. . 65
3.12 Supplement to Chapter 3: Seafloor reflection of a single shot. 66
3.13 Supplement to Chapter 3: Shot-gathers, shot-sorted 3D single channel data. . 66
3.14 Supplement to Chapter 3: Average frequency content of each channel. 67
3.15 Supplement to Chapter 3: Location of profiles of 3D and 2D re-processed reflection seismic data for comparison of shallow subsurface data quality. . . . 68
3.16 Supplement to Chapter 3: Visual comparison: Inline 3 (3D) and Channel 01 - 83 (2D). 69
3.17 Supplement to Chapter 3: Visual comparison: Inline 72 (3D) and Channel 01 - 29 (2D). 70
3.18 Supplement to Chapter 3: Visual comparison: Inline 77 (3D) and Channel 01 - 25 (2D). 71
3.19 Supplement to Chapter 3: Visual comparison: Inline 98 (3D) and Channel 01 - 09 (2D). 72
3.20 Supplement to Chapter 3: Visual comparison: Inline 127 (3D) and Channel 01 - 67 (2D). 73

3.21 Supplement to Chapter 3: Visual comparison: Inline 202 (3D) and Channel 01 - 07 (2D). 74
3.22 Supplement to Chapter 3: Profile through the by-pass zone of Ana Slide showing Channel 01 - 85 (2D). 75
3.23 Supplement to Chapter 3: TOPAS sub-bottom parasound profile through Ana Slide (Lastras et al., 2004). 75
3.24 Supplement to Chapter 3: TWTT (s) map of the Ref reflector (3D). 76
3.25 Supplement to Chapter 3: TWTT (s) map of the R3 reflector (3D). 76
3.26 Supplement to Chapter 3: TWTT (s) map of the R2 reflector (3D). 77
3.27 Supplement to Chapter 3: TWTT (s) map of the SFR reflector (3D). 77
3.28 Supplement to Chapter 3: TWTT (s) map of the R1 reflector (2D). 78
3.29 Supplement to Chapter 3: TWTT (s) map of the SFR reflector (2D). 78

4.1 Regional map and local overview map of Ana Slide. 84
4.2 Pre-failure seafloor reconstructions of Ana Slide. 88
4.3 Conceptual models of submarine landslide volume assessment. 92
4.4 Workflow for submarine landslide volume assessment. 96
4.5 Supplement to Chapter 4: 'Straight-line ' pre-failure seafloor reconstruction approach. 103
4.6 Supplement to Chapter 4: 'Horizon-flattening' pre-failure seafloor reconstruction approach. 104

5.1 Location of the study area in the Western Mediterranean Sea. 108
5.2 Data overview map in the Eivissa Channel. 109
5.3 Bathymetry of Ana Slide. 112
5.4 Re-processed 2D reflection seismic profile (Channel 1 - Line 37). 113
5.5 Re-processed 2D reflection seismic profile (Channel 1 - Line 83). 114
5.6 Isochron maps of stratigraphic units. 120
5.7 Profiles west of Ana Slide and south of Joan Slide. 123
5.8 Bathymetry and profiles through Joan Slide. 124
5.9 Bathymetry and profiles through Nuna Slide. 126
5.10 Bathymetry and profiles through Jersi Slide. 127
5.11 Profile north-south through the Eivissa Channel. 129
5.12 Activity diagram of slope failure and tectonic activity. 132
5.13 Supplement to Chapter 5: Extent of Messinian Units in the Balearic Promontory. 142

List of Tables

2.1 Short geomorphometric table of Eivissa Channel landslides. 11

3.1 Overview of profiles. 64

4.1 Results from volume estimations of Ana Slide. 91

5.1 Short geomorphometric table of Eivissa Channel landslides. 121

6.1 Available geophysical data from submarine landslides in the Eivissa Channel. 160

6.2 Geomorphometric table of landslides in the Eivissa Channel. 167

Acknowledgements

I thank all people involved in this PhD project. First, my supervisors Morelia Urlaub and Christian Berndt which I am indebted for providing funding and academic guidance throughout the project and agitating discussions on submarine landslides, 3D reflection seismic data and methods, and the scientific method – we fought extensive discussions that improved the quality of my work and challenged me as a researcher. Secondly, I thank my project partner Pauline Kaminski from the TUHH for excellent collaboration between the fields of reflection seismic analysis and geotechnical engineering. I especially thank her for fruitful discussions and great patience with my "interesting" questions. Thirdly, I thank my co-authors Galderic Lastras and Miquel Canals (University of Barcelona) for their fruitful discussions on landslides within the Eivissa Channel – unfortunately a meeting in Barcelona or Kiel was never possible. I thank Cord Papenberg (GEOMAR) for re-processing the seismic data. His patience in discussing seismic processing was great fun alongside being a detective in discovering the ghost.

I thank my dear friends Benjamin, Helene, Lara, Bruna, Carlos, Megan, Anna, Louisa, Florian, Johanna, Anders, and Jesper for considering me their friend. Furthermore, my badminton club (Sören, Ullvi, Paul, Valeska, Linus, Timo, Mirek, Daniel) and the box made my time in Kiel bearable.

At last, I want to thank my family Hans-Hermann (Opa), Annegret, Michael, Britta, Stefan, Valeska, Andreas, and as of recently Emil for their tremendous support during my time in Kiel.

Your dear friend, grandson, son, brother, nephew, brother-in-law, and uncle Thore.

Curriculum Vitae

Removed according to data protection regulations.

Aus datenschutzrechtlichen Gründen entfernt.

List of Publications

ORCID ID: 0000-0001-8777-2350

Peer Reviewed

Sager, T. F., Urlaub, M., Kaminski, P., Lastras, G., Canals, M., Papenberg, C., Berndt, C. (2022). Development and Emplacement of Ana Slide, Eivissa Channel, Western Mediterranean Sea. Geochemistry, Geophysics, Geosystems (G^3), https://doi.org/10.1029/2022GC010469

Kaminski, P., Grabe, J., **Sager, T. F.**, Urlaub, M. (2022). Decline in Slope Stability as a Consequence of Gassy Soil in Submarine Slopes on the Balearic Promontory. ASME 2022 41st International Conference on Ocean, Offshore and Arctic Engineering, https://doi.org/10.1115/OMAE2022-81151

Kaminski, P., **Sager, T. F.**, Grabe, J., Urlaub, M. (2021). A New Methodology to Assess the Potential of Conjectural Trigger Mechanisms of Submarine Landslides Exemplified by Marine Gas Occurrence on the Balearic Promontory. Engineering Geology, https://doi.org/10.1016/j.enggeo.2021.106446

Under Review

Sager, T. F., Urlaub, M., Kaminski, P., Lastras, G., Canals, M., Berndt, C. Destabilizing Factors for Submarine Landslides in the Eivissa Channel, Western Mediterranean Sea. Geochemistry, Geophysics, Geosystems (G^3)

Sager, T. F., Urlaub, M., Berndt, C. Assessment of submarine landslide volume. Geo-Marine Letters

Sager, T. F., Urlaub, M., Kaminski, P., Lastras, G., Canals, M., and Berndt, C. (2021) Evolutionary development and volume balance calculations of the Ana Slide in the Eivissa Channel, Western Mediterranean. vEGU General Assembly 2021, online, 19–30 April 2021, EGU21-2118, https://doi.org/10.5194/egusphere-egu21-2118

Sager, T. F., Urlaub, M., Kaminski, P., Lastras, G., Canals, M., Berndt, C. (2021). Development and Volume Balance Calculations of the Ana Slide in the Eivissa Channel, Western Mediterranean. ISSMMTC (International Symposium of Submarine Mass Movements and Their Consequences) 2020 (2021), online, Dublin, Ireland.

Sager, T. F., Urlaub, M., Geersen, J., Berndt, C. (2022). Volume Balance of Frontally Confined Submarine Landslides – A Case Study of the Ana Slide, Eivissa Channel, Western Mediterranean Sea. EGU General Assemly 2022, in-person, 23-27 May 2022, Vienna, Austria, EGU22-4343: https://doi.org/10.5194/egusphere-egu22-4343

Sager, T. F., Urlaub, M., Berndt, C. (2022). The Seafloor Morphology of Submarine Landslides – What can it tell us about Landslide Development? International Conference on Seafloor Landforms, Processes and Evolution 2022, in-person, 4-6 July 2022, Valetta, Malta.

Appendix

Here, a table gathering all geophysical data acquired during several cruises to the Eivissa Channel previously presented in Chapter 2.5.1 (Table 6.1) is presented that comprises the database of this thesis. Furthermore, from detailed analysis of geophysical data a complete geomorphometric table of submarine landslides in the Eivissa Channel, western Mediterranean Sea is presented in Table 6.2. This table uses geomorphometric parameters previously presented by Clare et al. (2019) and shows additional parameters specifically related to studies presented in Chapters 3, 4, and 5 covering the Ana, pre-Ana, Joan, Nuna, and Jersi slides.

Cruise	Year	Vessel	Bathymetry	Sub-Bottom Profiler Data (TOPAS)	Reflection seismic data	Side-scan sonar images	Additional data	Jersi Slide	Nuna Slide	Joan Slide	Ana Slide	Publication
BIG'95	1995	BIO Hespérides	50 x 50 m (EM12)	very low quality, no digital	-	-	-	bathymetry	bathymetry	bathymetry	bathymetry	Lastras et al., 2004; Lastras et al., 2006; Berndt et al., 2012
MARINADA	2002	BIO Hespérides	50 x 50 m (EM12)	High quality (TOPAS PS018)	-	-	-	bathymetry, sediment echosounder	bathymetry, sediment echosounder	bathymetry, sediment echosounder	bathymetry, sediment echosounder	Lastras et al., 2004; Lastras et al., 2006; Lafuerza et al., 2012
COBAS	2004	R/V Urania	-	-	Sparker reflection seismic profiles (?)	Chirp-sonar (?)	Gravity cores (?)	-	-	-	?	mentioned by Lafuerza et al., 2012, abandoned manuscript G. Lastras, *personal communication*, December 16, 2022
CD178	2006	RRS Charles Darwin	5 x 5 m (EM12)	-	3D reflection seismic data	-	re-processed 2D profiles (presented by Sager et al. (2022))	-	-	-	bathymetry, 3D seismic	CD178, 2006; Berndt et al., 2012; Lafuerza et al., 2012; Panieri et al., 2012; Sager et al., 2022
BALICAT TTR-14 Leg 2b	2006	R/V Professor Logachev	-	-	-	MAK-1M 30 kHz (2 x 2 m)	-	side-scan sonar	side-scan sonar	side-scan sonar	side-scan sonar	Lastras et al., 2006
PRISM	2007	R/V L'Atalante	-	-	-	-	CPTu measurements and gravity cores	-	-	-	CPTu and corings	Lafuerza et al., 2012
EUROLEON	2007	BIO Hespérides	20 x 20 m (EM120), 2 x 2 m (EM3000 in up slope region of Ana Slide)	low quality (TOPAS PS018)	-	-	SeaEye Linx, video transects	bathymetry, sediment echosounder	bathymetry, sediment echosounder	bathymetry, sediment echosounder	bathymetry	
HERMESIONE	2009	BIO Hespérides	25 x 25 m (EM120)	High quality (TOPAS PS018)	airgun 2D reflection seismic profiles	-	multi-corer and gravity cores	bathymetry, sediment echosounder, sediment sampling, 2D seismic	bathymetry, sediment echosounder, sediment sampling, 2D seismic	bathymetry, sediment echosounder, 2D seismic	bathymetry, sediment echosounder	HERMESIONE, 2009

Table 6.1: All available geophysical data for submarine landslides on the eastern slopes of the Eivissa Channel including Jersi, Nuna, Joan, and Ana (pre-Ana) slides used in this thesis. Detailed information about seismic processing of reflection seismic data acquired during cruise CD178 is presented in Sections 2.5.1.3 and 2.5.3.

			pre-Ana Slide	Ana Slide	Joan Slide	Nuna Slide	Jersi Slide	Comment
1	ID	Sequential number of each landslide entry in the database	-	-	-	-	-	-
2	Parent ID	Parent refers to the landslide complex; individual ID numbers are for each mapped landslide	-	-	-	-	-	-
3	Name	Published name for landslide	pre-Ana Slide	Ana Slide	Joan Slide	Nuna Slide	Jersi Slide	-
4	Aliases	Other names for the landslides	-	-	-	-	-	-
5	Frontal confinement	'Frontally-confined', 'frontally-confined with overrunning flow', 'frontally-emergent', 'frontally unconfined' or 'not identified'	frontally confined	frontally confined - frontally confined with overrunning flow	frontally confined with overrunning flow	frontally confined	frontally confined	-
6	Attachment	Attached or detached as defined by Moscardelli and Wood, 2008	-	-	-	-	-	-
7	Object type	Single event (mass-transport deposit) or multiple events (mass-transport complex). Multiple events should be linked to a parent ID	multi-staged retrogressive landslide	multi-staged retrogressive landslide	multi-staged retrogressive landslide	multi-staged retrogressive landslide	multi-staged retrogressive landslide	single event or multi-staged landslide (retrogressive) - constrained from the shape of the headscarp or landslide front
8	Depth below seafloor (TWTT in ms)	For landslides measured from subsurface data, this is the depth to the top of the landslide deposit. If calculated from seismic data, the two-way travel time (TWTT) should also be referenced. If mapped from seafloor data without seismic or core sample calibration this will not be possible to complete	in the sink area (approximately): 73 ms = 54.75 m (with V_p 1500 m/s) in the source area (approximately): 20 ms = 15 m (with V_p 1500 m/s)	buried beneath a ca. 2.5 - 3 m thick post-landslide drape	buried beneath a ca. 2.5 - 3 m thick post-landslide drape	buried beneath a ca. 2.5 - 3 m thick post-landslide drape	buried beneath a ca. 2.5 -3 m thick post-landslide drape	-
9	Depth below seafloor (m)	For landslides measured from subsurface geophysical data, this is the depth in TWTT to the top of the landslide deposit	-	-	-	-	-	-
10	Depth below seafloor (m)	For landslides measured from subsurface geophysical data, this is the depth in TWTT to the top of the landslide deposit	-	-	-	-	-	-
11	Latitude and longitude (WGS)	Centre-point of the mapped feature. It is recognised that the entirety of a landslide may not be visible due to data coverage limitations; hence, this is primarily intended to locate the feature on a global database	Latitude: $38°38'30''$ Longitude: $0°48'20''$	Latitude: $38°38'25''$ Longitude: $0°48'50''$	Latitude: $38°41'00''$ Longitude: $0°47'25''$	Latitude: $38°43'20''$ Longitude: $0°47'35''$	Latitude: $38°47'20''$ Longitude: $0°47'10''$	measured from the central point (relatively subjective measurement)
12	Water depth minimum (m)	Minimum water depth for mapped landslide (only possible from multibeam data)	buried MTD	635 m	610 m	705 m	750 m	-
13	Water depth maximum (m)	Maximum water depth for mapped landslide (only possible from multibeam data)	buried MTD	790 m	870 m	855 m	905 m	-

			pre-Ana Slide	Ana Slide	Joan Slide	Nuna Slide	Jersi Slide	Comment
14	Total length L_t (m)	Total mappable length of slide from the upslope limit of the headscarp to the downslope limit of the connected deposit (excludes out-runner blocks). This is measured along the axial course of the landslide if possible (e.g., from multibeam echosounder (MBES) data), otherwise this is a straight line (e.g., measured from 2D seismic data) and is an 'apparent' length measurement. Detail on the method should be listed as accompanying metadata	5.3 km	4.1 km	7.7 km	5.9 km	4.5 km	measure from the headscarp to the landslide front (maximum length) - straight line
15	Deposit length, L_d (m)	Total mappable length of the slide deposit (excludes outrunner blocks). This is measured along the axial course of the landslide if possible and, hence, is not necessarily a straight line (e.g., from MBES data); otherwise, this is a straight line (e.g., measured from 2D seismic data) and is an 'apparent' length measurement. Detail on the method should be listed as accompanying metadata	-	-	-	-	-	length of the deposit meaning length of the sink area (addressed below as the length of the accumulation sink area)
16	Evacuated length, L_e (m)	Length of the scar from the headscarp to the upslope limit of deposit measured along the axial course of the landslide. Should be equal to L_t minus L_d	-	-	-	-	-	length of the evacuational source area (addressed below)
17	Length metadata	For example, is this measured from a section and is it an apparent measurement (and thus may be an underestimate), or otherwise how was the distance calculated?	-	-	-	-	-	length of the by-pass zone (measure from profiles)
18	Scar perimeter length, L_s (m)	Length of scar perimeter including side scarps. A spline should be fitted to the mapped scarp to ensure consistency at different data resolutions	-	-	-	-	-	measured from picked polygons (little inconsistency) - not measured from Kingdom
19	Headscarp height, H_s (m)	Height difference from the maximum convex point at the top of the headscarp to the maximum concave point at the bottom	-	30 m	20 m	50 m	15 m	measured from Lastras et al., 2004
20	Evacuation height, H_e (m)	Height from the upslope limit of the landslide deposit to the upslope limit of the headscarp	-	-	-	-	-	-
21	Scar width, W_s (m)	Maximum scar width	2.1 km	1.6 km	4.0 km	2.2 km	2.1 km	-

			pre-Ana Slide	Ana Slide	Joan Slide	Nuna Slide	Jersi Slide	Comment
22	Scar surface nature	Descriptive explanation (e.g., concave, stepped, etc.)	-	-	-	-	-	add more to this (overall morphology - are compressional ridge presented - how far do they extend and where are they located, grooves or longitudinal features throughout the middle part i.e. the translational domain (by-pass zone)... etc.
23	Maximum deposit width, W_d (m)	Maximum deposit width (measured orthogonal to the deposit length, L_d)	2.1 km	1.6 km	4.0 km	1.6 km	2.0 km	width of the sink area
24	Maximum deposit thickness, $T_{d\ max}$ (TWTT in ms)	Maximum measured deposit thickness in metres. Detail should be provided in the accompanying metadata as to how this was measured (e.g., from height on bathymetry or from seismic data) (and where)	65 ms = 48.75 m (with V_p 1500 m/s) complete seismic coverage	52 ms = 39 m (with V_p 1500 m/s) complete seismic coverage	70 ms = 52.5 m (with V_p 1500 m/s)	60 ms = 45 m (with V_p 1500 m/s)	55 ms = 41.25 m (with V_p 1500 m/s)	calculated as the maximum thickness of all affected sediment and material
25	Maximum deposit thickness, $T_{d\ max}$ (m)	Maximum measured deposit thickness in TWTT	20 m (this study)	15 m (Sager et al., 2022)	16.5 m	9 m	11.25 m	calculated by horizon-flattening of Ref with assumed predictable thickness between Ref and SFR 5
26	Maximum unconfined deposit thickness, T_u (TWTT in ms)	Maximum measured unconfined deposit thickness	-	-	-	-	-	similar to the thickness of accumulated landslide material inside the sink area
27	Maximum unconfined deposit thickness, T_u (m)	Maximum measured unconfined deposit thickness in TWTT	-	-	-	-	-	similar to the thickness of accumulated landslide material inside the sink area
28	Thickness metadata	How was the thickness calculated? For example, derived from multibeam data, measured from seismic (with which assumed seismic velocity?) or calibrated with core sampling data?	reflection seismic data	reflection seismic data	sub-bottom parasound	sub-bottom parasound	sub-bottom parasound	-
29	Total height drop, H_t (m)	Height from the downslope limit of the landslide deposit and the upslope limit of headscarp	-	155 m	250 m	150 m	155 m	calculated from the water depth min to water depth max
30	Slope gradient, S (°)	Measured laterally away from the scar outside of the zone of deformation. This is intended to give an estimate of the gradient of the unfailed slope	-	2.2°	1.1°	1.5°	2°	calculated from the total height drop, H_t (m) and the total length, L_t (m)
31	Slope gradient metadata	Notes added here to indicate the distance of the lateral offset of the measurement, distance over which the gradient was measured and any uncertainties, etc.	-	CD178 bathymetric map (5 m grid)	HERMESIONE bathymetric map (25 m grid)	HERMESIONE bathymetric map (25 m grid)	HERMESIONE bathymetric map (25 m grid)	-

			pre-Ana Slide	Ana Slide	Joan Slide	Nuna Slide	Jersi Slide	Comment
32	Slope gradient of the headscarp, S_s (°)	Maximum slope of the headscarp	-	25°	18°	20°	22°	highly dependent on the resolution of the bathymetric maps
33	Slope gradient of the headscarp metadata	Notes added here to indicate where this was measured, the distance over which the gradient was measured and any uncertainties, etc.	-	CD178 bathymetric map (5 m grid)	HERMESIONE bathymetric map (25 m grid)	HERMESIONE bathymetric map (25 m grid)	HERMESIONE bathymetric map (25 m grid)	-
34	Slope gradient at the toe, S_t (°)	Measured in front of the toe outside of the zone of deformation.	-	1°	1°	1°	1°	-
35	Slope gradient at the toe metadata	Notes added here to indicate the distance of the lateral offset of the measurement, the distance over which the gradient was measured and any uncertainties, etc.	-	CD178 bathymetric map (5 m grid)	HERMESIONE bathymetric map (25 m grid)	HERMESIONE bathymetric map (25 m grid)	HERMESIONE bathymetric map (25 m grid)	-
36	Basal surface type	Description of the basal surface, if mappable (e.g., rugose, planar, etc.)	no mappable (planar)	no mappable (planar)	no mappable (planar)	no mappable (planar)	no mappable (planar)	-
37	Upper surface type	Description of the upper surface, if mappable (e.g., rugose, smooth, etc.)	rugose with compressional ridges	rugose with compressional ridges	rugose with compressional ridges	rugose with compressional ridges	rugose with compressional ridges	-
38	Volume (km^3)	Calculated deposit volume	0.040 km^3	0.016 km^3	-	-	-	Deposited volume should refer to landslide material accumulated inside the sink area, thus what was calculated for Ana Slide (Chapter 4) - requires 3D data for pre-Ana Slide
39	Volume metadata	How was the volume calculated? What are the assumptions? Which published method was used (if any?)	-	-	-	-	-	-
40	Age (years BP)	If known, this is the age of the landslide in years. This may be an absolute value or a constrained age (e.g., 45 ka.)	-	61.5 ka.	assumed to be similar to Ana Slide (see discussion below)	assumed to be similar to Ana Slide (see discussion below)	assumed to be similar to Ana Slide (see discussion below)	-
41	Age error	Where available, the error ranges of the dates should be presented	-	-	-	-	-	-
42	Age metadata	Information on the dating method, uncertainties, where the sample was taken (location and depth relative to the landslide deposit) and any assumptions should be referenced. Here the source of the age should also be referenced	-	Cattaneo et al., 2011 (EGU abstract)	-	-	-	-
43	Seafloor features	Which seafloor features are present - how do they look like, correlation with the landslide (sources?)	-	pockmarks in the vicinity of the landslide (Lastras et al., 2006) - no reflection seismic evidence	pockmarks in the vicinity of the landslide (Lastras et al., 2006) - no sub-bottom parasound coverage	pockmarks in the vicinity of the landslide (Lastras et al., 2006) - no sub-bottom parasound coverage	pockmarks in the vicinity of the landslide (Lastras et al., 2006) - no sub-bottom parasound coverage	-

			pre-Ana Slide	Ana Slide	Joan Slide	Nuna Slide	Jersi Slide	Comment
41	Age error	Where available, the error ranges of the dates should be presented	-	-	-	-	-	-
42	Age metadata	Information on the dating method, uncertainties, where the sample was taken (location and depth relative to the landslide deposit) and any assumptions should be referenced. Here the source of the age should also be referenced	-	Cattaneo et al., 2011 (EGU abstract)	-	-	-	-
43	Seafloor features	Which seafloor features are present - how do they look like, correlation with the landslide (sources?)	-	pockmarks in the vicinity of the landslide (Lastras et al., 2006) - no reflection seismic evidence	pockmarks in the vicinity of the landslide (Lastras et al., 2006) - no sub-bottom parasound coverage	pockmarks in the vicinity of the landslide (Lastras et al., 2006) - no sub-bottom parasound coverage	pockmarks in the vicinity of the landslide (Lastras et al., 2006) - no sub-bottom parasound coverage	-
44	Seafloor features metadata	Useful additional information about seafloor features in the vicinity or in association with the landslide deposit, such as evidence of fluid expulsion (e.g., pockmarks)	evidence for subsurface fluid and has migration (Berndt et al., 2012)	evidence for subsurface fluid and has migration (Berndt et al., 2012). Lastras et al., 2004 indicate the presence of pockmarks and volcanic centres on the eastern slopes of the Eivissa Channel	Lastras et al., 2004 indicate the presence of pockmarks and volcanic centres on the eastern slopes of the Eivissa Channel	Lastras et al., 2004 indicate the presence of pockmarks and volcanic centres on the eastern slopes of the Eivissa Channel	Lastras et al., 2004 indicate the presence of pockmarks and volcanic centres on the eastern slopes of the Eivissa Channel	-
45	Data type	Data on which the mapping was based. High-level statement (e.g., bathymetry, combined bathymetry and geophysics, core, deep seismic).	combined bathymetry and geophysics - 2D and 3D reflection seismic data	combined bathymetry and geophysics - 2D and 3D reflection seismic data, recurrent bathymetric survey, side-scan sonar images	combined bathymetry and geophysics - sub-bottom parasound profiles, recurrent bathymetric survey, side-scan sonar images	combined bathymetry and geophysics - sub-bottom parasound profiles, recurrent bathymetric survey, side-scan sonar images	combined bathymetry and geophysics - sub-bottom parasound profiles, recurrent bathymetric survey, side-scan sonar images	-
46	Data type metadata	Data on which the mapping was based – more details can be provided here on combinations of sources (e.g., hull-mounted multibeam data, AUV data, 2D/3D seismic, sediment cores, etc.). This may be a combination of sources	BIG'95, MARINADA, BALICAT TTR-14, CD178, PRISM	BIG'95, MARINADA, BALICAT TTR-14, CD178, PRISM	BIG'95, MARINADA, BALICAT TTR-14, EUROLEON, HERMESIONE	BIG'95, MARINADA, BALICAT TTR-14, EUROLEON, HERMESIONE	BIG'95, MARINADA, BALICAT TTR-14, EUROLEON, HERMESIONE	BALICAT TTR-14
47	Data source	Reference to where the data came from (e.g., the data provider and the cruise, etc.). This should, ideally, include a hyperlink(s)	see above	see above	see above	see above	see above	-
48	Data repositories	Where can the raw/processed data be found if they are available? This should include a hyperlink if available	see above	see above	see above	see above	see above	-
49	Publication source	Where is the peer-reviewed source? If there is not one, then link to a cruise report or equivalent. If not published, then this needs to be flagged. This should include a hyperlink	see separate table for more information (coverage, publication, data type, etc.)	see separate table for more information (coverage, publication, data type, etc.)	see separate table for more information (coverage, publication, data type, etc.)	see separate table for more information (coverage, publication, data type, etc.)	see separate table for more information (coverage, publication, data type, etc.)	-

			pre-Ana Slide	Ana Slide	Joan Slide	Nuna Slide	Jersi Slide	Comment
50	Depth below seafloor metadata	Notes to accompany the depth. For instance, is it the only measurable depth, an average depth or maximum depth? What was the assumed (or calibrated) seismic velocity?	all volume and thickness estimates have been made by using a seismic velocity of 1500 m/s	all volume and thickness estimates have been made by using a seismic velocity of 1500 m/s	all volume and thickness estimates have been made by using a seismic velocity of 1500 m/s	all volume and thickness estimates have been made by using a seismic velocity of 1500 m/s	all volume and thickness estimates have been made by using a seismic velocity of 1500 m/s	-
51	Data contact	Who is the contact for this dataset?	-	-	-	-	-	-
52	Database entry attribution	Who entered the data in the database?	-	-	-	-	-	-
53	Database entry notes	Any specifics to the data that were entered. For example, was the length recalculated from that in the original published material?	-	-	-	-	-	-
54	Data horizontal resolution	What is the horizontal resolution of the data from which the measurements were made?	see separate table for more information (coverage, publication, data type, etc.)	see separate table for more information (coverage, publication, data type, etc.)	see separate table for more information (coverage, publication, data type, etc.)	see separate table for more information (coverage, publication, data type, etc.)	see separate table for more information (coverage, publication, data type, etc.)	-
55	Data vertical resolution	What is the vertical resolution of the data from which the measurements were made?	see separate table for more information (coverage, publication, data type, etc.)	see separate table for more information (coverage, publication, data type, etc.)	see separate table for more information (coverage, publication, data type, etc.)	see separate table for more information (coverage, publication, data type, etc.)	see separate table for more information (coverage, publication, data type, etc.)	-
56	Additional notes	Comments on any other information/considerations that should be borne in mind when using these data	-	-	-	-	-	-
57	Shape of the landslide	Hour-glass (narrow middle corridor), downslope-widening, downslope narrowing, central bulge?	hour-glass (narrow middle corridor)	hour-glass (narrow middle corridor)	plum - downslope widening	if considered as two several landslides - hour-glass (narrow middle corridor)	-	-
58	Volume of all affected sediment and material	Use the best terminology to determine the landslide volume (Ve and Va versus volume of all affected sediment and material)	0.254 km^3	0.120 km^3 (Lastras et al., 2006; Sager et al., 2022)	0.40 km^3 (Lastras et al., 2006)	0.31 km^3 (Lastras et al., 2006)	0.19 km^3 (Lastras et al., 2006)	-
59	Shape of the headscarp	Irregular, outlines several amphitheatre headscarp, smooth (form described otherwise)	unknown southern extent - irregular	outlines several amphitheatre headscarps	outlines several amphitheatre headscarps	outlines several amphitheatre headscarps	outlines several amphitheatre headscarps	
60	Shape of the landslide front	Irregular, outlines several stages of failure, smooth (form described otherwise)	outlines several stages of failure	relatively smooth (several stages of failure - biggest one reached the landslide front and later ones were smaller)	relatively smooth (no coverage)	relatively smooth (several stages of failure - diverging towards the NW)	relatively smooth (several stages of failure - diverging towards the NW)	-
61	Extensional and/or compressional ridges present on the surface	-	compressional ridges inside the sink area (CD178 3D reflection seismic data)	extensional and compressional ridges (observed from side-scan sonar images acquired during the BALICAT TTR-14 cruise)	extensional ridges (observed from side-scan sonar images acquired during the BALICAT TTR-14 cruise) - compressional ridges not observed (not covered by the data)	extensional and compressional ridges (observed from side-scan sonar images acquired during the BALICAT TTR-14 cruise)	extensional and compressional ridges (observed from side-scan sonar images acquired during the BALICAT TTR-14 cruise)	observed from side-scan sonar images acquired during the BALICAT TTR-14 cruise

			pre-Ana Slide	Ana Slide	Joan Slide	Nuna Slide	Jersi Slide	Comment
62	Metadata for surficial extensional and/or compressional ridges	Where are these feature visible	2D and 3D reflection seismic data	bathymetric maps, side-scan sonar images, 2D and 3D reflection seismic data	bathymetric maps, side-scan sonar images, sub-bottom parasound	bathymetric maps, side-scan sonar images, sub-bottom parasound	bathymetric maps, side-scan sonar images, sub-bottom parasound	-
63	Relative complexity of the surrounding seafloor	-	relatively simple - small landslide	relatively simple - small landslide	relatively simple - large landslide	complex	relatively simple - small landslide	-
64	Presence of local faults	-	local seafloor synthetic faults and a seafloor anti-thetic en-echelon fault system	local seafloor synthetic faults and a seafloor anti-thetic en-echelon fault system	local fault presents inside the source area	local faults present beneath the transitional domain (by-pass zone), overrun by the slope failure thus active prior to failure	no faults observed	-
65	Buried and overrun faults	-	yes	yes	yes	yes	-	see Chapter 5
66	Thickness of evacuated landslide material (source area)	-	-	negative 20 m	-	-	-	requires pre-failure seafloor reconstruction
67	Thickness of accumulated landslide material (sink area)	Thickness calculated for accumulated landslide material in the sink area (e.g., between present-day seafloor and reconstructed pre-failure seafloor)	20 m (this study)	15 m 5	16.5 m	9 m	11.25 m	-
68	Straight landslide movement or diverged course?	Movement direction (main translation and movement orientation at the landslide front)	East to west	East to west	East to west	East to west	East to NNW	-
69	Areal extent of the landslide scar	-	8.2 km^2	4.8 km^2	ca. 23.6 km^2	10.2 km^2	8.1 km^2	landslide scar represents the outline of the landslide

Table 6.2: Geomorphometric table of landslides in the Eivissa Channel. Parameters 1 - 59 follow Clare et al. (2019) with additional descriptions and parameters added (60 - 69).

References

Berndt, C., S. Costa, M. Canals, A. Camerlenghi, B. de Mol, and M. Saunders (2012). Repeated Slope Failure Linked to Fluid Migration: The Ana Submarine Landslide Complex, Eivissa Channel, Western Mediterranean Sea. In: *Earth and Planetary Science Letters*, pp. 65–74. DOI: 10.1016/j.epsl.2011.11.045.

Cattaneo, A., D. Minisini, A. Asioli, M. Canals, G. Lastras, A. Remia, N. Sultan, and M. Taviani (2011). Age Constraints and Sediment Properties of Ana Slide (Balearic Sea, Western Mediterranean) and Implications on Age Dating of Submarine Landslides. In: EGU 2011 - Abstract. DOI: 10.1007/978-90-481-3071-9_42.

CD178 (2006). *Cruise Report No. 03 R.R.S. Charles Darwin cruise CD178*. Douglas G. Masson and Christian Berndt: National Oceanography Centre (NOC), Southampton; 14th March -11th April: 2006 3D Seismic Acquisition over Mud Volcanoes in the Gulf of Cadiz and Submarine Landslides in the Eivissa Channel, Western Mediterranean Sea. URL: https://www.bodc.ac.uk/resources/inventories/cruise_inventory/report/7117/.

Clare, M., J. Chaytor, O. Dabson, D. Gamboa, A. Georgiopoulou, H. Eady, J. Hunt, C. Jackson, O. Katz, S. Krastel, R. Le0n, A. Micallef, J. Moernaut, R. Moriconi, L. Moscardelli, C. Müller, A. Normandeau, M. Patacci, M. Steventon, M. Urlaub, D. Völker, L. Wood, and Z. Jobe (2019). A Consistent Global Approach for the Morphometric Characterization of Subaqueous Landslides. In: *Geological Society, London, Special Publications* 1, pp. 455–477. DOI: 10.1144/SP477.15.

HERMESIONE (2009). *Cruise Report BIO Hesperides Research cruise HERMESIONE*. Antoni M. Calafat and Miquel Canals: University of Barcelona, Spain; Institut National de Recherche Halieutique, Morocco; Consejo Superior de Investigaciones Científicas, Spain: Gibraltar Strait – Western Mediterranean (Cartagena – Cartagena) 15th September – 9th October 2009: Hotspot Ecosystem Research on Europe's Deep-Ocean Margins (HERMES), Hotspot Ecosystem Research and Man's Impact on European Seas (HERMIONE), and Ocean Tracking Network (OTN).

Lafuerza, S., N. Sultan, M. Canals, G. Lastras, A. Cattaneo, J. Frigola, S. Costa, and C. Berndt (2012). Failure Mechanisms of Ana Slide from Geotechnical Evidence, Eivissa Channel, Western Mediterranean Sea. In: *Marine Geology*, pp. 1–21. DOI: 10.1016/j.margeo.2012.02.010.

Lastras, G., M. Canals, D. Amblas, M. Ivanov, B. Dennielou, L. Droz, A. Akhmetzhanov, and TTR-14 Leg 3 Shipboard Scientific Party (2006). Eivissa Slides, Western Mediterranean Sea: Morphology and Processes. In: *Geo-Marine Letters* 4, pp. 225–233. DOI: 10.1007/s00367-006-0032-4.

Lastras, G., M. Canals, R. Urgeles, J. E. Hughes-Clarke, and J. Acosta (2004). Shallow Slides and Pockmark Swarms in the Eivissa Channel, Western Mediterranean Sea. In: *Sedimentology* 4, pp. 837–850. DOI: 10.1111/j.1365-3091.2004.00654.x.

Moscardelli, L. and L. Wood (2008). New Classification System for Mass Transport Complexes in Offshore Trinidad. In: *Basin Research* 20.1, pp. 73–98. DOI: 10.1111/j.1365-2117.2007.00340.x.

Panieri, G., A. Camerlenghi, I. Cacho, C. S. Cervera, M. Canals, S. Lafuerza, and G. Herrera (2012). Tracing Seafloor Methane Emissions with Benthic Foraminifera: Results from the Ana Submarine Landslide (Eivissa Channel, Western Mediterranean Sea). In: *Marine Geology*, pp. 97–112. DOI: 10.1016/j.margeo.2011.11.005.

Sager, T. F., M. Urlaub, P. Kaminski, C. Papenberg, G. Lastras, M. Canals, and C. Berndt (2022). Development and Emplacement of Ana Slide, Eivissa Channel, Western Mediterranean Sea. In: *Geochemistry, Geophysics, Geosystems*. DOI: 10.1029/2022GC010469.